Formation of Perovskite Type Oxide Artificial Lattices by Laser Molecular Beam Epitaxy and Their Electrical Properties.

The Institute of Scientific and Industrial Research
Osaka University

Hitoshi Tabata

Formation of Perovskite Type Oxide Artificial Lattices by Laser Molecular Beam Epitaxy and Their Electrical Properties.

The Institute of Scientific and Industrial Research
Osaka University

Hitoshi Tabata

Contents

7. Appendix

Chapter 1

1. General introduction

3d-transition metal-oxides have strong electron correlation. Their electrical and magnetical properties can be changed from insulating to metallic (in some cases, superconducting) and from anti-ferromagnetic to paramagnetic properties, respectively.[1] Form the view point of crystalchemistry, "perovskite structure" is one of the typical crystal structures among the 3d transition metal-oxides.[2] The perovskite type transition metal-oxides show various valence combination and strength of electron correlation without changing in crystal structure.

Oxide ferroelectric compounds were discovered in 1940's[3-6] and a lot of researches about these materials, such as $PbTiO_3$ and $BaTiO_3$, have been performed. These ferroelectric compounds have a long history and well studied in bulk samples. Various phenomena have been reported in the experimental works. The oxide superconductors (ex. La_2CuO_4 and $Bi_2Sr_2Ca_{n-1}Cu_nO_{2n+4}$), on the other hand, were discovered in recent years[7,8]. But a lot of studies, as same as ferroelectric materials, have been performed during this several years.

Both of the oxide superconductors and ferroelectric materials are commonly well studied in bulk samples as solid solutions. Nevertheless, the essential points , such as the origin of superconductivity or ferroelectricity and the relation between crystal structures and electric properties, of these materials have not been clear.

Artificial superlattices offer the unique opportunity to answer us these questions.

From the view point of crystalchemistry, typical features of the oxide superconductors and ferroelectric materials are that they are essintially copper oxide (Cu-O) and titanium oxide (Ti-O), respectively. The electronic configuration of Cu-O and Ti-O compounds are mostly Cu^{2+}; $[Ar][3d^9]$ and Ti^{4+}; $[Ar][3d^0]$.

So when the unit cell is divided at atomic or molecular layer scale, the sequence of $[CuO_2^{2-}]/[M_2O_2^{2+}]$ (M=La, Sm etc.) and $[TiO_2^0][MO^0]$ (M=Sr, Ba, Pb etc.) are expected. Therefore, the film formation of Ti-oxides is expected at atomic scale and Cu-oxide is at unit-cell scale or the sub-unit cell scale keeping the charge neutrality. (Fig.1-1)

In chapter 2, the laser ablation method is introduced form the view point of thin film and artificial lattice formation of the transition metal-oxides.

In chapter 3, the basic factors for the film formation of 3d-transition metal-oxides by the laser ablation are discussed.

In chapter 4 and 5, artificial superconductors and ferroelectrics are created by layer-by-layer successive deposition. In the superconducting artificial lattices, atoms are replaced site-selectively as we desire. The superconductivity appears by doping charge carriers into the anti-ferromagnetic insulator. The artificial substitution at atomic scale is demonstrated for the first time by the laser ablation. (in chapter 4)

In the artificial ferroelectrics, large stress can be introduced with the combination of two kinds compounds having different lattice constants. Furthermore, phase transition is controlled by the strain induced at the interfaces in the strained-superlattices. (in chapter 5)

References

1) J.Zaanen, G.A.Sawatzky and J.W.Allen ; Phys.Rev.Lett. 55 (1985) 418.

2) T. Arima, Y. Tokura and J. B. Torrance ; Phys. Rev. B 48 (1993) 17006.

3) H. Mueller ; Phys. Rev. 57 (1940) 829.

4) J.C.Slater ; J. Chem. pHys. 9 (1941) 16.

5) A von Hippel, R.G.Breckeridge, F.G.Chesley and L.Tisza ; Ind., Eng. Che.. 38 (1946) 1097.

6) B. Wul and I. M. Goldman ; Compy.rend.Acad.Sci.U.R.S.S. 46 (1945)139.

7) J.G.Bednorz and K.A.Muller ; Z. Phys. B 64 (1986) 189.

8) H.Maeda, Y.Tanaca, M.Fukutomi and T.Asano ; Jpn.J.Appl.Phys. 27 (1988) L209.

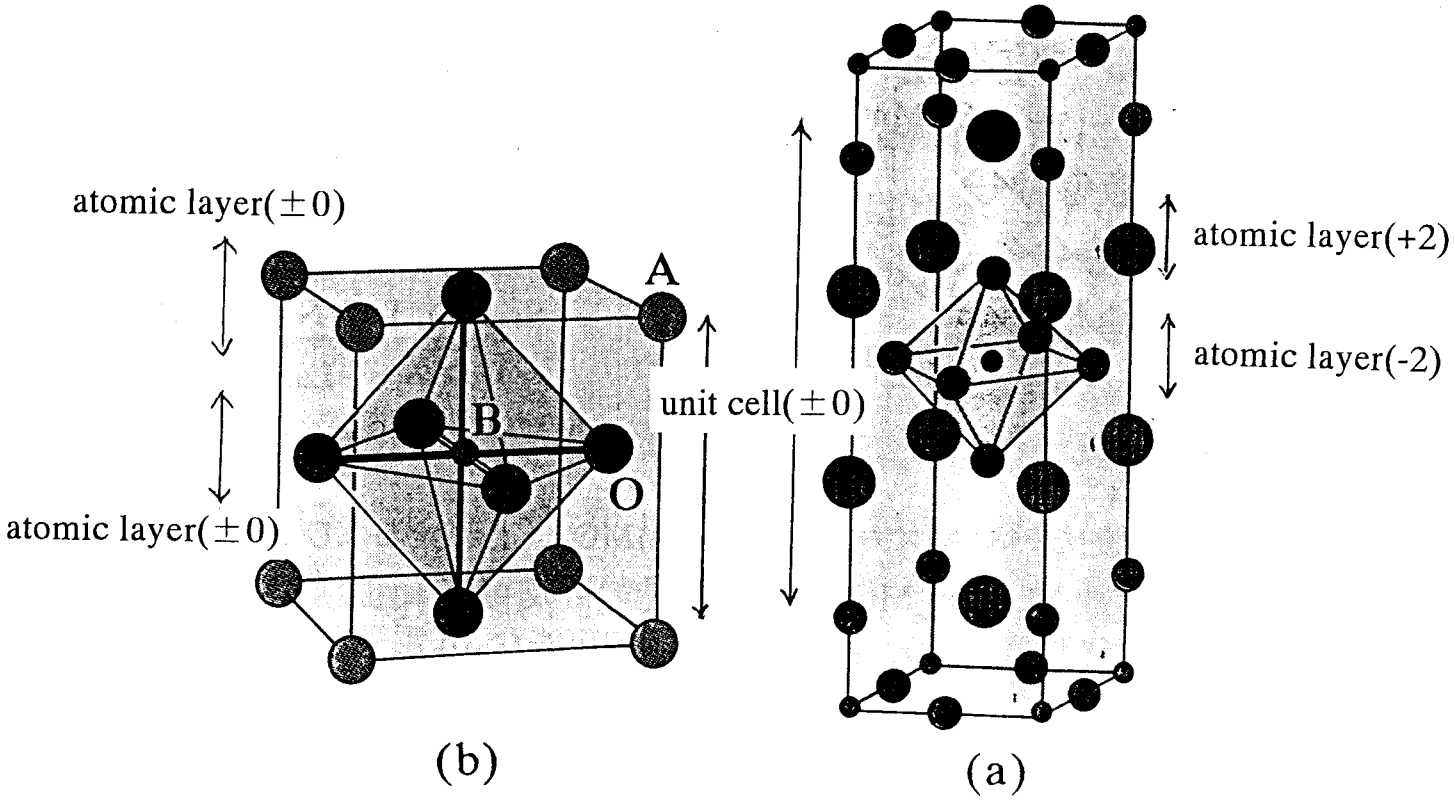

Fig. 1-1. Schematic models of crystal structures of

(a) copper oxide base superconductor, (b) titanium oxide base ferroelectrics.

Chapter 2

2. Laser ablation for thin film crystal growth

2-1 Characteristic feature of laser ablation

Pulsed laser ablation has become an increasingly utilized technique for the deposition of a variety of materials in thin film form. Its schematic illustration is shown in Fig.2-1. A high power laser beam is introduced into a vacuum chamber and focused on a target of the aimed material. The resulting plume of vaporized material is then collected on a nearby substrate to grow a film. At the laser powers commonly used for pulsed laser ablation, the vapor plume will typically consist of atoms, molecules, ions, free electrons and in some cases clusters.[1-9)]

The laser ablation method has several features as follows. Foremost among these is the capability of generating films that match the stoichiometry of the target. This is of particular importance in the deposition of materials such as the mixed oxide complexes such as high temperature superconductors[9-12)] where conventional thermal evaporation or sputtering can lead to non-stoichiometric deposits. Other advantageous feature is the capability with use of small targets in contrast to the large targets required for sputtering, and with deposition in reactive gas environments in contrast to conventional evaporation, where hot filaments or crucibles could be oxidized. In addition, high energy of the depositing species (10 - 100 eV) can have beneficial effects on film properties[13-15)].

The pulsed laser ablation process can be classified into three separated regimes: (1) interaction of the laser beam with the bulk target[16,17)], (2) plasma formation, heating and initial three dimensional expansion[18-22)], and (3) adiabatic expansion and deposition of thin films.[23-25)]

Recently, excimer lasers have been used to deposit semiconducting and high-

T_c superconducting thin films from bulk targets.

The deposition characteristics of the pulse laser ablation technique for the formation of the thin films have been found to be significantly different from other vaporization methods such as, rf-magnetron sputtering[26], chemical vapor deposition(CVD) [27] and molecular beam epitaxy(MBE)[28]. In particular, the laser deposition method has proven a suitable method for the growth of highly crystalline oxide thin films. Experimentally, this method involves ablation of a target using a high energy pulsed laser and subsequent deposition of the ablated material onto a substrate to yield a thin film product. A scheme of thin film formation by laser deposition under high vacuum condition which is called Laser MBE is shown in Fig. 2-2. Molecular beam epitaxy (MBE) refers to a deposition process which occurs under the molecular beam condition. The MBE condition is defined as that the mean free path of particles emitted from a solid target are much larger than the distance between the target and the substrate on which the film is formed. Under this condition, the particles emitted from the target can reach the substrate surface without any collisions with ambient gases.

Within a few nanoseconds of laser irradiation to the target surface, material evaporates rapidly. The luminous high- temperature plasma formed in the laser evaporation of the targets elongates preferentially perpendicular to the surface. The kinetic energies of the ejected species are in the range of 10-100 eV for excimer laser irradiated Y-Ba-Cu-O targets whereas the thermal evaporation energies are approximately an order of magnitude lower. The characteristics of laser-generated plasma have been attributed to the high evaporation flux rates and the interaction of the laser irradiation with the evaporated material.

The ablated plasma plume contains energetic particles in neutral and ionized states, which is characteristic of the relatively low temperature plasmas(1-2 eV)[14,15] produced by the laser ablation process(Fig.2-1). The plasma particle density is in the range of 10^{19}-$10^{21}$$cm^{-3}$, depending upon the stage of the

expansion process. The energy deposited by the laser beam on the target is equal to the energy needed to vaporize the surface layers plus the conduction loss by the plasma. This is given by the energy threshold, which represents the minimum energy above which appreciable evaporation is observed. In the excimer laser ablation, the energy threshold value varies from 0.3-0.4 J/cm^2 for oxide superconductors[3].

2-2 Historical review

The use of pulsed laser ablation was first reported by Smith and Turner[29], who used a pulsed ruby laser (wavelength; λ =694nm, intensity of 10^6 W/cm^2 and pulse duration; τ =1ms or Q-switch with 10^8 W/cm^2) to produce 'optically satisfactory' films of Sb_2S_3, As_2S_3, Se, ZnTe, Te, MoO_3, $PbCl_2$, PbTe and Ge. Other materials investigated (with less success) included CdTe, ZnO, InSb and InAs. Soon after, Zavitsanos and Sauer[30] reported the deposition of crystalline Ge and GaAs films on glass and NaCl substrates held at room temperature. This was followed by the work of Schwarz and Tourtellotte[31], who used a Nd-glass laser(λ =1060 nm, 100J/pulse and τ =2ms) to deposit films of Cr, W, Ti, C, ZnS, $SrTiO_3$ and $BaTiO_3$. By the early 1980s, a wide variety of oxide and fluoride dielectrics had been deposited[32,33], as well as very high quality elemental and compound semiconductors and their superlattices[32,34].

Interest in pulsed laser ablation was increased in 1987 with the discovery[35] that this process could be used to deposit thin films of high temperature superconductors with a degree of stoichiometric control much superior to that achieved with evaporation, sputtering or chemical vapor deposition(CVD). The first $YBa_2Cu_3O_7$(YBCO) films produced by laser ablation were deposited in vacuum, and required high temperature (800-900℃), post-annealing in an O_2

atmosphere to achieve the desired (superconducting) perovskite phase[35,36]. 'Superconducting-as-deposited' film where the deposition process includes in-situ anneal in a few hundred Torr of oxygen at a temperature below the deposition temperature having a superconducting transition temperature Tc of >80K were produced in an ambient of 5 mTorr O_2 on substrate at 650 ℃.[37] This was quickly followed by the demonstration that epitaxial films with a Tc of 90K could be produced in an ambient 70-200 mTorr of O_2 at 650-750℃.[38-43]

The success of laser ablation for the high temperature superconducting perovskite has motivated work on other complex materials systems, such as the ferroelectric perovskite materials.[44-47] Nevertheless, in many a number of studies about metal-oxide films, the relationship between crystal structures and electrical properties have not been elucidated in details. Therefore, I have formed artificial lattices to make clear these relations, controlling structures and properties artificially.

References

1) J.Cheung and J.Hotwitz, MRS Bulletin / February (1992) 30-36.

2) O.Auciello; Materials & Manufacturing Process 6 (1991) 32-52.

3) R.K.Singh and J.Narayan; Phys.Rev.B (1990) 8843-8859.

4) X.D.Wu et al.; MRS proceedings, 191 (1990) 129-140.

5) "Chemical processing with lasers" edit. by D.Bauerle (1986) Springer-Verlag.

6) "Laser-beam interactions with materials" edit. by M.Allmen (1986) Springer-Verlag.

7) "Laser processing of thin films and microstructures" edit. by Ian W.Boyd (1986) Springer-Verlag.

8) K.L.Saenger, Proceeding of Advanced Materials (1993) 2, 1-24.

9) J.G.Bednorz andK.A.Muller; Zeitschrift fur Physics, B64 (1986) 189.

10) M.K.Wu, L.R.Ashburn, C.J.Toyng, PH.hor, R.L.Meng,L.Gao, Z.J.huang, Y.Q.Wang and C.W.Chu; Phys.Rev.Lett. 58 (1987) 908.

11) H.Maeda, T.Tanaka, M.Fukutomi and T.Asano; Jpn.J.Appl.Phys. 27 (1988) L209.

12) Z.Z.Sheng and A.M.Hermann; Nature 332 (1988) 138.

13) E.W.Dreyfus; J.Appl.Phys. 69 (1991) 1721-1729.

14) J.P.Zheng, Z.Q.Huang, d.T.Shaw and H.S.Kwok; Appl.Phys.Lett. 54 91989) 280.

15) J.P.Zheng, Q.Y.Ying, s.Witanachchi, Z.Q.Huang, D.T.Shaw and H.S.Kwo; Appl.Phys.Lett. 54 (1989) 954.

16) C.H.Becker and J.B.Pallix; J.Appl.Phys. 64 (1988) 5152-5156.

17) S.Komuro, Y.Aoyagi, T,Morikawa and S.Namba; Jpn.J.Appl,Phys. 27 (1988) L34.

18) O.Eryu, K.Murakami, K.Musuda, A.Kasuya and Y.Nishuda; Appl.Phys.Lett. 54 (1989) 2716.

19) O.Auciello, S.Athavale, O.E.Hankins, M.Sito, A.F.Schreiner and N.Biunno; Appl.Phys.Lett. 53 (1988) 72.

20) D.Subhash, E.W>Rothe, G.P,Reck, T.Kushida and Z.G.Xu; Appl.Phys.Lett. 53(1988) 2698.

21) K.L.Saenger ; J.Appl.Phys. 66 (1989) 4435.

22) C.E.Otis and R.W.Dreyfus; Phsy.Rev.Lett. 67 (1991) 2102.

23) O.Auciello, A.R.Krauss, J.Santiago-Aviles, A.F.Schreiner and D.M.Gruen; Appl.Phys.Lett. 52 (1988) 239.

24) T.Vemkatesan, X.D.WU, A.Inam, Y.Jeon, M.Croft, E.W.Chase, C.C.Chang, J.B.Wachtman, R.W.Odom,, F.R.di Brozolo and C.A.Magee; Appl.Phys.Lett. 53 (1988) 1431.

25) U.Sudarsan, N.W.Cody, M.J.Bozack and R.Solanki; J.Matrials.Res. 13 (1988) 825.

26) H.Adachi, S.Kobayashi, K.Setsune, T.Misyuyu and K.Wasa; Jpn.J.Appl.Phys. 27 (1988) L1883.

27) J.N.Eckstein, I.Bozovic, K.E.von Dessonneck, D.G.Schlom, J.S.Harris and S.M.Baumann; Appl.Phys.Lett. 57 (1990) 931.

28) T.Yamashita, M.Era, S.Noge, A.Irie, H.yamane, T.Hirai, H.Kurosawa and T.Mastui; jpn.J.Appl.Phys. 29 (1990) L74.

29) H.M.Smith and A.F.Turner; Appl.Optics. 4 (1965) 147

30) P.D.Zavitsanos and W.E.Sauer; J.Electrochemical Soc. 115 (1968) 109

31) H.Schwarz and H.A.Tourtellotte; J.Vac.Sci,Technol.; 6 (1969) 373

32) V.S.Ban and D.A.Kramer; J.Mat.Sci. 5 (1970) 978

33) H.Sankur; Proc. MRS symp. 29 (1984) 373.

34) J.T.Cheung, G.Niizawa, J.Moyle, N.P.Ong, B.M.paine and

35) D.Dijikaamp, T.Venkatesan, X.D.Wu, S.A.Shaheen et al.; Appl.Phys.Lett. 51 (1987) 619.

36) J.Narayan, N.Biunno, R.Sinngh, O.W.Holland and O.Auciello;

Appl.Phys.Lett. 51 (1987) 1845.

37) X.D.WU, a.Inam, T.Venkateasn, C.C.Chang, E.W.Chase, P.Barboux, J.M.Trascon; Appl.Phys.Lett. 52 (1988) 754.

38) J.Fronhlingsdorf, W.Zander and B.Strizker; Solid State Comm. 67 (1988) 965.

39) G.Koren, E.Polturak, B.Fisher, D.Cohen and G.Kimel; Appl.Phys.Lett. 53 (1988) 2330.

40) B.Roas, L.Schultz and G.Endres; Appl.Phys.Lett. 53(1988) 1557.

41) A.I.Golovashikin, E.V.Ekimov, S.I.Krasnosvobodtev and E.V.Pechen; Physica C153-155 (1988) 1455.

42) T.Venkatesan, X.D.Wu, A.Inam et al.; Appl.Phys.Lett.54 (1989) 581.

43) G.Koren, A.Gupta et al. Appl.Phys.Lett. 54 (1989) 1054.

44) H.Kidoh and T.Ogawa; Appl.Phys.Lett. 58 (1991) 2910.

45) D.B.Chrisey, J.S.Horwitz et al. Apll.Phys.Lett. 59 (1991) 1565.

46) S.Kh.Esayan et al. Sov.Tech.Phys.Lett. 16 (1990) 857.

47) K.L.Saenger, R.A.Roy, K.F.Etzold and J.J.Cuomo; MRS symp.proc.200 (1990) 115.

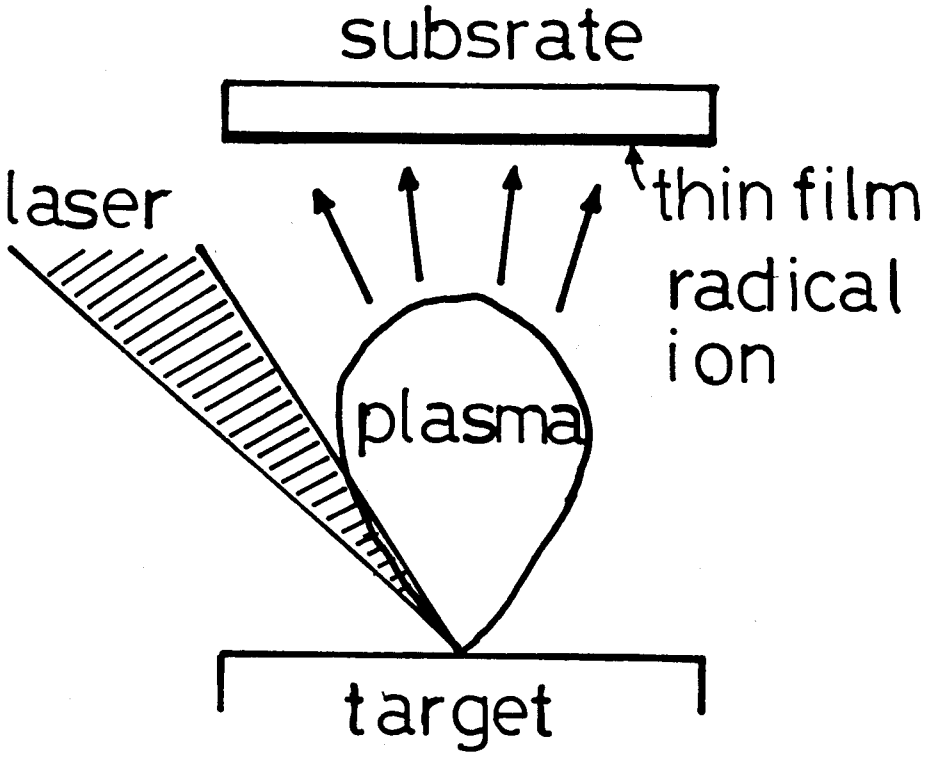

Fig. 2-1. Scheme of thin film formation with laser ablation

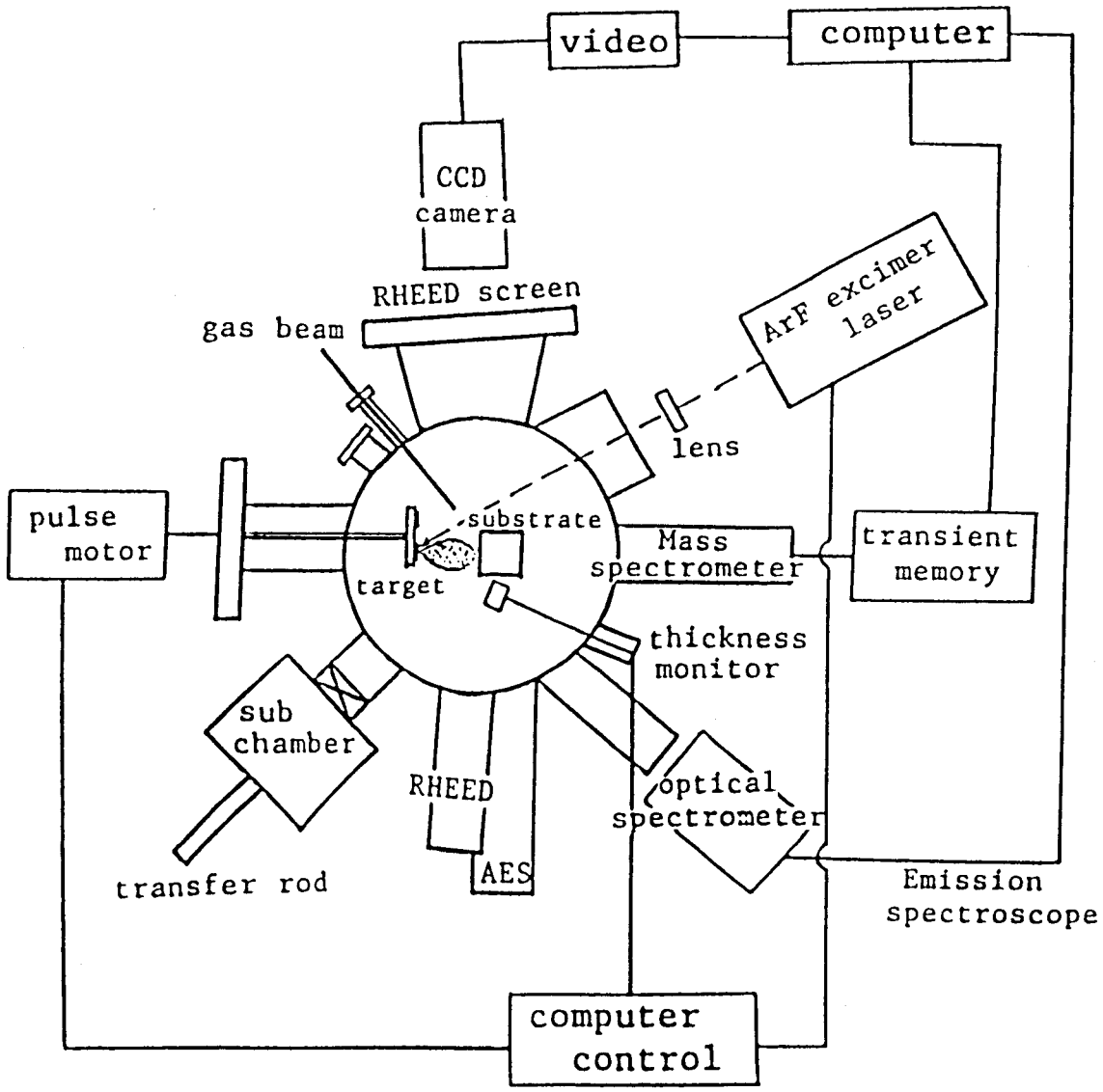

Fig.2-2. Schematic diagram of laser MBE apparatus .

Chapter 3

3. Thin film single crystal growth.

3.1 Introduction

The excimer laser ablation technique has been shown to be advantageous for making thin films of oxide materials[1-3]. Various thin films can be formed under a wide range of ambient pressure and at relatively low temperature[4-5]. Using this method, we have formed epitaxial 3d-metal oxide compounds thin films. In order to apply metal oxide materials to applications and to elucidate the mechanism in their electrical properties, thin film formation is important. Furthermore, highly controlled stoichiometry and crystallinity of the films are required.

For constructing the artificial lattices, the important parameters in the formation of the metal oxide film are summarized in the following three points.

① control the phase formation of the film by changing the atmosphere (oxygen partial pressure) and substrate temperature during the film construction.

②control of the starting composition.

③ control the film orientation (epitaxial growth).

The purpose in this chapter, to get the single crystal thin film which composition, crystal structure and electrical behavior is quite similar to that of bulk single crystal.

3-2. Basic condition for single crystal film formation

3-2-1. Effect of pressure and temperature - PbTiO3 film -

Abstract

Ferroelectric $PbTiO_3$ films have been formed on $SrTiO_3(100)$ substrate using ArF laser ablation as a function of substrate temperature and oxygen pressure. Perovskite $PbTiO_3$ is constructed around the substrate temperature of 450℃ and oxygen pressure of 10-40 mTorr. Pyrochlore $Pb_2Ti_2O_{7-x}\{111\}$, on the other hand, is formed at higher temperature and lower oxygen pressure than those of perovskite phase formed. And PbO films are obtained under similar formation condition to that of the perovskite phase formed. This result suggests that the PbO formation plays an important role for the construction of $PbTiO_3$ structure.

Introduction

Ferroelectric materials with perovskite structure have attracted much attention for various electronic applications. For example, $PbTiO_3$ and $SrTiO_3$ are promising for use in nonvolatile memory devices and capacitors[7,8]. $LiTaO_3$ and $LiNbO_3$ films are used for non-linear optics[9,10]. $Pb(Zr,Ti)O_3$ (PZT) and $(Pb,La)(Zr,Ti)O_3$ (PLZT) are well known as piezoelectric devices[11]. In order to apply these materials to devices, thin film formation is important. Furthermore, highly controlled stoichiometry and crystallinity of the films are required. For this reason, studies on the ferroelectric thin films have been carried out by various methods, such as rf-sputtering[12], and chemical vapor deposition (CVD)[13].

I have examined film formation using a laser ablation method. The advantage of the pulsed laser deposition technique is the ability to control the film formation conditions, because the laser beam is introduced from outside the reaction chamber. We can control temperature and pressure independently, and because of this, well-crystallized films are formed even at low pressure in comparison to other techniques, such as sputtering[14] and CVD[15,16].

So far, few studies of ferroelectric films have been reported on the correlation between substrate temperature and oxygen pressure over wide ranges. The aim in this study is to clarify the correlation between temperature, oxygen pressure and formation phase. Furthermore, we have formed PbO and TiO_2 films for discussing the essential factor in the construction of the $PbTiO_3$ structure.

Experiment

Figure 3-1 shows a schematic representation of the apparatus for ArF excimer laser ablation used in this experiment. The film growth was carried out in a vacuum chamber with an O_2 and O_2+O_3(8%) mixed gas with pressure in the range of $1x10^{-3}$-$3x10^{-1}$ Torr. The target was a 10 mmϕ disk of bulk single phase $PbTiO_3$ which was set at the center of the vacuum chamber. The laser beam was focused on the target with an energy density of 1 J/cm^2 at a frequency of 10 Hz. The thin film was deposited on the substrate located at the opposite side of the target in the presence of O_2 gas.

The target was a 10 mmϕ pellet of stoichiometric and single-phase $PbTiO_3$, which was set at the center of the vacuum chamber. The $PbTiO_3$ target was prepared by pressing $PbTiO_3$ powder (99.99%) with $1-2x10^3$ kgf/cm^2 and

sintering at 950℃ for 24 hours in air atmosphere. PbO and TiO_2 targets were prepared by pressing PbO powder(99.9%) and TiO_2 powder at $2.0x10^3 kgf/cm^2$, respectively.

The substrates used were MgO(100) and $SrTiO_3$(100) single crystals heated to 300-700℃. The heater was sandwiched with two pieces of substrates.The $PbTiO_3$ thin film was deposited of the substrate located at the front side, and a thermocouple was mounted in contact with that of back side. The substrate temperature was measured with this thermocouple. Deposition rate was about 10Å/min, and the film was quenched to room temperature after film formation. The film thickness was about 1000Å. Film thickness was measured by quartz crystal oscillator during film formation and it was checked by the multiple beam interferometry method after formation.

Pb/Ti ratios for the films made at various deposition temperatures, and ambient oxygen pressures were determined with energy dispersive x-ray spectroscopy (EDX). The crystal structure and crystallographic orientation of the films were evaluated with x-ray diffraction and the reflection high energy electron diffraction (RHEED) method. The surface morphology of the film was observed by scanning electron microscope (SEM).

Results and discussion

Figure 3-2-1 shows the Pb/Ti ratio of the film deposited under various ambient O_2 pressures. The Pb content decreases rapidly under O_2 pressure below $1x10^{-1}$ Torr. Under this condition, Pb, which has a low melting point and therefore a high vapor pressure, may revaporize from the film. For this reason, the composition of the film changes from the stoichiometric ratio of $PbTiO_3$

(Pb:Ti=1:1). For ambient O_2 pressures above $1x10^{-1}$ Torr, Pb and Ti atoms are well oxidized to the $PbTiO_3$ compound. Consequently, the $PbTiO_3$ film can be formed without stoichiometric change under O_2 pressures greater than $1x10^{-1}$ Torr. Fig.3-2-2 shows the X-ray diffraction pattern of $PbTiO_3$ films formed at O_2 pressure of $1x10^{-3}$Torr(a) and $1x10^{-1}$ Torr(b). On the other hand, when $O_2+O_3(8\%)$ gas is used for oxidation atmosphere, Pb/Ti ratio is kept constant at the pressure of $3x10^{-2}$ Torr. Because of the strong oxidizing effect of ozone (O_3)[16-18], Pb and Ti can be stabilized as metal oxide ($PbTiO_3$) at relatively low oxygen pressure comparing with pure oxygen (100% O_2).

Figure 3-2-3 shows the formation diagram for the phases of the $PbTiO_3$ films deposited under various oxygen (O_2+8% O_3) pressures and substrate temperatures. This diagram can be divided into three regions. One is the region where c-axis-oriented perovskite $PbTiO_3$ is formed at the substrate temperature around 450℃ in the oxygen pressure of 10~40 mTorr. The second is the region where the {111}-oriented pyrochlore $Pb_2Ti_2O_{7-x}$[19,20] is formed around the temperature of 580℃ and oxygen pressure of 10mTorr. In the region of higher temperature above 670℃ and lower oxygen pressure, titanium oxide is obtained.In the third region of "pyrochlore{100}" around 380℃, the films formed are also pyrochlore with {100} orientation. At the lower temperature than "pyrochlore{100}", amorphous phase is obtained.

Thermodynamically, the interaction of the Pb and Ti cations with the oxygen is given by

$$Pb + 1/2xO_2=PbO, \quad (3\text{-}1)$$

$$Ti + O_2=TiO_2, \quad (3\text{-}2)$$

the standard enthalpy change and the entropy change are

ΔH_{PbO}° =-219.73 kJ/mol, ΔS_{PbO}° =-101.62 J/K mol in Eq. (1) and

ΔH_{TiO2}° = -941.78 kJ/mol,

ΔS_{TiO2}° = -179.66 K/k mol in Eq. (3-2), respectively, (at 700 K).[21-23]

The Gibbs' free energy can be represented by the equation

$$\Delta G^{\circ} = \Delta H^{\circ} - \Delta S^{\circ} T, \qquad (3\text{-}3)$$

where ΔG° is the Gibbs' free energy. The Gibbs's free energy change in the reaction of PbO (1) and TiO_2(2) are -148.6 kJ/mol and -186.1 kJ/mol, respectively. Namely, lead oxide (PbO) is far less stable than TiO_2. Therefore Pb atoms tend to decompose during the film formation. High oxygen partial pressure (above 0.1 Torr) is required in order to prevent Pb, which is a volatile element, from revaporizing during film formation. This guide line is similar to the Cu-O formation in the copper-oxide superconductors[24-33].

Analysis of X-ray diffraction patterns shows that the crystallographic phases in the film also depend strongly on the substrate temperature. The perovskite structure ($PbTiO_3$) is formed in the temperature range of 380-550℃ under the O_2 pressure of $1x10^{-1}$ Torr.(Fig.3-2-4(b)) The film show pyrochlore $Pb_2TiO_2O_7$ [19,20] below 350℃ (Fig.3-2-4(a)) and mixed structures of $PbTi_3O_7$ and TiO_2 above 550℃ (Fig.3-2-4(c)). Pb/Ti ratio for the films is almost constant up to 500 ℃. However, the ratio decreases rapidly above 550℃ due to the decomposition of the lead component from the film. Above 550℃, we have to add Pb of 10-15 mol % to the target to get the $PbTiO_3$ film having stoichiometric composition.

The surface morphology of the film having the perovskite structure has mirror like very smooth surface in the scanning electron microscope (SEM) image (Fig.3-2-5).

Conclusion.

$PbTiO_3$ films have formed as a function of substrate temperature ad oxygen pressure using ArF laser ablation. The pyrochlore phase is formed at lower temperature than that of the perovskite. Perovskite $PbTiO_3$ phase locates at the substrate temperature around 450℃ and in the oxygen pressure of 10-40 mTorr. The stability of PbO phase plays an important role for the $PbTiO_3$ film formation. Namely, one of the most important factors of metal oxide with low melting point (PbO) rather than that of high melting point (TiO_2). This is the guiding principle to form the metal oxide film which is constructed with the combination of high melting points and low melting point compositions.

References

1) D.Roy, S.B.Krupanidhi and J.P.Dougherty; J.Appl.Pys. 69 (1991) 7930.

2) H.Kidoh, T.Ogawa, H.yashima, A.Morimoto and T.Shimuzu; Jpn.J.Appl.Phys. 30 (1991) 2167.

3) J.Lee and A.Safari, R.L.Pfeffer; Appl.Phys.Lett. 61 (1992) 1643.

4) D.Roy, S.B.Krupanidhi; J.Mater.Res. 7 (1992) 2521.

5) S.B.Krupanidhi and D.Roy; J. Appl.Phsy. 72 (1992) 620.

6) L.Sheppard; Am.Ceram.Soc.Bulletin 72 (1993) 45.

7) J.T.Evans and R.Womack; IEEE J.SOlid-State Circuits 23 (1988) 1171.

8) S.Yamauchi, T.Sakuma, K.Takemura and Y.Miyasaka; Jpn.J.Appl.Phys. 30 (1991) 2193.

9) T.Kanata, Y.KObayashi and K.Kubota; Appl.Phsy.Lett. 62 (1987) 2989.

10) R.C.Baumunn, T.A.Rost and T.A.Rabson ; Appl.Phsy.Lett. 68 (1990) 2989.

11) K.Kushida and H.Takeuchi; Appl.aphsy.Lett. 50 (1987) 1800.

12) M.Okuyama, Y.Matsui, H.Nakano, T.Nakagawa and Y.Hamakawa; Jpn. J. Appl. Phsy. 18 (1979) 1633.

13) S.Mochizuki, S.Kimura and R.Makabe ; Jpn.J.Appl.Phys. 28 (1989) 15.

14)K.Torii, T.Kage, K.Kushida, H.Takeuchi and E.Takeda; Jpn.J.Appl.Phys. 30 (1991) 3562.

15) M.de Keijser, G.J.M.Dormans, J.F.M.Dormans, J.F.M.Cillessen and D.M.de Leeuw; Appl.Phys.Lett. 58 (1991) 2636.

16) D.G.Schlom, A.F.Marshall, J.T.Sizemore, Z.J.Chen, J.N.Ecksrein, I.Bozovic, K.E.von Dessonneck, J.S.Harris, Jr. and J.C.Bravman; J.Crys.Growth 102 (1990) 361.

17) Y.Nakayama, H.Ochimizu, A.Maeda, A.Kawazu, K.Uchiokura and S.Tanaka; Jpn.J.Appl.Phys. 28 (1989) L1217.

18) R.O.Suzuki, P.Bohac and L.J.Gauckler; J.Am.Cream.Soc. 75 (1992) 2833

19) S.Otsubo, T.Maeda, T.Minimikawa, Y.Yonezawa, A.Morimoto and T.Shimizu; jpn.J.Appl.Phys. 29 (1990) L133.

20) T.Mihara, S.Mochizumi, S.Kimura and R.Makabe; Jpn.J.Appl,Phys. 31 (1992) 1872.

21)JANAF Thermochemical Tables (American Chemical Societyand American Institute of Physic for National Bureau of Standard, New York, 1971) 2nd. edition editted by D.R.Stull and H.Prophet.(NSRD-NBS37)

22)T.B.Lindemer, F.A.Washburn, C.S.MacDougall, R.Fenstra and O.B.Cavin ; Physica C 178 (1991) 93.

23)R.Fenstra, T.B.Lindemer, J.D.Budai and M.D.Galloway, T.Hashimoto, H.Koinuma and K.Kishio; Jpn.J.Appl.Phys. 30 (1991) 1685.

24)I.Iguchi, A.Sugishita, M.Yanakisawa, S.Hosaka, Y.Yokoyama and H.Asano ; Jpn.J.Appl.Phys. 27 (1988) L992.

25)B.T.Ahn, V.Y.Lee, TBeyer, T.M.Guer and R.A.Huggins; Physica C 162-164 (1989) 883 and 167 (1990) 529.

26)T.Aselage and K.Keefer; J.Mater.Res. 3 (1988) 1279.

27)J.E.Ullman, R.W.McCallum and J.D.Verhoeven; J.Mater.Res. 4 (1989) 752.

28)B.-J.Lee and D.N.Lee ; J.Am.Ceram.Soc. 72 (1989) 314.

29)U.Balanchandran, R.B.Poeppel, J.E.Emerson, S.A.Johnson, M.T.Lanagan, C.A.Youngdahl, D.Shi, K.C.Goretta and N.G>Eror; Mater.Lett. 8 (1989) 454.

30)R.K.Williams, K.B.Alexander, J.Brynestad, T.J.Henson, D.M.Kroeger, T.B.Lindemer, G.C.Marsh and J.O.Scarbrough; J.Appl.Phys. 67 (1990) 6934.

31)E.D.Specht, C.J.Sparks, A.G.Dhere, J.Brynestad, O.B.Cavin and D.M.Kroeger; Phys.Rev.B 37 (1988) 7426.

32)D.Shi, D.W.Capone II, K.C.Goretta, K.Zhang and G.T.Goudey; J.Appl.Phys. 63 (1988) 5411.

33)J.C.MacCallum, C.W.White and L.A.Boaatner; Mater.Lett. 6 (1988) 374.

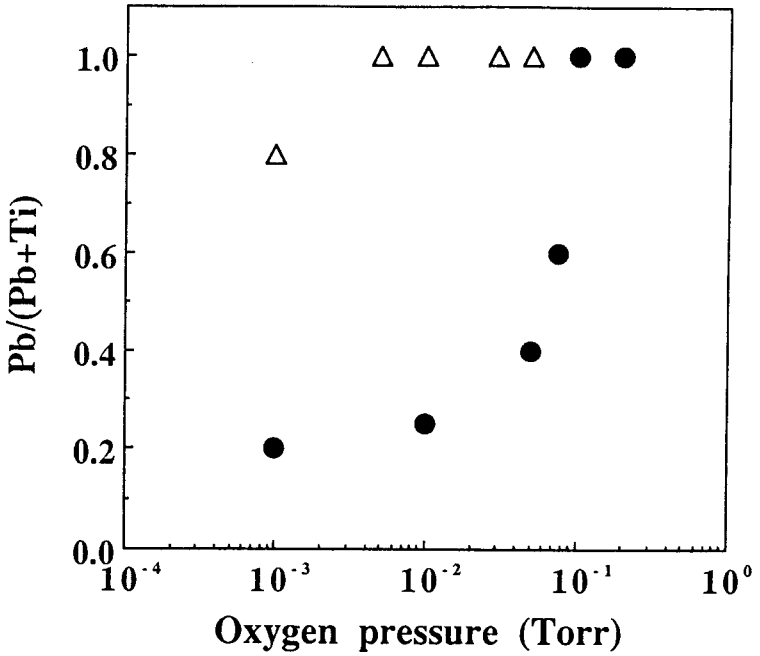

Fig. 3-2-1. Pb/Ti ratio in the $PbTiO_3$ film at various ambient O_2(●) and O_3 (△) pressure

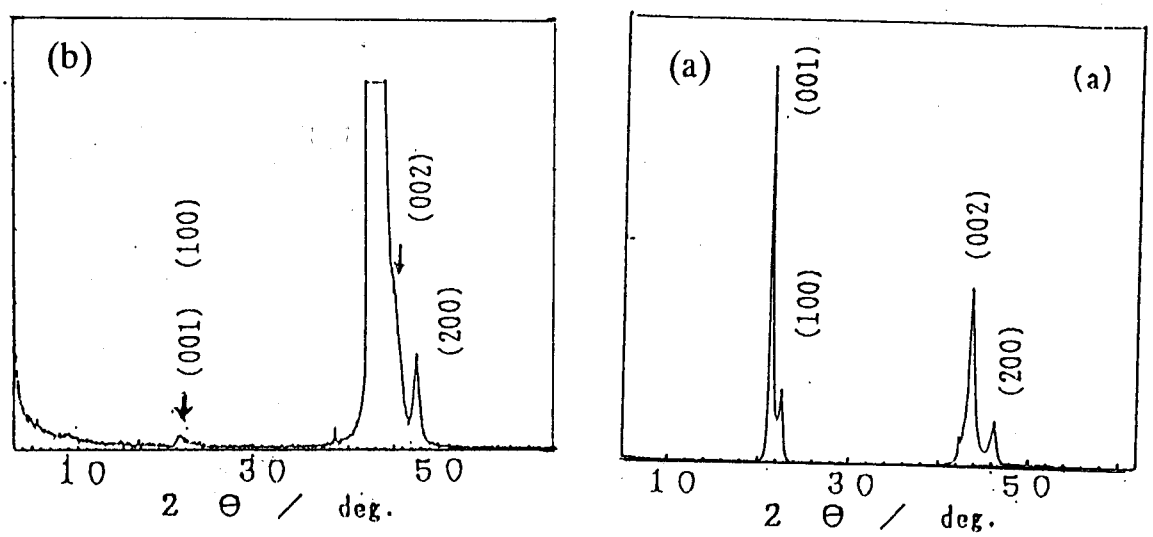

Fig. 3-2-2. X-ray diffraction pattern of $PbTiO_3$ film formed under the O_2 pressure of (a) 1 mTorr and (b) 100 mTorr.

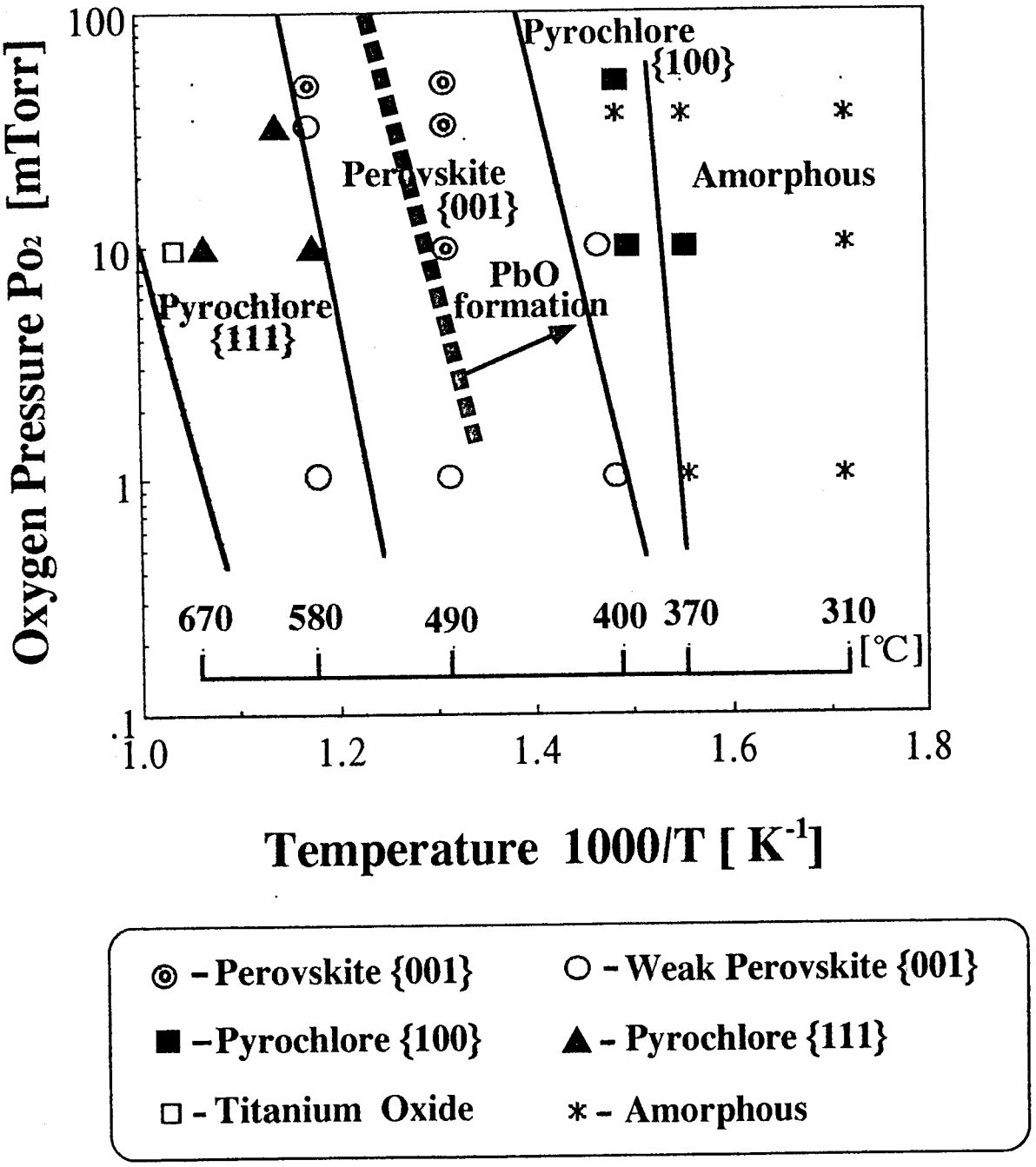

Fig. 3-2-3. O_2+O_3(8%) partial pressure vs temperature diagram for $PbTiO_3$ and PbO film formation.

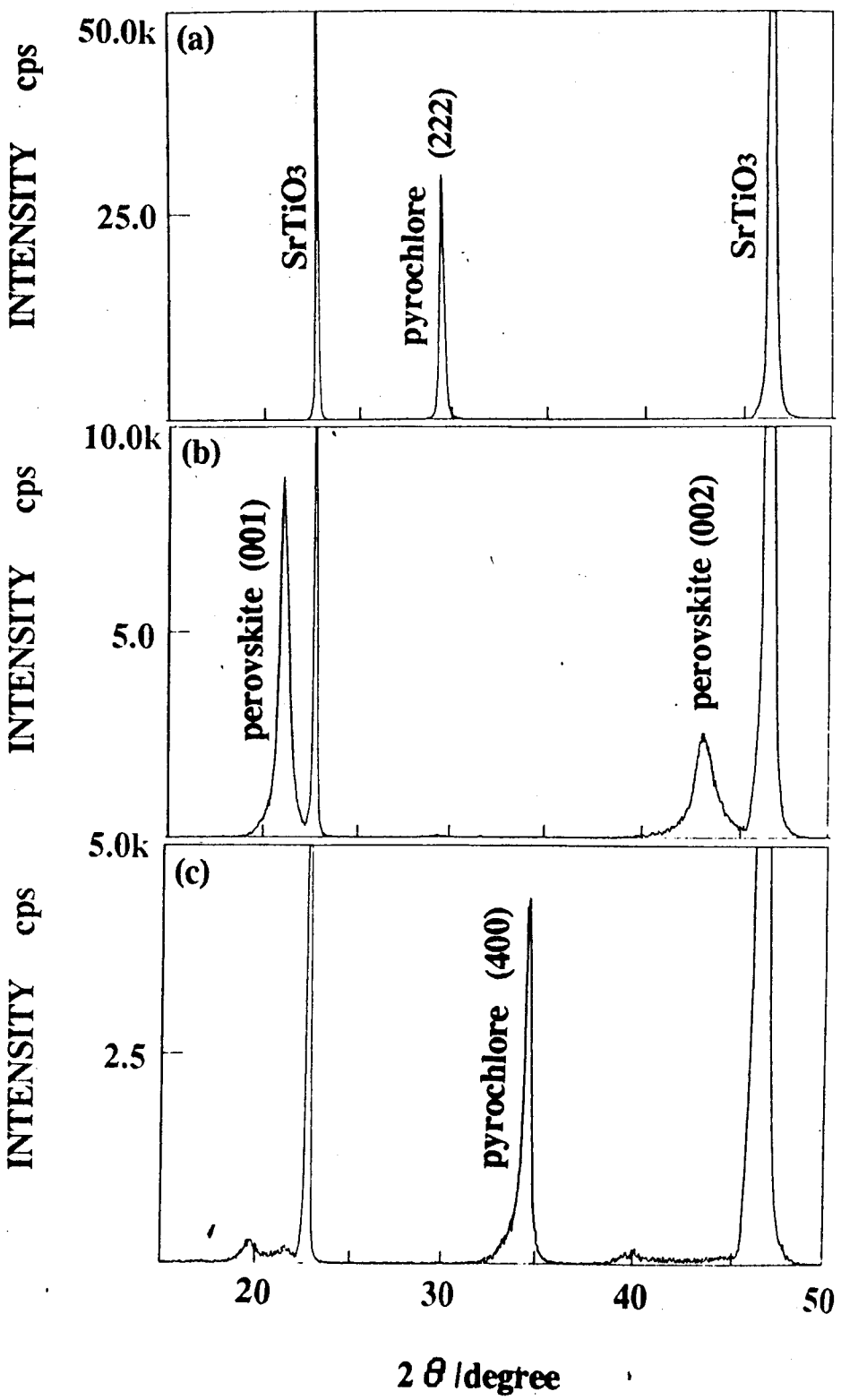

Fig. 3-2-4. X-ray diffraction pattern of $PbTiO_3$ films formed at substrate temperature and oxygen pressure of (a) 580℃, 35 mTorr, (b) 490℃, 35mTorr and (c) 400d℃, 50 mTorr.

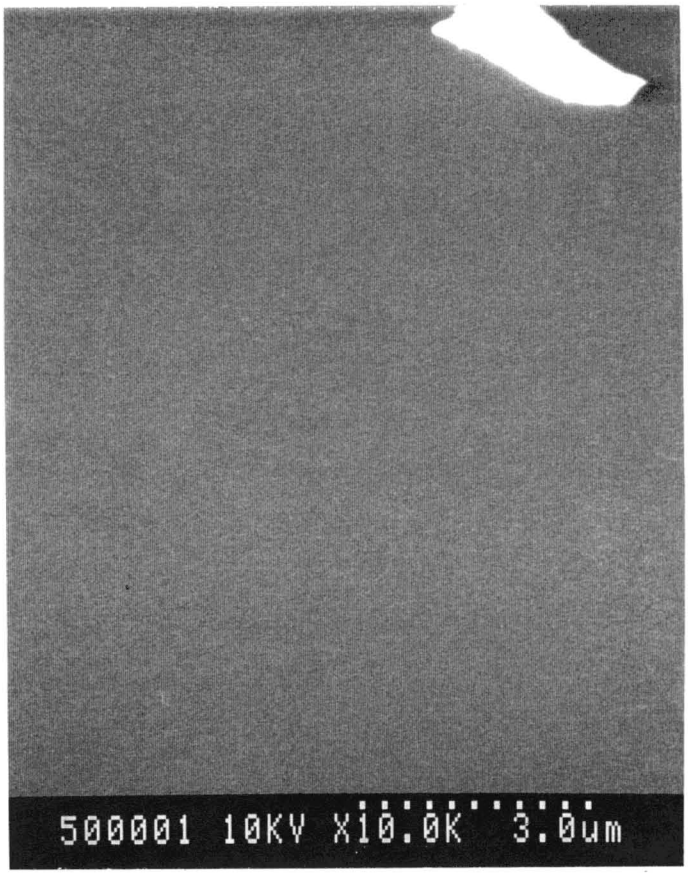

Fig. 3-2-5. SEM image of laser ablated $PbTiO_3$ film.

3-2-2. Effect of pressure, temperature and starting composition - $Bi_2Sr_2Ca_{n-1}Cu_nO_{2n+4}$ system -

Abstract

Three phases of $Bi_2Sr_2Ca_1Cu_2O_{2n+4}$ superconductors, i.e. $Bi_2Sr_2Cu_1O_6$(2201), $Bi_2Sr_2Ca_1Cu_2O_8$(2212) and $Bi_2Sr_2Ca_2Cu_3O_{10}$ (2223), have been controlled by a laser ablation method. The 2201,2212 and 2223 phases are selectively formed by controlling substrate temperature, starting composition of targets and ambient pressure. The oxygen partial pressure plays the important role in these three parameters. Under the pressure higher than $6x10^{-2}$ Torr, 2201 phase is dominantly formed in the wide range of substrate temperature and composition. Under the lower oxygen partial pressure (from $3x10^{-3}$ to $6x10^{-2}$ Torr), on the other hand, the control of the three phases, 2201, 2212 and 2223, is possible for as-deposited films only by changing the target compositions.

Introduction

In the bulk samples of $Bi_2Sr_2Ca_{n-1}Cu_nO_{2n+4}$ (BSCCO) superconductors, there have been a lot of reports of phase control by changing starting composition, ambient pressure and sintering temperature [1][2]. Nevertheless, in the thin films, especially for as- grown films, a relation between phases of BSCCO thin films and the parameters for making thin films has not been fully established[3]. The BSCCO superconductor has typical phases such as, $Bi_2Sr_2CuO_6$(2201), $Bi_2Sr_2Ca_1Cu_2O_8$(2212) and $Bi_2Sr_2Ca_2Cu_3O_{10}$(2223), containing one, two and three layers of CuO_2 planes in half a unit cell. They show critical temperatures (T_c) of 7K(or semiconductor), 80K and 110K, respectively[4][5]. In the present

experiments, we have attempted the phase control of as-deposited BSCCO thin films by controlling ambient pressure, substrate temperature and composition of the ablation targets using laser ablation method. It has become possible to discriminate these 2201,2212,2223 thin films in the as-deposited state by controlling these parameters.

Experimental

The thin films were formed by an ArF excimer laser ablation (193nm). Ions and atoms were injected from targets, and thin films of superconductors were formed on an MgO(100) single crystal substrate. The targets of BSCCO for the laser ablation were prepared by a soled-state reaction with various starting compositions. The starting composition of the targets were at first fixed to $Bi_{4.2}Sr_{3.0}Ca_{3.0}Cu_{6.0}O_y$ in order to make clear a relation between the phases of the thin films and ambient pressure or substrate temperature, Then we fixed the ambient pressure and the substrate temperature to the suitable condition, and the composition of the targets was changed to make clear a relation between starting composition and film phases. The ambient pressure was a mixture of N_2O and O_2 with the ratio of 1 to 1. The mixed gas of O_2 and N_2O was selected by following reasons. N_2O gas is effective in crystallization at low temperature and is known to get rid of impurities (CuO etc.)[7]. The structures of the films were determined by X-ray diffraction measurement (Cu Kα), and the surface morphology of the films was observed by scanning electron microscope(SEM). Compositional analysis of the thin films was performed by energy dispersion of X-ray micro analyzer. Superconductivities of the films were measured with a standard four-prove technique using a calibrated germanium temperature sensor.

Results and discussion

1. Phase control by ambient pressure and substrate temperature

At an ambient pressure higher than $6x10^{-2}$ Torr, the 2201 phase is formed for the an-grown state under wide range of substrate temperature between 500℃ and 670℃(see Fig.3-2-6). The 2212 phase is formed under the oxygen partial pressure between $3x10^{-1}$ Torr and $6x10^{-2}$ Torr. The conditions getting the single 2212 phase and well crystallized structure have been further investigated. The well crystallized 2212 single phase can be formed between $6x10^{-3}$ Torr and $1x10^{-2}$ Torr and at 550℃ to 650℃ (Fig.3-2-6). No peak of impurity phase is observed in the X-ray diffraction pattern. Under the conditions out of the area B, the 2201 phase tends to mix with the 2212 phase. Under the oxygen partial pressure lower than $3x10^{-3}$ Torr, no crystallization occurs, indicating amorphous state or decomposition. The 2223 phase is not formed with this composition of the target. It is interesting that the phase control is possible only when the ambient pressure is changed with the starting composition is fixed at $Bi_{4.2}Sr_{3.0}Ca_{3.0}Cu_{6.0}O_y$.

One possible explanation for that the 2201 phase is formed under the higher oxygen partial pressure, is as follows. The 2201 and the 2212 phases consist of excess oxygen in the Bi_2O_2 layer. Therefore,under the condition of relatively higher ambient pressure which force to introduce excess oxygen, the 2201 phase having higher symmetry may be more stable than the 2212 phase.

2.Phase control by the starting compositions

When the ambient pressure is fixed at $6x10^{-3}$ Torr, three phases of 2201,2212 and 2223 can be independently formed by controlling the target composition. Fig.3-2-6 shows that the amount of Sr and Ca is important to form these phases.The 2201 phase (Fig.3-2-6(b)-(1)) is formed in an area of relatively Ca and Sr-poor region , but the 2223 phase (Fig.3-2-6 (b)-(3)) is formed in the Ca

and Sr-rich (Ca-rich) region (Fig.3(L,H,K,P). The 2212 phase (Fig.3-2-6(b)-(2)) is formed in the area around B, C, D (Fig.3-2-6(a)). These results suggest that the amount of Ca and Sr plays an important role for controlling these three phases as well as Bi and Cu. It is important that the 2223 phase is not formed even when only Ca and Cu (1:1) are added to the ideal 2212 composition. The reason of this phenomenon is considered that it is important to increase Ca (Sr) atoms around the CuO_2 planes when the more $CaCuO_2$ planes are formed in the BSCCO. In this way, phase control of 2201,2212 and 2223 compounds are possible only when the ambient pressure, substrate temperature and starting composition are suitably selected.

Conclusion

(1) The 2201 phase is formed under the ambient oxygen pressure higher than $6x10^{-2}$ Torr (the condition of high ambient pressure). The 2212 phase is formed in the ambient oxygen pressure between $3x10^{-3}$ Torr and $6x10^{-2}$ Torr(condition of low ambient pressure). Under this condition, each phase is formed at wide range of substrate temperature between 500℃ and 670℃. In other words, phases are mainly controlled by oxygen ambient pressure for the starting composition of the $Bi_{4.2}Sr_{3.0}Ca_{3.0}Cu_{6.0}O_y$.

(2) Under the condition of low ambient pressure, the 2201, 2212 and 2223 phases of as-grown films are controlled independently by changing the starting compositions.

(3) The 2223 phase formation is strongly determined by Ca and Sr content. In this way, the control of 2201, 2212 and 2223 phase and of superconducting properties is possible only when the conditions of ambient pressure, substrate temperature and starting composition are suitably selected.

REFERENCES

1)E. Takayama-Muromachi, Y. Uchida, A. Ono, F. Izumi, M. Onoda, Y. Matui, K. Kosuda, S. Takekawa and K. Kato :Jpn. J. Appl. Phys. 27 (1988) L365.

2)U. Endo, S. Koyama and T. Kawai :Jpn. J. Appl. Phys. 27 (1988) L1476.

3) T. Kawai, M. Kanai, O. Murata and S. Kawai :Jpn. J. Appl. Phys. 28 (1989) L430.

4)M. A. Subramanian, C.C. Torardi, J.C. Calabrese, J. Gopalakrishnan, K.J. Morrssey, T.R. Askew, R.B. Flippen, V. Chowdahri and A.W. Sleight :Science 239 (1988) 1015.

5)H. Nobumasa, K. Shimizu, Y. Kitano and T. Kawai :Jpn. J. Appl. Phys. 27 (1988) L846.

6)M. Kanai, T. Kawai, M. Kawai and S. Kawai :Jpn. J. Appl. Phys. 27 (1988) L1293.

7)M. Kanai, K. Horiuchi, T. Kawai and S. Kawai :Appl. Phys. Lett. Dec.17 issue (1990).

8)H. Yamane, H. Kurosawa, T. Hirai, H. Iwasaki, N. Kobayashi and Y. Muto :Jpn. J. Appl. Phys., 27(1988) L1495.

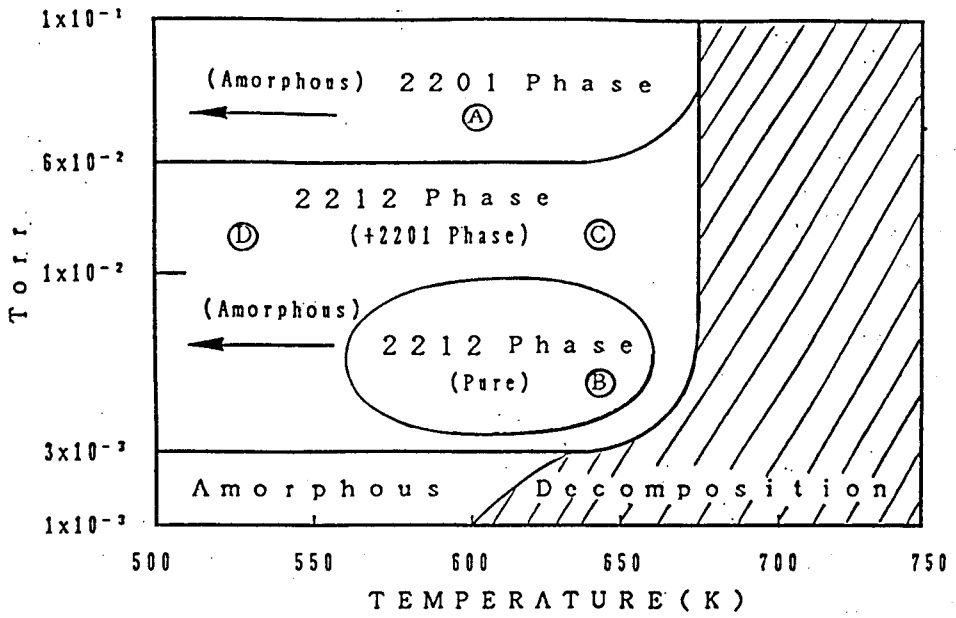

Fig.3-2-6. Ambient pressure-substrate temperature diagram for as-grown thin films formed from the $Bi_{4.2}Sr_{3.0}Ca_{3.0}Cu_{6.0}O_y$ target. A: 2201 phase and amorphous at lower temperature. B: Single 2201 phase. C: 2212 phase containing 2201 phase. D: Amorphous like 2212 phase. Slash: BSCCO structures are not formed.

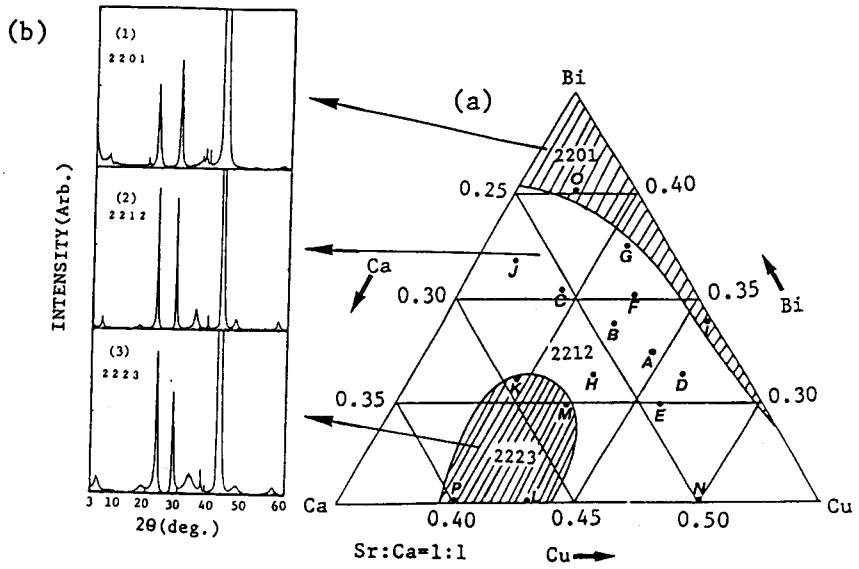

Fig.3-2-7. A diagram of starting compositions for the formation of the 2201, 2212 and 2223 phase of as-grown thin films (a) and X-ray diffraction patterns of the 2201, 2212 and 2223 phase of as-grown thin films(b). The starting compositions are Bi:Sr:Ca:Cu:=A)4.2:3.0:3.0:5.7 B)4.2:3.0:3.0:5.2 C)4.2:3.0:3.0:4.7 D)4.2:3.0:3.0:6.2 E)3.7:3.0:3.0:5.7 F)4.7:3.0:3.0:5.7 G)5.2:3.0:3.0:5.7 H)4.2:3.5:3.5:5.7 I)3.7:2.5:2.5:5.2 J)4.2:3.0:3.0:4.2 K)3.7:3.5:3.5:4.7 L)3.7:4.7:4.7:6.2 M)3.7:3.5:3.5:5.2 N)3.0:3.0:3.0:6.0 O)4.0:2.2:2.2:3.8 P)2.5:3.5:3.5:4.0

3-2-3. Control of the crystal orientation

Abstract

Orientation of the ferroelectric $PbTiO_3$ thin films can be controlled with changing the cooling rate after the film formation. In these experiments, ferroelectric $PbTiO_3$ epitaxial thin films have been formed on a base electrode of Pt(100)/MgO (100) using ArF excimer laser ablation. The X-ray diffraction patterns of these films show c-axis orientation with a rocking angle of 0.5° when the film is cooled faster than 75℃ /min after the deposition. The films exhibit clear and large ferroelectric hysteresis loops. The dielectric constant of the films is 130. The very large remnant polarization(Pr) of $80\mu C/cm^2$ is observed for the first time. This Pr values are almost the same as those theoretically predicted.

Introduction

In the perovskite type materials such as tetragonal $BaTiO_3$, $PbTiO_3$ (ferroelectric materials) and La_2CuO_4(superconducting materials), they have anisotropy in their crystal structures and electrical behaviors. Therefore, control of the orientation in the film growth is very important forl the physical properties of the films. In this chapter I report the formation of preferential c-axis oriented $PbTiO_3$ epitaxial films using pulsed laser ablation, and describe the electric and pyroelectric behavior of $PbTiO_3$ films deposited on a platinum(100).

A considerable amount of research has been focused on the growth and device fabrication of ferroelectric thin films for a variety of applications

including: nonvolatile memories[1]; ultrasonic sensors[2]; and infrared(IR) detectors[3]. Recently, epitaxial ferroelectric films, such as $PbTiO_3$, PZT and PLZT, have been successfully grown by a number of deposition techniques[4-6]. A pulsed laser ablation technique, on the other hand, has been widely used with great success in producing high-quality thin films for high temperature superconductors[7,8]. These superconductors are multicomponent oxides and have a perovskite structure just like many ferroelectric materials. Many advantages of the pulsed laser deposition process recognized for superconducting thin films should also be applicable to the fabrication of ferroelectric thin films[9 - 13].

The unique advantage of the pulsed laser deposition technique is its ability to produce highly oriented stoichiometric films at a low substrate temperature in a high pressure oxygen atmosphere. In this section I report the formation of preferential c-axis oriented $PbTiO_3$ epitaxial films using pulsed laser ablation, and describe the electric and pyroelectric behavior of $PbTiO_3$ films deposited on a base electrode of platinum(100).

Experiment

The deposition system was already described in the earlier reports. Laser pulses from an ArF excimer laser, energy density of 1 J/cm^2, were focused onto a stoichiometric sintered $PbTiO_3$ target. A heated substrate was set parallel to, and at a distance of, 3 cm from the target. The wavelength. the pulse width, and repetition rate were 193 nm. 25 ns. and 10 Hz. respectively. The substrate used was platinum-coated MgO [Pt(100)/MgO(100)]. The substrate was heated to temperatures in the range of 400-550℃ and the temperature (T_s) was measured with an IR pyrometer and a chromel-alumel thermocouple clamped to the back

of the substrate.The deposition experiments were carried out in an ambient oxygen/ozone atmosphere [O_2/O_3 (8%)] of 1-100 mTorr. The deposited films were cooled from Ts to room temperature at a rate between 10 and 1000℃/min. The deposition rate was about 5nm/min and the thickness of the films was 1 μm.

The dielectric properties along the c axis of the $PbTiO_3$ film using a LCR meter were measured. with a standard parallel plate geometry, with an aluminum top electrode and the bottom platinum electrode. Ferroelectricity was investigated by observing the polarization hysteresis using a Sawyer-Tower circuit at a frequency of 60 Hz. Other electrical properties, namely resistivity, dissipation factor (tan δ), and pyroelectric voltage were also measured.

Results and discussion

Figure 3-2-8 shows the tendency of the crystal orientation (preferred c-axis orientation) of the laser ablated $PbTiO_3$ films as the cooling rate is varied after deposition at 550℃.The value of the c-axis orientation is determined by the intensity rate of (001)/[(001)+(100)] in the x-ray diffraction patterns. The faster the cooling rate, the greater the preferred c-axis orientation.a-axis oriented films are formed at cooling rates less than 10℃/min. On the contrary, almost all c-axis oriented films are formed at a cooling rate faster than 75℃/min.

It is an established fact[14,15] that the effect of the substrate on the crystal orientation of the film can be explained by the mechanical stress on the film to force c-axis orientation that is caused by the difference between the thermal expansion coefficients of the film and substrate. It is certain that this phenomenon is one of the important factors for producing oriented films as indicated by

$$\sigma = \varepsilon \times E \qquad (3\text{-}4),$$

$$\sigma = (a \times dT / L)E \qquad (3\text{-}5),$$

where σ, ε, E, a, L, a and dT are a stress, strain, Young's modulus, thermal expansion coefficient, sample size, and the change of substrate temperature during cooling, i.e., the difference between the deposition temperature and room temperature. Therefore, in the case of $PbTiO_3$ film formation on a Pt/MgO substrate, the stress should be determined only by the temperature difference, and can be estimated as about 400-500 MPa.

Nevertheless, this mechanism does not explain the tendency for c-axis orientation based on the cooling rate demonstrated in our experiment. We have produced different crystal orientations by changing the cooling rate; that is, the cooling rate (strain rate) affects the crystal orientation of the film. There is the following relationship between the strain rate ($d\varepsilon/dt$) and thermal activation energy(Q):

$$d\varepsilon / dt = A \exp(-Q/kT) \qquad (3\text{-}6),$$

where A is a constant, k is Boltzmann constant, and T is formation temperature. This shows that when the strain rate is large, the excited energy is small. Further, the activation energy plays an important role as a driving force for the formation of defects. such as dislocation, which is a kind of pinning center for inducing the stress which drives c-axis orientation. In the case where k and T are constant, if the strain rate ($d\varepsilon/dT$) is large, the activation energy excites the dislocations. Therefore the dislocation cannot be moved. In this case, the thermal stress along the plane of the film is induced effectively at the interface between the film and the substrate during cooling from T_S to room temperature. This may be the reason why there is a relation between the c-axis orientation and the cooling rate.

The phase transition energy is also an important factor for the film orientation . There is a phase transition from the cubic to the tetragonal phase at

around 500℃ owing to the Curie point (T_c) of $PbTiO_3$ at 490 ℃. The crystal orientation of the films is enhanced by this kinetic energy of phase transition. When the films are deposited at the substrate temperature of 400℃ (below the T_c), the cooling rate does not make as much difference as when deposited at 550 ℃.

With the technique described above, the perfect c-axis orientation of the $PbTiO_3$ film can be formed. Figure 3-2-11(a) shows the x-ray diffraction patterns of $PbTiO_3$ thin films on Pt(100)/MgO(100). The films are of a perovskite single phase and oriented in the 100% (001) direction with a rocking angle of 0.5 in the electrode substrate (Pt/MgO). This film is formed at a cooling rate of 150℃/min.Further, in order to observe the in-plane orientation, We have measured the orientation of the $PbTiO_3$ film with a four-circle x-ray diffractometer. The results are shown in the form of a pole figure in Fig.3-2-11(b). The four {111} reflections of the $PbTiO_3$ film are located with the same direction of Pt bottom electrode {111}.This result shows that the Pb TiO_3 film grows epitaxially on the Pt electrode with a high orientation along the c-axis direction.

The dielectric constant of the excimer laser ablated films with a thickness of 1 μm was determined to be 120-130 with a dissipation factor (tan δ) of 0.03-0.05 at 1 kHz. Ferroelectricity has been investigated by observing the polarization hysteresis and the results are shown in Fig. 3-2-12(a), indicating clear and large remnant polarization (P_r) of 80 $\mu C/cm^2$ and coercive field of 280 kV-cm. This remnant polarization value is almost similar to that of the theoretically predicted value (Pr=81 $\mu C/cm^2$.)[16,17]. And slightly larger than another value (Pr=66 $\mu C/cm^2$) calculated by semiempirical estimation.[18,19] A large Pr value is also reported in the highly oriented PZT film by Tottle et al. Another $PbTiO_3$ film with the c-axis orientation of 90% has a remnant

polarization and corcive field of 60 $\mu C/cm^2$ and 50 kV/cm, respectively. Resistivity is in the range of $>10^{10}$ Ωcm. The SEM images revealed that only those possess a very smooth surface.

conclusion

In summary, ferroelectric $PbTiO_3$ thin films have been formed by an ArF excimer laser ablation technique. The crystal orientation of the films can be controlled by changing the cooling rate and the perfect c-axis oriented film can be formed with a cooling rate faster than 75℃/min.The laser ablated films exhibit good ferroelectric properties. The dielectric constant and remnant polarization of the Pb TiO_3 films are in the range of 120-130 and 80 $\mu C/cm^2$.

References

1) M.H.Francombe and S.Krishnaswany ; J.Vac.Sci Technol. A 8 (1990) 1382.

2) M.Koijima, M.Sugawa, H.Sato, Y.Matsui, O.Okuyama and Y.Hamakawa, Proc. 2nd Sensor Symposium (Springer, Tokyo, 1982) 241.

3) K.Iijima, I.Ueda and K.Kugimiya ; Jpn.J.Appl.Phys. 30 (1991) 2149.

4) M.Okada and K.Yominaga ; J.Appl.Phys. 71 (1992) 1955.

5) G.Yi, Z.Wu and M.Sayer ; J.Appl.Phys. 64 (1988) 2717.

6) K.Screenivas and M.Sayer ; J.Appl.Phys. 64 (1988) 1484.

7) X.X.Xi, Q.Li, C.Doughty, C.Kwon, S.Bhattacharya, A.T.Findikoglu and T.Venkatesan ; Appl.Phys.Lett. 59 (1991) 3470.

8)K.L.Saenger, R.A.Roy, K.F.Etzold and J.J.Cuomo; Mat.Res.Soc.Symp.Proc. 225 (1990) 115.

9) C.K.Chiang, L.P.Cook, P.K.Schenck, P.S.Brody and J.M.Benedetto ; Mat.Res.Soc.Symp.Proc. 225 (1990) 133.

10) T.Imai, M.Okuyama and Y.Hamakawa ; Jpn.J.Appl.Phys. 30 (1991) 2163.

11)H.Kidoh, T. Ogawa,H.Yashima, A.Morimoto and T.Shimizu: Jpn.J.Appl.Phys., 30, 2167 (1991).

12)D.Roy and S.B.Krupanidhi: Appl.Phys.Lett., 62, 1056 (1993).

13) J.Kong, T.Yoko and S.Sakka ; Jpn.J.Appl.Phys. 30 (1991) 2182..

14)T.Ogawa, A.Senda and T.Kasanami: Jpn.J.Appl.Phys., 30, 2145 (1991).

15)S.Mastubara, S.Miura, Y.Miyasaka and N.Shohata: J.Appl.Phys., 66, 5826

(1989).

16)Yu.N.Venevtsev, G.S.Zhdanov, S.P.Solovev and V.V.Ibanova: Kristallografiya, 4, 255 (1959).

17)B.A.Tottle, J.A.Voigt, D.C.Goodnow, D.L.Lamppa, T.J.Headby, M.O.Eatough, G.Zender, R.D.Nasby and S.M.Rodgers, J.Am.Ceram.Soc. 767, 1537 (1993)

18) .G.Bhide, M.S.Hedge and K.G.Deshmukh ; J.Am.Ceram.Soc. 51 (1968) 565.

19) M.S.Ameen, T.M.Graettinger, S.H.Rou, H.N.Al-Shareef, K.D.Gifford, O.Auciello and A.I.Kingon ; Mater.Res.Soc.Symp.Proc. 200 (1990) 297.

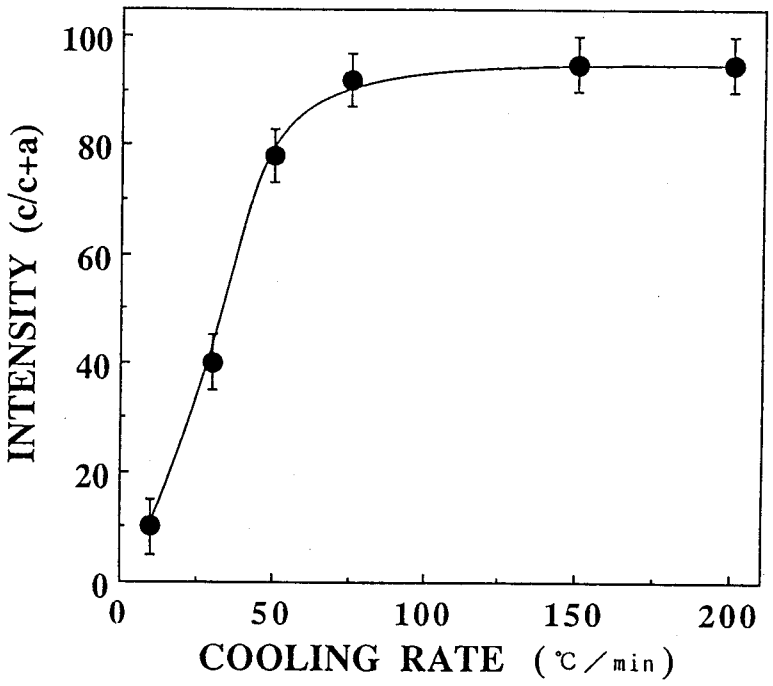

Fig. 3-2-8. A relation between cooling rate and rate of c-axis prefered crystal orientation

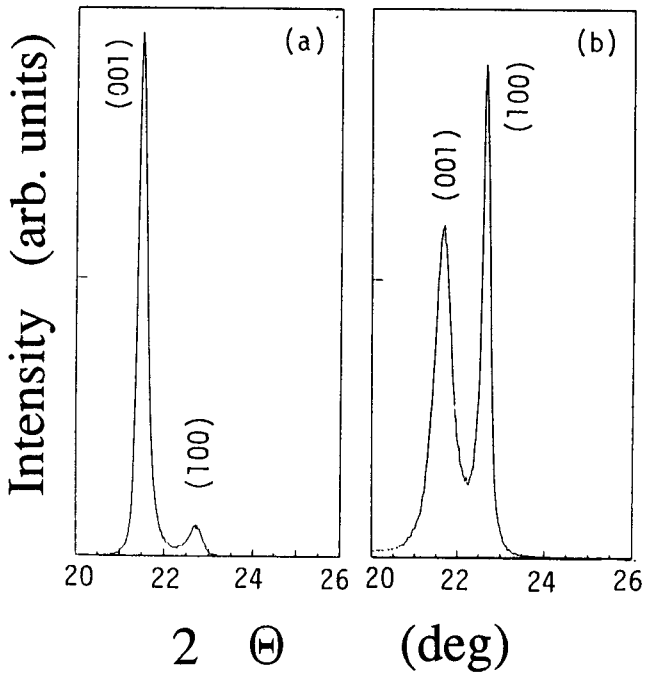

Fig.3-2-9 X-ray diffraction patterns of PbTiO3 thin films with the preferred c-axis orientation of (a) 95% (cooling rate; 100℃/min) and (b) 40%(30℃/min.).

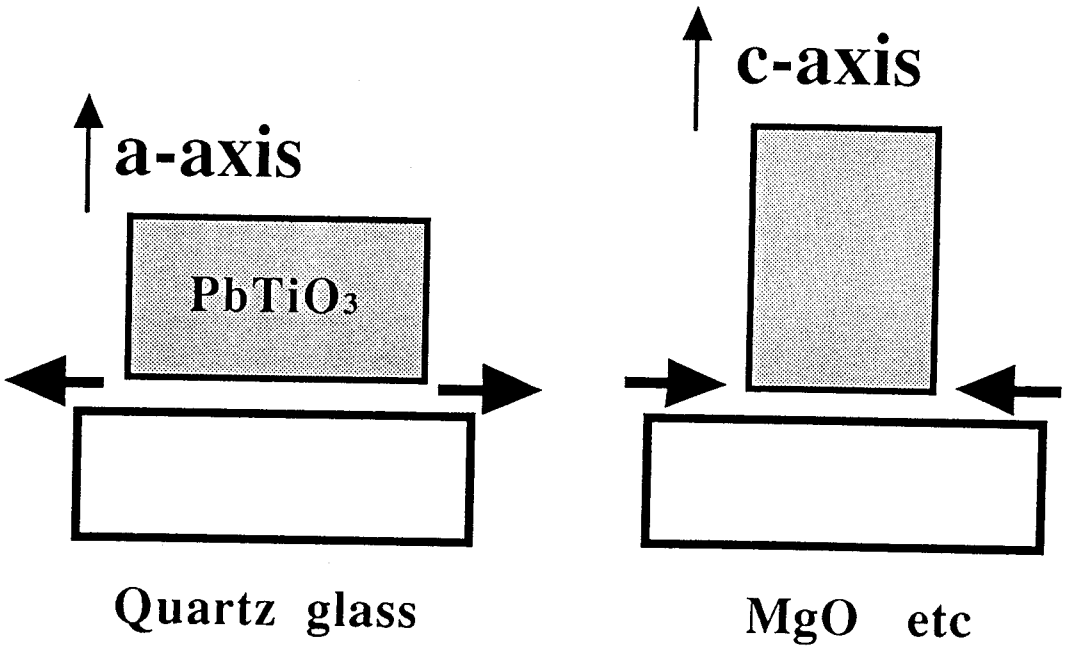

Fig.3-2-10 Model of preferred orientation of a-axis and c-axis by the substrate effect. film; PbTiO3, substrate; glass and MgO

(a)

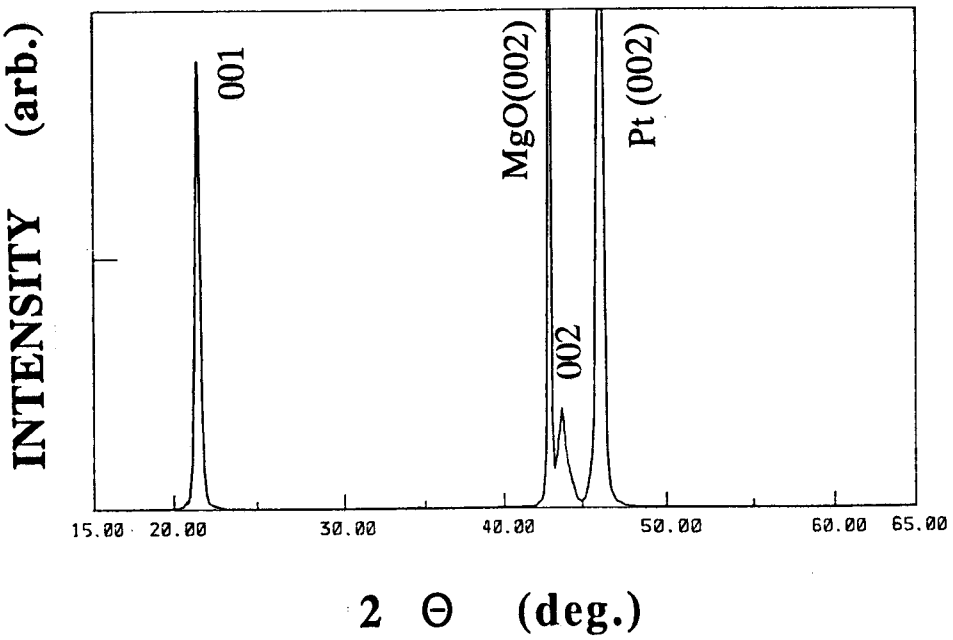

(b)

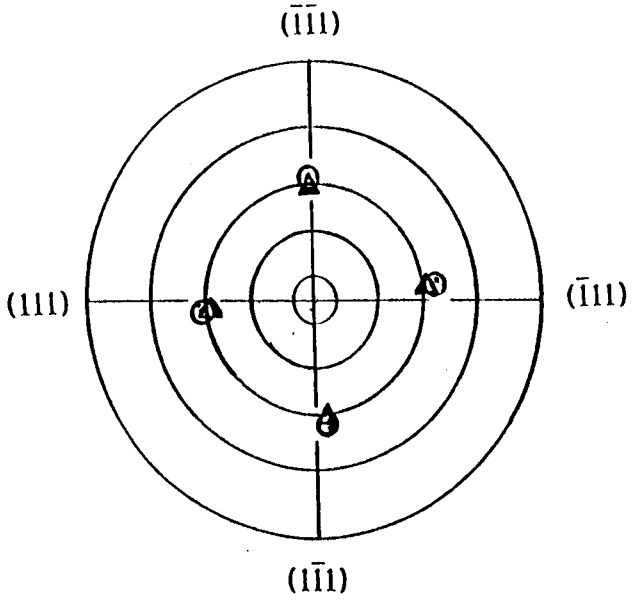

Fig. 3-2-11 (a) X-ray diffraction patterns of $PbTiO_3$ films formed with cooling rate of 150℃/min. (b) X-ray pole figure of the c-axis oriented $PbTiO_3$ film.

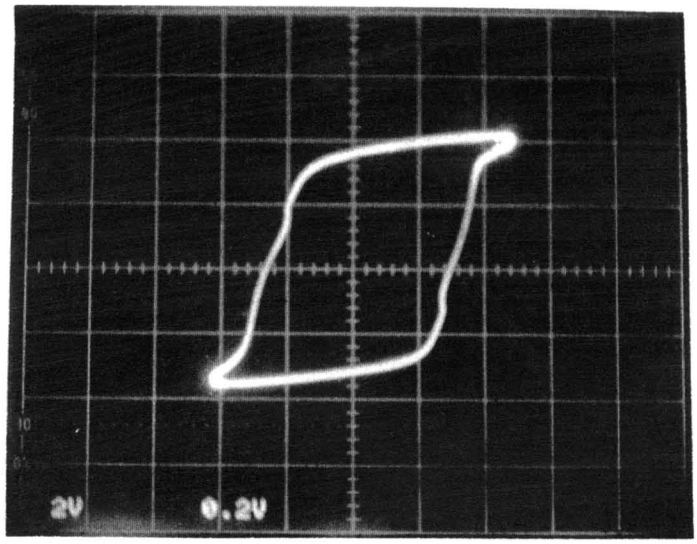

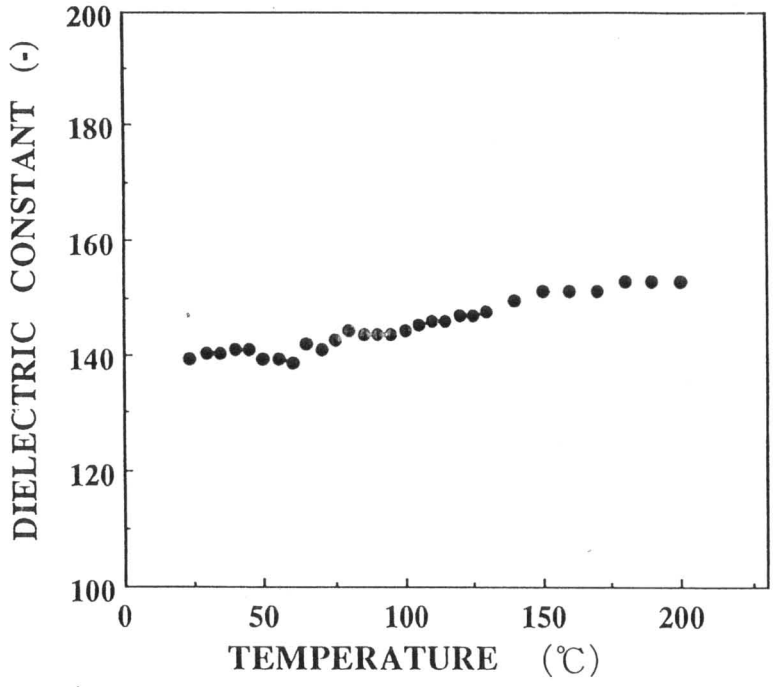

Fig. 3-2-12 (a) Typical D-E hysteresis loop of $PbTiO_3$ film deposited on Pt/MgO substrate at 450 ℃.(vertical;46 μ C/cm^{2}div, horizontal ;190kV/cmdivat applied frequency of 60Hz, at RT)
(b) dielectric constant vs temperature (from RT to 200℃)

3-3. Effect of laser irradiation

Abstract

The unique advantage of the pulsed laser deposition technique is its ability to produce highly oriented stoichiometric films at a low substrate temperature in a high pressure oxygen atmosphere. The formation of $PbTiO_3$ thin films at a particularly low substrate temperature, i.e., 350℃, is posssible on a $SrTiO_3$ single-crystal substrate and based electrode of Pt or oxide superconductor ($(La,Sr)_2CuO_4$) using excimer laser ablation. A second laser irradiation at the substrate surface is quite effective for crystallization of the films at low substrate temperature below 400 ℃. The suitable energy density of the irradiation laser is in the range of 30-100 mJ/cm^2. X-ray diffraction patterns of $PbTiO_3$ thin films show c-axis orientation, with a rocking angle of 1.0 - 0.5° . These films exhibit ferroelectric hysteresis loop. A dielectric constant and remanent polarization of the $PbTiO_3$ films are in the range of 120-150 and 20-25 $\mu C/cm^2$, respectively.

Introduction

The unique advantage of the pulsed laser deposition technique is its ability to produce highly oriented stoichiometric films at low substrate processing temperature in a high pressure oxygen ambient. I reported the formation of $PbTiO_3$ thin film at low particularly low substrate temperature of 350℃ on $SrTiO_3$ single crystal substrate by the excimer laser ablation technique and I

showed that the second laser irradiation at the substrate surface during the thin film formation is quite effective to the crystallization at low substrate temperature[1].

On the other hand, it is reported that the ablated species can be classified into groups corresponding to their difference velocities by the spectroscopic experiments[2-10]. Therefore, for the film formation at further lower substrate temperature, it is important to irradiate the species with the second laser at the time the species reach the substrate surface.

In this section we discuss the effect of the second laser irradiation by changing the delay time to excite the species selectively. Furthermore, the electrical behavior is shown for the $PbTiO_3$ thin film deposited on base electrode of Pt or oxide superconductors ($Y_1Ba_2Cu_3O_y$, $(La,Sr)_2CuO_4$) which is metallic at room temperature.[9-10]

Experiment

Fig.3-3-1 shows a schematic diagram of the experimental set up. The target is set at the center of the vacuum chamber and the substrate is located at the opposite side of the target with the distance of 3 cm. The target used is stoichiometric $PbTiO_3$ sintered pellet. The substrate is heated at a temperature in the range of 350 ℃-500 ℃. The deposition is carried out in an oxygen pressure in the range of 10^{-3}-10^{-1} Torr. The thickness of $PbTiO_3$ film is typically 1000 Å.

The ablation laser is focused on the target at an energy density of 1 J/cm2 with the repetition rate of 10-15 Hz. Furthermore the second laser irradiates the substrate surface during the film formation with the intensity in

the range of 0 - 150 mJ/cm^2.

First of all, the ablated particles are observed by a Q-Mass spectroscopy(TOF:Time Of Flight) to determine the kinds of the ablated species and their average velocities. The detected mass numbers are 48, 207, 64, 80 and 223 are corresponding to Ti, Pb, molecules TiO, TiO_2 and PbO, respectively.

Next, the delay-time of the second laser is controlled by a delay generator in order to irradiate the ablated components selectively. This is expected to improve the crystallinity if the film by re-exciting these components during the deposition process. Then, the intensity of the irradiation laser beam is changed.

Finally, the electrical behaviors, such as resistivity, dielectric constant and remanent polarization, are measured.

Results and discussion

1).Substrate irradiation effect

Fig.3-3-3 shows the time of flight measured (a)Ti and (b)Pb atoms by a Q-Mass spectroscopy . The broken lines are obtained when the filament in ionization chamber is turned off, so these lines show the amount of cations. The solid lines show the data with turned on the filament, so these show the total amount of ions are produced. The result shows that a large number of monovalent ions (more than 80%) is produced comparing with neutral atoms. Molecules, such as TiO(mass number:64), TiO2(80) and PbO(223), divalent ions or clusters can not be detected. The profile of observed TOF is different from that of calculated assuming a Maxwell-Boltzmann distribution of Pb or Ti atom. This result shows that the the thin films are formed with not thermal mechanism but photo-chemical mechanism by the excimer laser ablation.

The average velocities of the species, ablated with the pulsed laser, are estimated about $5x10^5$ cm/s from these results. By calculating from the average velocities of the ablated components, the ablated component is estimated to come to the substrate surface at 6 μs after the ablation laser. Therefore, the controlled second laser with delay times of 6 μs.

Figure 3-3-4 shows the rocking curves of x-ray diffraction patterns of $PbTiO_3$ thin films(100 peaks). No-irradiate(c) and irradiate with the delay time of (a)6 μs and (b)30 μs deposited at 400 ℃. This result indicates that the second laser irradiation is the most effective for the second ablated component with the delay time of 6 μs. Furthermore, these experiments were done in the various delay time from -10μs to +150 μs.(Fig.3-3-5) But in these cases, the crystallinities of the films are not changed so much comparing with the film formed with the delay time of 6 μs. The species excited with high photon energy (6.4 eV) of the second ArF excimer laser are enhanced their migration energy at the film surface. Therefore their crystallinities become better at low substrate temperature of 400 ℃.

Next the delay time is fixed at 6 μs and the fluence of the irradiate laser is changed. Figure 3-3-6 shows the X-ray diffraction patterns of $PbTiO_3$ thin films with the second laser irradiation at the intensity of (a) 0 mJ/cm^2, (b) 10 mJ/cm^2 and (c) 30 mJ/cm^2. The higher the energy density of irradiate laser is the more the film crystallized. At the irradiation energy of 120 mJ/cm^2, the surface of the film becomes rough owing to the decompose of the film.(Fig.3-3-8) Therefore the suitable energy density of the second irradiation laser is in the range of 50 - 80 mJ/cm^2. In this energy range, the laser beam may play not thermally but photo chemically. The perovskite $PbTiO_3$ thin films can be formed at 380 ℃ with this technique. Until now, this kinds of film can not be formed below 450 ℃.(Fig.3-3-9) Therefore, this laser ablation

technique with irradiation by the second laser is essential method for the film formation at lower substrate temperature such as 350 ℃.

The films are of a perovskite single phase and oriented in the (001) direction with the rocking angle of 1.0 - 0.5° on the electrode substrate(Pt/MgO or oxide superconductor/MgO). The typical remanent polarization(Pr) and the coercive field(Ec) of these films formed at 400～450℃ are 20 μC/cm^2 and 180 kV/cm, respectively. (Fig.3-3-10) Another electrical behaviors, such as resistivity and dielectric constant, are in the range of > 10^{10} ohm cm and 120 - 150, respectively.

2). Vapor irradiation effect

There is a question that the substrate irradiation effect is caused by a thermal effect or the photo-chemical effect. To elucidate the mechanism of the irradiation effect, the vapor irradiation experiments were done. In this case (vapor irradiation experiments), the delay time was fixed at 5 μs and the laser beam was focused at the point 5 mm above the substrate surface.

Fig.3-3-11 shows the X-ray diffraction patterns of the $PbTiO_3$ films formed with the vapor irradiation of (a) 12 mJ/cm^2, (b) 25 mJ/cm^2 and 50 mJ/cm^2.

The higher the energy density of irradiate laser is the more the film crystallized just like as substrate irradiation. Figure 3-3-12 shows the relation between the irradiation intensity and full width at half maximum (FWHM) of the X-ray diffraction patterns ((a); substrate irradiation and (b) ; vapor irradiation). FWHM indicate crystallinities of these $PbTiO_3$ films. In both of cases, suitable irradiation intensity is about 50-80 mJ/cm^2.

Furthermore, Fig.3-3-13 shows the X-ray diffraction pattern of (a)the

substrate irradiation and (b)vapor irradiation with intensity of 30 mJ/cm^2 formed at 400℃. These two patterns show quite similar behavior in the intensity and shape of the profile and this suggest that the laser irradiation is not the thermal effect but the photo-chemical effect. The high laser energy of ArF excimer laser (193nm) may be absorbed by the O+(208nm) and Pb(217nm)[11] and changed to migration energy at the surface of the films.

CONCLUSION

In summery of this section, Ferroelectric $PbTiO_3$ thin films have been formed by an ArF excimer laser ablation technique with a second laser irradiation. The second laser irradiation at the substrate surface is quite effective for crystallization of the films. The suitable energy density of the irradiation laser is in the range of 50-80 mJ/cm^2 in both substrate irradiation and vapor irradiation. And the laser irradiation effect is some kinds of photo chemical effect. These films exhibit ferroelectric hysteresis loop. A dielectric constant and remanent polarization of the $PbTiO_3$ films deposited at 400℃ are in the range of 120-150 and 20-25 μC/cm^2, respectively.

References

1) H.Kidoh, T.Ogawa, H.Yashima, A.Morimoto and T.Shimizu ; Jpn. J. Appl. Phys. 30 (1991) 2167.

2) T.Imai, M.Okuyama, Y.Hamakawa ; Jpn.J.Appl.Phys. 30 (1991) 2163.

3) O.Eryu, K.Murakami, K.MasudaK.Shihaya and T.Mochizuki ; Jpn.J.Apppl. Phys. 31 (1991) L86. and Appl.Phys.Lett. 54 (1989) 2716.

4) P.E.Dyer, A.Issa and P.H.Key ; Appl.Phys.Lett. 57 (1990) 186.

5)X.D.Wu, B.Dutta, M.S.Hegde, A.Inam, T.Venkatesan, E.W.Chase, C.C.Chang and R.Howard ; Appl.Phys.Lett. 54 (1989) 179.

6) Q.Y.Ying, D.T.Shaw and H.S.Kwok ; Appl.Phys.Lett. 53 (1988) 1762.

7) C.H.Becker and J.B.Pallix ; J.Appl.Phys. 64 (1988) 5152.

8) S.Preuss, M.Spath, Y.Zhang and M.Stuke.

9) H.L.Kao, J.Kwo, R.M.Fleming, M.Hong and J.P.Mannaerts ; Appl.Phys.Lett. 59 (1991) 2748.

10) K.Tanabe, Y.Enomoto, H.Asano and Syugo Kubo ; Jpn.J.Appl.Phys. 32 (1993) 1626.

11) "The Identification of Molecular Spectra" (by R.W.B.Pearse and A.G. Gaydon , London 1976) Chapman and Hall.

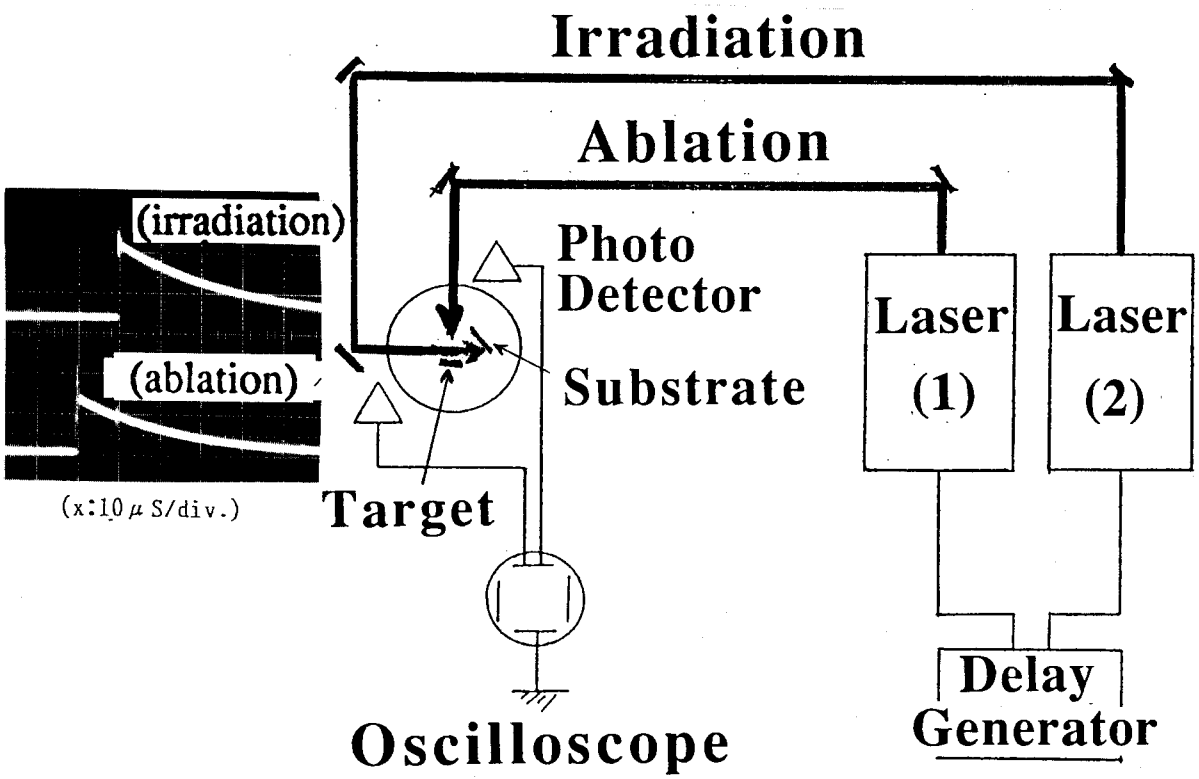

Fig. 3-3-1 Schematic diagram of the experimental setup for double laser irradiation

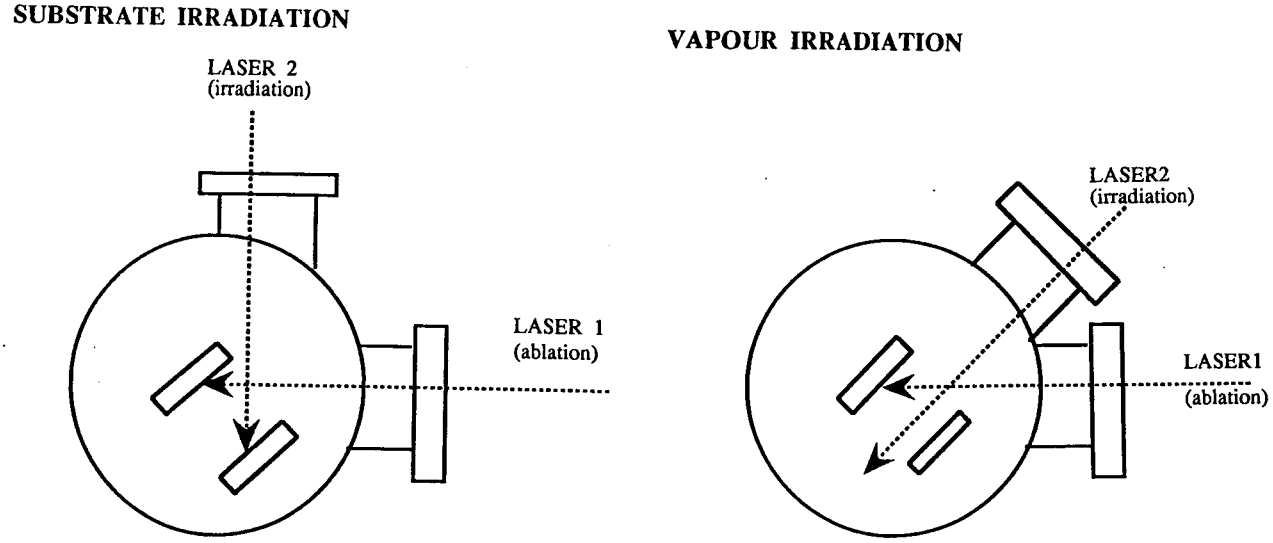

Fig. 3-3-2 schematic image of (a) substrate irradiation and (b) vapor irradiation.

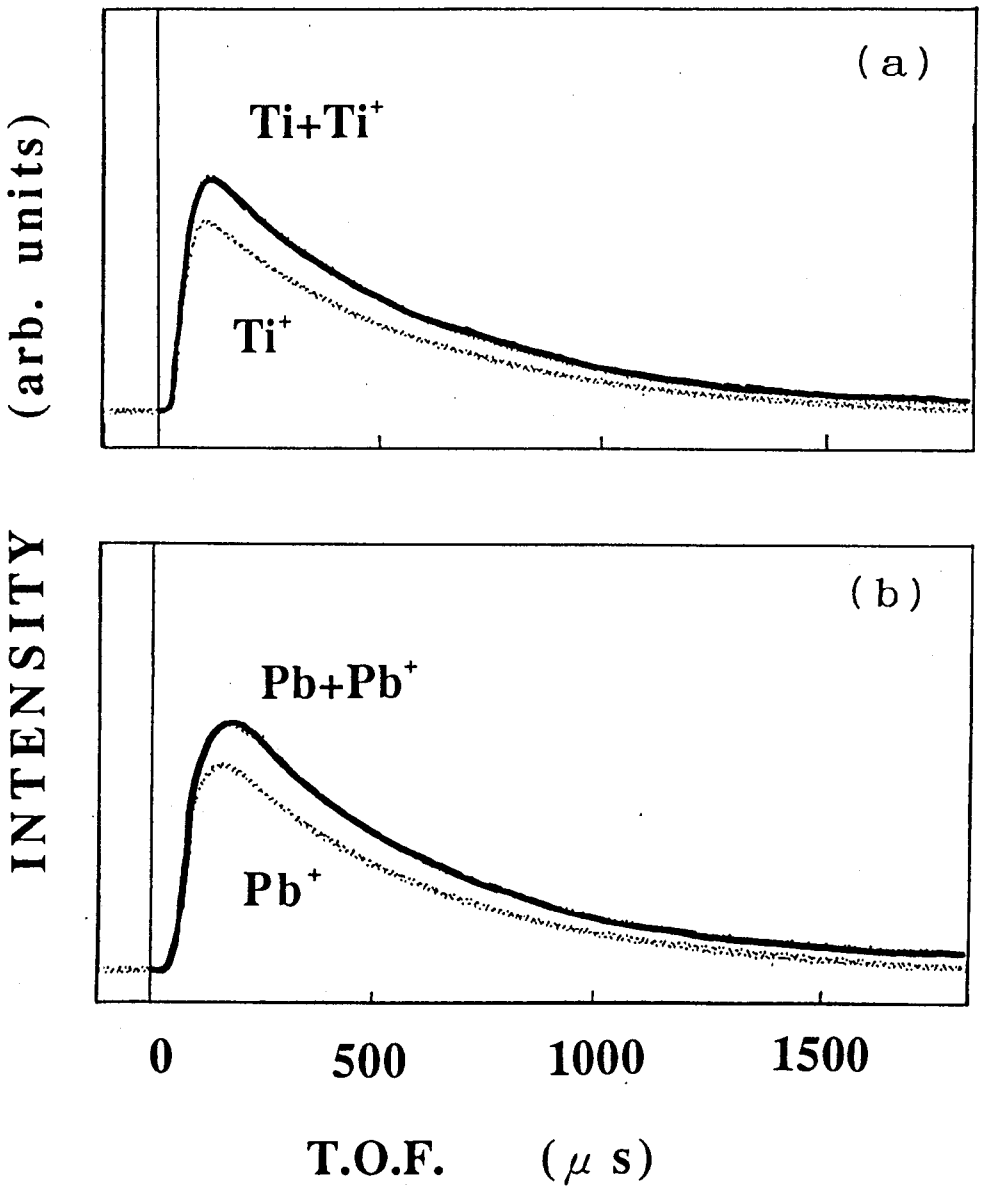

Fig. 3-3-3. Time resolved spectrum for (a) Pb^+, $Pb+Pb^+$ and (b) Ti^+, $Ti+Ti^+$ by laser ablation with the intensity of 200-300 mJ/cm^2. X-axis shows TOF(time of flight) and Y-axis shows the intensity of signal.

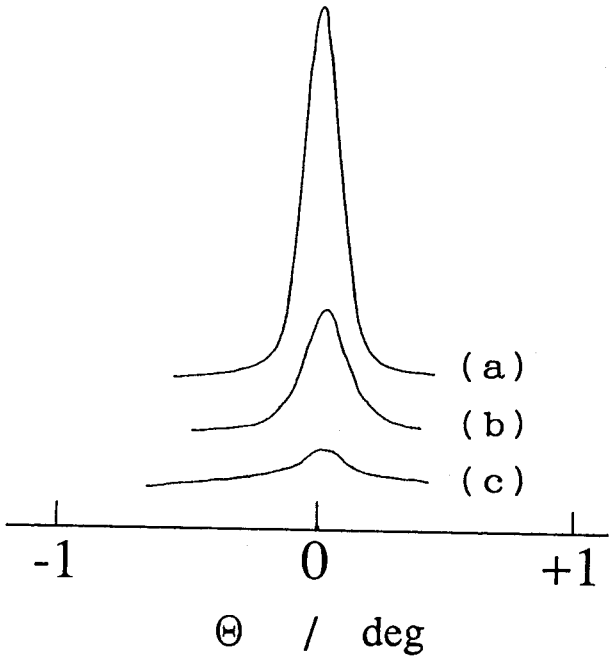

Fig. 3-3-4. Rocking curves of (001) peaks of PbTiO3 thin films formed with the delay time of (a) 6 μs (b) 30 μs and (c) no irradiation.

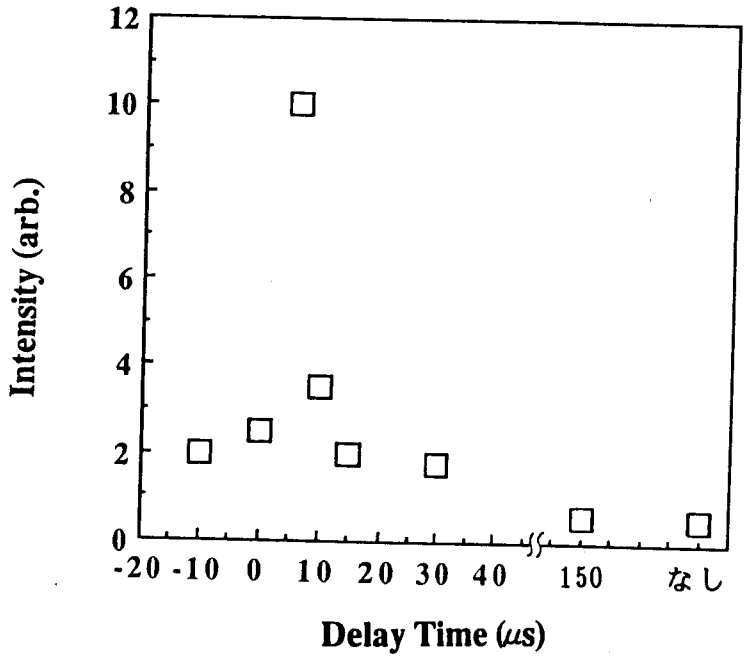

Fig. 3-3-5. Delay time of irradiation laser for substrate vs intensity of the X-ray diffraction pattern of $PbTiO_3$ films

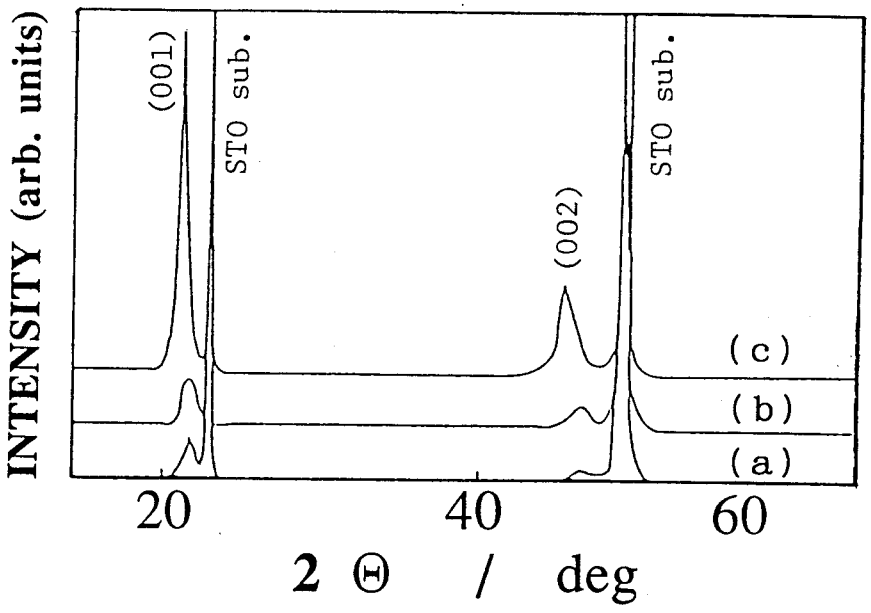

Fig. 3-3-6. X-ray diffraction patterns of PbTiO3 films formed with the fluence of the irradiation laser (a) 0 J/cm^2, (b) 10 J/cm^2 and (c) 30 J/cm^2.

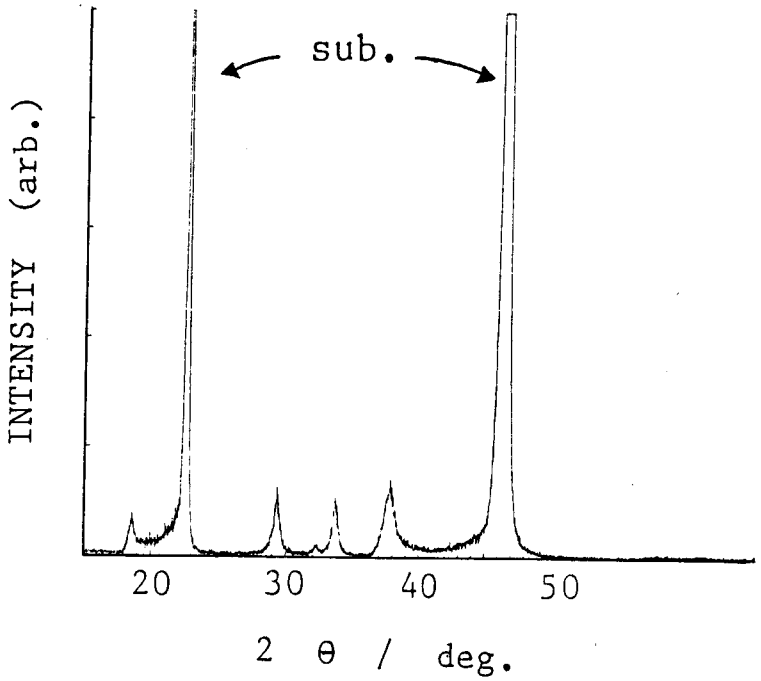

Fig. 3-3-7. X-ray diffraction patterns of $PbTiO_3$ films formed with the second laser irradiation of 120 mJ/cm^2.

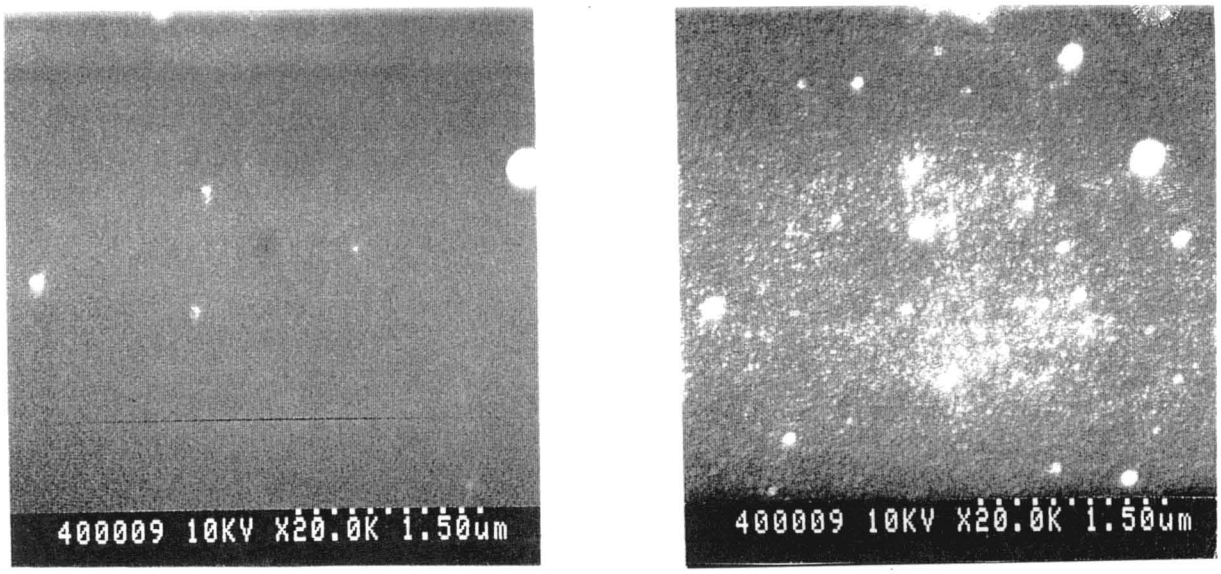

Fig. 3-3-8. SEM images of the PbTiO3 films formed with the second laser irradiation with the fluence of 30mJ/cm^2 and 120mJ/cm^2

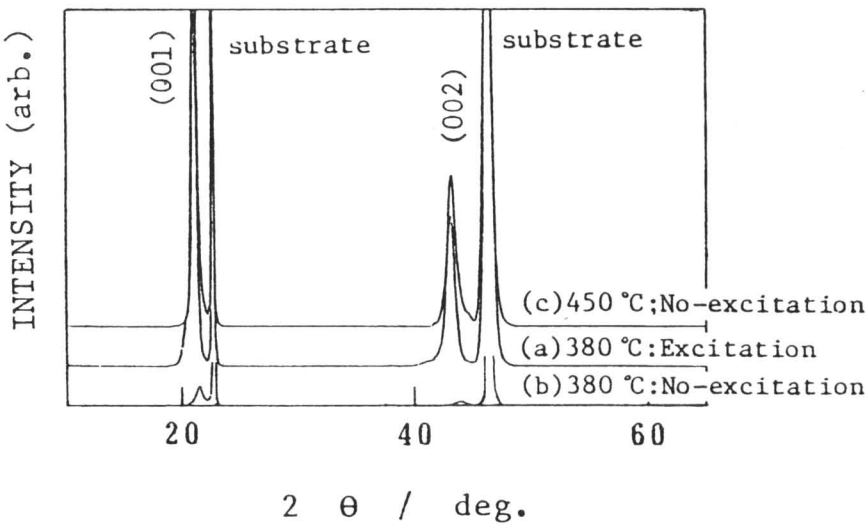

Fig. 3-3-9. X-ray diffraction patterns of PbTiO3 films (a) with and (b) without laser irradiation of the substrates during the film formation at 380℃ and (c) no irradiation at 450℃

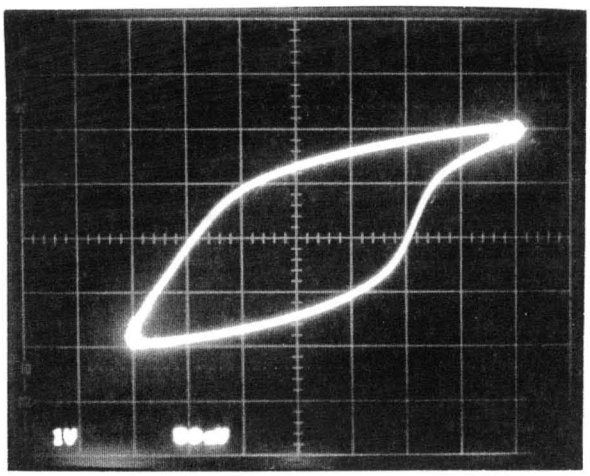

Fig. 3-3-10. Typical D-E hysteresis loop of $PbTiO_3$ thin film deposition on Pt/MgO substrate (vertical; 10 μ C/cm_2div, horizontal; 90 kV/cmdiv at applied frequency of 60 Hz).

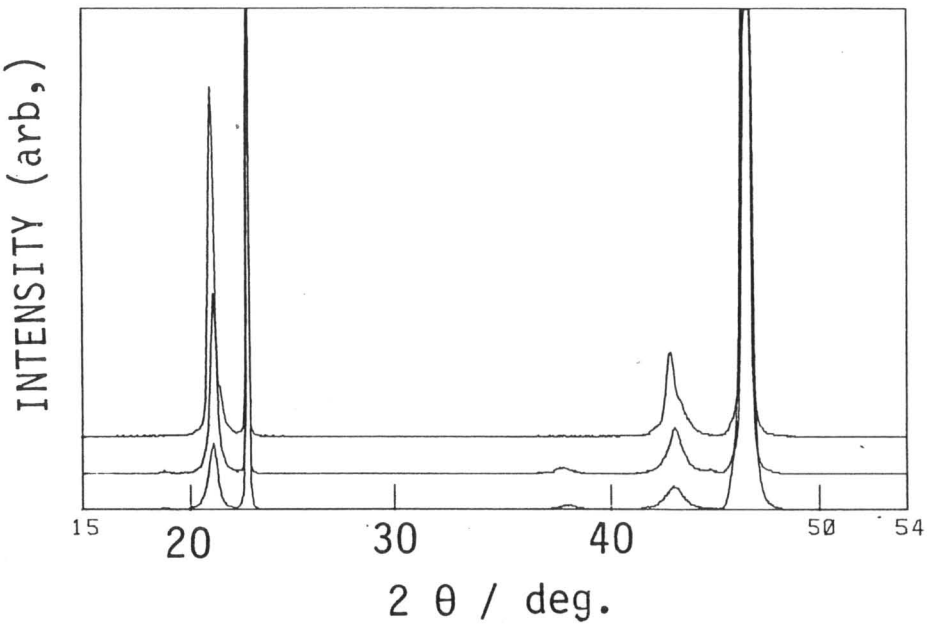

Fig. 3-3-11. X-ray diffraction patterns of PbTiO3 thin films with the vapor irradiation intensities of (a) 12 mJ/cm^2, (b) 25 mJ/cm^2 and (c) 50 mJ/cm^2.

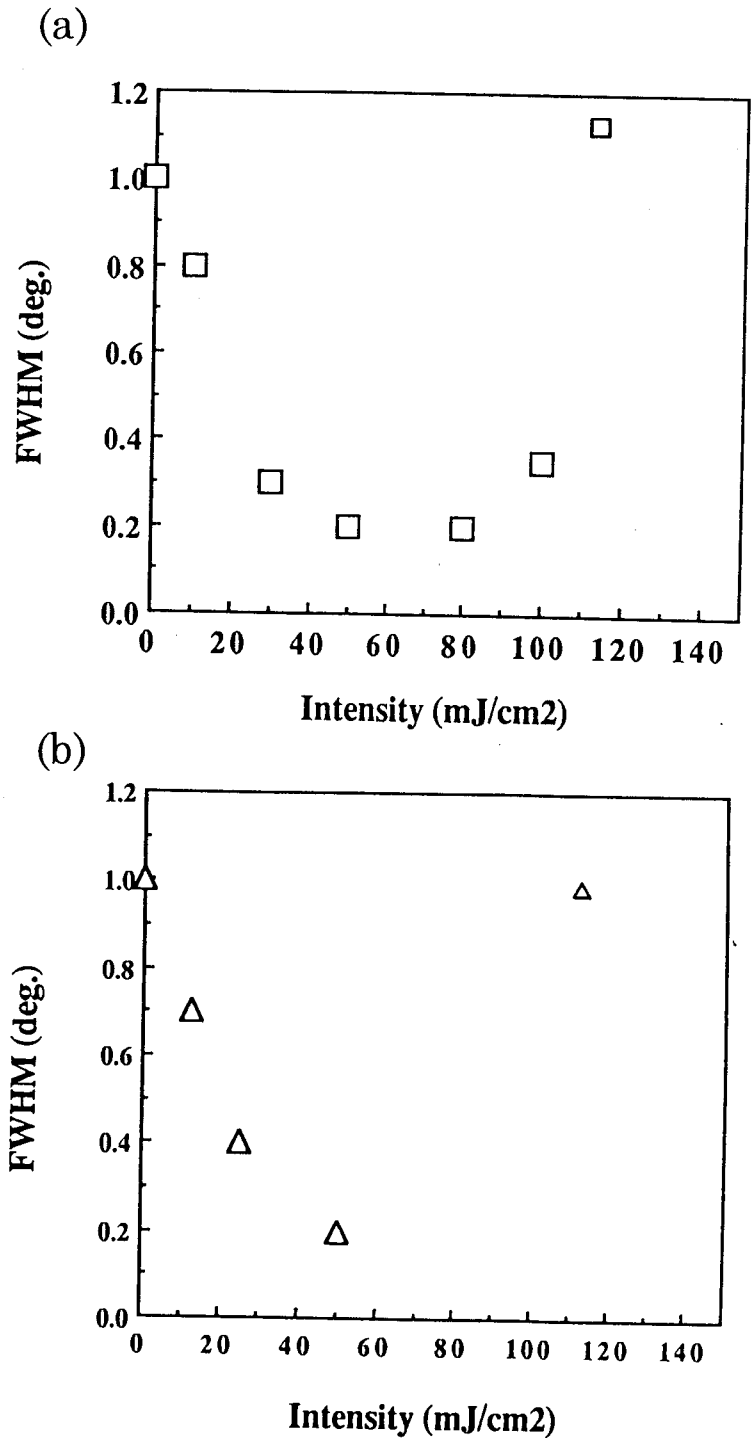

Fig. 3-3-12. Intensity of the irradiation laser vs FWHM(full width at half maxim) of the PbTiO3 films. (a) substrate irradiation and (b) vapor irradiation.

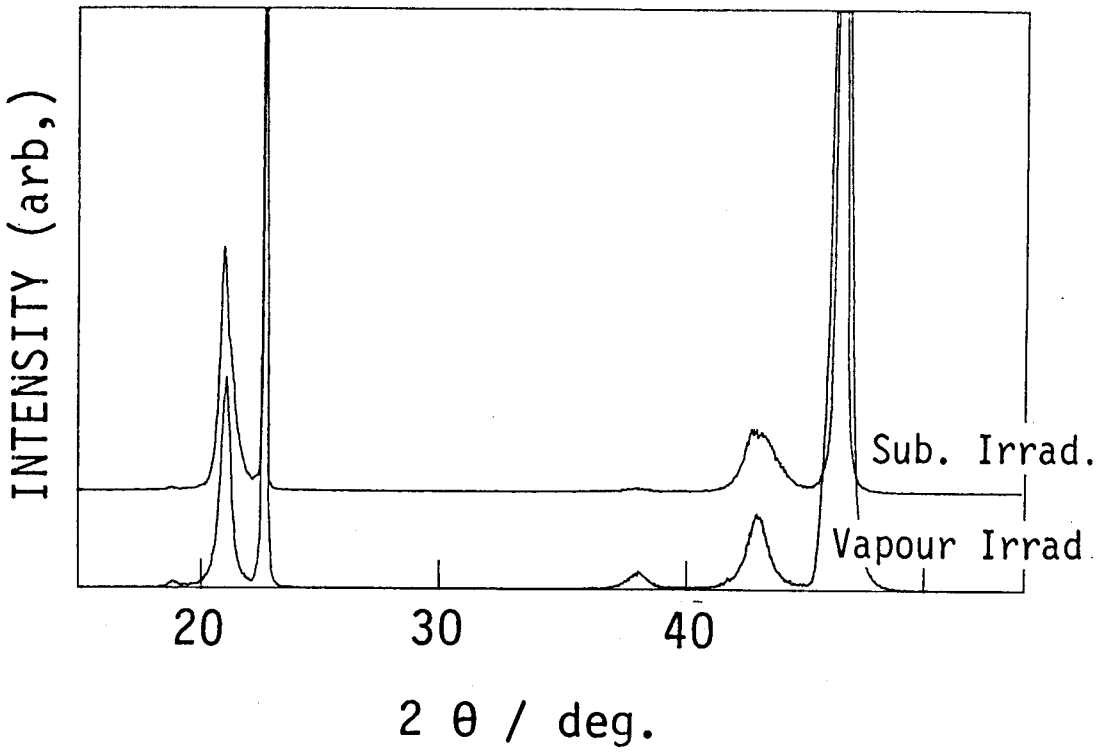

Fig. 3-3-13. X-ray diffraction patterns of PbTiO3 films formed with laser irradiation by 2nd laser. (a) substrate irradiation and (b) vapor irradiation with the fluence of 30 mJ/cm^2.

Chapter 4

4. Superconducting Artificial Lattices.

4-1. Basic concept & abstract

High T_c oxide superconductors can be classified in terms of well known structural types, such as perovskite or layered perovskite (K_2NiF_4). In the copper-based high T_c oxide superconductors, the common structural feature is CuO_2 sheets[1]. Any structure of the copper-oxide superconductors can be constructed by inserting various kinds of layers into the infinite stacking of the CuO_2 layers[2,3]. As shown in Fig.4-4-1, the high Tc materials are represented by the combination of infinitely stacked CuO_2 sheets with La_2O_2, $SrO/Bi_2O_2/SrO$, Ca, SrO/PbO/SrO and Y, BaO/CuO chain/BaO, corresponding to La-Cu-O[4], Bi-Sr-Ca-Cu-O[5], Pb-Sr-(Ca,Y)-Cu-O[6,7] and Y-Ba-Cu-O[8], respectively. Based on this concept, artificially layered new compounds are expected to be synthesized by periodic insertion of the blocking layer into the infinite layers of $CaCuO_2$, which are well known as a parent structure of the superconductors[9-14].

It has also been recognized that two kinds of unit layers are playing important roles for separating the CuO_2 sheets and constructing the structure. One is a thick layer, called "Blocking layer", such as Bi_2O_2, Tl_2O_2 or La_2O_2 to stabilize the structure, and the other is a thin layer, called "Mediating layer" such as Ca or Y which plays as charge reservoir for the superconductivity[15,16]. Any type of the high T_c superconductor can be constructed by the combination of the units of $CaCuO_2$ layer with the primary structures , such as $Bi_2Sr_2CuO_6$, $Tl_2Ba_2CuO_6$ or La_2CuO_4.

Laser ablation has become one of the most widely used techniques for synthesizing high temperature superconducting thin films[17-22]. We have

demonstrated that layer-by-layer successive deposition is an excellent method to form various artificial thin films with this technique. In the $Bi_2Sr_2Ca_{n-1}Cu_nO_{2n+4}$ artificial lattices, the numbers of CuO_2 planes are changed from one to even eight in the unit formula.(Chapter 4-2-1) The layer-by-layer laser ablation method has been applied to the site-selective incorporation of +1,+2 and +3 ions at Ca and Sr sites of $Bi_2Sr_2Ca_1Cu_2O_8$. The correlation between T_c and the lattice parameter c is explained on the basis of the distance between CuO_2 layers, indicating the importance of the interaction among CuO_2 layers.(Chapter 4-2-2) Furthermore superconducting superlattices have been formed and the pressure effects are studied in the strained superlattices. In the case of $La_{1.85}Sr_{0.15}CuO_4/Sm_2CuO_4$ superlattices, lattice constant a and b in the LSCO layer are forced to expand and T_c decreases as the number of stacking periodicity decreases. For $La_{1.85}Sr_{0.15}CuO_4$ / $La_{1.6}Sr_{0.35}CuO_4$ superlattices, we calculate the superconducting critical temperatures under the proximity effect using de Geenes-Werthamer's theory in the normal layer($La_{1.6}Sr_{0.3}CuO_4$). In these superlattices, the change of the lattice constant along a,b axes is proved to be one of the important controlling factors for the T_c value. (Chapter 4-2-3)

Refereces

1) T.Siegrist, S.M.Zakurak, D.W.Murphy and R.S.Roty ; Nature 334 (1988) 231.

2) M.Kanai, T.Kawai and S.Kawai ; Appl.Phys.Lett. 57 (1990) 198.

3) P.J.Dobson, B.A.Joyce, J.H.Neave and J.Zhang ; J.Cryst.Growth 81 (1987) 1.

LSCO

4) J.B.Bednorz and K.A.Mullar ; Z.Phys.B 64 (1986) 189.

YBCO

5) H.Maeda, Y.Tanaca, M.Fukutomi and T.Asano ; Jpn.J.Appl.Phys. 27 (1988) L209.

6) R.S.Liu, S.F.Hu, D.A.Jefferson, P.P.Edwards and P.D.Hunneyball; Physica C 217 (1993) 1

7) S.F.Hu, D.A. Jefferson, R.S.Liu and P.P.Edwards; J.Solid State Chem. 103 (1993) 208.

8) M.K.Wu, J.R.Ashburn, C.J.Torng, P.H.Hor, R.J.Meng, L.Gao, Z.J.Huang, Y.Q.Wang and C.W.Chu; Phys.Rev.Lett. 58 (1987) 908.

9) M.Takano, Y.Takeda, H.Okada, M.Miyamoto and K.Kusaka ; Physica C 159 (1989) 375.

10) M.G.Simith, A.Manthiram, J.Zhou, J.B.Goodenough and J.T.Markert ; Nature 351 (1991) 549.

11) G.Er, Y.Miyamoto, F.Kanamaru and S.Kikkawa ; Physica C 181 (1991) 206.

12) M.Takano, M.Azuma, Z.Hiroi, Y.Bando, Y.Takeda ; Physica C 176 (1991) 441.

13) M.Azuma, Z.Hori, M.Takano, Y.bando and Y.Takeda ; Nature 356 (1992) 775.

14) S.Adachi, H.Yamaguchi, S.Tanaka and N.Mori ; Physica C 208 (1993)226.

15) H.Nobumasa, K.Shimizu and T.Kawai ; Z.Phys.B 88(1991) 7.

16) S.Uchida ; Jpn.J.Appl.Phys. 32 (1993) 3784.

17) J.M.E.Harper, R.J.Colton and L.C.Feldman, (Eds.), American Insitutute of Physics Conference Proc. 165 (1988) 100

18) D.Dijkkamp, T.Venkatesan, X.D.Wu, S.A.Shaheen, N.Jisrawi, Y.H.Min-Lee, W.L.McLean and M.Croft ; Appl.Phys.Lett.151 (1987) 619.

19) J.Narayan, N.Biunno, R.Simgh, O.W.Holland and Auciello ; Appl.Phys.Lett. 151 (1987) 1845.

20) U.Sudardan, N.W. Cody, M.J.Bozack , andR.Solanki ; J.Mat.Res. 3 (1988) 825.

21) T.Venkatesan, X.D.WU, A.Inam, Y.Jeon, M.Croft, E.W.Chase, C.C.Chang, J.B. Wachtman, R.W.Odom, F.R.di Bronzolo and C.A.Magee ; Appl.Phys.Lett. 53 (1988) 1431.

22) D.Roy, S.Krupanidhi and J.P.Dougherty ; J.Appl.Phsy. 69 (1991) 7930.

23) C.K.Chiang, W.Wong-ng, P.K.Schench, L.P.Cook, M.D.Vaudin, P.B.Brondy, B.J.Rod andK.W.Bennet; MRS symp.proc., 230 (1992) 321.

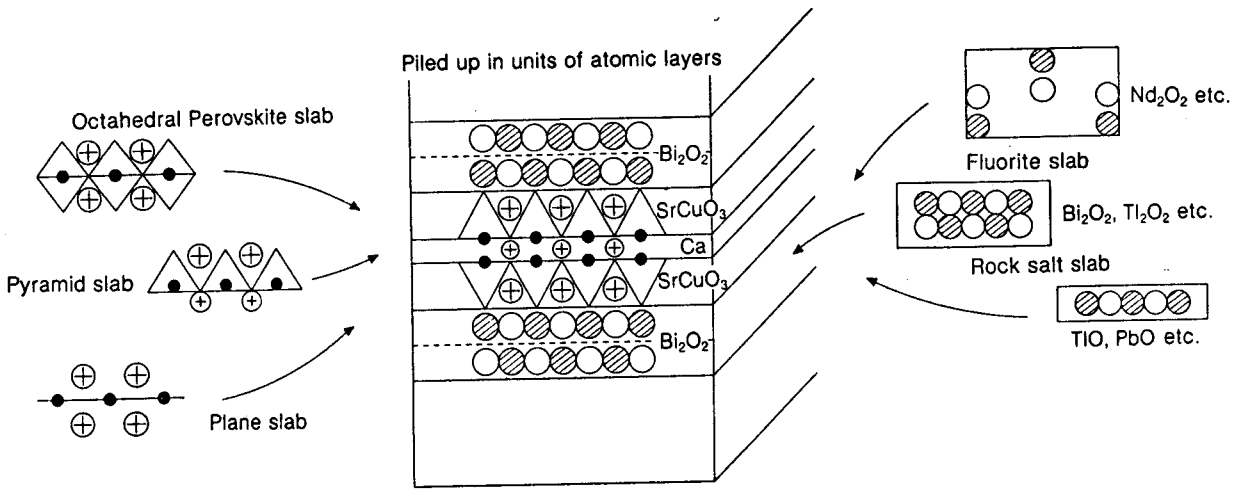

Fig. 4-1-1. Typical crystal structure of Copper oxide superconductors.

4-2. Artificial control with sub-unit cell scale

4-2-1. Control of the number of Cu_2O layers

- New $Bi_2Sr_2Ca_{n-1}Cu_nO_{2n+4}$ (n=6-8) compounds based on the parent structure of layered $Ca(Sr)CuO_2$-

Introduction

In a series of $Bi_2Sr_2Ca_{n-1}Cu_nO_{2n+4}$[1-4]) and $Tl_2Ba_2Ca_{n-1}CunO_{2n+4}$ superconductors[5-9], the basic structural units are $Ca(Sr)CuO_2$ layers and n=1 compound, i.e. $Bi2Sr_2CuO_6$ or $Tl2Ba_2CuO_6$. For example, the combination of one $Ca(Sr)CuO_2$ layer with $Bi_2Sr_2CuO_6$ makes $Bi_2Sr_2CaCu_2O_8$(n=2), and two layers of $CaCuO_2$ make $Bi_2Sr_2Ca_2Cu_3O_{10}$ (n=3). Thus, the combination of $Bi_2Sr_2CuO_6$ and (n-1)$CaCuO_2$ leads to any type of $Bi_2Sr_2Ca_{n+1}Cu_nO_{2n+4}$.(Fig.4-2-1) In these compounds, the numbers of $CaCuO_2$ layers in the unit formula are definitely important for the Tc value. The Tc Value changes from zero to 110K or 125K for different n values of $Bi_2Sr_2Ca_{n+1}CunO_{2n+4}$[1-4]) and $Tl_2Ba_2Ca_{n+1}Cu_nO_{2n+4}$[5-9]). Even for the $La_2Ca_{n-1}Cu_nO_{n+4}$ compounds, the n=1 compound, $(La,Sr)_2CuO_4$ shows the Tc of 40K and n=2 $(La,Sr)_2CaCu_2O_6$ shows 60K only by the increase of one $CaCuO_2$ layer.[10-13]) In this sense, the $Ca(Sr)CuO_2$ is the key compound and has been called "the parent material of the high T_c superconductor".[14]) Based on this basic concept(Fig.4-2-1), we have actually accumulated the layers of $Ca(Sr)CuO_2$ of desired n on a substrate and periodically inserted the $Bi_2Sr_2CuO_6$ unit layer by using laser MBE method. Using this particular

synthesis method, we have formed not only the $Bi_2Sr_2Ca_{n+1}CunO_{2n+4}$ of n=1 to n=5 which have been already reported[15,16], but also we have formed those of n=6, 7 and 8 for the first time. The $Ca(Sr)CuO_2$ is used as "the parent compound" to discriminate the structures.

Experiment

The formation of the compounds in the form of thin films has been carried out using the laser MBE method which have been described previously.[17] In the present experiment, two targets are used. One is $Ca_{0.86}Sr_{0.14}CuO_2$ to form the infinite $Ca(Sr)CuO_2$ layers and the other is $Bi_2Sr_2CuO_6$ target to deposit this layer. These two targets are alternately ablated with appropriate duration with monitoring the thickness of the layer by quartz thickness monitor. Typical experimental conditions are as follows: substrate used is $SrTiO_3(100)$ with 5Å surface flatness, substrate temperature is 500 to 630℃, ambient pressure of O_2 gas is $6x10^{-3}$ Torr, laser intensity is $1.0J/cm^2$ and the repetition rate is 20Hz. O_2 gas is used during the formation of the film and the mixture of O_2 and $O_3(8\%)$ is flowed for the oxidation of the films during cooling process.

Results and discussion

The formation of the infinite layers of $Ca(Sr)CuO_2$ is the first step for the synthesis of any type of $Bi_2Sr_2Ca_{n-1}CunO_{2n+4}$. Since the (100) surface of $SrTiO_3$ has lattice constant a of 3.9 Å, the a-axis length of $Ca(Sr)CuO_2$ (3.8 Å) coincides

with it within the mismatch of 3%. Figure 4-2-2 shows the X-ray diffraction pattern of the films formed on the $SrTiO_3$(001) surface at 590℃ using the $Ca_{0.86}Sr_{0.14}CuO_2$ target. The diffraction peaks at 27.5° (001) and 56.4° (002) in the pattern indicate that the infinite Ca(Sr)CuO_2 layer[2] is actually formed under this condition with 0its c-axis perpendicular to the substrate surface. Unless Ca is partially substituted by Sr in $CaCuO_2$ targets, the c-axis oriented layer is not formed. The Reflection High Energy Electron Diffraction(RHEED) pattern of the film surface shows a streak pattern with the spacing of 3.8Å, indicating that the film growth is epitaxial having smooth and uniform surface. The substrate temperature to form the c-axis oriented Ca(Sr)CuO_2 film ranges from 500℃ to 600℃.

The next step is the insertion of $Bi_2Sr_2CuO_6$ layer to discriminate the different n values of $Bi_2Sr_2Ca_{n-1}CunO_{2n+4}$.(see Fig.4-2-1) The numbers of the Ca(Sr)CuO_2 layer sandwiched by $Bi_2Sr_2CuO_6$ layer can be controlled by monitoring the thickness of the Ca(Sr)CuO_2 layers with quartz thickness monitor which has been calibrated for the actual thickness of the films. The numbers of the Ca(Sr)CuO_2 layers are also confirmed by the oscillation of the RHEED intensities that is described in detail elsewhere.[18] The selection of the structures from n= 1 to even 8 of $Bi_2Sr_2Ca_{n-1}Cu_nO_{2n+4}$ is successful using this method just by changing the numbers of the deposited layers of Ca(Sr)CuO_2 sandwiched by $Bi_2Sr_2Cu_1O_6$ layer. Figure 4-2-3 shows the X-ray diffraction pattern of the newly formed $Bi_2Sr_2Ca_5Cu_6O_{16}$ (n=6) compound. The diffraction pattern has been calculated for the n=6 to 8 compounds based on the ideal crystal structures using the crystallographic date.[19] Not only the peak position of (002) peak at 2θ =3.0° coincides with that of the expected c-axis length for n=6 compound(c= 58.8Å), but also the

total feature of the X-ray pattern coincides with the calculated pattern, indicating that the synthesis of the n=6 compounds is achieved by this method. In the similar manner, not only the thin films of n=1,2,3,4,5 but also the films of n=6,7,8 which has not been reported can be formed by this technique. Figure 5 shows the changes of the (002) peak positions of the corresponding compounds.

The superconducting transition temperatures(T_{czero}) of n=1, 2 and 3 compounds are zero(semiconductor), 80K and 102K, respectively. The compounds with higher n value(5 to 8) are semiconductor presumably because the concentration of carriers for the superconductivity supplied from Bi_2O_{2+y} layer are not enough in these materials. The details are now under investigation.

From the view point of the growth mechanism of $Bi_2Sr_2Ca_{n-1}Cu_nO_{2n+4}$ compounds, the present result suggests that the basic structural units are $Ca(Sr)CuO_2$ layers which has essentially a perovskite structure and also the n=1 compound; $Bi_2Sr_2Cu_1O_6$. So far, the formation of n=1 to 5 compounds was achieved but that of n=6-8 was not successful. We believe that this is because the growth of $Ca(Sr)CuO_2$ layer, the parent material, has not been carefully undertaken.

Conclusion

In summary, the new layer-by-layer technique enables us to control the larger number of the CuO_2 layers sandwiched by the thick $Bi_2Sr_2CuO_6$ layers. This basic concept and the particular synthesis technique will be useful to understand the mechanism of the high T_c superconductivity and also to create new compounds. This method will be applied to the other high T_c superconductors, since all the copper based superconductor have layered structure based on the $(Ca,Sr)CuO_2$ layers.

references

1) H.Maeda, Y.Tanaca, M.Fukutomi and T.Asano ; Jpn.J.Appl.Phys. 27 (1988) L209.

2) K.Imai, I.Nakai, T.Kawashima, S.Sueno and A.Ono ; Jpn.J.Appl.Phys. 27 (1988) L1661.

3) J.L.Tallon, R.G.Buckley, P.W.Gillberd, M.R.Presland, I.W.M.Brown, M.E.Bowden, L.A.Christian and R.Goguel ; Nature 333 (1988) 153.

4) A.Maeda, M.Hase, I.Tsukada, K.Noda, S.Takebayashi and K.Uchinokura ; Phys.Rev.B 41 (1990) 6418.

5) Z.Z.Sheng and A.M.Hermann ; Nature 332 (1988) 138.

6) P.Somasundaram, R.Vijayaraghavan, R.Nagarajan, R.Sehadri, A.M.Umauji and C.N.R.Rao ; Appl.Phys.Lett. 56 (1990) 487.

7) S.H.Liou, K.D.Aylesworth, N.J.ianno, B.Johs, D.Thompson, D.Meyer, J.A.Woollam and C.Barry ; Appl.Phys.Lett. 54 (1989) 760.

8) R.S.Liu, W.C>Shih, K.Scott, P.P.Edwards, W.A.Phillips and A.L.Greer ; J.Appl.Phys. 71 (1992) 4085.

9) Torardi, C.C. et al.,Science 7124071, 632-633 (1988).

10) H.K.Kao, J.Kwo, R.M.Fleming, M.hong and J.P.Mannaerts ; Appl.Phys.Lett. 59 (1991) 2748.

11) A.Levy, M.J.Lercel, J.P.Falck, M.A.Kastner, A.A.Bright and A.W.Kleinsasser ; J.Appl.Phys. 71 (1992) 1764.

12) M. Suzuki ; Phys. Rev. B 39 (1989) 2312.

13) M.Z.Cieplak, S.Guha, H.Kojima, P.Lindenfeld, G.Xiao, J.Q.Xiao and C.L.Chien ; Phys. Rev. B 46 (1992) 4518.

14) Siegrist,T., Zahurak,S.M., Murphy,D.W. and Roth,R.S., Nature 7133471, 231-232 (1988).

15) Adachi,H. Kohiki,S., Setsune,K. Mitsuyu,T. and Wasa,K., Jpn. J. Appl. Phys., 712771, L1883-1885 (1988).

16) Kanai,M., Kawai,T. and Kawai,S., Appl.Phys.Lett. 725472 1802-1804 (1989).

17) Kanai,M., Kawai,T. and Kawai,S., Appl.Phys.Lett., 725772 198-200 (1990)

18) Kanai,M., Kawai,T. and Kawai,S., submitted.

19) Gao,Y., Lee,P., Coppens,P., Subramanian,M.A. and Sleight, A.W., Science 7224172 954 (1988).

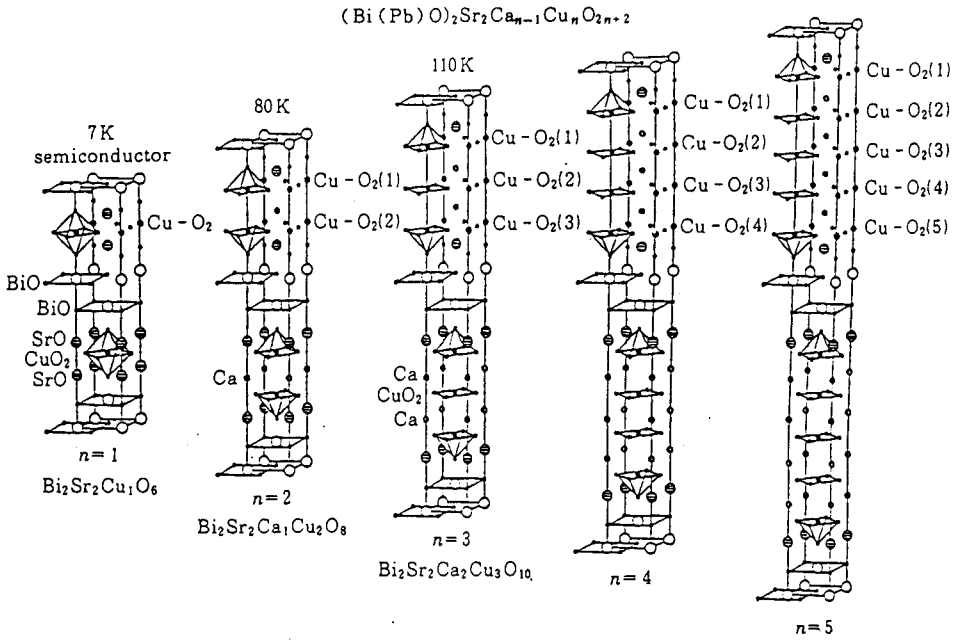

Fig. 4-2-1. The typical crystal structures of $Bi_2Sr_2Ca_{n-1}Cu_nO_{2n+4}$.

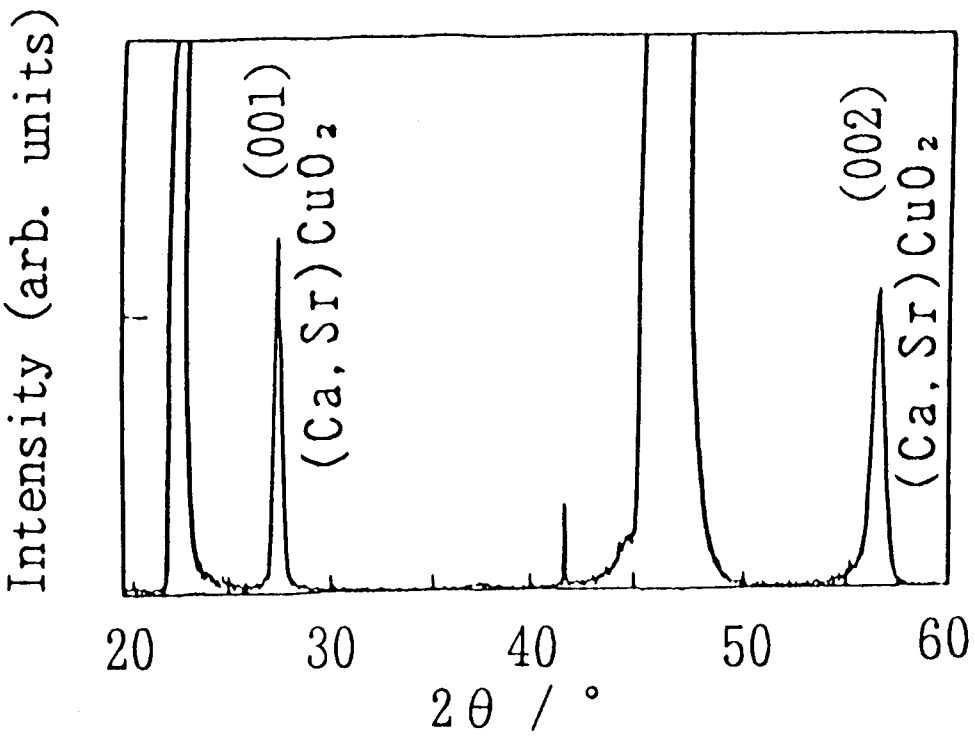

Fig. 4-2-2. X-ray diffraction patterns for the $(Ca_{0.86}Sr_{0.14})CuO_2$ film prepared on the $SrTiO_3$ substrate.

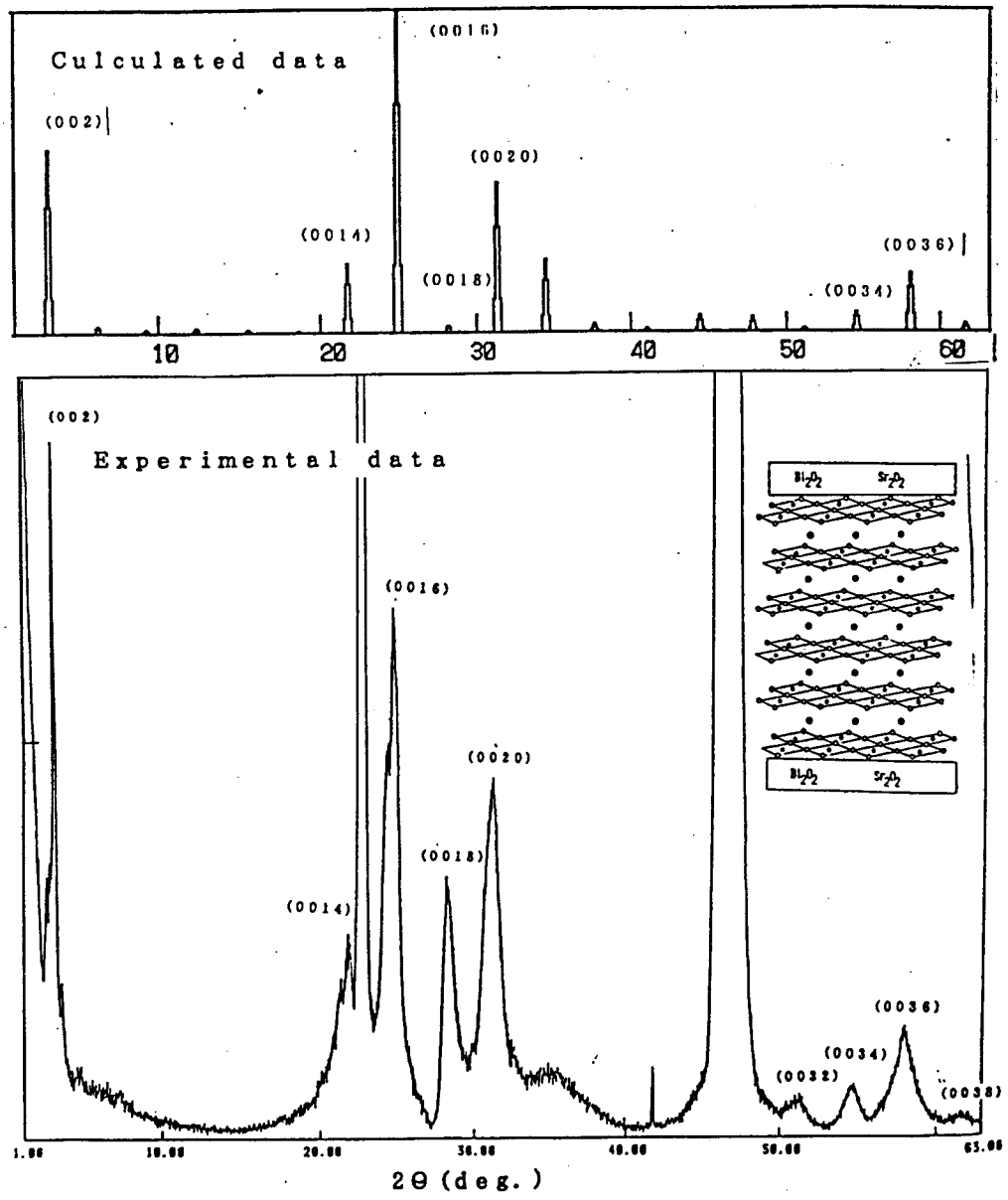

Fig. 4-2-3 X-ray diffraction pattern of the $Bi_2Sr_2Ca_{n-1}Cu_nO_{2n+4}$ film with n=6. The calculated pattern based on the structure in the inset ($Bi_2Sr_2Ca_5Cu_6O_{16}$) coincides with the observed X-ray diffraction pattern.

4-2-2. Control of the distance between CuO_2 layers and carrier density - site selective substitution of Ca and Sr -

Abstract

Layer-by-layer successive deposition utilizing laser ablation has been applied to the site-selective substitution of +1, +2 and +3 ions having different ionic radii at the Ca and the Sr site of $Bi_2Sr_2Ca_1Cu_2O_y$ superconducting films. With this technique, we can control the crystal structure (lattice parameter) and the carrier parameter. The substitutions at the Sr and the Ca site exhibit quite different behaviors in the superconductivity and the structural parameters. For the substitution of larger ions at the Ca site, lattice parameter c increases showing the higher value Tc, while the substitution at the Sr site does not elongate the c-axis and does not increase the T_c. Furthermore we demonstrate the independent control of the lattice parameter and carrier parameter. When the +3 ion such as Y is incorporated at the Ca(+2) site, the carrier density decreases. On the other hand when the +2 ion, such as Ba, is incorporated at this site it dose not. These changes have been explained by the structure models, and the correlation between T_c and the lattice parameters is explained by the changes of the distance between CuO_2 layers, indicating the importance of the interaction between CuO_2 layers.

Introduction

As described in chapter 4-2-1, CuO2 sheets are the essential feature of the copper-oxide based superconductor.[1-5] The high T_c superconductivity appears by doping charge carriers into the CuO_2 sheets. Positive ions, such as Y, Ba, Bi, Sr, Ca and Tl, are playing roles to construct structural framework and to control the amount of charge carriers in the superconductor.[6,7] Thus, the control of the structures based on the CuO_2 sheets together with the control of charge carriers are necessary for the elucidation and improvement of the superconductivity.

Fig.4-2-4(a) shows important structural factors of the CuO_2 based structures for the example of $Bi_2Sr_2Ca_1Cu_2O_8$(Fig.4-2-4(b)).; When the number of the CuO_2 layers are fixed, the structural feature of the CuO_2 layers are (1)the distance between CuO_2 layers, (2) the bond length of Cu-O and (3) the distance between Cu and O(apex). These factors can be controlled either by accumulation of CuO_2 layers or the insertion of exotic atoms with different ionic radii into Ca layer or SrO layer.

The carrier density can be changed by the control of;(1) the amount of oxygen and (2) the substitution of the atoms with different valence state. This is performed by the incorporation of ions with different valence state into Ca, SrO or Bi_2O_2 layer.

For these controls of the composition at the atomic layer scale, we have demonstrated that layer-by-layer successive deposition is excellent method in which each constituent layer is piled up on a substrate layer-by-layer to form the artificial crystal structure and compositions.

In this chapter, we will report on the site selective substitution of ions

with different ionic radii and valence state taking advantage of layer-by-layer successive deposition. By means of this technique, the formation of a new oxide superconductor which is hardly attainable as a bulk phase will be possible. As shown in Fig.1, the ions we have chosen for the substitutions are , Mg, Ca, Sr and Ba, the 2+ ions, Li, Na and K, the 1+ ions, and Y, Nd and La, the 3+ ions. These ions are systematically substituted at either Ca site or Sr site, and the changes of the properties such as lattice parameter and the superconductivity are thoroughly studied. These "tailored superconducting films" have been proved to be useful to elucidate the mechanism of the superconductivity and be useful as a sophisticated technique for the device application of the superconductor.

II. EXPERIMENTAL

The films are prepared by a layer-by-layer successive deposition method using a pulsed ArF excimer laser(193nm). The laser beam is sequentially focused on the multi-targets to form a film on a substrate placed at the opposite side in the presence of N_2O and/or O_2 gas atmosphere.[8] Typical experimental conditions are : energy density for ablation after focusing = 0.5 J/cm^2, and repetition rate = 10 Hz. The substrate used was a MgO(100) single crystal heated at 600 - 620℃. The thickness of the thin film was measured by and oscillating film thickness monitor in situ, and the total thickness was measured by optical thickness monitor.

For the deposition, sintered disks of $Bi_7Pb_3O_y$, $Sr_1Cu_1O_y$, $Ca_1Cu_1O_y$, $Ba_1Cu_1O_y$ and $Y_1Cu_1O_y$(nominal compositions) are used as targets and the layers are successively deposited as we desire. These targets are prepared by calcining the mixture of Bi_2O_3, PbO, $SrCO_3$, $CaCO_3$, Li_2CO_3, K_2CO_3,

$BaCO_3$, Y_2O_2, La_1O_3 and/or $NdCO_3$ with appropriate ratios. The $Bi_7Pb_3O_y$, NaCuO and KCuO target are prepared by heating in air at 630℃ for three hours, and the rest by heating at 800 ℃ for 10 hours.

[Layer control with sub-unit cell accuracy]

[layer control]

First of all we measured the relation between the laser focusing time on the $BiPbO_y$-target and the amount of the deposited Bi-atom. Then the layer was piled up on the substrate layer-by-layer to form the artificial crystal. In the case of piling up, we piled up (1)the unit-layer as 1 layer of theoretical level and (2) the unit-layer as 3 layers of theoretical amount; it is piled up three times as much as ideal amount of 1-layer for every unit layer.

[construction of the standard crystal structure]

It is essential for getting these artificial thin films to control the composition at the atomic layer scale. So we have demonstrated that the layer-by-layer successive deposition can control each constituent layer at atomic level which is piled up on a substrate layer-by-layer to form the artificial crystal structure with compositions. To form the standard BSCCO film, we used the multi-targets such as $BiPbO_y$, $SrCuO_y$ and $CaCuO_y$. The laser beam is sequentially focused on these multi-targets to form a film on a substrate. The sequence for the successive deposition was $BiPbO_y$-$SrCuO_y$-$CaCuO_y$-$SrCuO_y$-$BiPbO_y$, which will simply be termed as A-B-C-B-A. This consist of one cycle which was repeated 30 times. Hereafter we call each layer one unit-layer.

[Substitution at the Ca-site]

Partial substitution of mono-(Li, Na and K), di-(Mg, Sr and Ba), and tri-valent(Y, La and Nd) ions for Ca has been examined. In this case, the

deposition was carried out successively from the targets, BiPbO-SrCuO-CaCuO-MCuO-CaCuO-SrCuO-BiPbO (M=Li, Na, K, Mg, Sr, Ba, Y, La and Nd). This consisted of one cycle which was repeated. The sequence can be abbreviated as A-B-C-M-C-B-A. (A;$Bi_7Pb_3O_y$, B;$Sr_1Cu_1O_y$, C;$Ca_1Cu_1O_y$ and D; $Ba_1Cu_1O_y$, for example) Typical irradiation periods for successive deposition are 25 s for $Bi_7Pb_3O_y$, 15 s for $SrCuO_y$, 10 s for $MCuO_y$ and 28 s for $CaCuO_y$. In the case of Ba substitution, for example, the replace ratio of Ba for Ca was changed form 0% to 100%.

[Substitution at the Sr-site]

Partial substitution of the ions for Sr has been performed as for the Ca site: The sequence is similar to the Ca substitution, except that the deposit from the $MCuO_y$ (M=Li, Na, K, Mg, Ca, Ba, Y, Nd and La) is sandwiched between the deposits from $SrCuO_y$. Typical irradiation periods for the successive deposition are 25 s for BiPbO(A), 5 s for SrCuO(B) or MCuO(M) and 65 s for CaCuO(C). That is ; the sequence is A-B-M-B-C-B-M-B-A.

The critical temperature (T_c) for the superconducting transition was measured by a standard four probe technique. The structures and the compositions of these films were determined by X-ray diffraction patterns using Cu Kα and EDX(observed area is 500x500 μm with accelerate voltage is 15 kV), respectively. And carrier density were measured by hole density with applied magnetic field of 1.2T.

RESULTS AND DISCUSSION

[Layer control]

Fig.4-2-5 shows the dependence of time of laser ablation on the Bi content. The content of Bi in the film increases linearly with increasing the ablated time of Bi_2O_3 target. So it shows that the film thickness (the contents of atoms) can be controlled by changing the ablation time.

When the 3 unit cells of each layer(Bi_2O_2, $SrCuO_y$ and $CaCuO_y$) was deposited as one cycle (3 layers = 45 Å), the perovskite BSCCO crystal structure can not be constructed. When the layers are pilled up with the sequence just 1 unit cell, on the other hand, the crystal structure was successfully constructed (Fig.4-2-6) This result suggests that there is no inter-diffusion beyond the one unit cell in the c-axis direction.

[Partial substitution of Ca-site and Sr-site by +2 ions]

In the case of Ba substitution at Sr or Ca site, the upper substitution limit is measured. Figure 4-2-7 shows the content of substituted Ba at the Sr and Ca site versus lattice constant c. The lattice constant c increase gradually with increasing the content of Ba replacement. The partial substitution of Ba for Sr by about 30-40 % of Sr atoms showed a clear X-ray diffraction pattern of double CuO_2 layered structure with no extra peaks due to Ba compounds, such as $BaCuO_2$ (see Fig. 4-2-11). In the bulk samples, $BaBiO_3$ and $BaCuO_2$ impurity phase appear with substituting Ba for Sr or Ca with only a few %.[ref] (Fig. 4-2-8), whereas in this particular successive deposited films, Ba was incorporated into BSCCO crystal structure, forming no other phases. Actually, an EDX analysis showed the presence of Ba for up to about 40% of the Sr atoms.(Fig.4-2-8(b)) When Ca is replaced with 50 % by Ba, perovskite structure of BSCCO can be constructed with containing impurity phase of $BaCuO_2$. (Fig.4-2-9)

When all atoms of Sr or Ca are replaced by Ba(100% substitution), the perovskite crystal structure can not be constructed any longer but only the $BaCuO_2$ structure disappears.(Fig.4-2-10) Therefore, the maximum of Ba substitution at Sr or Ca site is about 40%. In these artificial BSCCO structure, the limit of Ba solid solution into Ca or Sr site can be expanded from 4-5% to 40-50 % comparing with that of bulk sample.

The partial substitution of Mg, Sr and Ba ions for Ca by about 30% shows broad X-ray diffraction patterns of double $Cu\text{-}O_2$ layered structure for all substituted patterns of double $Cu\text{-}O_2$ at 800℃. The films showed X-ray pattern of the single phase of double CuO_2 layers structure with their c-axis perpendicular to the substrate surface (Fig.4-2-11,12) . No apparent impurity peaks have been observed, indicating that these atoms are incorporated into the BSCCO crystal structure.

The lattice parameter c is found to depend on the ionic radii of the incorporated ions for both Ca and Sr site, but with different manner. When small ion such as Mg is incorporated at the Ca site, the c-axis shrink. On the other hand, with the incorporation of the larger ions such as Ba, the lattice constant c increases. (Fig.4-2-13) On the other hand, when the Sr is replaced by large ion, the lattice constant c does not increase much. These behavior is expected by the structure model presented in the next section. Thus quite different behaviors are expected and actually have been observed for the Ca and Sr site substitution.

[Structural models for the site selective substitution at Ca and Sr site in $Bi_2Sr_2Ca_1Cu_2O_8$ crystal.]

Fig. 4-2-14(a) shows estimated changes of the lattice parameter c with the incorporation of Ba, the larger ion(rion=1.49Å), and Mg, the smaller ion(rion=0.86Å) at the Ca site. The Ca ion is osculating with the neighboring oxygen ions in the standard $Bi_2Sr_2Ca_1Cu_2O_8$ structure[3,4]. Consequently, for the incorporation of small Mg ion, the c-axis is expected to shrink down, while for the incorporation of large Ba ion, expansion of the c-axis is expected(see Fig.4-2-14(a)).

As shown in Fig.4-2-14(b), on the other hand, it is reported from the crystallographic analysis of $Bi_2Sr_2Ca_1Cu_2O_8$ single crystal that there is a room between Sr and oxygen above, since close contact is achieved by Bi and oxygen beside them. Accordingly, it shrinks the c-axis, while the incorporation of Ba may give a small changes for the c-axis length(see Fig.4-2-14(b)).

The most important difference between the Ca site substitution and Sr site substitution is that large expansion of the distance between CuO_2 sheets is expected for the Ca site, while it is not expected for the incorporation at the Sr site. The present experiment is aimed to perform these site-selective substitution to see whether these expected crystallographic changes are achieved or not, and to see the correlations between these structural changes and the superconductivities.

[Substitution by +1 and +3 ions at Sr or Ca- site]

The changes of the lattice parameter c by the incorporation of +1 ions, Li and Na, and +3 ions, Y, Nd and La have also been examined (Fig.4-2-13). the

mono-valent ions show similar behavior to the divalent alkaline earth ions, that is, the larger ions leads to the larger lattice constant. The trivalent ions, on the other hand, show distinct shrinking of the c-axis. This is presumably because highly positive valency works to attract negative oxygen ions.

[Superconducting properties of the tailored films]

These tailored films in which Sr or Ca ion is substituted by +1, +2 or +3 ions show systematic change in the resistance -temperature (R-T) curves. For example, the R-T curves for the incorporation of +2 ions, Mg, Ca, Sr and Ba, at the Ca site are shown in Fig. 4-2-15. It is clearly observed that the larger the substituted ion is, the higher the T_c is. The highest T_c is observed for the Ba substitution, Tc_{onset}=to be 95K and Tc_{mid}=83K even for the 300Å thin films. Accordingly the correlations are observed between T_c and ionic radii of the substituted ions, in other word, T_c and lattice parameter c, as shown in Fig.4-2-16. For the substitution of ions at Sr site, on the other hand, both larger and smaller ions other than Sr lower T_c. (Fig.4-2-15; Sr→Ba) Furthermore, the replacement of other ions than Sr seems to make the superconductivity worse presumably because of the introduction of randomness at the SrO layer.

In this manner, the site-selective partial substitution of Sr and Ca site by exotic atoms shows drastic difference in superconductivity depending on the ionic radii and valence state.The replacement of larger ions at the Ca site makes c-axis longer, while that at the Sr site does not. Accordingly, the spacing between double CuO_2 planes can be changed artificially by this technique, and we found that this spacing between CuO_2 planes has an strong effect on the T_c value. It has been reported that there might be a hopping of Cooper pairs between CuO_2 layers and this kind of interaction between layers

is important for the T_c value. In addtion, dimensionality is the essential factor for the superconducting behaviors. The present experimental results indicate that the distance between the layers is really important as the determining factor of the T_c value.

The R-T curves for the incorporation of +3 ions, show semiconducting behavior for all ions. This is because of the decrease of hole concentration by +3 ion incorporation instead of the +2 ion. (Fig.4-2-17)

Conclusion

1. With the layer-by-layer successive deposition method utilizing laser ablation, site selective partial substitution of +1, +2 and +3 ions at the Ca and Sr site has been performed.
2. The incorporation of smaller +2 ion, Mg, at the Ca site makes the c-axis shrink, while that of larger Sr and Ba ions makes the c-axis longer. On the other hand, the incorporation of even Ba at the Sr site does not elongate the c-axis so much.
3. This phenomenon is explained by the structure model in which there is a capacity to incorporate the large Ba ion at the Sr site.
4. The T_c value has correlation with the expansion of c-axis due to the incorporation of exotic atoms. The larger lattice parameter c produces higher T_c.
5. It is suggested from these results that the spacing between CuO_2 planes is important structural factor for the T_c, suggesting the strong interaction between CuO_2 layers.

References

1) M.Takano, Y.Takeda, H.Okada, M.Miyamoto and K.Kusaka ; Physica C 159 (1989) 375.

2) M.G.Simith, A.Manthiram, J.Zhou, J.B.Goodenough and J.T.Markert ; Nature 351 (1991) 549.

3) G.Er, Y.Miyamoto, F.Kanamaru and S.Kikkawa ; Physica C 181 (1991) 206.

4) M.Azuma, Z.Hori, M.Takano, Y.bando and Y.Takeda ; Nature 356 (1992) 775.

5) M.A.Subramanian, C.C.Torardi, J.C.Calabrese, J.Gopalakrishnan, K.Morrissey, T.R.Askew, R.B.Flippen, U.Chowdhry and A.W.sleight, Science, 26, 1015(1988).

6) K.Imai, I.Nakai, T.Kawashima, S.Sueno and A. Ono, Jpn.J.Appl.Phys., 27, L1661(1988).

7) J.M.Wheatley, T.C.Hsu and P.W. Anderson, nature, 333, 121(1988).

8) M.Kanai, T.Kawai, M.Kawai and S.Kawai: Jpn.J.Appl.Phys., 27 (1988) L1293.

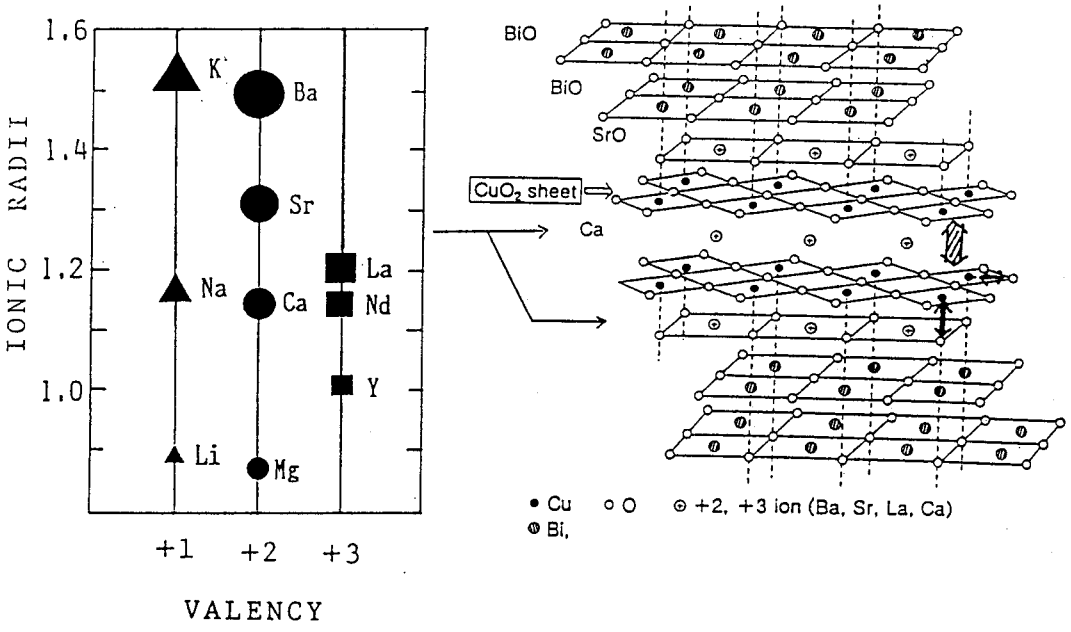

Fig.4-2-4(a). Schematic structure of layered $Bi_2Sr_2Ca_1Cu_2O_8$ superconductor. Important structural factors based on CuO_2 sheets and carrier concentration can be changed by an incorporation of ions with different radii and valence state.

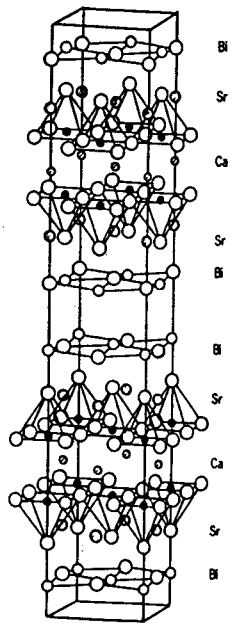

Fig. 4-2-4(b). Crystal structure model of $Bi_2Sr_2Ca_1Cu_2O_8$.

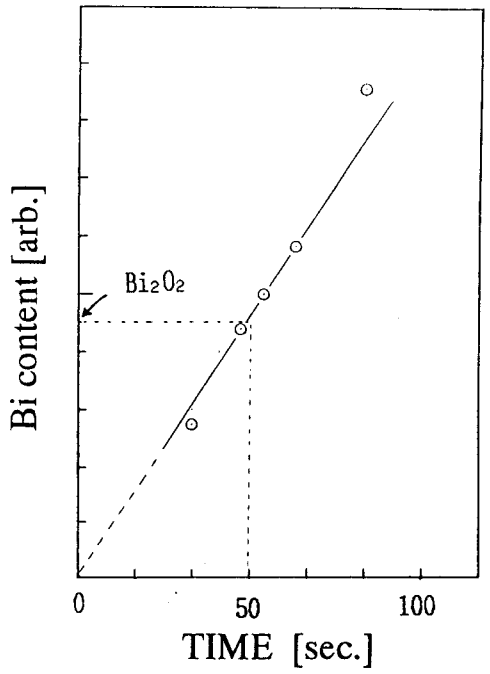

Fig. 4-2-5. The relation between deposition time of Bi_2O_3 layer and the thickness of Bi_2O_3 layer.

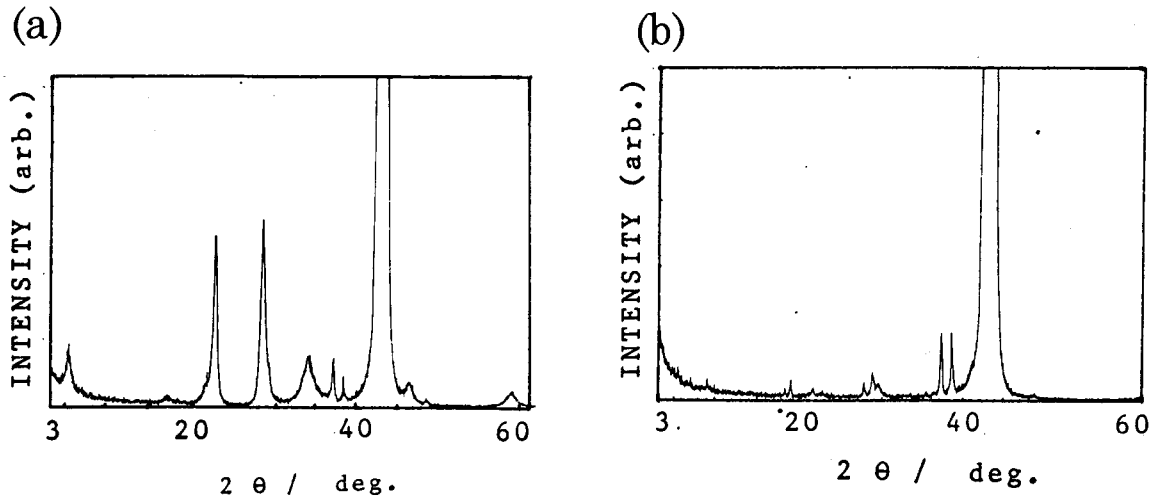

Fig. 4-2-6. A schematic representation of multi target successive deposition for Bi-Sr-Ca-Cu-O film. And the X-ray diffraction patterns of $Bi_2Sr_2Ca_1Cu_2O_8$ films with the stacking of (a) 1 half unit cell cycle and (b) 3 half unit cell cycle.

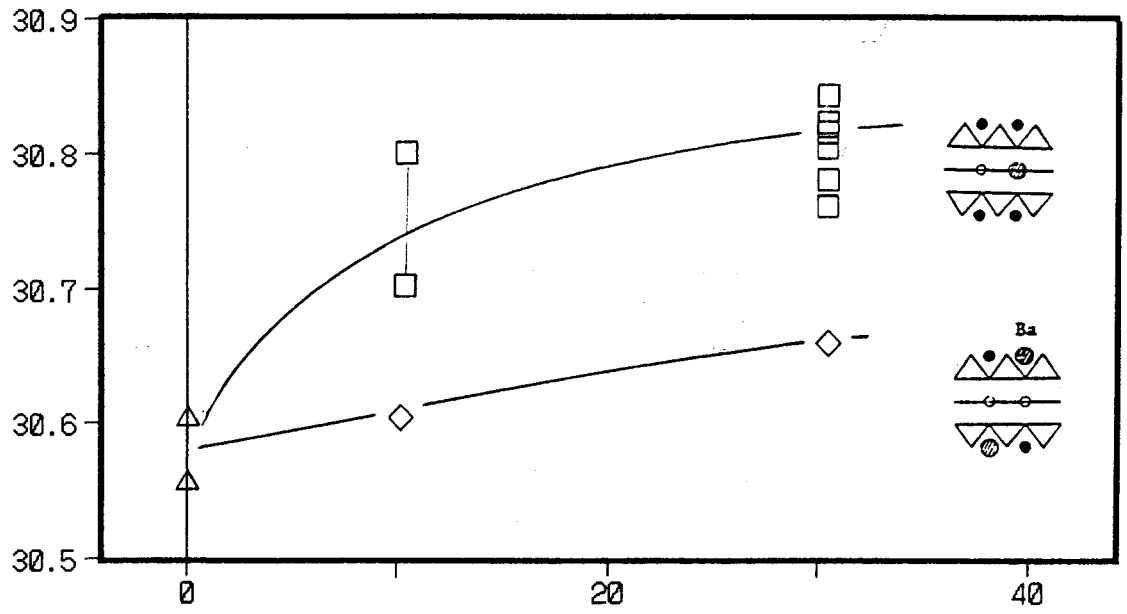

Fig. 4-2-7. Lattice constant c vs concentration of substituted Ba for Sr-site(◇) and Ca-site(□).

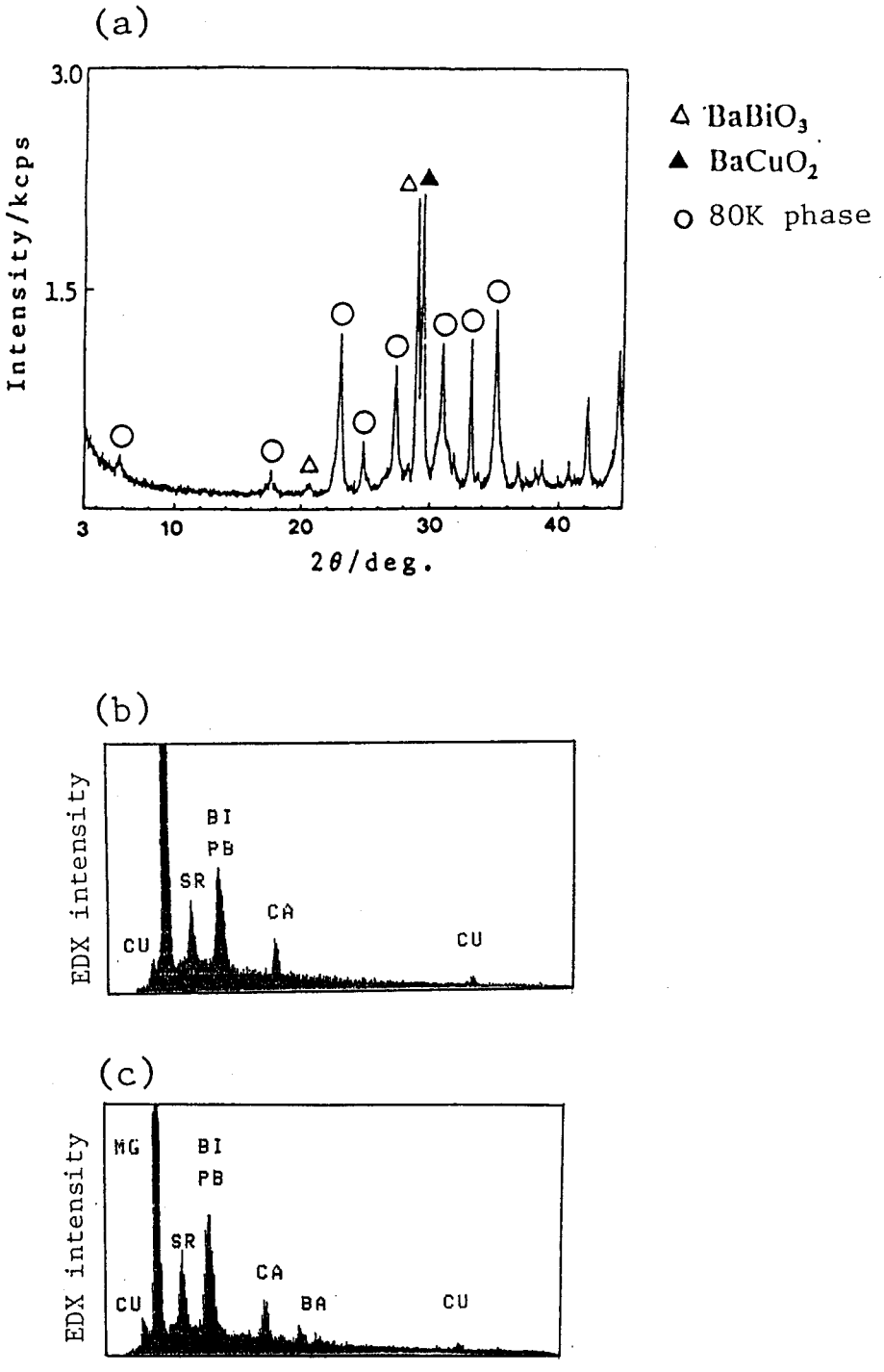

Fig. 4-2-8. (a) X-ray diffraction pattern of bulk $Bi_2Sr_{1.6}Ca_1Cu_2Ba_{0.4}O_8$ sample. And the EDX spectra of the thin films. (b) standard BSCCO film, (c) the film in which 30 to 40 % of Ca is substitute by Ba.

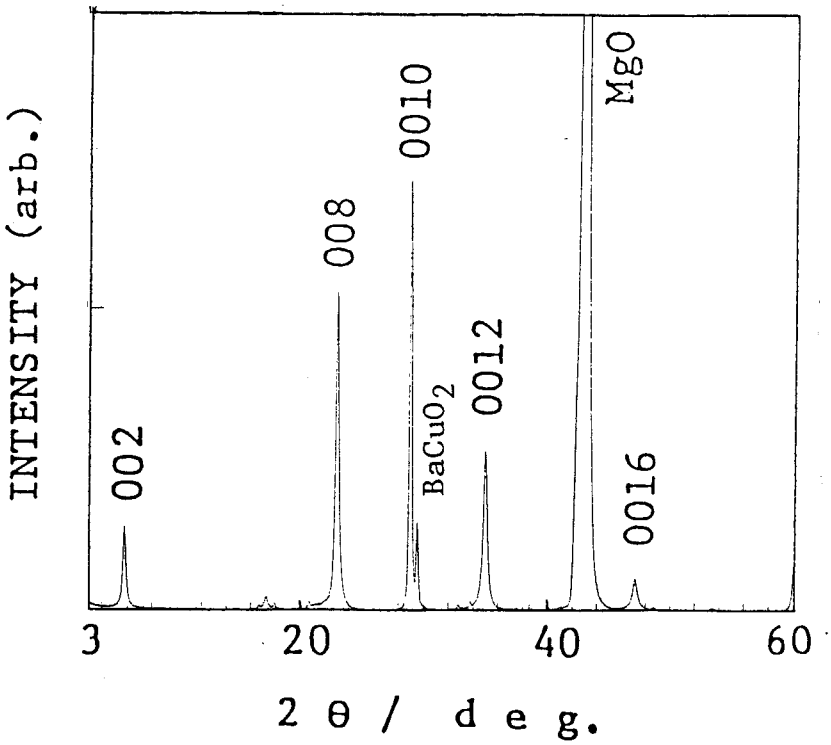

Fig. 4-2-9. X-ray diffraction pattern of the $Bi_2Sr_2Ca_{0.5}Ba_{0.5}Cu_2O_8$ films in which Ba is substituted for Sr by 50 %.
($BaCuO_2$ peaks can be observed)

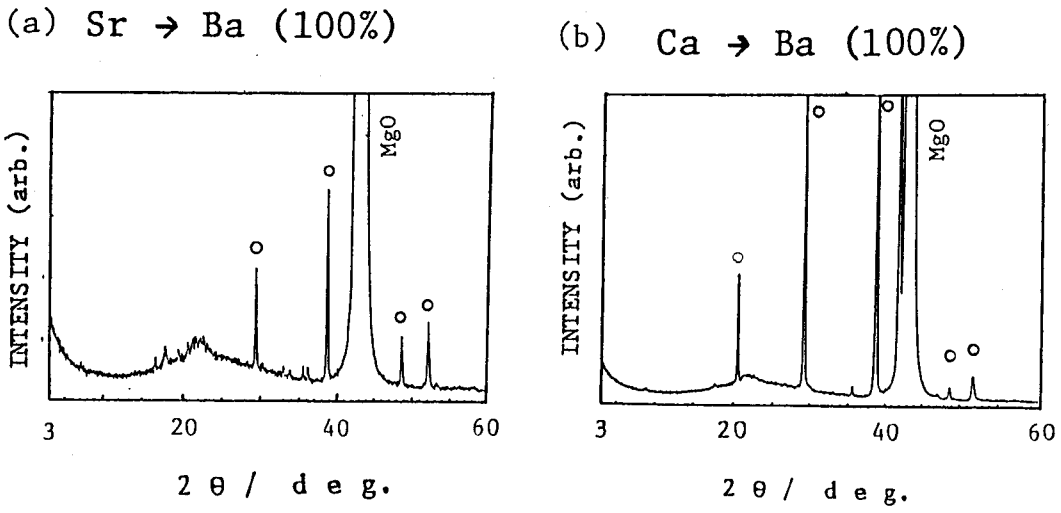

Fig. 4-2-10. The X-ray diffraction patterns of the thin films for (a) complete substitution of Ba for Sr (b) complete substitution of Ba for Ca. ○; $BaCuO_2$ peaks

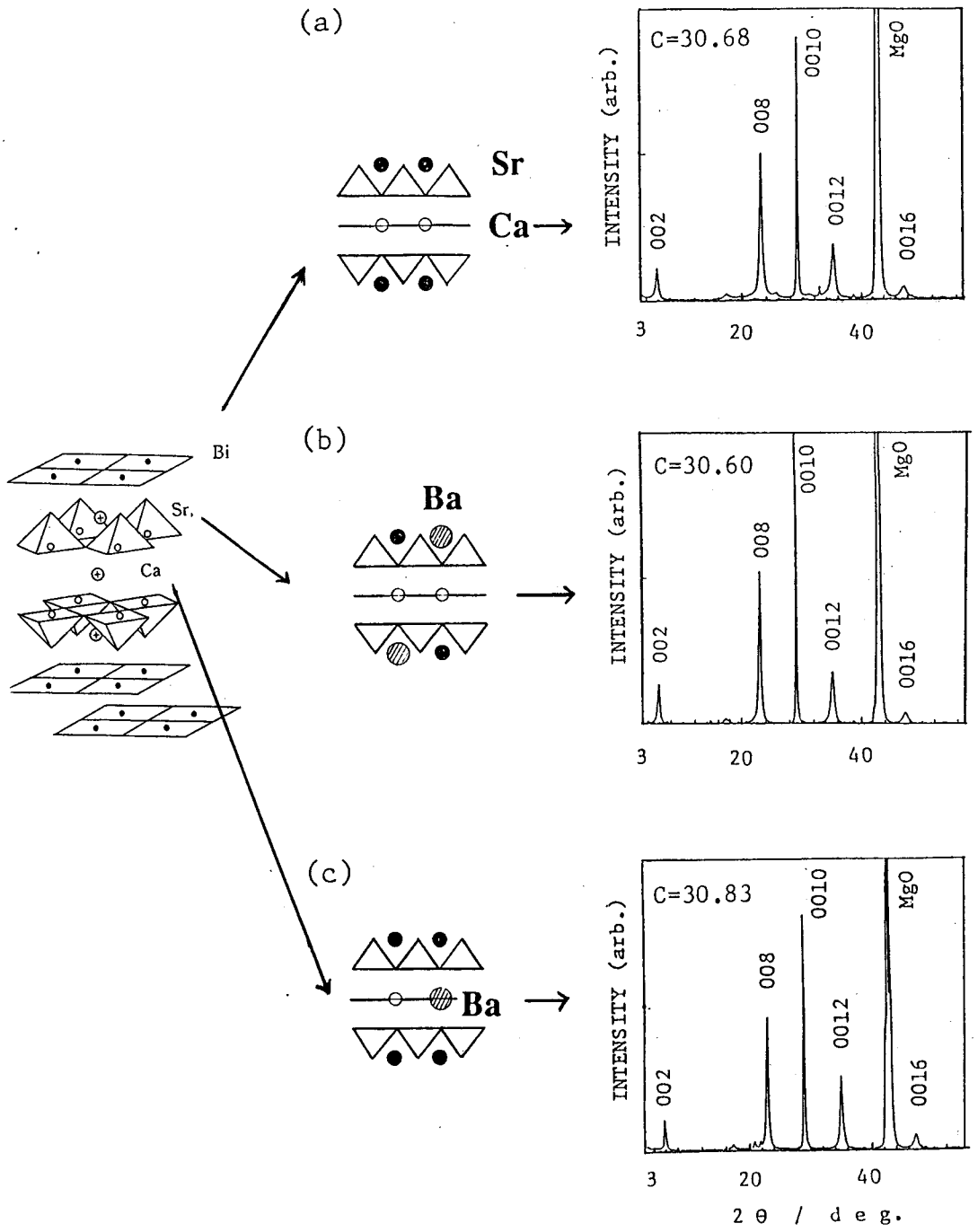

Fig. 4-2-11. Schematic representation for the partial substitution of Ba for the Sr or Ca site, and the X-ray diffraction patterns of the corresponding thin films. (a) BSCCO film without Ba substitution, (b) partial substitution of Ba for Sr by 30-40 % (c)partial substitution of Ba for Ca by 30-40%.

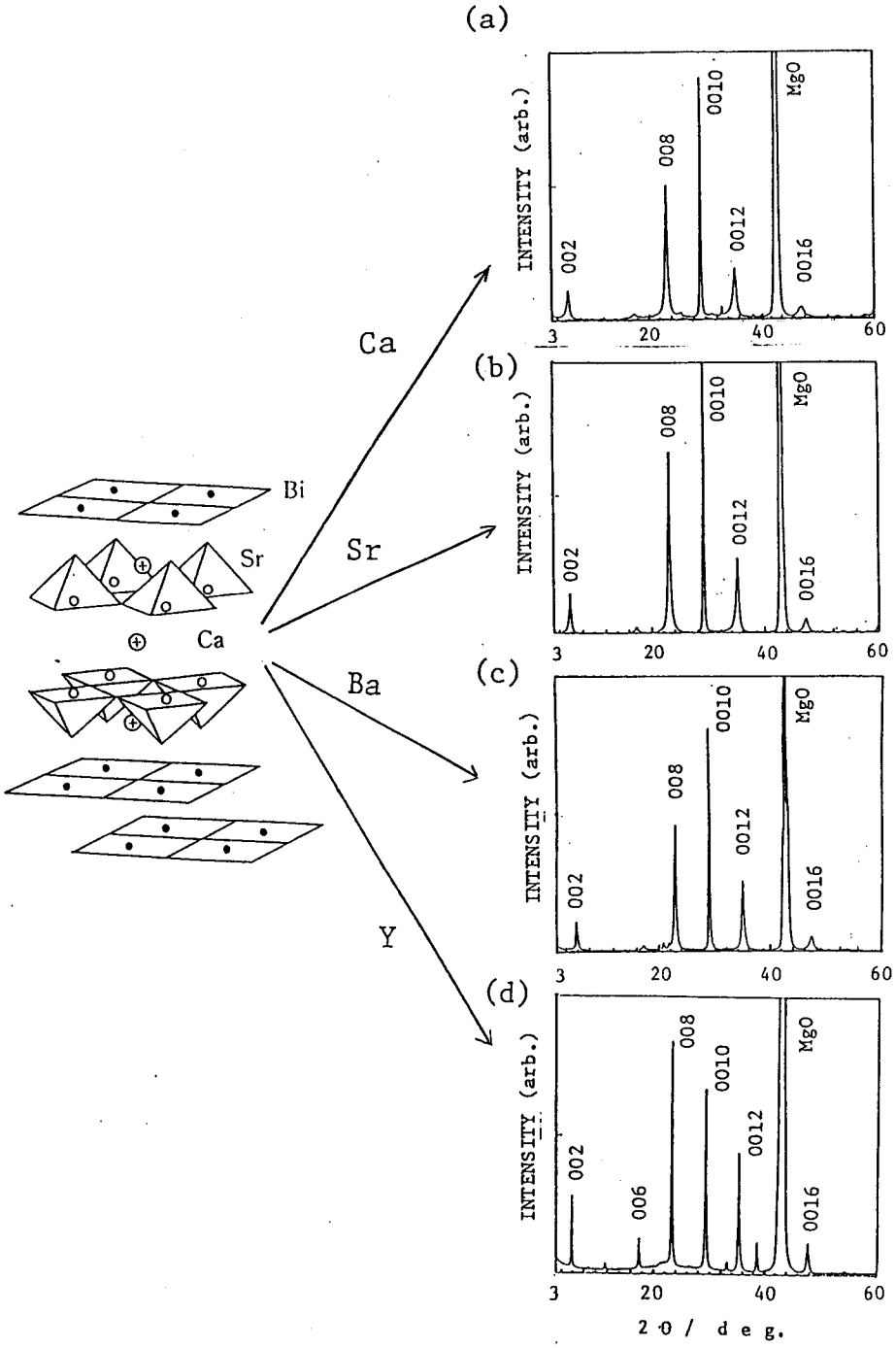

Fig. 4-2-12. Schematic representation for the partial substitution of Ca by Sr, Ba and Y, and the X-ray diffraction patterns of the corresponding thin films, (a) Ca, (b) Sr, (c) Ba and (d) Y at the Ca layer.

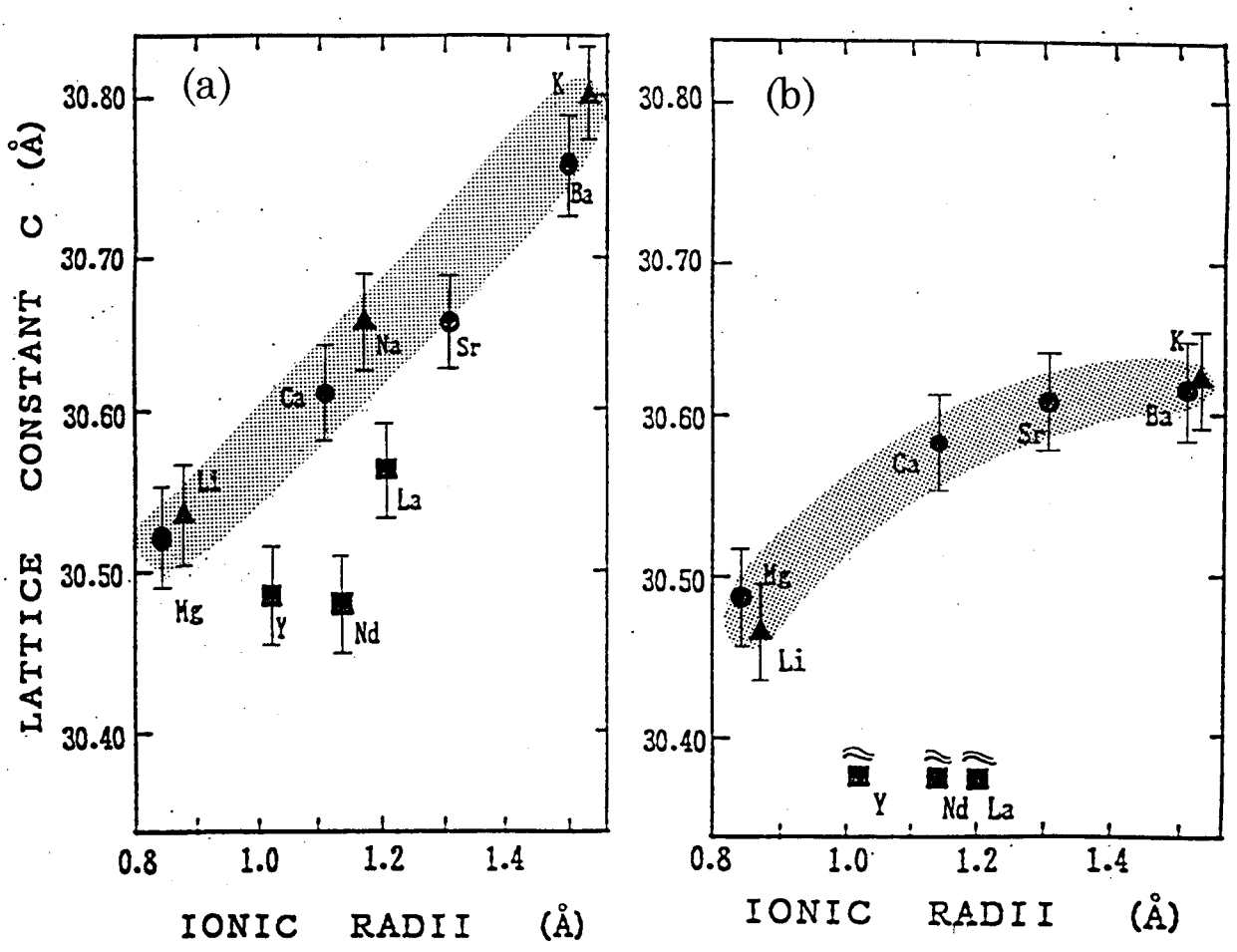

Fig. 4-2-13. (a) Lattice constant c versus ionic radii of the ions incorporated at the Ca site in the BSCCO films, and (b) lattice constant c versus ionic radii at the Sr site. The c-axis is expanded most evidently for the Ba substitution at Ca site.

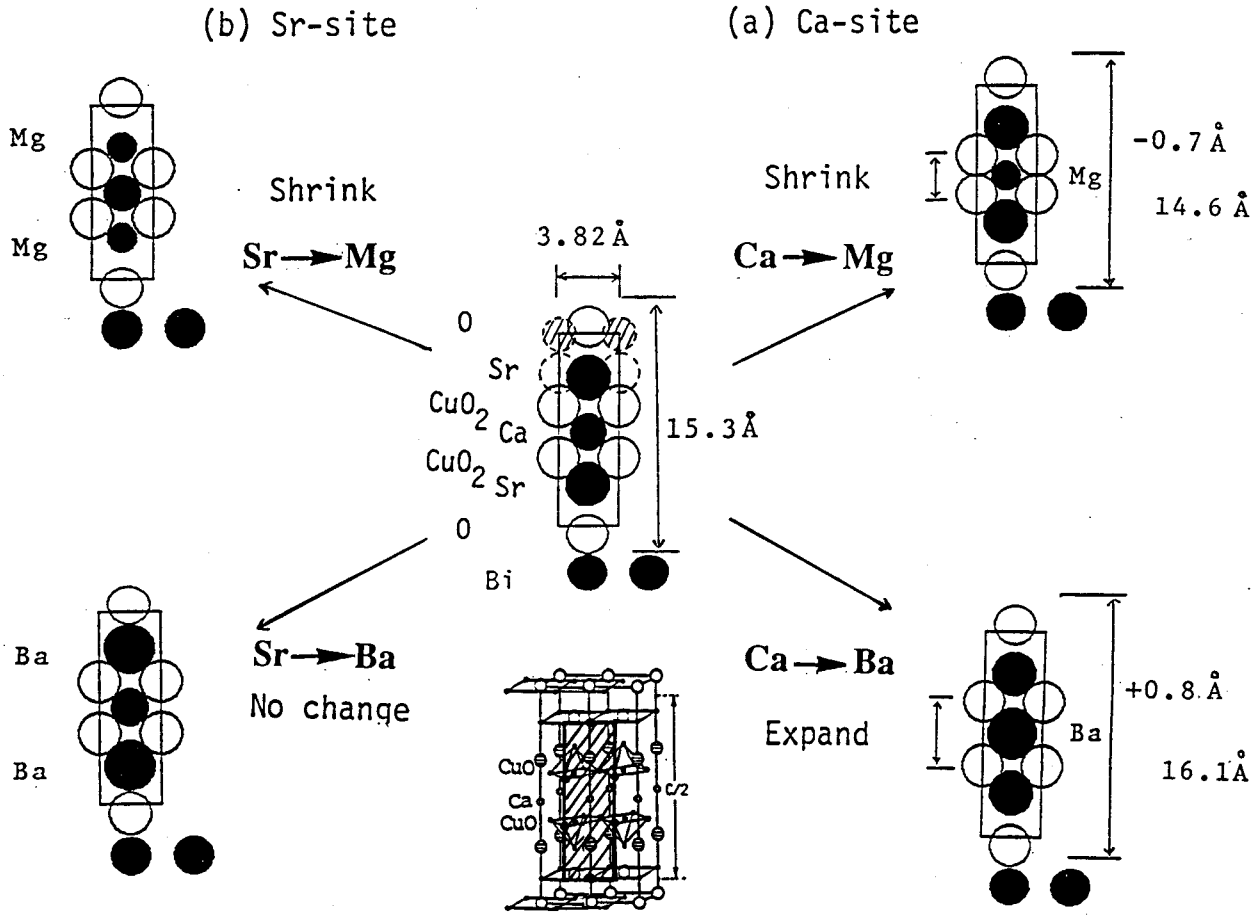

Fig. 4-2-14..Structure model of $Bi_2Sr_2Ca_1O_8$, and the changes of the lattice parameter c by the incorporation of Mg and Ba. (a)substitution at the Ca site, (b) substitution at the Sr site. For Mg incorporation, the c-axis is shrunk. For Ba incorporation at Ca site c-axis becomes longer, while it does not change much for the Sr site substitution.

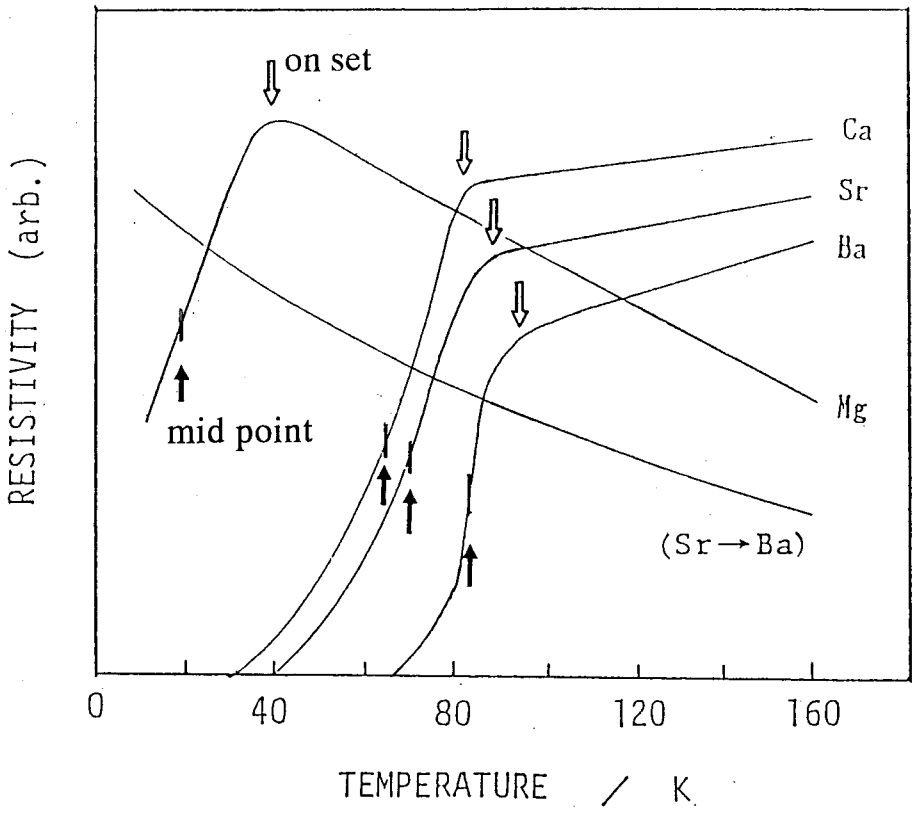

Fig. 4-2-15. Temperature-resistivity curves for the BSCCO films which contain various +2 ions (Mg, Ca, Sr, Ba) at the Ca site.

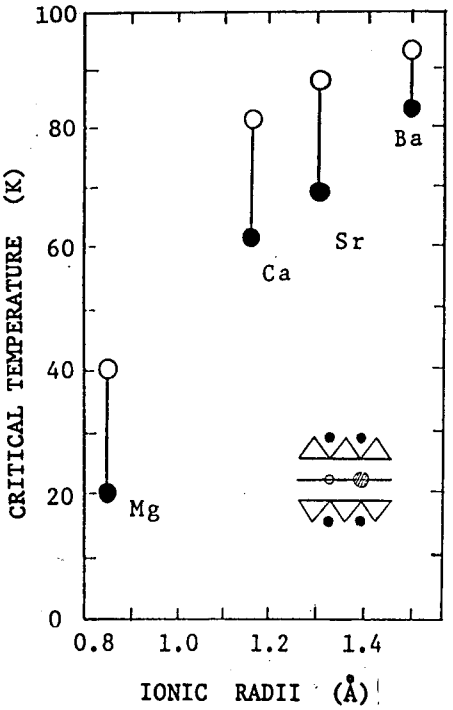

Fig. 4-2-16. Critical temperature versus ionic radii of the ions incorporated at the Ca site.

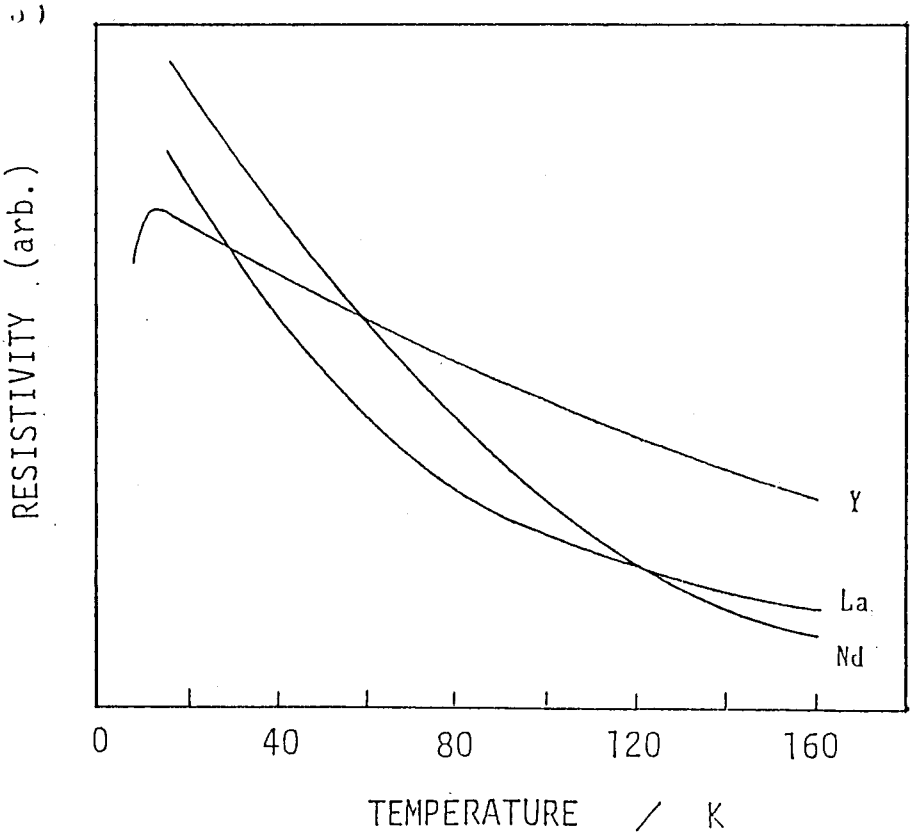

Fig. 4-2-17. Temperature-resistivity curves for the BSCCO films which contain various +3 ions (Y, La, Nd) at the Ca site.

4-3. Artificial control with unit cell scale
- $(La,Sr)_2CuO_4/Sm_2CuO_4$ superlattices -

Abstract

We have grown superlattices of $(La,Sr)_2CuO_4/Sm_2CuO_4$onto $SrTiO_3$ substrates at unit cell accuracy by an excimer laser deposition technique. These superlattices can be classified into three regions. The stacking periodicity of (La, $Sr)_2CuO_4/Sm_2CuO_4$ is changed from 1/1 (one $(La,Sr)_2CuO_4$ and one Sm_2CuO_4 layer) to 120/120 combinations. For the short periodicity of the stacking up to 4/4, new structures are constructed having a large unit cell made of a CuO_5 pyramid, CuO_6 octahedral, and CuO_4 sheet. For the large periodicity more than 60/60, the superlattices exhibit the same superconducting behavior as the standard $(La,Sr)_2$ CuO_4. The superlattices of the intermediate periodicity, from 60/60 to 15/15 on the other hand show changes in the critical temperature against the variation of the stacking periodicity. This phenomenon is explained to be derived from a pressure effect caused by a lattice mismatch between (La, $Sr)_2CuO_4$ and Sm_2CuO_4 layers. Furthermore controlled variations of the in plane Cu-O bond length and interlayer proximity coupling have been produced in various superlattices $La_{1.85}Sr_{0.15}CuO_4$(LSCO) based superlattices. In LSCO/Sm_2CuO_4 strained superlattices, the in-plane lattice constant of the LSCO layers is increased and the transition temperature (T_c) is decreased. We estimate the effective pressure to be -8 GPa and conclude the in plane Cu-O bond length is an important factor controlling T_c. For the LSCO/$La_{1.65}Sr_{0.35}CuO_4$(metallic) superlattices, a proximity-induced coherence length of 50Å is calculated for the metallic layer using the de Gennes-Werthamer theory.

Introduction

A variety of theories have been proposed to explain the superconducting mechanism in copper oxide superlattices.These include proximity effect[1-7], carrier concentration[8-10], pressure effect[11,12], tunneling effect[13,14] and a 3D-2D crossover (Kosterlitz-Thouless transition)[15-18]. Hydrostatic pressure studies on bulk oxide superconductors have revealed that the transition temperature (T_c) depends strongly on the pressure[11,12]. However, the use of hydrostatic pressure obscures the intrinsic anisotropy of these materials, since both in-plane lattice spacing a (b) and the out-of-plane c axis are isostatically compressed. Superlattice and multi layer films offer the unique opportunity to separate the roles of the bond lengths within the CuO_2 planes and along the Cu-O apex. In-plane compressive or tensile stress can be easily applied by adjusting the lattice mismatch between the alternate layers[19-23].

In addition, the study of the proximity effect between high-Tc superconductors and normal metals in superlattice structures is both scientifically and technologically of great importance. The coupling between the superconducting and normal-metal layers will help us to better understand the nature and origin of superconductivity in the high-T_c cuprates.

In this chapter, we compare the properties of three series of multi layer films containing the superconducting oxide $La_{1.85}Sr_{0.15}CuO_4$. Layers of undoped, semiconducting La_2CuO_4 of Sm_2CuO_4 were inserted in a controlled manner in the LSCO compound using a multi target, laser-ablation technique to study the effect of in -plane Cu-O bond length variation. Alternatively, layers of over doped, metallic $La_{1.65}Sr_{0.35}CuO_4$ were inserted to study the proximity effect.

Because of the relatively small structural differences between these compounds, complete epitaxy was obtained at the interfaces. Thus systematic trends with the stacking periodicity could be identified, reflecting the changes in the in-plane Cu-O bond length and proximity coupling.

In this chapter I describe in situ epitaxial growth of $(La,Sr)_2CuO_4/Sm_2Cu_4$ superlattices, having various periodicity from the very short to large periodicity. These superlattices are classified into three regions: new compounds, strained superlattices, and multi layers, depending on the periodicity of the stacking of $(La,Sr)_2CuO_4$ and Sm_2CuO_4 layers. The new compounds contain three kinds of basic structures such as CuO_5 pyramid, CuO_6 octahedral, and CuO_4 sheet in one unit cell. We have chosen the combination of Sm as Ln, since Sm is contained both in the p-type superconductor: (La, Sr)$_1$Ln$_1$CuO$_4$[24-26]) and in the n-type one: $(Ln,Ce)_2CuO_4$ (Ln=Sm, Eu, Nd and Gd) [27,28]. Furthermore Sm_2CuO_4 has a relatively small lattice constant, a, among the Ln_2CuO_4 compounds, coming close to that of $(La,Sr)_2CuO_4$.(Fig.4-3-1)

Experiment

The films were prepared by a laser deposition technique using the ArF excimer laser(193 nm). Targets were set at the center of a vacuum camber and a laser beam was focused on these targets with the intensity of 1-2 J/cm^2 and the frequency of 15 Hz. Thin films were formed on substrates placed at the opposite side of the targets in the presence of O_2/O_3(8%) atmosphere. The substrates used are MgO(100) and $SrTiO_3$(100) single crystals. The target compositions for the respective layers were $La_{1.85}Sr_{0.15}CuO_4$(LSCO), Sm_2CuO_4 (SmCO), La_2CuO_4 (s-LCO), and $La_{1.65}Sr_{0.35}CuO_4$ (m-LSCO; metal-LSCO). These targets for the

laser ablation were made by a conventional solid-state reaction with sintering at 800℃ for 24 hours in air. These targets were set at the center of the vacuum chamber with background pressure of 1 x 10^{-6} Torr. To produce multi layers, the laser beam was focused on these targets alternately with the fluence of 1 J/cm^2 and the repetition frequency of 15 Hz.

In order to form multi layers, elucidation of the synthetic condition of the thin films using single target is necessary. For the search of the condition in which the thin films of both LSCO and SCO can be formed each thin film was at first deposited independently under various conditions. Substrate temperature was varied from 550℃ to 750℃, and oxygen (O_2+8%O_3)partial pressure was varied from 10^{-1} to 10^{-3} Torr. Then we have determined the suitable conditions for the formation of superlattices, and the LSCO and SCO layers were piled up with the cycle of n/m. Then/m means n-layers of $(La,Sr)_2CuO_4$ and m-layers of Sm_2CuO_4 by using LSCO and SCO targets alternately. We have repeated n=m to be 1 - 120 (1/1 - 120/120) for several tens cycles. (Fig.4-3-2)

A periodicity of 1/1 means the periodic stacking of a half unit cell of LSCO and a half unit cell of SmCO (or s-LCO, of m- LSCO). The two layers define one cycle and this cycle was repeated several times. The superconductivity was measured by a standard four-probe method.

We have formed three series of superlattices as shown in Fig.4-3-3, namely $La_{1.85}Sr_{0.15}CuO_4/Sm_2CuO_4$ (LSCO/SmCO; superconductor/ semiconductor), $La_{1.85}Sr_{0.15}CuO_4/La_2CuO_4$ (LSCO/s-LCO; superconductor/semiconductor), $La_{1.85}Sr_{0.15}CuO_4/La_{1.65}Sr_{0.35}CuO_4$ (LSCO/m-LSCO; superconductor/normal metal).

Note that in the latter two cases, only the Sr doping level was varied between the successive layers. Since the in-plane lattice parameter a varies only weakly with Sr content over this composition range, negligible interfacial stress was expected for these multi layers. On the other hand, large stress effects were

expected for the LSCO/SmCO superlattices, because of the relatively large lattice mismatch of 3.4% (LSCO, 3.78 Å; SmCO 3.91 Å) for these materials, resulting in an expansion of the a axis of the LSCO layers. A necessary condition for the existence of proximity coupling between a superconductor and a normal metal is that the superconducting order parameter extend into the normal metal. The penetration depth of the order parameter depends strongly on the carrier concentration of the normal metal Thus, different penetration depths were expected for the LSCO/m-LSCO and LSCO/s-LCO superlattices, respectively, because of the different carrier concentrations.

The total thickness of the multi layers was 1000 Å. The thickness of the thin films was monitored by a quartz crystal oscillating thickness monitor in situ and confirmed by an optical microscope ex situ. The structures of the films were determined by X-ray diffraction patterns. The superconductivity was measured by a standard four-probe method. The surface morphology was determined by scanning electron microscopy (SEM) (JEOL; JSM-840) and the Two-dimensional surface structure was studied by reflection high-energy electron diffraction(RHEED) and four circle X-ray diffractometer. And the crystal structure of the superlattices were checked by the SIMS (secondary ion mass spectroscopy)(ATOMIKA Co.; A=DIDA3000) with O_2^+, 4kV. Furthermore, TEM(transmittance electric microanalysis.) images have also been observed.

Results and discussion.

The LSCO and SCO thin film can be formed in situ at the substrate temperature of more than 600℃. The LSCO SCO can be made in situ under relatively higher oxygen partial pressure: more than 10^{-2} Torr. The typical X-ray diffraction patterns of LSCO and SCO of the single phase thus formed are shown in Figs.4-3-4(a) and 1(b), respectively. We have formed the superlattices under the conditions in which both LSCO and SCO can be crystallized in situ at the substrate temperature of 700 ℃and the oxygen pressure of 1×10^{-1} Torr. The LSCO SCO layers were piled up with the cycle of n/m:[n layers of $(La,Sr)_2CuO_4$ and m layers of Sm_2CuO_4] by using LSCO and SCO targets alternately. We have repeated n=m to be 1,2,3,4,15,30,60,and 120 for several tens cycles.

The LSCO/SCO superlattices formed here are classified into three regions, according to the number of the stacking periodicity. The first one is the compounds of short periodicity, such as 1/1,2/2,3/3, and 4/4. The second one is the strained superlattice which is in the regions of 15/15 to 30/30 periodicity. The third is the so-called multi layer of $(La,Sr)_2CuO_4/Sm_2CuO_4$, keeping each original property.

Figure 4-3-5 shows the X-ray diffraction patterns and calculated peak position and intensities of the superlattices of LSCO/SCO with the periodicity of: (a) 1/1,(b)2/2,(c)3/3, and (d)30/30. The pattern of Fig.4-3-5(a) is similar to that of the known La (Sr)$SmCuO_4$ having a CuO_5 pyramid structure. The observed X-ray diffraction pattern shows quite similar pattern to that of calculated one in the peak position and the relative intensities of 004($2\theta=28°$) and 006($2\theta=43°$) peaks. In Fig.4-3-5(b) and (c), satellite peaks are observed characteristic of superlattices. The larger the periodicity of each layer, the lower the intensity of the main peak in the X-ray diffraction patterns becomes. Instead, the satellite peaks grow and eventually the main peak separates into two peaks originated

from the LSCO and SCO above the periodicity of 15/15 [see Fig. 4-3-5(d) for 30/30].

From the viewpoint of crystal chemistry, the superlattices of 2/2 and 3/3 can be regarded as new compounds having a long unit cell by the combination of CuO_5 octahedral, CuO_5 pyramid, and CuO_4 sheet in one unit cell. In the stacking periodicity of 2/2 and 3/3, the superlattices do not have their original characters of LSCO and SCO in the crystal structures. Therefore these can be called the new compounds having the combination of CuO_6 octahedral, CuO_5 pyramid, and CuO_4 sheet. The resistivity-temperature curves for these compounds show semiconducting behavior within the treatment done in this experiment (Fig.4-3-6:1/1-4/4).

In the periodicity more than 15/15, the longer the periodic cycle is, the higher the Tc becomes. The superlattices of 15/15, 30/30, and 60/60 show the Tc_{on} of 15, 25 and 38K (Fig.4-3-6), while the LSCO film exhibits the Tc_{on} of 40K and Tc_{zero} of 38K (see Fig.4-3-6). This phenomenon is explained by a pressure effect due to the strain by the lattice mismatch which is observed in bulk samples and also in the $Y_1Ba_2Cu_3O_7/(Nd,Ce)_2CuO_4$ system.[29] The a-axis lengths of LSCO and SCO are 3.78 and 3.91 Å, respectively. The CuO_6 octahedral slab of LSCO is forced to expand in the a direction but the CuO_4 sheet slab of SCO is forced to shrink. Accordingly, the bond distance of Cu-O in the CuO_2 sheet of LSCO is expanded for the sake of mismatching the lattice parameters between LSCO and SCO. Figure 4-3-7(a) shows the changes of the lattice parameter c against the stacking periodicity. In the range of short periodicity (1/1-4/4) the c axis is defined as the compound of the long unit cell, whereas in the region of 15/15-60/60, the X-ray peaks due to original LSCO and SCO emerge and the peak position gradually shifts toward the original compounds due to the relaxation of the strain above 60/60 periodicity. After annealing the sample under 50GPa of O_2

at 450℃, the lattice constant c of the film dies not change. this result shows that the oxygen is well incorporated in the crystal structure at the as-deposited state.

For these stacking sequences. the in-plane lattice constant a is expected to be expanded for LSCO and compressed for SmCO. In order to observe these changes. we have measured the lattice constants a and c with a four-circle x-ray diffractometer. The results are shown in the form of a pole figure in Fig. 4-3-8(a). The figure shows that the LSCO layers and SmCO layers grow epitaxially on the $SrTiO_3$ substrate. The most important observation of Fig. 4-3-8(a) is the difference between the two in-plane lattice parameters for LSCO and SmCO. The variation of the in-plane lattice constant a with the stacking periodicity is shown in Fig. 4-3-8(b). It is seen that the parameter a of the SmCO layer decreases with decreasing stacking periodicity below 60/60. On the other hand, for the LSCO layer, a increases from 3.78 Å at great thicknesses to 3.84 Å at a periodicity of 15/15 with decreasing layer thickness. The changes in c have the opposite sign of those in a. By comparison, for the LSCO/s-LCO multi layer, a remains constant at 3.84 Å. Thus the expansion of a in the LSCO/Sm CO layers may be attributed to an in-plane pressure effect due to the large lattice mismatch. The changes in the lattice constant a correspond to changes in the in-plane Cu-O bond length in LSCO which is forced to expand parallel to the layer interface as the individual layers become thinner. The pressure at the interface of the strained LSCO layers may be estimated using data for bulk LSCO under isostatic pressure, $dP/da=1.6x10^2$ Pa/a [30]. In the case of the15/15 multi layer, a is expanded from its normal value for LSCO of 3.78Å to 3.84Å . The corresponding pressure is 8 GPa.

The pressure effect can also be discussed from another point of view. We consider two sheets in elastic contact and estimate the stress using elasticity theory. In this case, the tensile stress (σ) in the LSCO layer can be written as follows:

$$\sigma = E_i (\alpha_1 - \alpha_2) dT \, dl/ti, \qquad (4\text{-}1)$$

where, dl,Ei, αi, and ti are the lattice mismatch, Young's modulus, thermal expansion coefficient, and thickness of each layer [i=1(LSCO), 2(SmCO)]. Using the values of dT=700 K and Ei =1.5 GPa, and a=10^{-5} K^{-1} [31], the stress in the LSCO layer can be estimated as 3.0 GPa. This value is similar to the pressure derived above from the experimentally observed changes in lattice parameter.(Fig.4-3-9)

Corresponding to the changes of the lattice constant, the critical temperature (T_c) of these strained superlattices decreases rapidly with decreasing number of half unit cells as shown in Fig. 4-3-10(a) (squares and solid line).It should be noted that the in-plane pressure effect is independently induced in these superlattices. Using the value -8 GPa, a negative pressure effect of -2.0 k/GPa can be estimated from the observed T_c decrease of Fig. 4-3-10(a).

Above the cycle of 60/60, the superlattice exhibits similar Tc to the standard LSCO films[Fig.4-3-6(b) for 60/60]. Accordingly, this is a normal multilayered thin film having original properties. The lattice mismatch is partially reduced in the superlattice made of $(La,Sr)_2CuO_4$/ Gd_2CuO_4(lattice constant a;3.89 Å. this superlattice shows the T_{Con} of 18K at the stacking periodicity of 15/15 which is 3 K higher than that of LSCO/SCO [Fig.4-3-6(b)]. This value is expected from the data of the pressure effect in the bulk samples.

For the unstrained superlattices, LSCO/s-LCO and LSCO/m-LSCO, of the other hand, the lattice constant a remains constant over the entire range of layer thicknesses.(Fig.4-3-11) For the former, T_c dose not change down to a periodicity of 15/15 multilayers. (Fig.4-3-12) The T_c reduction for layer thicknesses less than 10/10 periodicity will be discusses later.

The variation of T_c for the super/normal super lattices is shown in Fig. 4-3-10(b). T_c decreases gradually with decreasing number of half unit cells; however,

the T_c decrease deviates markedly from that of the strain at the interface of each layer. Therefore. the question is why the Tc of this kind of superlattice decreases with decreasing stacking periodicity in the absence of lattice mismatch.

There are several possible explanations for this tendency of T_c, such as interlayer coupling[32], 3D-2D (Kosterlitz-Thouless) transition[15-18] , and proximity effect[1-7].

In the following we will examine the possibility of proximity coupling in greater detail. It is well known that the Cooper pairs penetrate from a superconductor into a normal metal, producing a lowering of T_c in the superconducting material [2,3]. In the case that each layer is relatively thick, we calculate T_c using the de Gennes Werthamer (dGW) theory [33,34]. For thin layers, the coupling is calculated according to the Cooper limit theory[35].

The relation between T_c and the thickness of each layer may be written as follows [36,37]:

$$\ln (T_{cs}/T_c)=X(\xi_s^2 k_s^2), \qquad (4\text{-}2)$$

$$[N\xi^2 k\tan(kd)]_s=[N\xi^2\tanh(kd)]_n, \qquad (4\text{-}3)$$

$$X(z)=\Psi(1/2+1/2_z)-\Psi(1/2), \qquad (4\text{-}4)$$

where Ψ is the digamma function and T_{cs}, T_c, k, and d_i are the T_c of superconductor, T_c of normal metal, Boltzmann constant, and thickness of each layer, respectively.

The open circles in Fig. 4-3-13 represent the calculated value using the parameters $V_F=8\times10^6$ cm sec^{-1} and $T_c=34$ K [38]. It is seen that for d>150Å, the dGW theory is in good agreement with the observed data (solid circles). However, below 150 Å, the measured T_c is significantly higher than that predicted by the dGW model. Instead, the observed values approach the value of the Cooper limit calculated using the average (N_0V) of the super/normal system

given by

$$(N_0V)=(N_s^2V_sd_s+N_n^2V_nd_n/(N_sd_s+N_nd_n) \quad (4\text{-}5)$$

and using

$$T_c= D/1.45\exp(-1/N_0V), \quad (4\text{-}6)$$

where D, N_i V_i, and d_i are the Debye temperature, the effective attractive interaction, and the thickness of each layer [i=s(super),n(normal)], respectively [35]. This limit simply corresponds to very thin layers where the electrons experience the average pairing interaction of the m (normal) and s (super) materials.

By fitting eq. (2)-(4) to the experimental data, a coherence length of 50 Å is estimated for the normal m-LSCO layers. According to the BCS theory, the coherence length of the oxide superconductors is very short because of their high superconducting critical temperature (T_c). Therefore weak interaction between electrons and phonons in the normal layer produces this large coherence length of 50 Å. This may be one possible explanation for the long proximity coupling length.

The stacking variation of the superlattices in LSCO/m-LSCO(metal) was changed from 1;1 to 1;2 and 1;3. That is; the number of stacking periodicity of the superconducting layer (LSCO) is fixed at 7 unit cells (42 Å) and that of normal metal layer (m-LSCO) is changed from 7 unit cells to 14 unit (84 Å) and 24 unit (126 Å). The superlattices with the stacking periodicity of 1;2 and 1;3 do not show superconducting behaviors. From the calculation in the Cooper's theory (eq. 4-5 and 4-6), the Tc of 1;2 and 1;3 stacking is predicted 7K and 4.5K, respectively. The Tc below the temperature of 10K is not measured with our apparatus.

Finally, it should be noted that the SEM images of these superlattice have shown good surface. Moreover the RHEED pattern shows streaked lines showing epitaxial growth with as smooth surface.(Fig.4-3-14) These results also assure

strict control of the crystal structure of unit cell order.

SIMS(secondary ion mass spectroscopy) and TEM image are shown in Fig.4-3-15 and Fig.4-3-16. In the result of SIMS, the concentration of Sr is oscillations. They indicate that the LSCO/SCO and LSCO/LCO superlattice are actually constructed as we desired without any inter diffusion at the interfaces. Furthermore, we have compared the R-T behavior of the two kinds of films. One is LSCO(Sr=0.15)/LSCO(Sr=0.35) superlattice and the other is solid soluted LSCO(Sr=0.25). If there is a inter-diffusion of Sr in the superlattice, both of these two films show similar behavior. But they are apparently different each other. This result also suggests that there is no inter-diffuision.

Conclusion

In conclusion, we have formed three series of multilayers, LSCO/SmCO, LSCO/s-LCO, and LSCO/m-LSCO by using a multi target pulsed-laser-ablation technique. The crystal structures and the superconductivity of the superlattice are classified into three regions according to the number of the stacking periodicity: the new compounds for 2/2 and 4/4, strained lattices for 15/15-60-60, and multilayers for more than 60/60.

In the case of LSCO/SmCO strained multilayers, the lattice constants a and c of the LSCO layers are expanded and contracted, respectively. In this superlattice, a pressure of 8 GPa at the interface can be estimated by comparing with isostatic pressure data in the bulk system. A value of 3 GPa is estimated from the thermal expansion elastic calculation.

In the strained lattice region, the critical temperatures become lower as the number of stacking layers decrease due to the pressure effect to the $(La,Sr)_2CuO_4$ by Sm_2CuO_4 layer. The superlattices of 2/2 and 3/3 show the definable main X-

ray peaks with satellites and can be regarded as new compounds with a large unit cell having the combination of CuO_6 octahedral, CuO_5 pyramid, and CuO_4 sheet in one crystallographic unit cell.

This result shows that uniaxial pressure, along the basal plane, giving rise to variations in the Cu-O bond length in the CuO_2 plane is one of the important factors determining T_c. In the case of the unstrained superlattices of LSCO/S-LCO, on the other hand, the lattice constants a and c do not depend on the layering sequence. The T_c decrease in the unstrained superlattices of superconducting/ overdoped-m-LSCO layers was discussed in terms of proximity coupling, and a large coherence length of 50 Å was estimated for the normal-metal layer.

References

1)J.-M.Triscone, D.Ariosa, M.G.Karkut and O.fishier, Phys. Rev.B35, (1987) 3238.

2) W.P.Lowe and T.H.Geballe, Phys.Rev.B29, (1984) 4961.

3) V.Z.Kresin; proc. of Int.Symp.Superconductivity in sendai 1991 p.969.

4)E.Polturak, G.Koren, D.Cohen and E.Aharoni; Phys.Rev.Lett. 67 (1991) 3038.

5)D.S.Dessau, B.O.Wells, Z.-X.Shen, W.E.Spicer, A.J.Arko, R.S.List, C.G.Olson C.B.Eom, D.B.Mitzi, A.Kapitulnik and T.H.Geballe; Appl.Phys.Lett. 58 (1991) 1332.

6)J.Z.Wu, C.S.Ting, W.K.Chu and X.X.Yao ; Phys.Rev.B44 (1991) 411.

7) G.Deutsher ; Physica C 185-189 (1991) 216.

8)T.Nishio, E.Yamada and U.Kawabe ; Phys.Rev.B33, (1986) 2042.

9) M.Z.Cieplak, S.Guha, H.Kojima, P.Lindenfeld, G.Xiao, J.Q.Xiao and C.L.Xiao ; Phys.Rev.B46 (1992)

10)G.E.Blonder, M.Tinkam and T.M.Klapwijk ; Phys.Rev.B (1982) 4515.

11)A,Gupta, R.Gross, E.Olsson, A.Segmuller, G.Koren and C.C.Tsuei ; Phys.Rev.Lett. 64 (1990) 3191.

12)K.Horiuchi, M.Kanai, T.Kawai and S.Kawai ; Phsy.REv.B45 (1992) 13152.

13) G.E.Blonder and M.Tinkham ; Phys.Rev.B 27 (1983) 112.

14) S.I.Park and T.H.Geballe ; Phsy.Rev.Lett. 57 (1986) 901.

15) M.Rasolt, T.Edis and Z.Tesanovic ; Phys.Rev.Lett. 66 (1991) 2927.

16) S.Vadlamannati, Q.Li, T.Venkatesan, W.L.McLean and P.lindenfeld ; Phys.Rev. B 44 (1991) 7094.

17) S.Vadlamannati, Q.Li, X.X.Xi, T.Vemkatesan, w.L.Mclean and P.Lindenfeld ; Physica C 185-189 (1991) 2051.

18) C.S.L.Chun, Guo-Guang Zheng, J.L.Vincentand I.K.Schuller ; Phys.Rev.B. (1984) 4915.

19) J.-M.Triscone, O.fishier, O.Brunner, L.Antognazz, A.D.Kent and M.G.Karkut ; Phys.Rev.Lett. 64 (1990) 804.

20) R.Gross, A.Gi[ta, E.Olsson, A.Segmuller and G.Koren ; Appl.Phys.Lett. 57 (1990) 203.

21) Q.Li, X.X.Xi, D.Wu, A.Inam, S.Vadlamannati, W.L.McLean, T.Venkatesan, R.Ramesh, D.M.Hwang, J.A.martinez and L.Nazar ; Phys.Rev.Lett. 64 (1990) 3086.

22) E.E.Fullerton, J.Guimpel, O.Nakamura and I.K.Schller ; Phys.Rev.Lett. 69 (1992) 3859.

23) S.M.Cui, C.H.Tsai ; Phys. Rev. B 42 (1990) 8615.

24) J.Akimitsu, S.Suzuki, M.Watanabe and H.Sawa ; Jpn.J.Appl.Phys. 27 (1988) L1859.

25) E.Takayama-Muromachi, Y.Matsui, Y.Uchida, F.Izumi, M,Onoda and K.Kato ; Jpn.J.Appl.Pjys. 27 (1988) L2283.

26) H.Sawa, S.suzuki, M.watanabe, J.Akimitsu, H.Matsubara, H.Watabe, S,Uchida, K.Kokusho, H.Asano, F.Izumi and E.Takayama-Muraomachi ; Nature 337 (1989) 347.

27) Hk. Muller-Buschbaum ; Angew. Chem. Int. Ed. Engl. 16 (1977) 674.

28) Y.Tokura, H.Takagi, S.Uchida ; Nature 337 (1989) 345.

29) R.Gross, A.Gupta, E.Olsson, A.Segmuller and G.Koren ; Appl.Phys.Lett. 57 (1990) 203.

30)S.Yomo, C.Murayama, H.Takahashi, N.Mori, K.Kishio, K.Kitazawa and L.Fueki ; Jpn.J.Appl.Phys. 26 (1987) L603.

31) X.-D.Xiang, J.W.Brill, L.E.Delong, L.C.Bourne, A.Zettl, J.C.Jones and L.A.RIce ; Solid State Commun.65 (1988) 1073.

32) Q.Li, X.X.Xi, D.Wu, A.Inam, S.Vadlamannati, W.L.McLean, T.Venkatesan, R.Ramesh, D.M.Hwang, J.A.Martines and L.Nazar ; Phys.Rev.Lett. 64 (1990) 3086.

33) P.G.de Gennes, Rev.Mod.Phys. 36 (1964) 225.

34) N.R.Werthamer ; Phys.Rev. 132 (1963) 2440.

35) L.N.Cooper, Phys.Rev.Lett. 6 (1961) 689.

36) "Superconductivity" edited by R.D.Parks Volume 2, pp.1005 1969 Marcel Dekker

37) "Superconductivity of Metals and Alloys" edited by P.G.de Gennes, pp.227, 1989, Advanced Book Classics.

38) S.A.Wolf and V.Z.Kresin, in Proceedings of the International Symposium on Superconductivity, edited by T.Ishiguro and K.Kajiimura (Springer-Verlag, Tokyo, 1989), p.447.

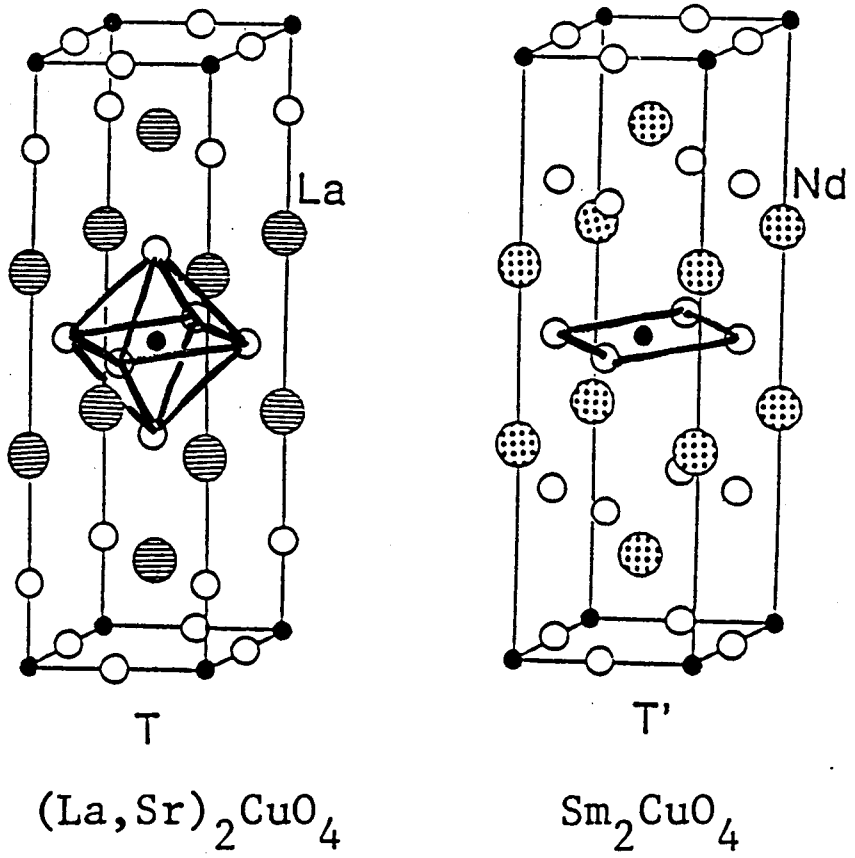

Fig. 4-3-1. Crystal structures of the row types of the copper oxide (T-type and T'-type). In the T-type crystal structure, the apical oxygen. Nevertheres, in the T'-type, there is not apical oxygen.

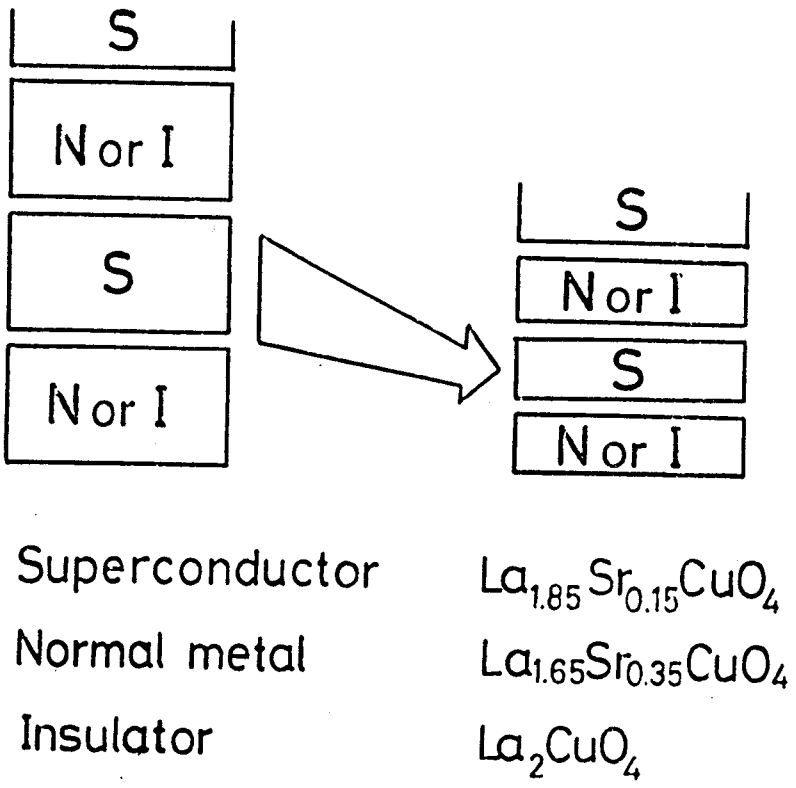

Fig. 4-3-2. Schematic model for the $La_{1.85}Sr_{0.15}CuO_4/La_2CuO_4$ and $La_{1.85}Sr_{0.15}CuO_4/L_{1.65}Sr_{0.35}CuO_4$ superlattices.

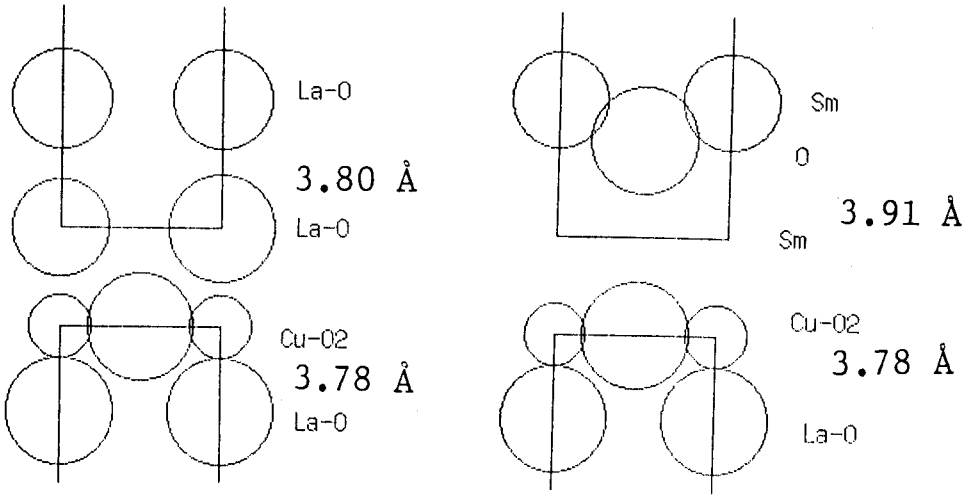

Fig. 4-3-3. Schematic model at the interface between $La_{1.85}Sr_{0.15}CuO_4$ layer and Sm_2CuO_4 layer.

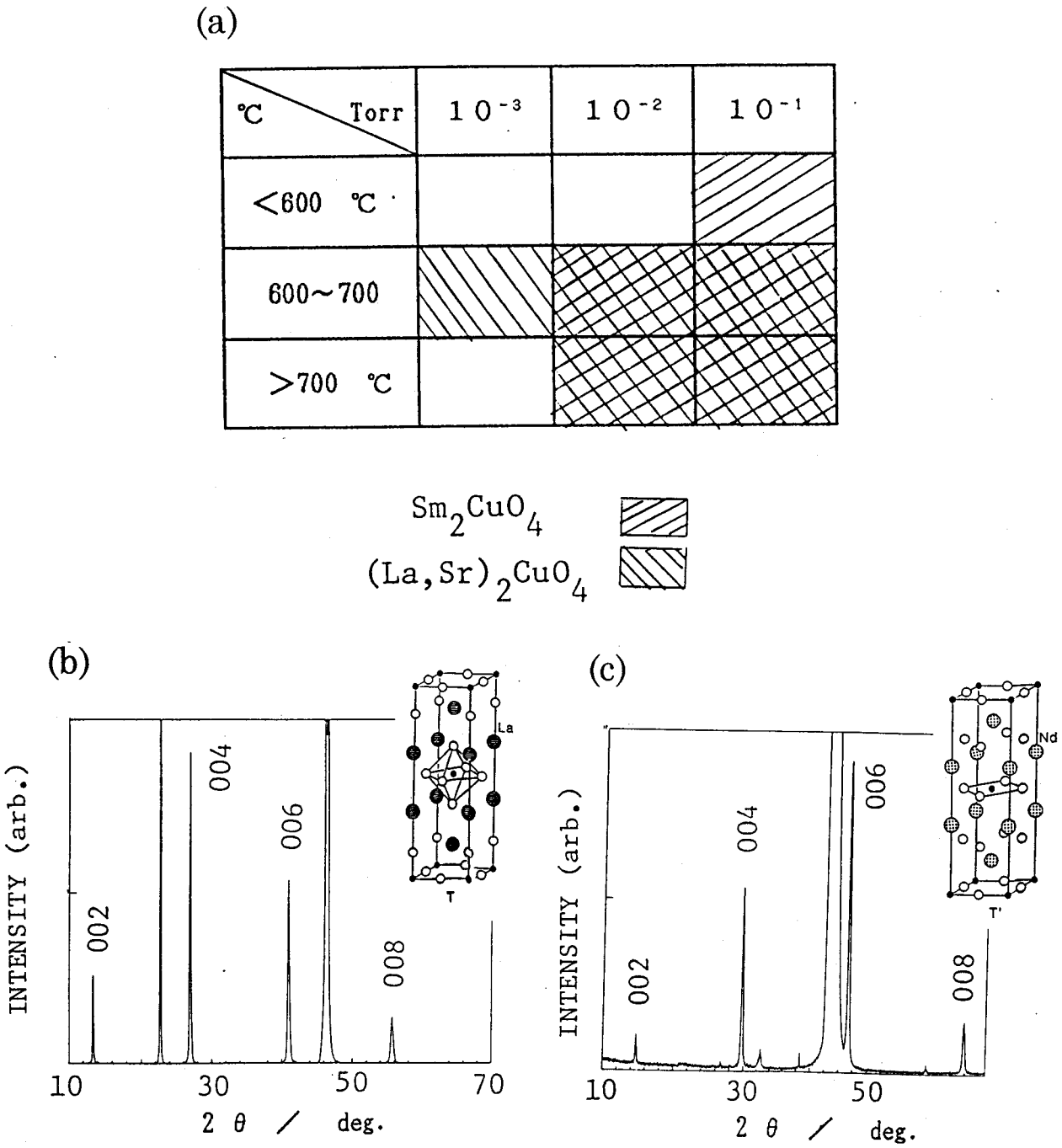

Fig. 4-3-4. (a)The correlation between the substrate temperature and oxygen partial pressure.and (b) X-ray diffraction patterns of as-deposited $La_{1.85}Sr_{0.15}CuO_4$ film(left) and $SmCuO_4$ thin film (right). The crystal structures are correspondence to T phase and T' phase.

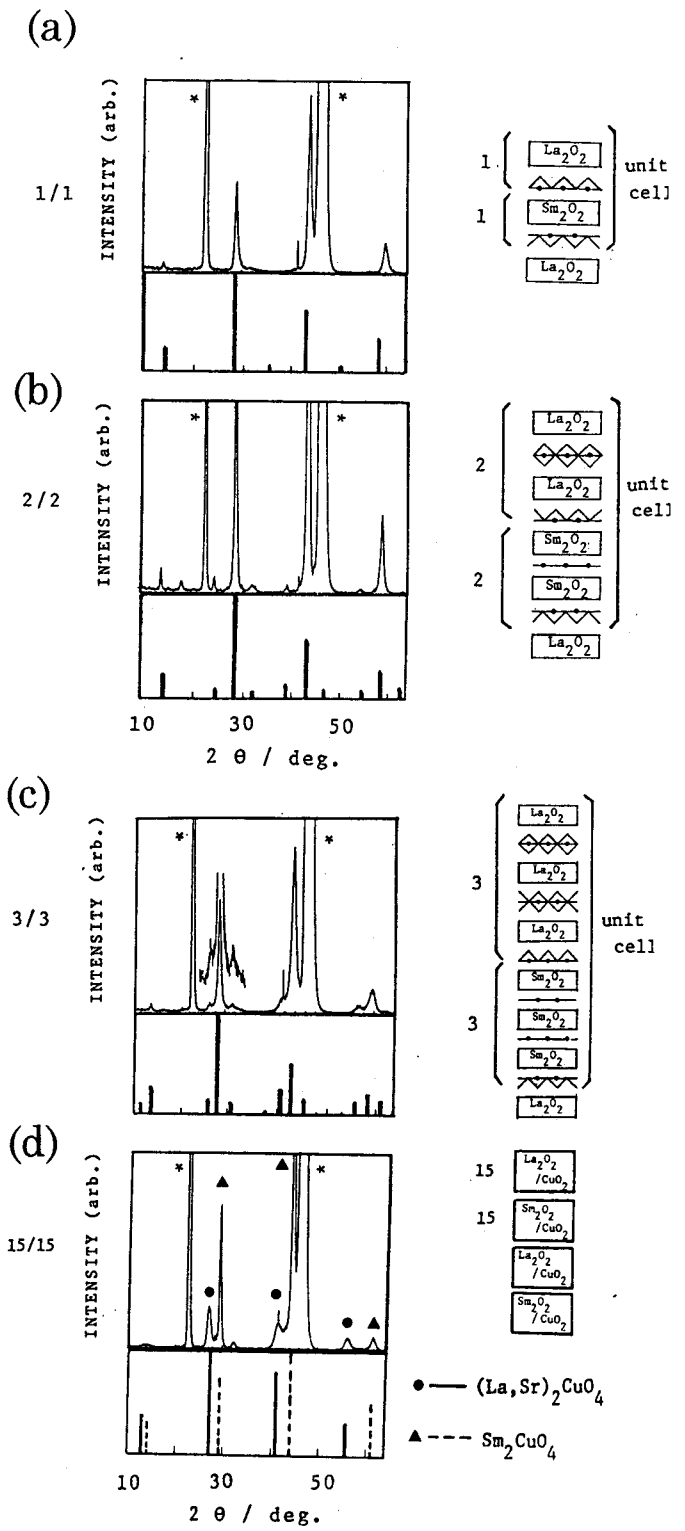

Fig. 4-3-5. Observed x-ray diffraction patterns of the superlattices and calculated patterns. The schematic ideal crystal structures are also shown for the stacking periodicity of (a)1/1, (b)2/2, (c) 3/3 and 15/15～30/30. (*) peaks of $SrTiO_3$ substrate.

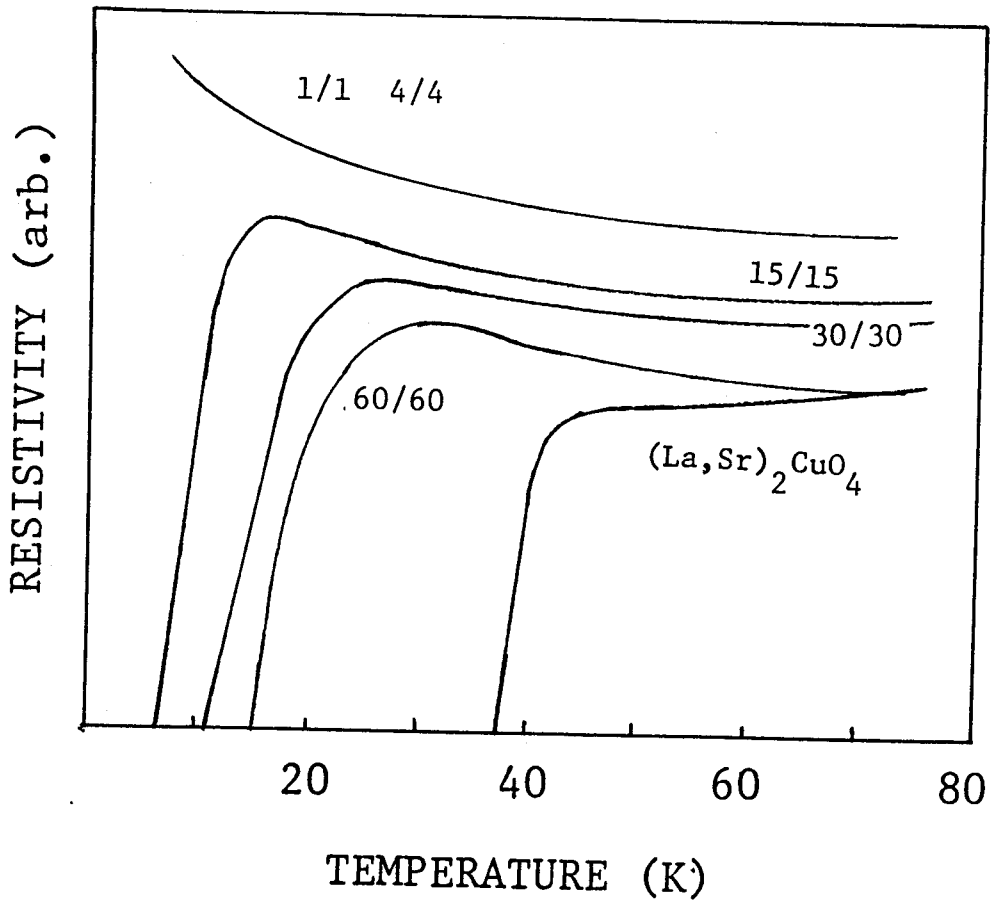

Fig. 4-3-6. Resistivity - temperature curves for the superlattice formed with various stacking periodicity (1/1, 2/2, 3/3 and 15/15 half unit cell) . The periodicities are shown in the figure.

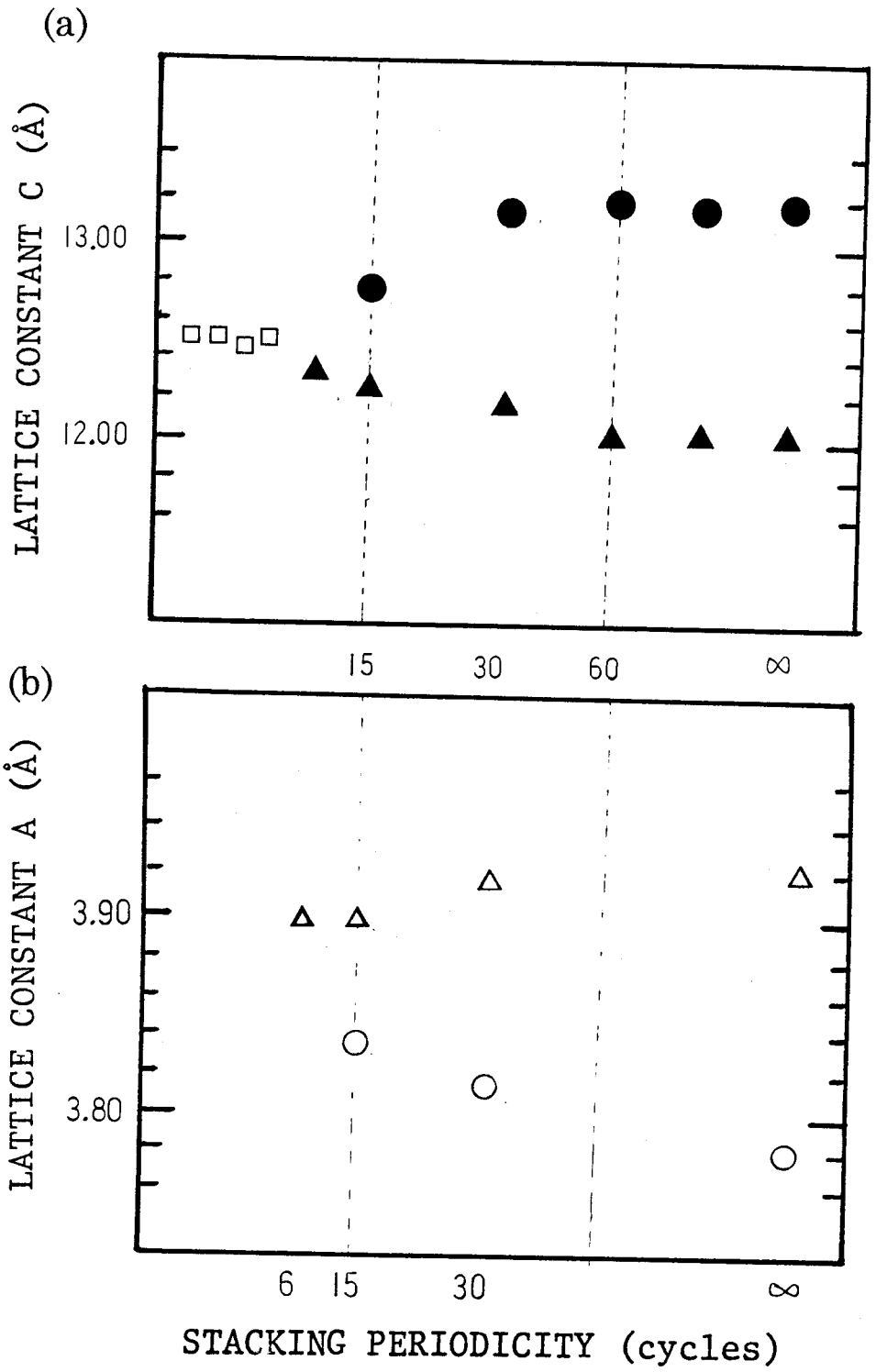

Fig. 4-3-7. Relation between stacking periodicity and the (a) lattice constant c and (b) lattice constant a.

●;lattice constant c of LSCO layer, ▲; lattice constant c of SmCO layer, ○; lattice constant a of LSCO, △;lattice constant a of SmCO.

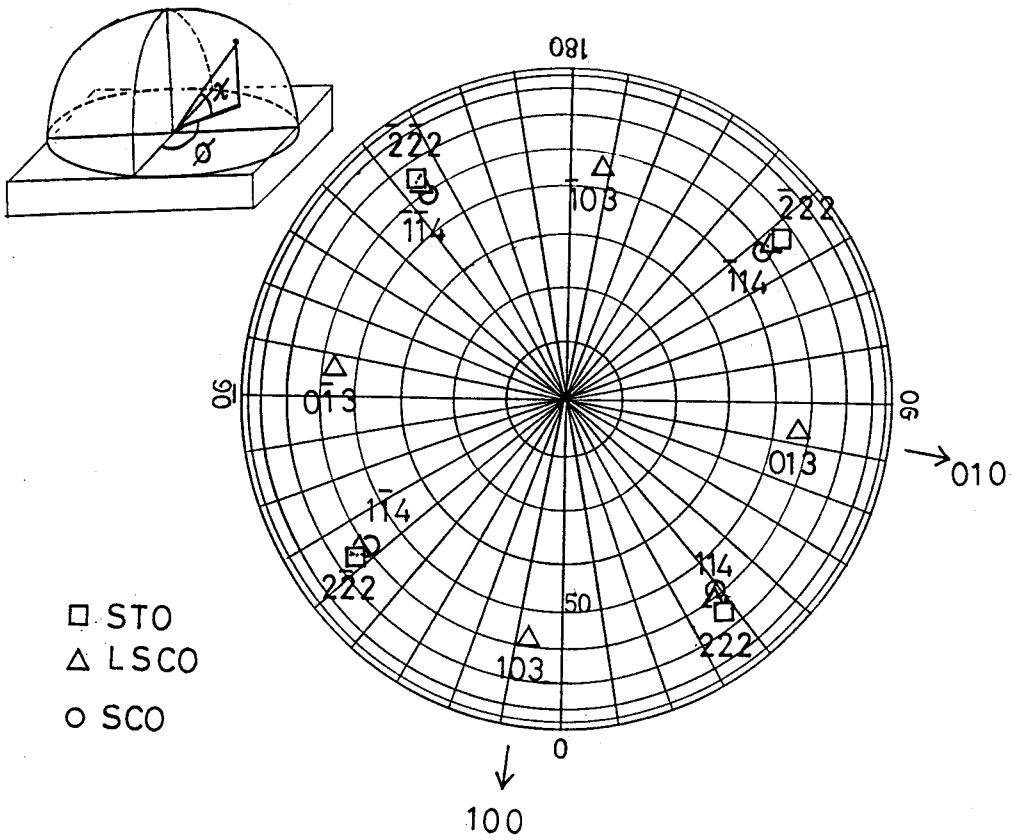

Fig. 4-3-8. Pole fugure of the LSCO/SmCO superlattice deposited on the $SrTiO_3$ substrate.

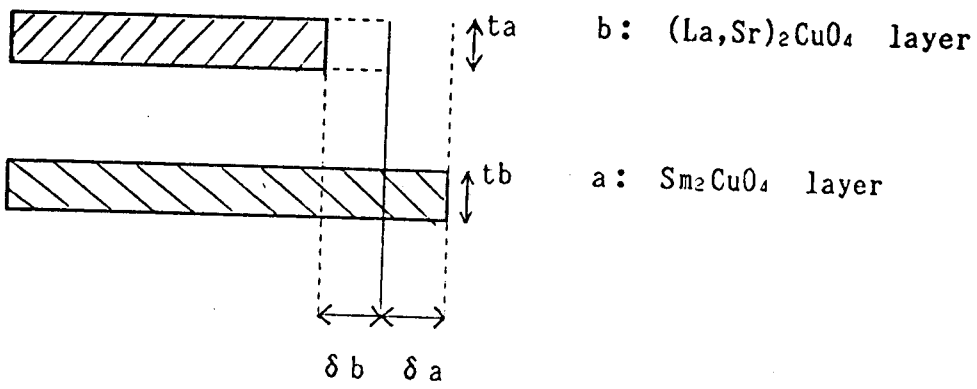

Fig. 4-3-9. Schematic model for the stress analysis by elastic calculation.

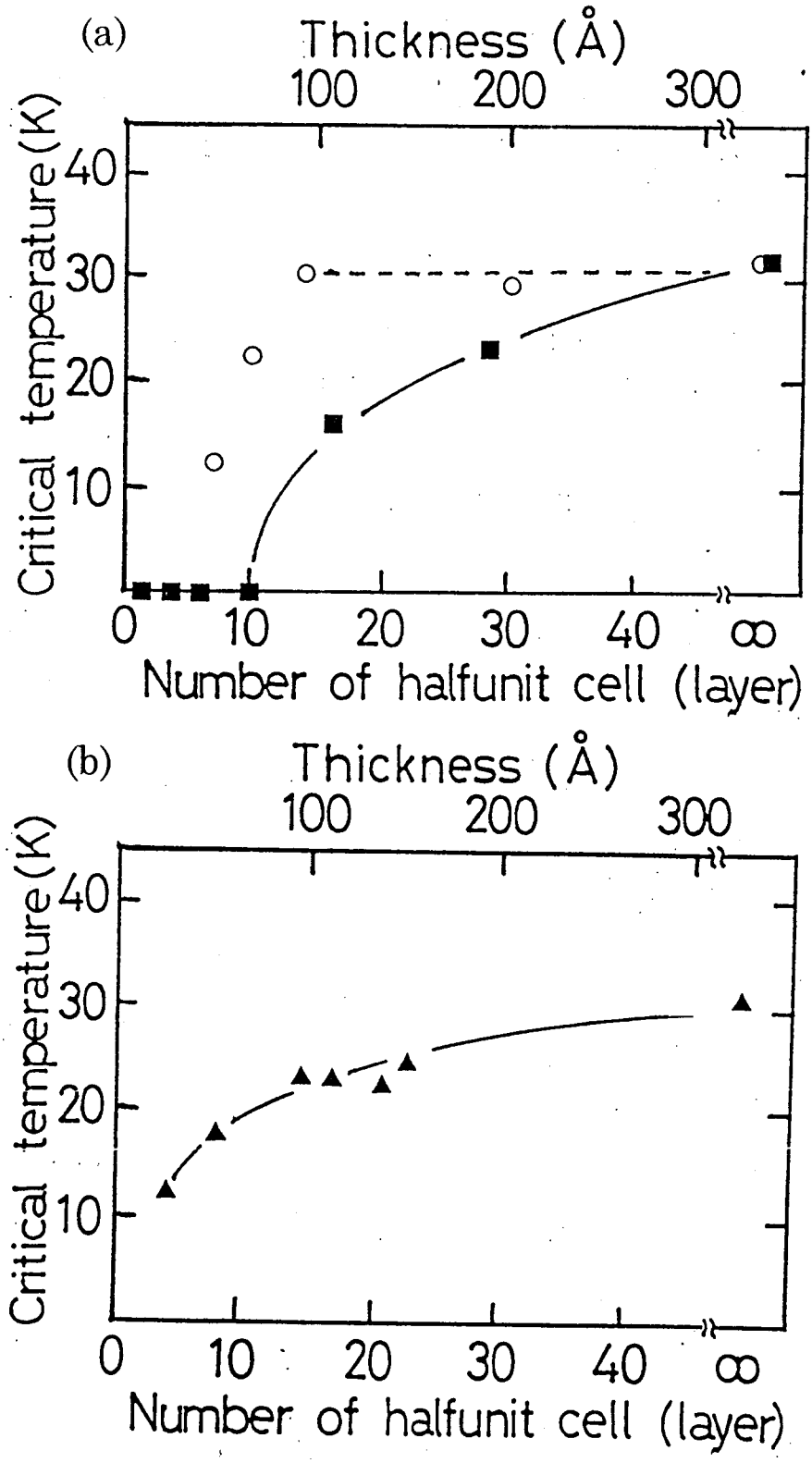

Fig. 4-3-10. Variation of the critical temperature Tc of (a) LSCO/SmCO (solid line), LSCO/LCO (supr/semiconductor, dashed line), and (b) LSCO/m-LSCO(super/normal metal) multilayer films as a function of the umber of half unit cells.

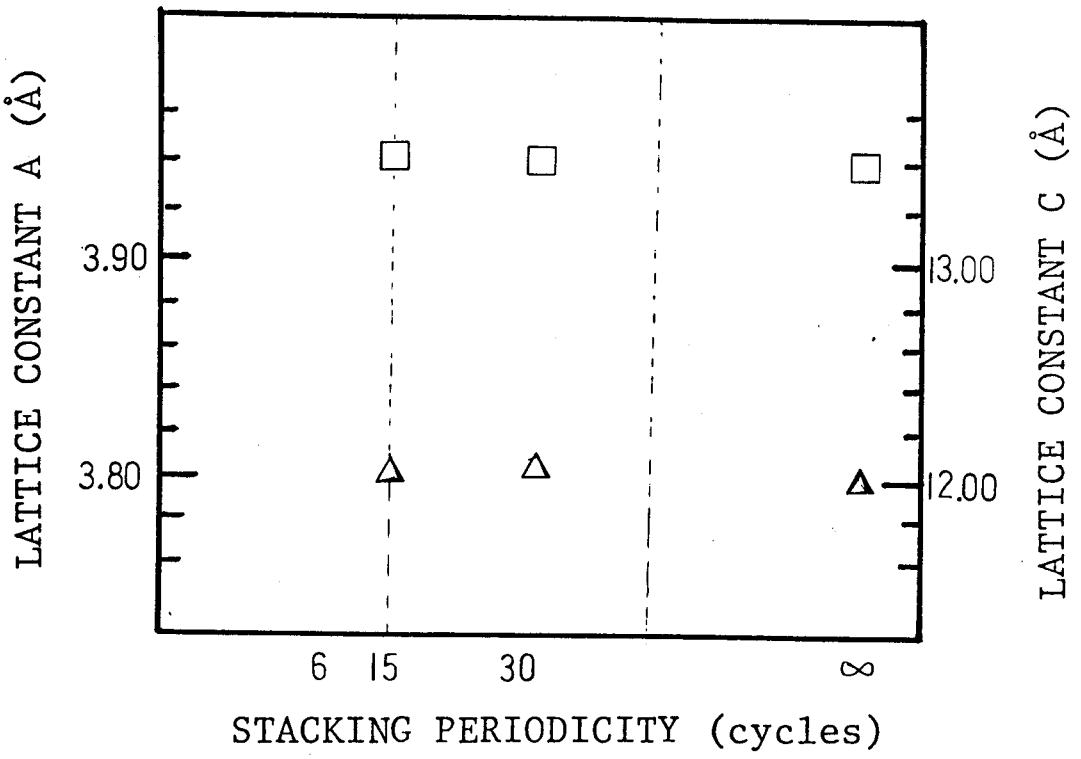

Fig. 4-3-11. The change of the lattice constant a (□) and c (△)of the $(La_{1.85}Sr_{0.15})CuO_4$ / La_2CuO_4 no-strained superlattices against the number of stacking periodicity.

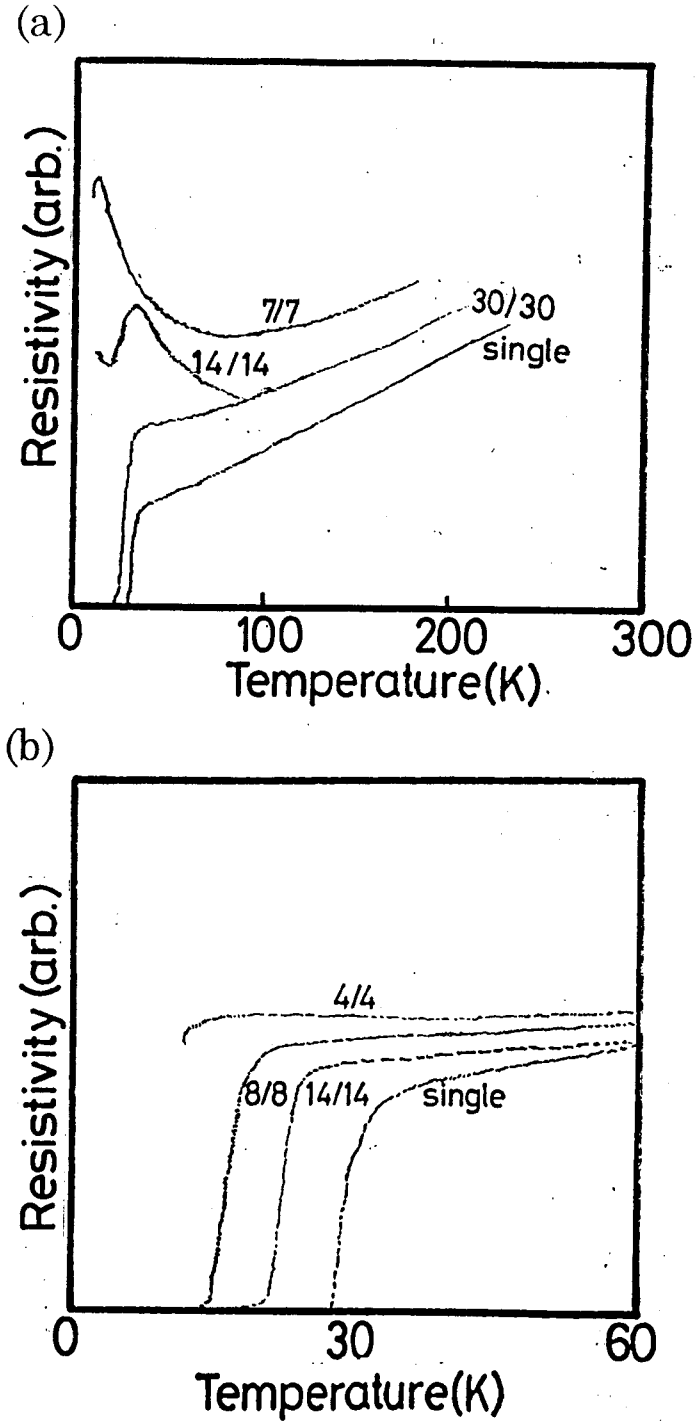

Fig. 4-3-12. Resistivity vs temperature curves of LSCO/LCO (superconductor / semiconductor) superlattices and (b) LSCO/m-LSCO (superconductor / normal metal) superlattices.

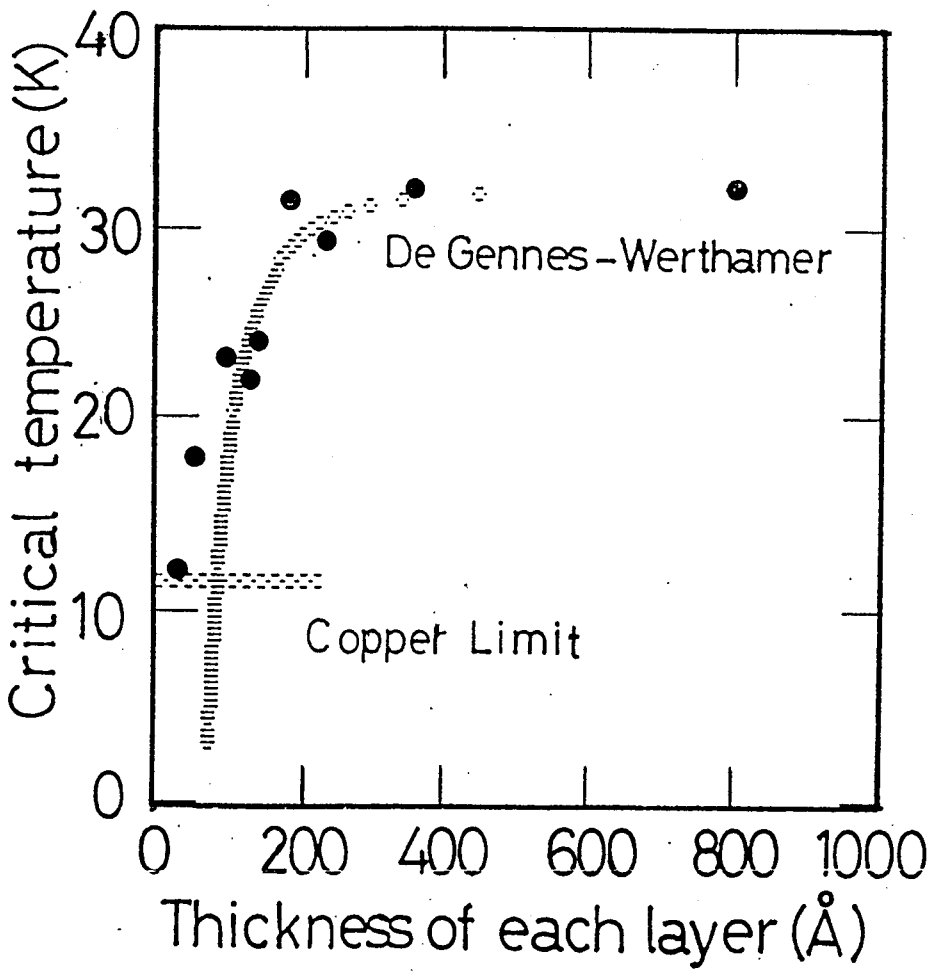

Fig. 4-3-13. Critical temperature of LSCO/SmCO superlattices as a function of the thickness of each stacking layer. Solid circles are the measured values and open circles are calculated using dGW theory and Cooper limit theory, respectively.

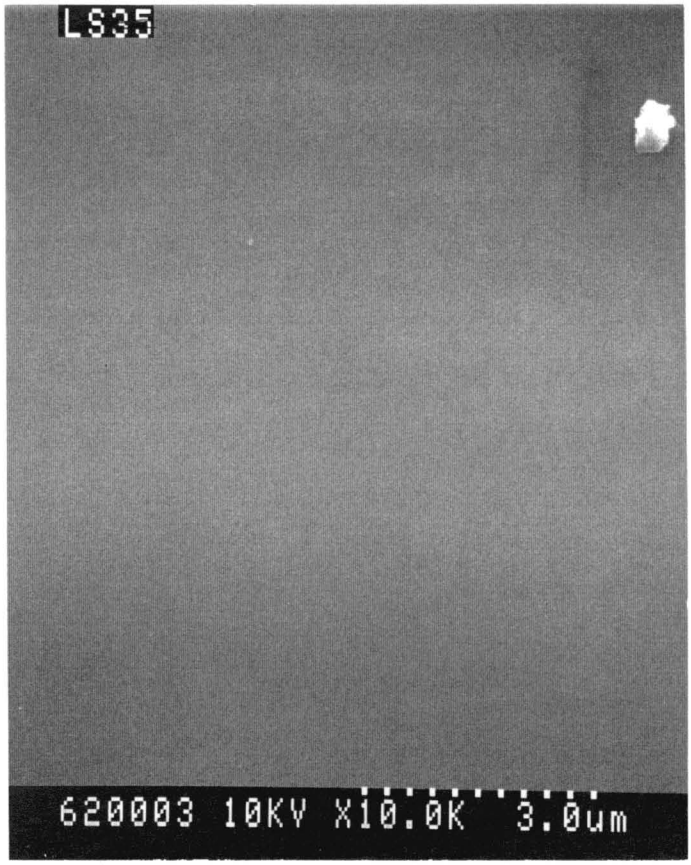

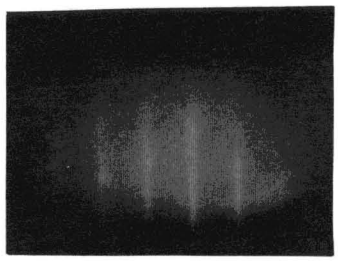

Fig. 4-3-14. SEM image and RHEED pattern of the $(La_{1.85}Sr_{0.15})TiO_3/Sm_2CuO_4$ superlattice.

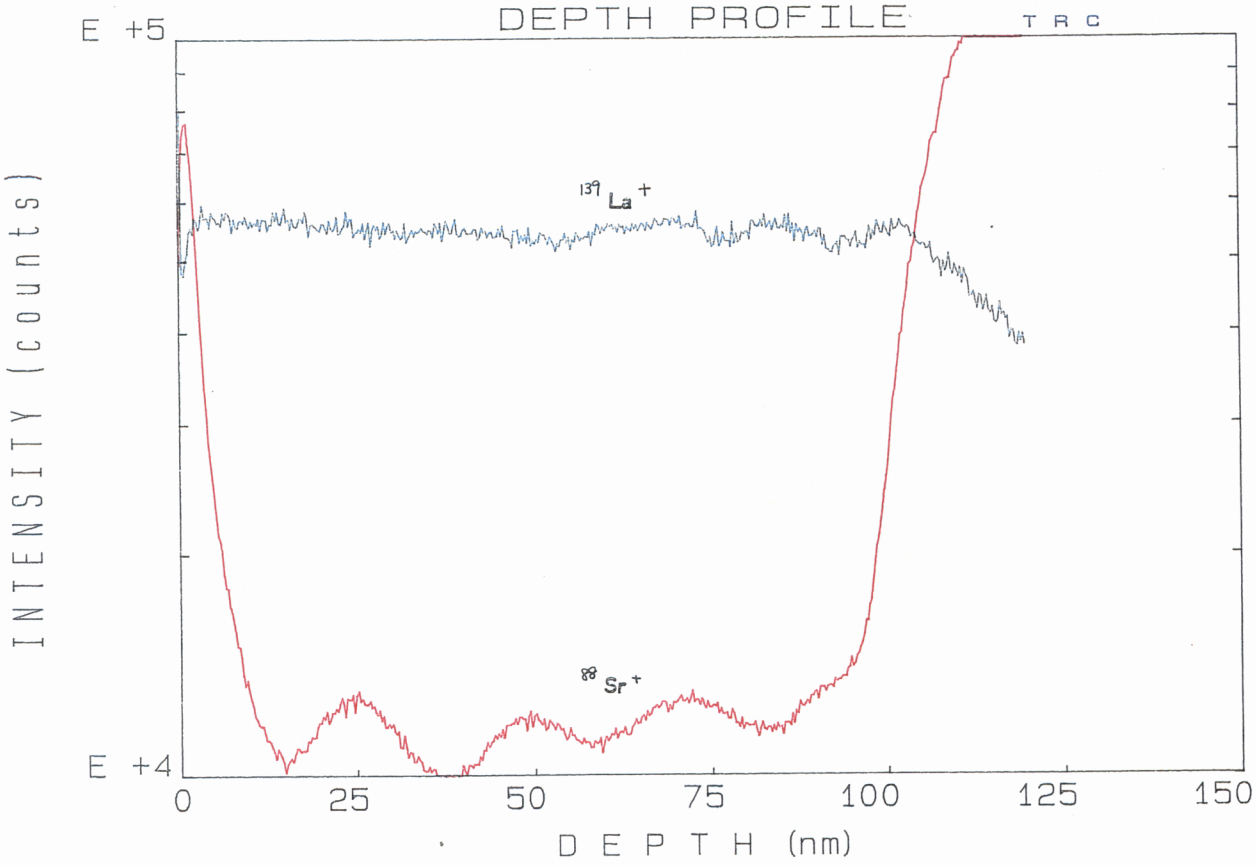

Fig. 4-3-15. SIMS (secondary ion mass spectroscopy) depth profile of LSCO/LCO superlattice. The oscillation of Sr concentration can be observed.

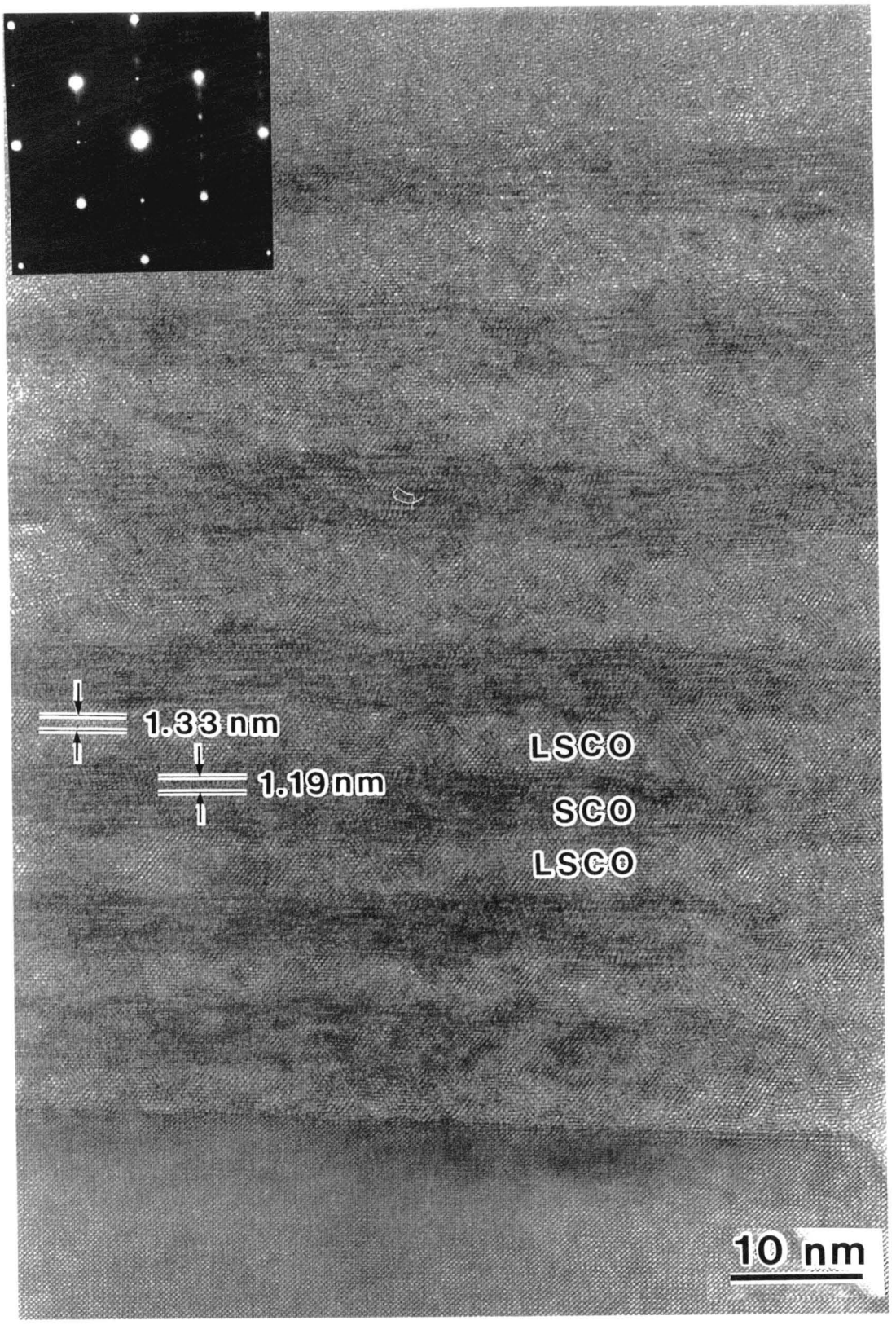

Fig. 4-3-16. TEM image and TED pattern of the cross section of the LSCO/SmCO superlattice.(stacking periodicity of 3/3 unit cell)

Chapter 5

5. Ferro/Di-electric Artificial Lattices

5.1 Introduction

A lot of ferroelectric films, such as $SrTiO_3$[1], $BaTiO_3$[2], $PbTiO_3$[3], $LiNbO_3$ and $LiTaO_3$[4], are of interest for a number of applications. Among them, barium titanate ($BaTiO_3$) is one of the most typical ferroelectric materials, not only because of its simple crystal structure (ferroelectric perovskite)but also because of its economical and scientific importance for applications, such as nonvolatile memories, electro-optic switches and detectors. Therefore, a large number of studies have been performed to elucidate the mechanism giving rise to the ferroelectricity of this material and to improve the properties[1]. To enhance the ferroelectric behavior of $BaTiO_3$, for example, various kinds of cations have been substituted for Ba and Ti. In particular, when Ba is replaced by Sr as a solid solution, the dielectric constant increase dramatically[2](Fig.5-1-1). Nevertheless, it have not been made clear the reason why the dielectric constant increases so high. Isostatic pressure is also effective to enhance the dielectric constant[3,4]. Superlattice, man-made materials, will be very essential approach to control the crystal structures and ferroelectric properties artificially. With this approach, atoms such as Ba and Ti in $BaTiO_3$ can be replaced site-selectively with an atomic order accuracy and strain can be introduced by a combination of different layers(Fig.5-1-2). In this chapter, we report for the first time the observation of novel super-dielectric properties in strained superlattices of $BaTiO_3$ and $SrTiO_3$ or $CaTiO_3$. The combination of $BaTiO_3$ - $SrTiO_3$ show the large dielectric value in their solid solution of $(Ba,Sr)TiO_3$. The combination of $BaTiO_3$ - $CaTiO_3$, on the other hand, show continuous change in their dielectric

constant(Fig.5-1-1).

The tetragonal form of $BaTiO_3$ exhibits ferroelectric distortions involving displacements of the cations(Ti^{4+}, Ba^{2+}) relative to the anions(O^{2-}), leading to a net dipole moment per unit volume(Fig.5-1-3). These soft mode distortions correspond to c axis /a axis lattice strain in tetragonal $BaTiO_3$. When $BaTiO_3$ layers (called BTO hereafter) are combined with $SrTiO_3$ layers (called STO hereafter) or $CaTiO_3$(CTO) as BTO/STO or BTO/CTO superlattices, there is a relatively large mismatch of 2.5% or 5.5% between the in-plane lattice parameters (BTO;3.990Å, STO;3.905Å and CTO;3.820). Thus, strain is induced by changing the periodicity of the strained superlattices. Larger ion shifts are expected in the case of larger lattice mismatch. In order to study the importance of the soft-mode coupling with the lattice strain, ferroelectric strained superlattice is also effective, because even is cases with small strain in BTO, the strain energy strongly affects the phase transition as was indicated in the bulk sample[5].

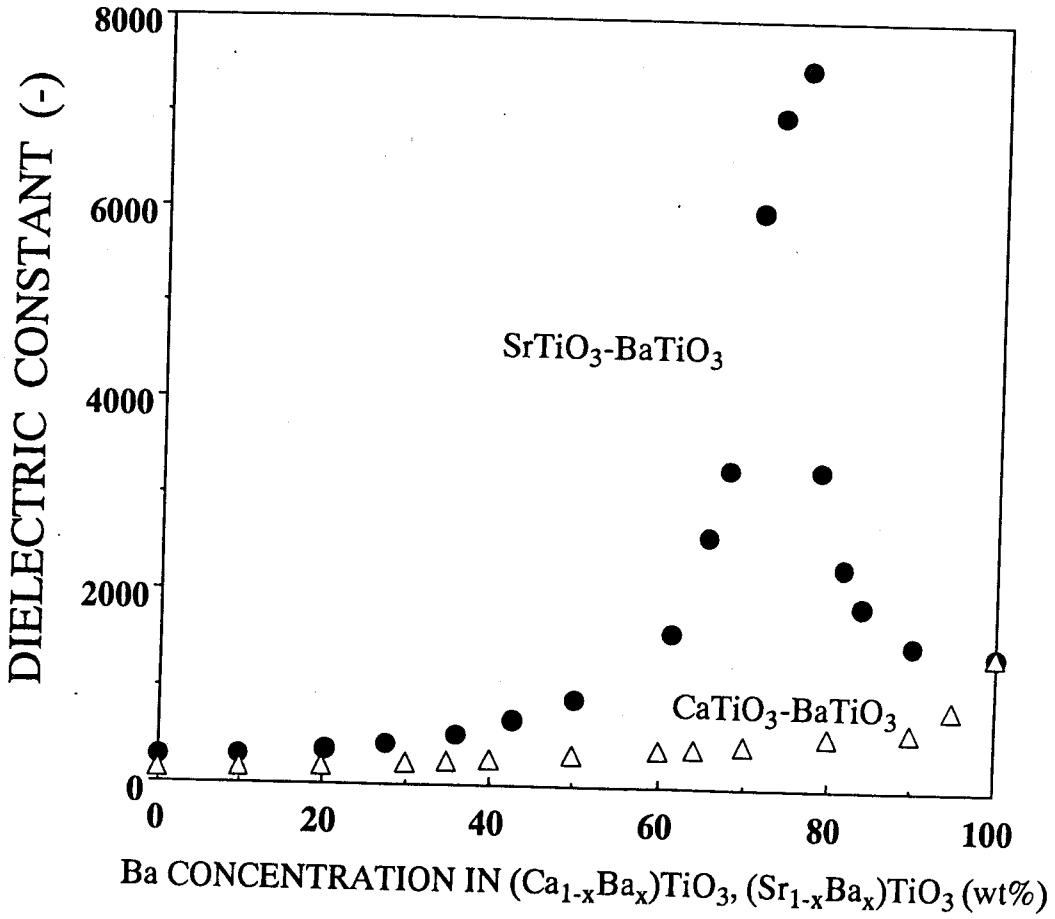

Fig. 5-1-1. The change of dielectric constant in the solid solution of $SrTiO_3$-$BaTiO_3$ and $CaTiO_3$-$BaTiO_3$.

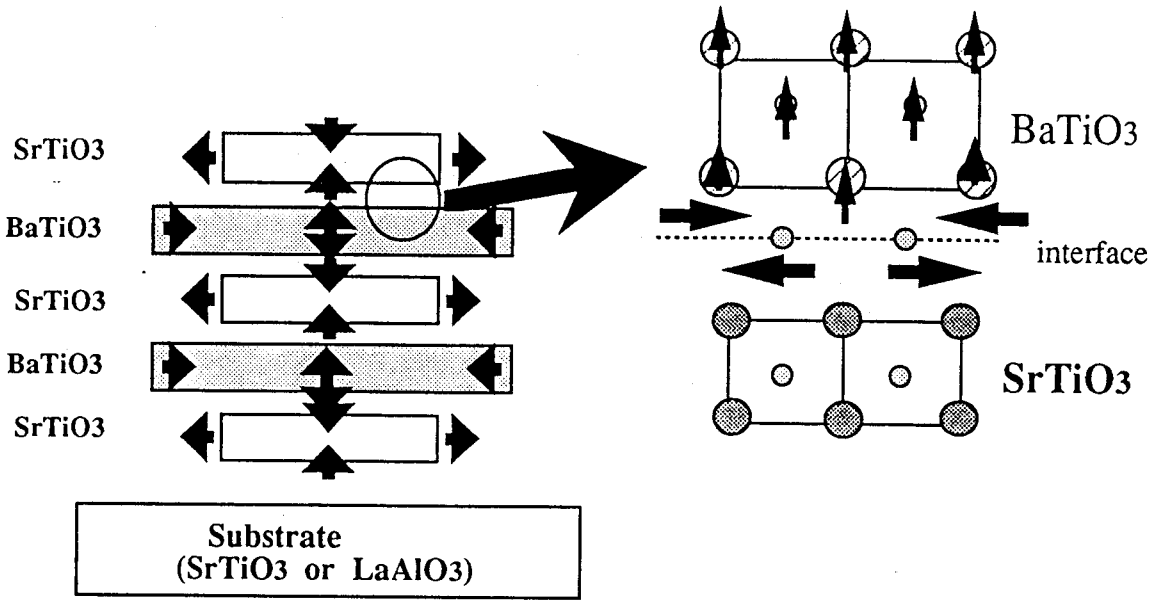

Fig. 5-1-2. A schematic model of strained $BaTiO_3/SrTiO_3$ superlattice.

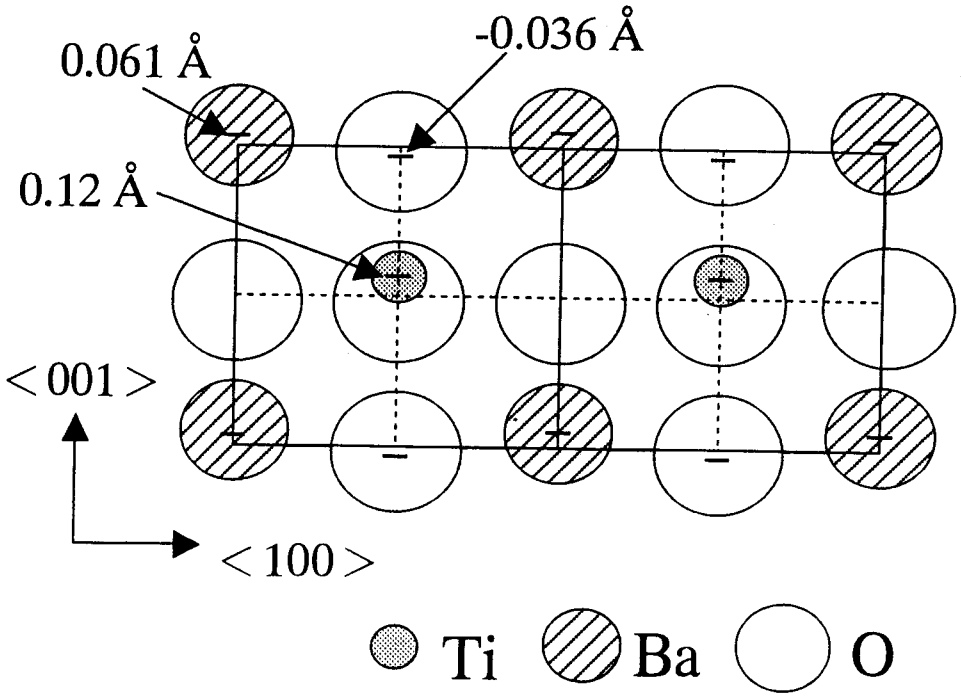

Fig. 5-1-3 Stricture of tetragonal $BaTiO_3$ projected on (010), showing atomic displacement.

5-2. Growth control of single phase thin film crystals

- $BaTiO_3$, $SrTiO_3$, $CaTiO_3$ -

Abstract

We have formed the films of ferroelectric or dielectric materials ($BaTiO_3$, $SrTiO_3$ and $CaTiO_3$)by the laser ablation on the $SrTiO_3$, $LaAlO_3$ and MgO single crystal (100) substrate. All the films can be formed epitaxially on the $SrTiO_3$ substrate with c-axis orientation. The electrical behaviors of these films such as dielectric constant and remnant polarization are quite similar to that of single crystals in bulk samples. These results are the bases parameter for constructing dielectric/ferroelectric superlattices (in chapter 5-3 and 5-4).

Experiment

In this study, the $BaTiO_3$ and $SrTiO_3$ or $CaTiO_3$ layers were stacked alternately by a multi target pulsed laser deposition technique. This technique offers advantages for film growth, including epitactic growth at low substrate temperatures; congruent deposition of materials with complex stoichiometries and facile deposition of materials with high melting points[6,7]. In our experiment, stoichiometric sintered $BaTiO_3$(BTO), $SrTiO_3$(STO) and $CaTiO_3$(CTO) pellets were used as ablation targets as described in chapter 5-1. An ArF excimer laser beam (wave length: 193 nm) was focused onto the target of BTO and STO or CTO alternately with an energy density of 500 mJ/cm^2, and the BTO and STO or CTO layers were deposited on conductive 1%-Nb doped single crystal $SrTiO_3$(100), $LaAlO_3$(100) and MgO(100) substrates which size were 10 x 5 x 0.5^t mm. The thickness of the BTO , STO and CTO films

were about 1000 - 3000Å. The films were formed at 600 - 650 ℃ in an oxygen/ozone(8%) ambient at a pressure of 1 - 3 mTorr. This condition is suitable for the formation of BTO, STO and CTO films commonly. The deposition rate was 10-15 Å/min. The change of lattice parameter of the films was measured by 2θ - θ X-lay diffraction (Rigaku, RAD-C) and four circle X-ray diffraction methods (Rigaku, RINT-9000). The epitaxy of the films was also confirmed by reflection high energy diffraction (RHEED) with acceleration voltage of 15 kV and by the pole figure obtained by the four circle X-ray measurement. Dielectric constants (ε r) of the films were measured by LCR meters with changing the temperature and applied frequency from 20 ℃ to 200 ℃ and from 10^1 to 10^6 Hz, respectively (WAYNE KERR, LCR Meter 4210).

Results and discussion

Figure 5-2-1 (a) and (c) show X-ray diffraction patterns of $SrTiO_3$(STO) and $BaTiO_3$ (BTO) films formed on the $LaAlO_3$(LAO) substrate (lattice constant a= 3.79Å). The STO and BTO films grown with 100% c-axis orientation perpendicular to the substrate surface on LAO substrates with a FWHM (full width at half maximum) of below 0.15° . Fig. 5-2-1 (b) and (d) show calculated X-ray diffraction pattern of STO and BTO, respectively with assuming the c-axis oriented crystal structures. The peak position and the intensity of the (001) and (002) diffraction of the calculated data are quite similar to that of experimental one. The lattice constant c of BTO and STO film are 4.040Å and 3.905Å, respectively.

We have measured the in-plane orientation of the BTO and STO films with a four-circle x-ray diffractometer. The results are shown in the form of a pole

figure in Fig. 5-2-2. The four {111} reflections of the $BaTiO_3$ film are located with the angle of 90° . This result shows that the BTO film oriented not only in c-axis but also a and b-axis, that is BTO film grown epitaxially on the substrate.

The dielectric constant of the excimer laser ablated BTO and STO films with a thickness of 0.1 μm are determined to be 400 and 300 at room temperature. The dissipation factor (tan δ) of these films have 0.01-0.02 at 1 kHz. Ferroelectricity of the BTO film has been investigated by observing the polarization hysteresis and the results are shown in Fig. 5-2-3, indicating clear and large remnant polarization (P_r) of 15 $\mu C/cm^2$ and coercive field of 10 kV-cm. This remnant polarization value is almost similar to that of the theoretically predicted value (Pr=25 $\mu C/cm^2$). The relatively higher coercive field of Fig.5-2-3 may be essential in the film samples associated with a crystallinity, micro structures of the domain. and the residual stress from the substrate. Resistivity is in the range of $>10^{10}$ Ωcm. The SEM images revealed that only those possess a very smooth surface.

Figure 5-2-4 shows X-ray diffraction patterns of $CaTiO_3$ films deposited on the various substrate of (a) $LaAlO_3$ (a=3.76Å), (b) $SrTiO_3$ (a=3.905Å) and (c) MgO (a=4.20Å) . Ii is interesting that $CaTiO_3$ film can growth with c-axis orientation on the $LaAlO_3$ and $SrTiO_3$. In these case, lattice mismatch is only 0.76% and 2.2%, respectively. In the film growth on the MgO substrate, on the other hand, (111) orientation occurs on be half of (100) orientation owing to quite large lattice mismatch (10.0%). In the case of $CaTiO_3$ film deposited on $SrTiO_3$ substrate, the CTO film epitaxially on the STO substrate from the result of pole figure measurement. The dielectric constant (ε r) and dispassion factor (tan δ Å) keep almost constant in the applied frequency between 1 kHz to 1 MHz.(Fig.5.2-6(a)) Furthermore, C-V curve show flat pattern indicate that the film is not the ferroelectric behavior. (fig.5-2-6(b))

X-ray diffraction pattern shows a c-axis preferred orientation and D-E hysteresis can be observed indicating the ferroelectric behavior. (Fig.5-2-7)

Conclusion

In conclusion, the ferroelectric or dielectric thin films such as $BaTiO_3$, $SrTiO_3$ and $CaTiO_3$ have been formed by the laser ablation on the $SrTiO_3$, $LaAlO_3$ and MgO single crystal (100) substrate. All the films can be formed epitaxially on the $SrTiO_3$ substrate with c-axis orientation. The electrical behaviors of these films such as dielectric constant and remnant polarization are quite similar to that of single crystals in bulk samples.

References

1) N.Inoue, I.Toyama, S.Kashiwabara, S.Toshima and R.Fujimoto ; J. Vacuum. Soc. Jpn. 36 (1993) 410.

2) C.S.Chern, J.Zhao, L.Lup, P.Lu, Y.Q.Li, P.Norris, B.Kear, F.Cosandey, C.J.Maggiore, B.Gallois and B.J.Wilkens ; Appl.Phys.Lett. 60 (1992) 1144.

3) H.Nakazawa, H.Yamane and T.Hirai ; Jpn.J.Appl.Phys.; 30 (1991) 2200.

4) B.S.Kwak, K.Zhang, E.P.Boyd and A.Erbil and B.J.Wilkens ; J.Appl.Phys. 69 (1991) 767.

5) K.Iijima, T.Terashima, K.Yamamoto, K.Hirata and Y.Bando, Appl. Phys. Lett., 56 (1990) 527.

6) K.Uchio, N.Y.Lee, T.Oba, N.Ushiki, H.Aburataniand Y.Ito ; J.Ceramic Soc.Jon. 100(1992) 1091.

7) K.Sreenivas, A.Mansingh and M.Sayer ; J.Appl.Phys. 62 (1987) 4475.

8) T.Hirano, M.Taga and T.Kobayashi ; Jpn.J.Appl.Phys. 32 (1993) L1730.

9) K.R.Carroll, J.M.pond, D.B.Chrisey, J.S.Horwitz, R.E.Leuchtner and K.S.Grabowski ; Appl.Phys.Lett. (1993) 1845.

10) M.Yoshimoto, H.Ohkubo, N.Kanda and H.Koinuma ; 31 (1992) 3664.

11) S.Yamamichi, T.Sakuma, K.Takemura and Y.Miyasaka ; Jpn.J.Appl.Phys. 30 (30) 2193.

12) H.Yamaguchi, S.Matsubara and Y.Miyasaka ; Jpn.J.Appl.Phys. 30 (1991) 2197.

13) K.Okuwada and S.Komatsu ; J. Ceramic Soc. Jpn. 100 (1992) 1085.

14)H.F.Cheng, M.H.Yeh, K.S.Liu and I.N.Lin ; Jpn.J.Appl.Phys. 32 (1993) 5656.

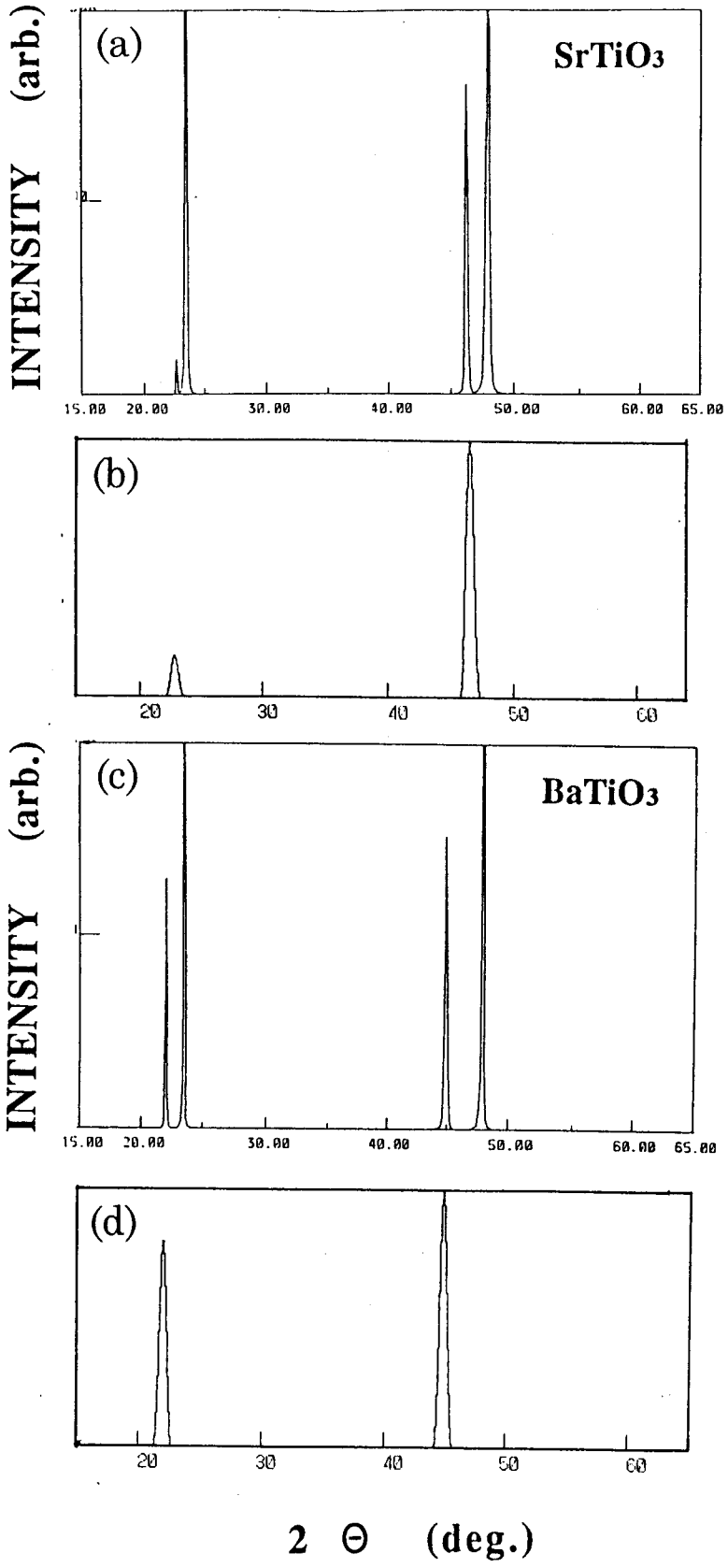

Fig. 5-2-1. X-ray diffraction pattern of $SrTiO_3$(a), (b) and $BaTiO_3$ (c), (d) deposited on $LaAlO_3$ (100) single crystals.
(a) and (c) are the observed X-ray diffraction pattern.
(b) and (d) are that of calculated pattern.

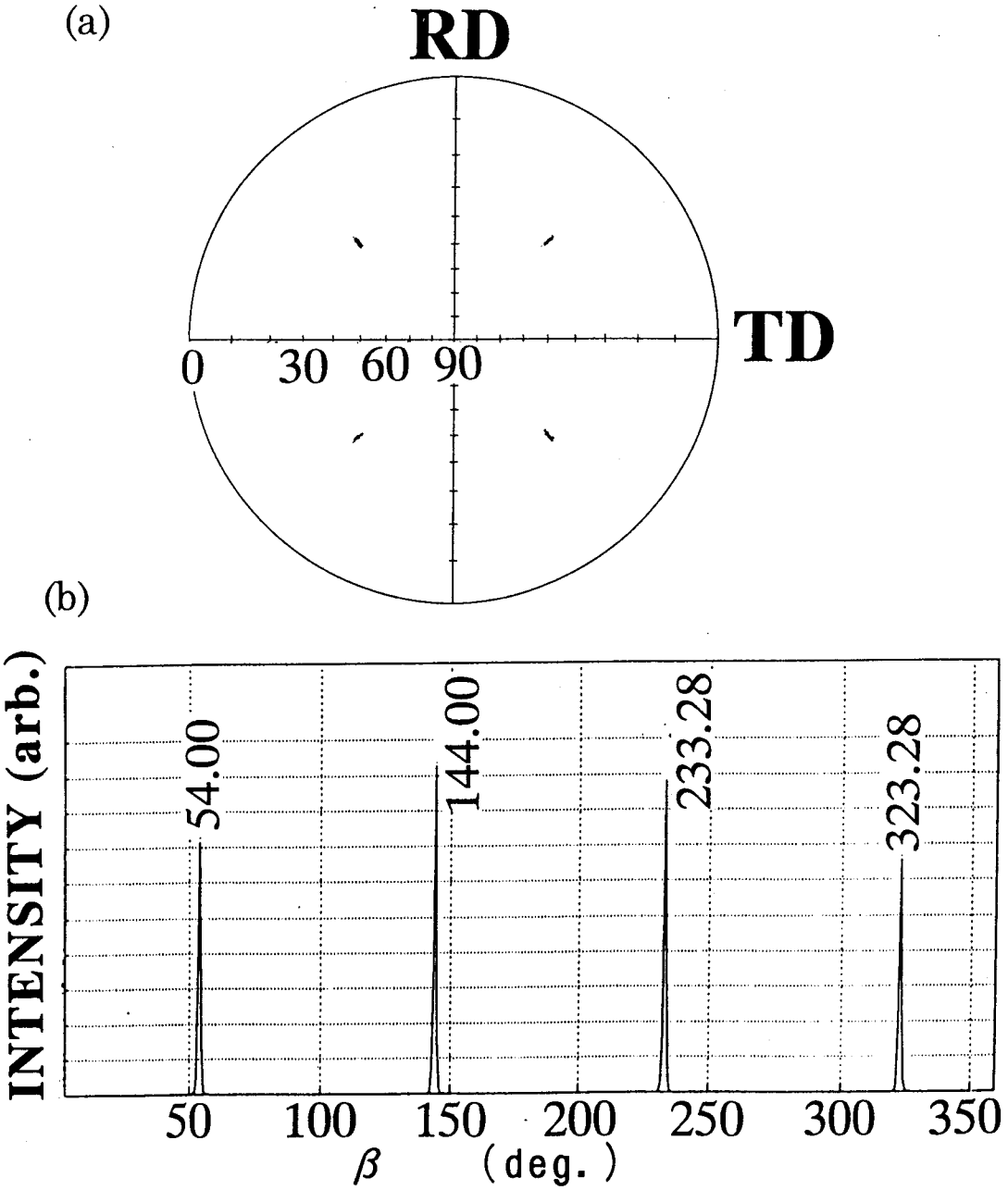

Fig. 5-2-2. X-ray pole figure(a) and β-scan of the $BaTiO_3$ films(b) in the X-ray diffraction patterns.

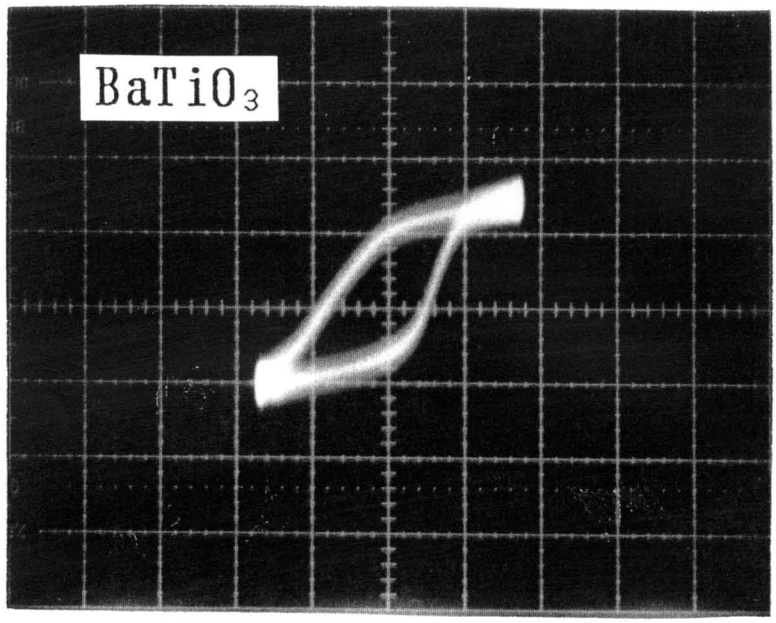

Fig. 5-2-3. D-E hysteresis curve of the $BaTiO_3$ film
(X; 20 kV/cmdiv., Y; 16 μ C/cm^2)
film thickness is 4000 Å, measured at RT.

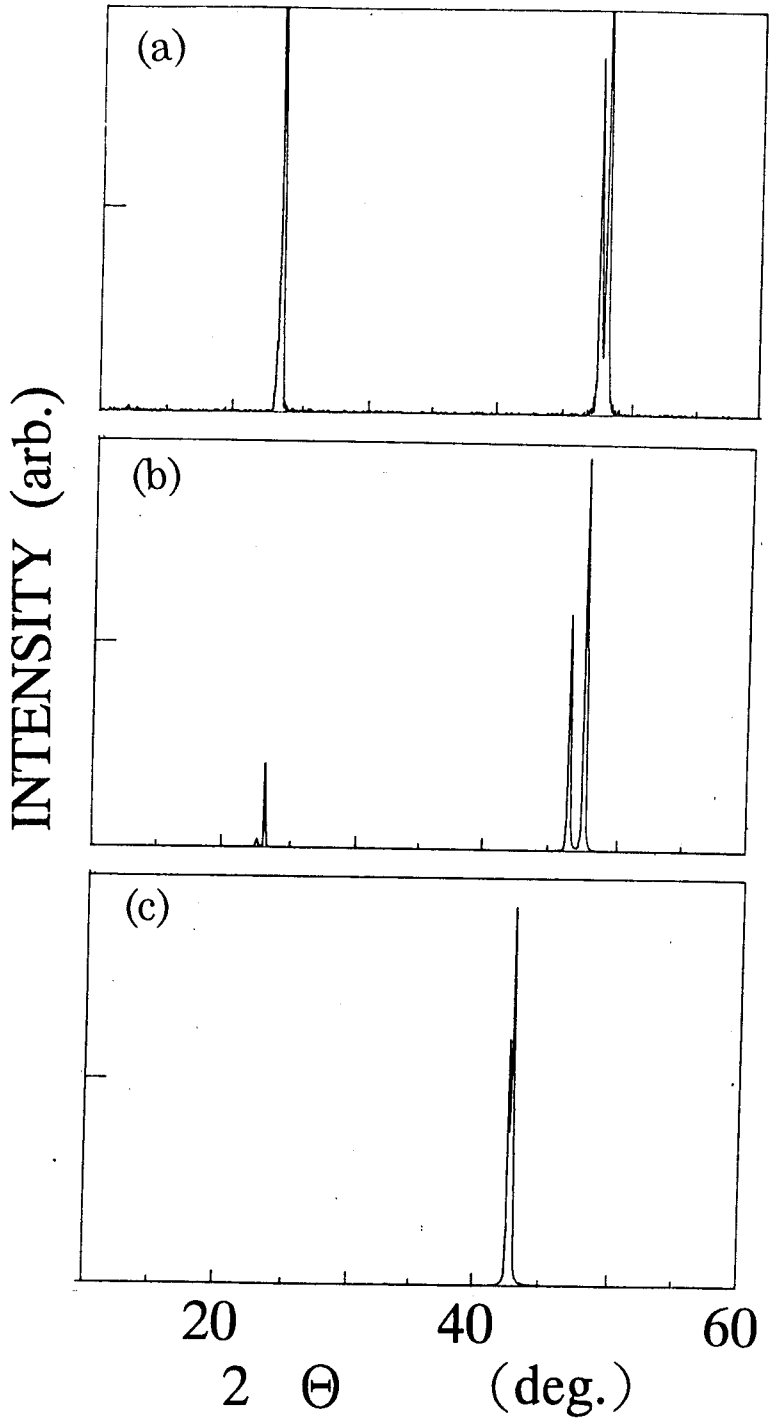

Fig. 5-2-4. X-ray diffraction pattern of CaTiO3 film deposited on (a)$LaAlO_3$(100), (b) $SrTiO_3$ (100) and (c) MgO(100) at 500℃ under the oxygen pressure of $1x10^{-3}$ Torr.

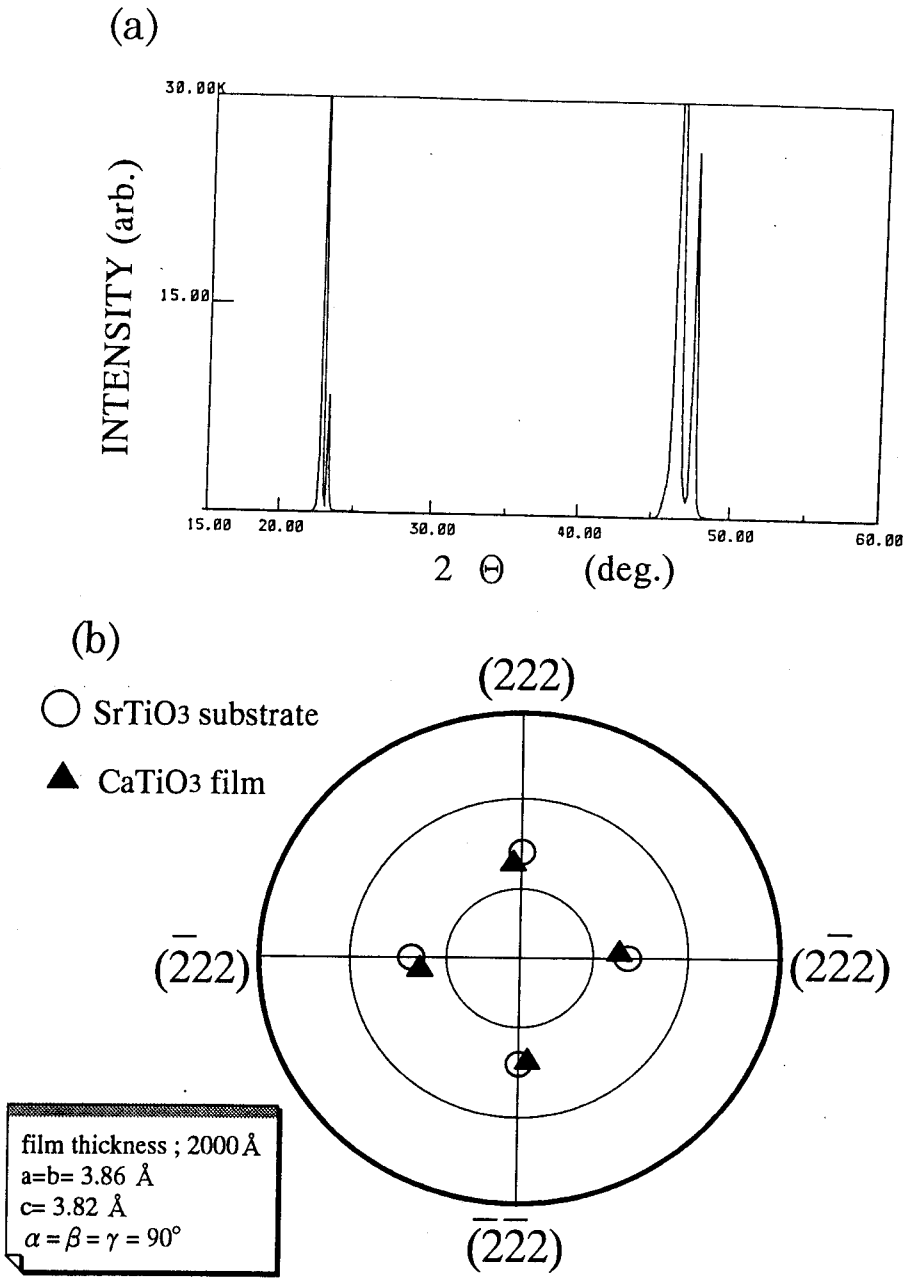

Fig. 5-2-5. (a)The X-ray diffraction pattern of $CaTiO_3$ film deposited on $SrTiO_3$ (100) substrate and (b) the pole figure.

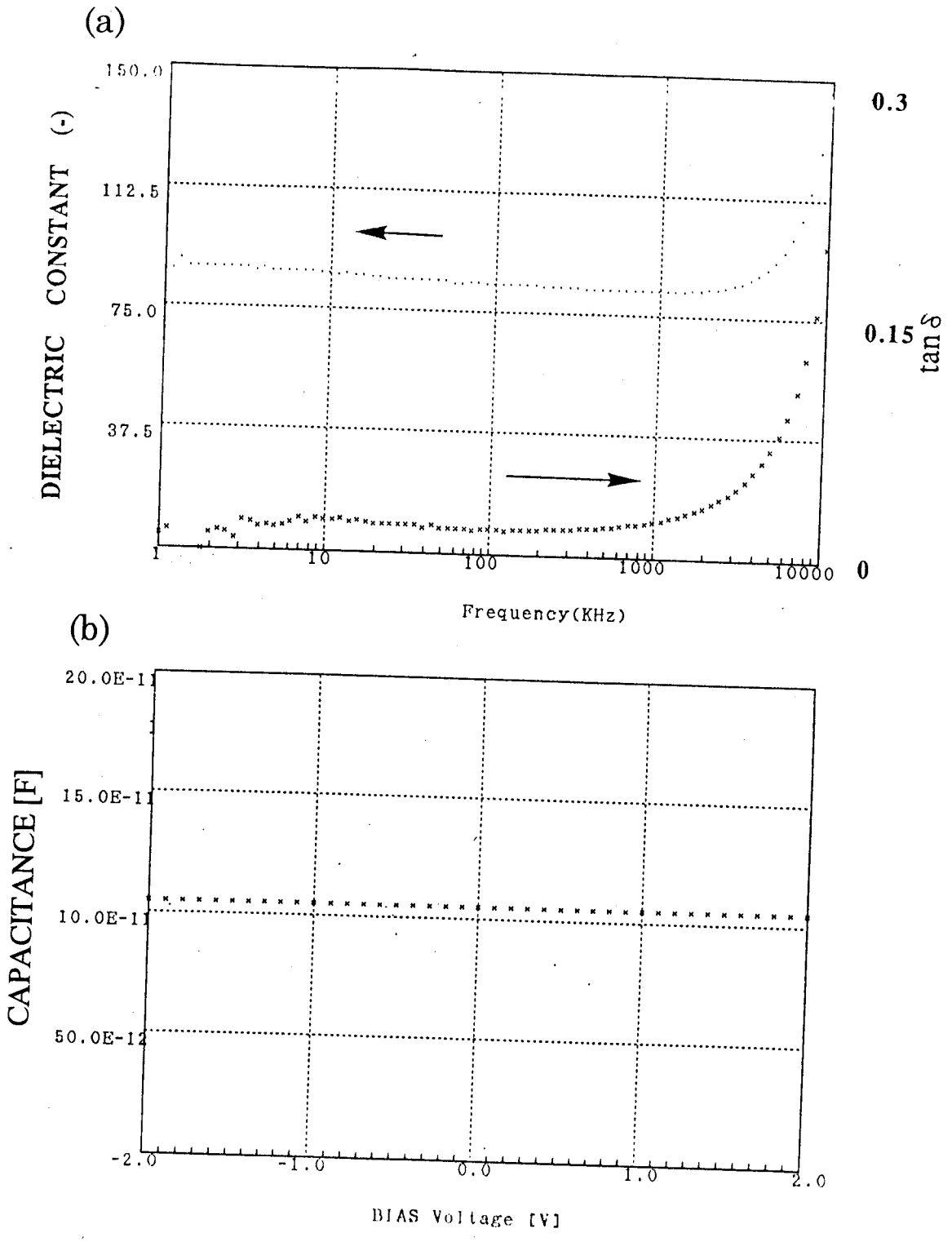

Fig. 5-2-6. (a) dielectric constant and dissipation factor (tan δ) vs applied frequency of the CaTiO3 film (thickness=1000Å) and (b) Capacitance-voltage (C-V) curve .

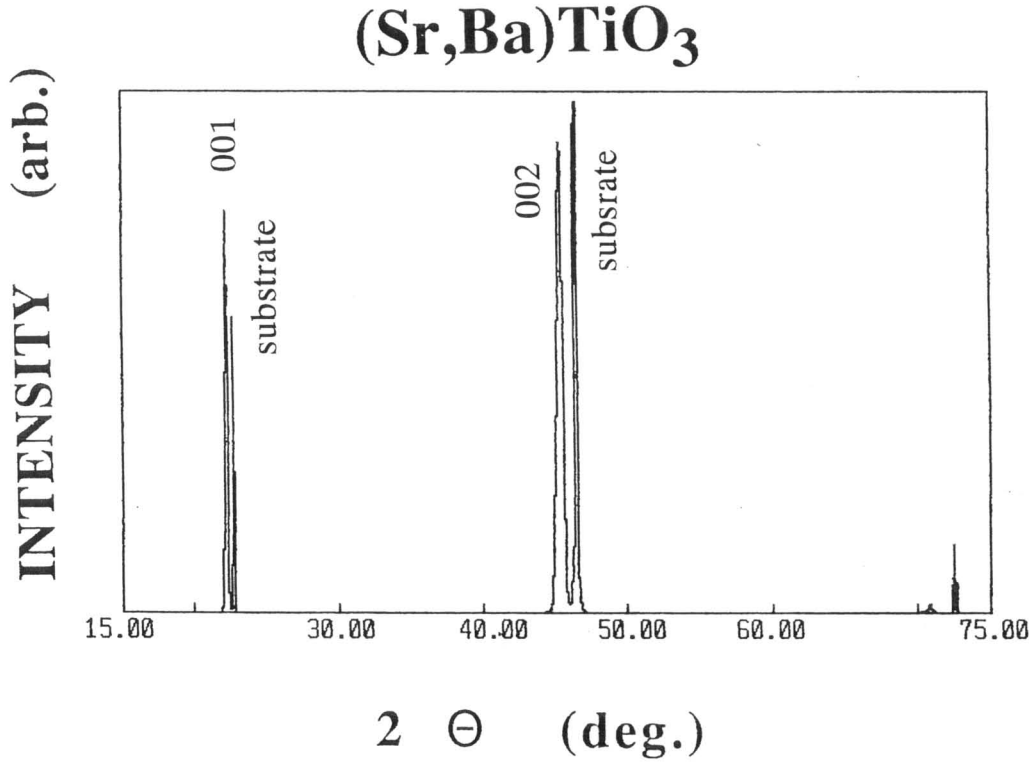

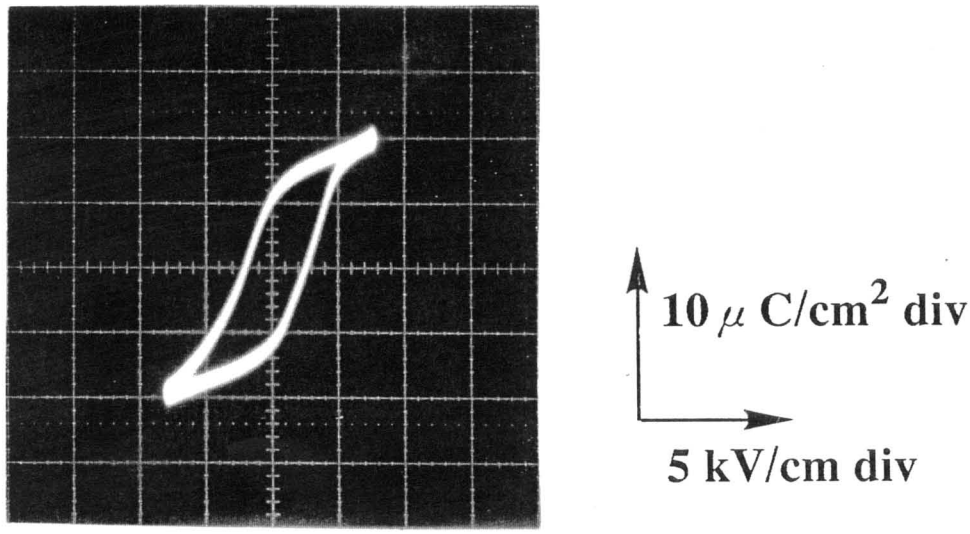

Fig. 5-2-7. X-ray diffraction pattern and D-E hysteresis loop of $Sr_{0.5}Ba_{0.5}TiO_3$ solid solution film.

5-3 Artificial control with unit cell scale

- $BaTiO_3/SrTiO_3$ and $BaTiO_3/CaTiO_3$ strained superlattices -

Abstract

Artificial dielectric superlattices of $SrTiO_3/BaTiO_3$(STO/BTO) and $CaTiO_3/BaTiO_3$(CTO/BTO) have been formed by a pulsed laser ablation technique with an in situ monitoring of RHEED(reflection high energy electron diffraction) oscillation. The crystal structures can be controlled with atomic order accuracy and a large strain of 400-500 MPa is introduced at the interface between the BTO and STO layers. The superlattices show higher dielectric constant than that of $(Sr_{0.5}Ba_{0.5})TiO_3$ films against the change of temperature or applied frequency. A large dielectric constant of 900 was observed for the superlattices with a stacking periodicity of 2 unit cells / 2 unit cells. The superlattices show drastically different electrical behavior from that of the solid solution $(Sr,Ba)TiO_3$ films, both with changing temperature or applied frequency. Broad maxima of the dielectric constants occur around 40-50 ℃ and the values remain large even for temperature above 200 ℃. On the contrary, in the case of CTO/BTO superlattices, lattice constants and dielectric constant do not change so much comparing with STO/BTO cases. Lattice mismatch in the STO/BTO and the CTO/BTO superlattices are 2.5% and 5.5%, respectively. In the case of CTO/BTO, the misfit dislocation such as stacking faults may occur at the interface between CTO and BTO layers owing to large lattice mismatch.Therefore, lattice strain is introduced effectively below the lattice mismatch of about 3 %.

Experiment

In this study, the BTO and STO or CTO layers were stacked alternately by a multi target pulsed laser deposition technique. This technique offers advantages for film growth, including epitactic growth at low substrate temperatures; congruent deposition of materials with complex stoichiometries and facile deposition of materials with high melting points[6,7]. In our experiment, stoichiometric sintered $BaTiO_3$(BTO), $SrTiO_3$(STO), $CaTiO_3$(CTO) and their solid solution of $(Sr_xBa_{1-x})TiO_3$ (SBTO) and $(Ca_xBa_{1-x})TiO_3$ (CBTO) pellets were used as ablation targets. An ArF excimer laser beam (wave length: 193 nm) was focused onto the target of BTO and STO or CTO alternately with an energy density of 500 mJ/cm^2, and the BTO and STO or CTO layers were deposited layer-by-layer on conductive 1%-Nb doped single crystal $SrTiO_3$(100) substrates which size were 10 x 5 x 0.5^t mm. The thickness of each layer of BTO and STO or CTO was varied in the range from 4 Å(1 unit cell) to 1000 Å(250 unit cells) and the total thickness of the superlattices was fixed at 2000 Å, at first. Then the total thickness of the superlattices was changed from 2000 Å to 250 Å. The films were formed at 650 ℃ in an oxygen/ozone(8%) ambient at a pressure of 1 - 3 mTorr. This condition is suitable for the formation of BTO, STO and CTO films. The deposition rate was 10-15 Å/min. The change of lattice parameter of the films was measured by 2θ-θ X-ray diffraction and four circle X-ray diffraction methods. The epitaxy of the films was also confirmed by reflection high energy diffraction (RHEED) with acceleration voltage of 15 kV (Physitec, RHG-1000) and by the pole figure obtained by the four circle X-ray measurement (Rigaku, RINT-9000). Dielectric constants (εr) of the films were measured by LCR meters with changing the temperature and applied

frequency from 20 ℃ to 200 ℃ and from 10^1 to 10^6 Hz, respectively (WAYNE KERR, LCR Meter 4210).

Results and Discussion

[$BaTiO_3/SrTiO_3$ superlattices]

Figure5-3-1 shows a RHEED intensity oscillation of the specular beam reflection observed <100> azimuth during the formation of STO/BTO superlattices by layer-by-layer successive deposition. When three unit cells of STO were deposited on the substrate, clear three oscillations of the RHEED intensity were produced with the streaky pattern. That is, three unit cells of STO are deposited on the substrate followed by three unit cells formation of BTO. The accurate total thickness of the films is confirmed by the thickness monitor after the film deposition. The RHEED patterns showed streaks throughout the film growth process, indicating that these materials can be formed by layer-by-layer growth with flat surfaces. It was confirmed that one cycle of the oscillation corresponds to one molecular layer growth of $SrTiO_3$ and $BaTiO_3$, by comparison with the number of the stacking cycles and the total thickness of the film. Monitoring the total diffraction pattern makes it possible to control the film growth with atomic accuracy.

Figure 5-3-2 shows the θ-2θ X-ray diffraction patterns and calculated peak position and intensities of the superlattices of STO/BTO with the periodicity of: (a) 125/125, (b) 6/6. The pattern of Fig.5-3-5(a) is similar to that of the known BTO and STO structure.

The changes of the lattice parameters a and c saturate at a stacking periodicity of approximately 40Å (10 unit cells). In this range, the superstructures can be also observed in the X-ray diffraction patterns ; that is, the combination of main peaks with satellite peaks.(Fig.5-3-2(b)) Therefore, crystallographically, these superlattices should be classified as new materials having a longer c-axis length.

In Figs. 5-3-2(b), satellite peaks are observed characteristic of superlattices. From the viewpoint of crystal chemistry, the superlattices of 1/1 - 5/5 can be regarded as new compounds having a long unit cell by the combination of SrO, BaO and TiO_2 layers in one unit cell. In the X-ray diffraction patterns, the relative intensities of diffraction pattern are similar to that of the calculated one. This result indicates that the BTO/STO superlattice was formed as designed, and the pole figure and scan patterns indicate that the STO and BTO films are in complete epitaxy with the substrate.

Fig.5-3-3 shows the variation of the ratio of lattice constant c and a of the STO and BTO layers as a function of the periodicity of each layer. The lattice parameter c of the BTO layers increases with decreasing stacking periodicity below 250(1000 Å)/250(1000 Å) unit cells.(Fig.5-3-3(a)) On the other hand, the lattice constant a decreases with decreasing periodicity, just opposite of lattice constant c. (Fig.5-3-3(b), Fig.5-3-4) Thus the expansion of c-axis in the BTO layers is attributed to an in-plane pressure effect due to the lattice mismatch of STO/BTO(2.5%).

The pressure at the interface of the strained BTO/STO layers may be estimated using data for bulk BTO under isostatic pressure, $dP/da=1.0x10^1$ Pa/a [10] (Fig.5-3-5). In the case of the25/25 superlattice, a is compressed from its normal value for BTO of 3.990Å to 3.925Å . The corresponding pressure is

0.5 GPa.

The pressure effect can also be discussed from another point of view. (Fig.5-3-6(a),(b)) We consider two sheets in elastic contact and estimate the stress using elasticity theory. In this case, the tensile stress (σ) in the BTO layer can be written as follows as described in chapter 4-3:

$$\sigma = E_i (\alpha_1 - \alpha_2) dT \, dl / ti, \qquad (5\text{-}1)$$

where dl,Ei, α i, and ti are the lattice mismatch, Young's modulus, thermal expansion coefficient, and thickness of each layer [i=1(BTO), 2(STO)]. Using the values of dT=600 K and Ei =1.1 GPa, and $\alpha = 10^{-6}$ K^{-1}, the stress in the BTO layer can be estimated as 0.4 GPa. This value is similar to the pressure derived above from the experimentally observed changes in lattice parameter. The pressure at the BTO layer induced by the STO layers is estimated to be about 400 - 500MPa from elastic calculations. (Fig.5-3-6(b)) Strictly speaking, stress in the strained superlattice has some distribution. To estimate the distribution, the in-plane stress in the BTO/STO superlattice is calculated by finite elements method. (Fig.5-3-6(c)) In the caser of 1000Å/1000Å stacking, the expansion stress (about -400 MPa) shows maximum in the BTO layer at the interface and decreases gradually toward the middle point of each stacking layer(almost zero).

The changes in the dielectric constant(ε r) of the BTO/STO superlattices as function of the stacking periodicity are shown in Fig.5-3-7 (▲). The dissipation factors (tan δ) are also shown in Fig.5-3-7 (□). The ε r does not change much for periodicities between 100Å and 1000Å(25 - 250 unit cells cycle). In the range between 100Å(25 unit cells) and 8Å(2 unit cells) stacking, however, ε r increases with decreasing stacking periodicity. The changes of the lattice constants are in good agreement with the change of the dielectric constant (ε r). This result indicates that there is the pressure effect

at the interface due to the large lattice mismatch between BTO and STO layers. At the one unit cell periodicity, εr decreases 500. This is presumably because by the fact that, in this 1/1 structure, the TiO_2 atomic layer is sandwiched between a BaO and SrO layer. This type of crystal structure is quite similar to that of $(Sr_{0.5},Ba_{0.5})TiO_3$ solid solutions in the sense that both Sr and Ba are included in he basic perovskite cell. In the case of superlattices with larger than 2/2 stacking periodicity, an original crystal structure of BTO is maintained in one unit cell; that is, TiO_2 layer is sandwiched by BaO layers. Therefore, the crystal structure is essentially different between the superlattice of 1/1 and those over 2/2.

The dissipation factors do not change so much in the all range of the stacking periodicity (tan δ = 0.06-0.08). Therefore, quality of the superlattices is almost constant in a series of stacking periodicity.

Figure 5-3-8 shows the dielectric constant vs total thickness of STO/BTO superlattices and $(Sr_{0.5}Ba_{0.5})TiO_3$ (SBTO) solid solution. The filled triangle (▲), filled circle(●), and empty square(□) indicate the dielectric value of 4/4, 2/2 and 1/1 superlattices, respectively. The filled square mark(■) show the εr of the SBTO solid solution. The dielectric constant(εr) of SBTO films decreases monotonously below the film thickness of 2000Å and becomes almost zero at the thickness of 250Å. The dielectric constants (εr) of superlattice, on the other hand, show almost constant value in the thickness range between 2000Å and 250Å comparing with that of solid solution of SBTO. It should be noted that the STO/BTO strained superlattices have high dielectric constants even at the film thickness of 250Å. The εr of $(S_{0.5},Ba_{0.5})TiO_3$ solid solution thin films, on the other hand, decreases monotonously below the film thickness of 2000 Å and becomes almost 10-20 at a thickness of 250 Å.(Fig.5-3-8) Considering these tendencies, the superlattice structure and the stress caused at the interface between the

STO and BTO layers, apparently, play an important role in the enhancement of the dielectric constant.

Temperature dependence of the εr measured of the superlattices (total thickness ; 2000Å) at R.T. with 10 kHz are of particularly interesting as shown in Fig.5-3-9. The dielectric constant of $(Sr_{0.5}Ba_{0.5})TiO_3$ solid solution thin films becomes zero at 35 ℃ because of the phase transition from tetragonal to the cubic structure. For the BTO/STO superlattices, on the other hand, broad peak of εr which is typical feature of ferroelectric film is observed around 50 - 60 ℃ and high ε r values are kept even at higher temperature of 200 ℃ in the superlattices of stacking periodicity of 1/1 and 4/4.(Fig.5-3-9(a)) This indicates that the ferroelectric phase transition occurs at high temperature in the superlattice. Furthermore, for the BTO/STO-25 unit superlattice, the εr value is further increasing up to 200 ℃. (the Curie temperature of simple BTO is known as 130 ℃.) Tetragonal phase of BTO may become stable due to the compressive stress along in-plane induced by the STO layers. In Fig.5-3-9(b), the total thickness of the superlattices are changed 2000Å(□), 1000Å(△) and 500Å(●). The superlattices of 2000Å and 1000Å thickness show similar behavior against the changing temperature. That is, the broad maximum of εr is observed at around 50 -60℃. The superlattice of 500Å thickness show double maximum of r at 50-60℃ and 90-100℃.

Furthermore, these large dielectric constants of the ferroelectric superlattice can be maintained at the high applied frequency of above 10^6 Hz.(Fig.5-3-10) Dielectric constants of the superlattices, in the stacking periodicity of 1 - 4 unit cells, decrease gradually with increasing the applied frequency. The dielectric value of STO-2 unit/BTO-2unit superlattice, however, it still as three times as large as that of $(Sr,Ba)TiO_3$ solid solution at the applied frequency of 10^6 Hz. In this frequency range, ionic factor plays an important role for the dielectric constant. (Fig.5-3-11) In the bulk samples, the strain energy

strongly affects the phase transitions[5]. In the superlattices of STO/BTO, large ion shifts are expected owing to the large lattice mismatch. Therefore, we believe that these phenomena observed in these particular superlattices should be called "super-dielectric properties" which are artificially induced in the man-made materials.

The FT-IR absorption spectra of SBTO film and STO/BTO superlattices(100/100 unit) deposited at substrate temperature of 650 ℃ are shown in Fig. 5-3-12(a) and (b), respectively. These measurements were carried out in the reflection mode. These peaks are due to resonance with the longitudinal optic(LO) phonon modes associated with STO and BTO films. The peaks at 610cm^{-1} indicates the typical spectrum of SBTO film(Fig.5-3-12(a)). And STO/BTO superlattice shows the two series of peaks derived from standard STO(590 cm^{-1}) and BTO(410, 540 cm^{-1}) and SBTO(610cm^{-1}). The peak at 610 cm^{-1} decreases with decreasing the stacking periodicity, and eventually disappears at 4/4 periodicity. The position of these peaks are in good agreement with those of reported by Myoren et al.[11,12]. Recently, Myoren et al. reported that the infrared polarized reflection spectra strongly depend on the STO film thickness, and discussed the relationship between the optical dielectricity and spectra.

In the "soft-mode" picture, the atoms primary occupy the ideal cubic sites at high temperatures. As the temperature is lowered, one of the transverse optical (TO) modes soften and becomes unstable, and the crystal transforms to the tetragonal phase with atomic displacements along the [001] direction.[8] In the case of these strained superlattices, the soft-mode may be frozen by the compressive stress in the film.

Fig. 5-3-13. shows capacitance-voltage curves of (a) $BaTiO_3$ single phase film, (b) STO/BTO (total 500Å) and (c) STO/BTO (total 250Å) with stacking 4/4 unit cells. In Fig.5-3-13(a) the butterfly type hysteresis

can be observed which is the typical feature of ferroelectricity. In Fig.5-3-13(b), a small hysteresis loop also observed in the thickness of the superlattice. But in Fig.5-3-13(c) that is 250Å case, it do not show any loops.

In these displacive type, the energy(U) which determine the ferroelectricity consists of short range force (U_{short}) and long range force(U_{long}),

$$U = U_{short} + U_{long} \qquad (5\text{-}2)$$

where U_{short} and U_{long} are contracted by as follows, respectively.

$$U_{short} = Wr(r) + Wf(r) \qquad (5\text{-}3)$$

Wr(r) ; Born repulsion and Wf(r) ; Van der Waals force

$$Wr(r) = c \exp\left(\frac{-r}{\rho^1+\rho^2}\right) \qquad (5\text{-}4)$$

$$Wf(r) = -\frac{3}{2}\frac{|\mu|^2}{(4\pi\varepsilon)^2}\frac{1}{r^6} \qquad (5\text{-}5)$$

$$U_{long} = Wa(r) + Wd(r) \qquad (5\text{-}6)$$

Wa(r) ; Coulomb's force and Wd(r) ; dipole-dipole interaction

$$Wa(r) = \frac{-z^1 z^2 e}{4\pi\varepsilon r} \qquad (5\text{-}7)$$

$$Wd(r) = -\frac{3(r\mu^1\, r\mu^2) - \mu 1 \mu 2 r}{4\pi\varepsilon r^5} \qquad (5\text{-}8)$$

In the case of superlattice, the short range force is same both of 500Å and 250Å thickness superlattices. Therefore, the long range force, such as Coulomb force or dipole-dipole interaction, plays an important role for the ferroelectric behavior. The lower limit of occur the ferroelectricity is around 250~500Å. This is consistent with that reported in the powder sample[23].

Conclusion.

In conclusion, we have formed dielectric superlattice of STO/BTO using pulsed laser deposition technique. The dielectric properties of the superlattices show quite different behaviors from those of $SrTiO_3$, $BaTiO_3$ and $(Sr,Ba)TiO_3$ single phase films. The dielectric and ferroelectric superlattices are the promising approach to create new super-ferroelectric materials and to make clear the mechanism of ferroelectricity.

[$CaTiO_3$/$SrTiO_3$ artificial superlattices]

Figure 5-3-15 (a), (b) shows the θ-2θ X-ray diffraction patterns of BTO(400Å)/STO(400Å) superlattice (a) and BTO(20Å)/CTO(20Å) superlattice (b), respectively. The diffraction pattern indicates that the BTO/CTO superlattice was formed as designed.

Fig.5-3-16(a) shows the variation of the ratio of lattice constant c (●) and a (▲) of the STO and BTO layers as a function of the periodicity of each layer. The lattice parameter c of the BTO layers and CTO layers do not change in the all range of stacking periodicity. From the view point of lattice matching, the lattice mismatch of STO/BTO and CTO/BTO are 2.5 % and 5.5%, respectively. Therefore, in the CTO/BTO superlattices, a misfit dislocation (stacking fault) may occur at the interface between CTO and BTO layers owing to the large lattice mismatch. Because of these misfit dislocation, the lattice strain may be relaxed and can not play effectively as the pressure effect. From the results of these experiments in the superlattices of STO/BTO superlattices and CTO/BTO superlattices, the threshold of the lattice for the strained superlattices is about 3%.

The critical thickness for the misfit dislocations can be estimated as follows by Matthews[24-25],

$$\varepsilon = \frac{b(1-\nu\cos\theta)}{4\pi(1+\nu)\cos\lambda}\frac{1}{hc}(\ln hc+1) \qquad (5\text{-}9)$$

where ε, b, hc, b, ν and θ are lattice mismatch, critical thickness, $\sqrt{2}$x a, Poisson ratio and the angle between the slip dislocation and the that direction in the film plane. (Fig.5-3-22) So in the case of STO/BTO superlattices in which misfit is 2.5%, the critical thickness is above 200Å. In the case of CTO/BTO

superlattices, on the other hand, that is around 50 Å.

5-3-2. $(Sr_xBa_{1-x})TiO_3$ / $(Ca_xBa_{1-x})TiO_3$ superlattices

From the results of Chapter 5-3-1, the critical lattice mismatch is about 3%. Therefore, we have formed the $(S_{0.3}Ba_{0.7})TiO_3$ / $(Ca_{0.52}Ba_{0.48})TiO_3$ superlattices which lattice mismatch of 2.5% is similar to that of $SrTiO_3/BaTiO_3$ strained superlattices. (Fig.5-3-20)

In these experiment, stoichiometric sintered $(S_{0.3}Ba_{0.7})TiO_3$ (SBTO) and $(Ca_{0.52}Ba_{0.48})TiO_3$ (CBTO) pellets were used. Total thickness and stacking periodicity were fixed at 500Å and16Å (4 unit cell). Another conditions are described in Chapter 5-3-1.

Results and discussion

The film of $(S_{0.3}Ba_{0.7})TiO_3$ solid solution, $SrTiO_3/BaTiO_3$ superlattice and $(S_{0.3}Ba_{0.7})TiO_3$ / $(Ca_{0.52}Ba_{0.48})TiO_3$ superlattices have the dielectric constants of 20-30, 550 and 900, respectively. (Fig. 5-3-21) It should be noted that the $(S_{0.3}Ba_{0.7})TiO_3$ / $(Ca_{0.52}Ba_{0.48})TiO_3$ superlattice show large dielectric constant value even at the film thickness of 500Å. This is because that the tetragonality in crystal structure is enhanced by the pressure effect.

References

1)Cohen R.E., Nature 358, 136-138 (1992).

2)Bunting,E.N., Shelton,G.R. & Creamer,A.S., J.Am.Ceram.Soc. 30 114-25 (1947).

3)Amirez,R., Lapena,M.F. & Gonzalo,J.A., Phys.Rev.B42 2604-2606 (1990).

4)Decker,D.L. & Zhao,Y.X. Phys.Rev.B39 2432-2438 (1989).

5)Marais,S., Heine,V., Nex,C. & Salje,E., Phys.Rev.Lett. 66, 2480-2483 (1991).

6)Wailenhorst,A., Doughty,C., Xi.X.X., Mao,S.N., Li,Q., Venkatesan,T. & Ramesh,R., Appl.Phys.Lett. 60, 1744-1746 (1992).

8)Harada,J., Axe,J.D. & Shirane,G., Phys.Rev.B 4, 155-160 (1971).

9) M.Y.Chern, A.Gupta, B.W.Hussey and T.M.Shaw, J.Vac. Sci. Technol. 11 (1993) 637.

10) R.A.McKee, F.J.Walker, J.R.Conner, E.D.Specht and D.E.Zelmon, Appl. Phys. Lett. 59 (1991) 782.

11) Y.Shibata, K.Kaya, K.Akashi, M.Kanai, T.Kawai and S.Kawai, Appl. Phys.Lett., 61 (1992) 1000.

12) E.N.Bunting, G.R.Shelton and A.S.Creamer, J.Am.Ceram.Soc. 30 (1947) 114.

13) A.Wailenhorst, C.Doughty, X.X.Xi, S.N.Mao, Q.Li, T.Venkatesan and R.Ramesh, Appl.Phys.Lett. 60, (1992) 1744.

14) Z.Q.Shi, Q.X.Jia and W.A.Anderson, J.Vac.Sci.Technol., 11 (1993) 1441.

15) K.Iijima, T.Terashima, K.Yamamoto, K.Hirata and Y.Bando, Appl.Phys.Lett., 56 (1990) 527.

16)S.Marais, V.Heine, C.Nex and E.Salje, Phys.Rev.Lett. 66 (1991) 2048.

17) K.Matsui, M.Taga and T.Kobayashi ; Jpn.J.Appl.Phys. 32 (1993) L796.

prssure effect in BTO

18) R.Ramirez, M.F.Lapena and J.A.Gonzalo ; Phys.Rev.B 42 (1990) 2604.

19)D.L.Decker and Y.X.Zhao ; Phys.rev.B 39 (1989) 2432.

20) E.Wiener-Avnear ; Appl.Phys.Lett. 65 (1994) 1784.

21) K.Iijima, T.Terashima, Y.Bando, K.Kamigaki and H.Terauchi ; J.Appl.Phys. 72 (1992) 2840.

22) H.Koinuma, M.Yoshimoto, H.Nagata and T.Tsukahara; Solid State Comm. 80 (1991) 9

23) Landolt-Bornstein Vol.16 Edt. T.Mitsui and S.Nomura (Springer-Verlag, New York 1981)

24) J.W.Matthews and A.E.Blakeskee; J.Crys.Growth 27 (1974) 118.

25) J.S.Speck, A.Seifert, W.Pompe and R.Ramesh; J.Appl.Phys. 76 (1994) 477.

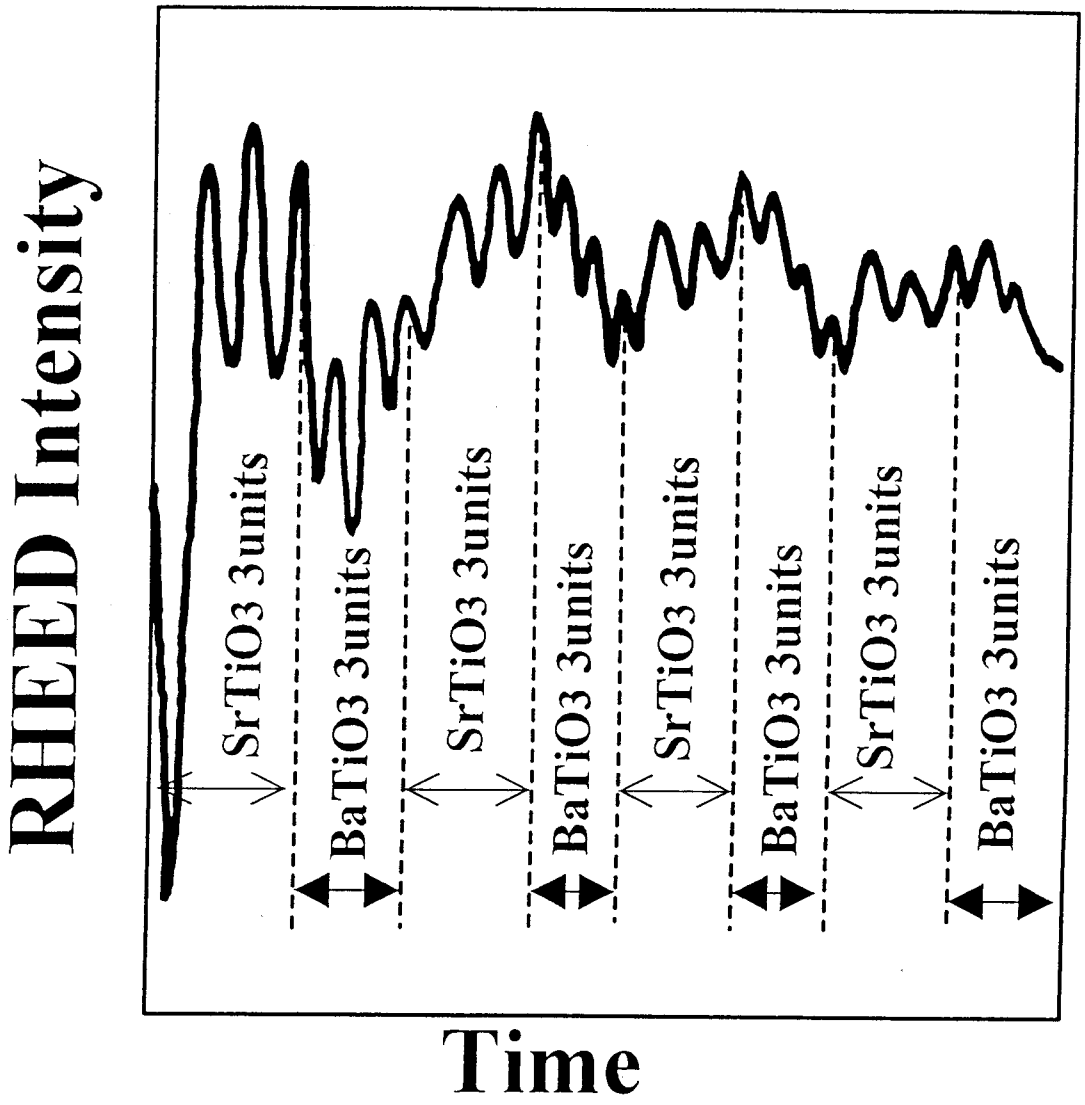

Fig. 5-3-1. The change of RHEED oscillation intensity during the growth of STO/BTO superlattice with the stacking combination of 3 unit cells / 3 unit cells of $SrTiO_3$ and $BaTiO_3$.

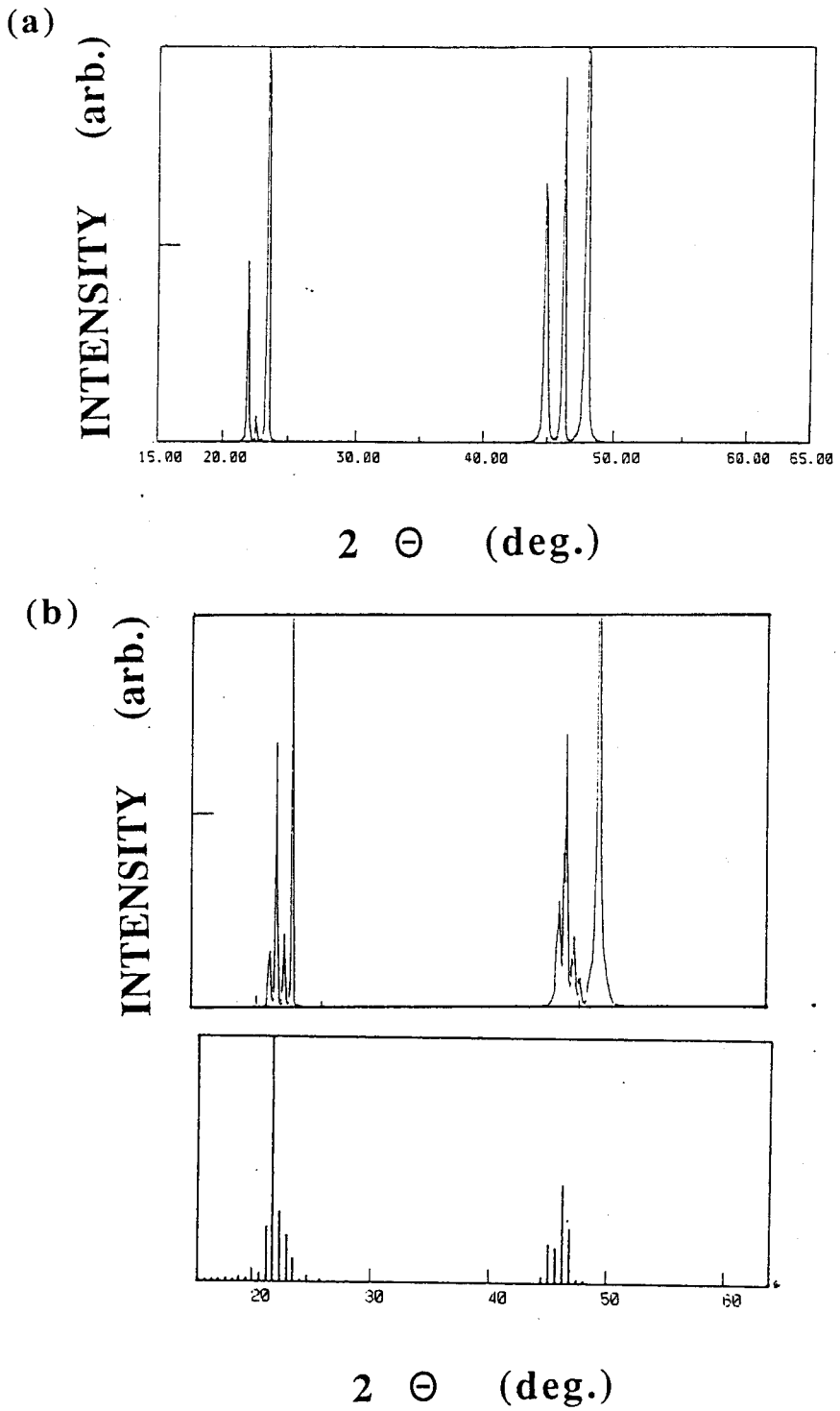

Fig. 5-3-5. (a) X-ray diffraction pattern of BTO/STO superlattice with stacking periodicity of 100 unit cell (400 Å) (b) The X-ray diffraction pattern of observed BTO(20 Å)/STO(20 Å) superlattice and calculated one with the stacking periodicity of 5 unit cells (20 Å).

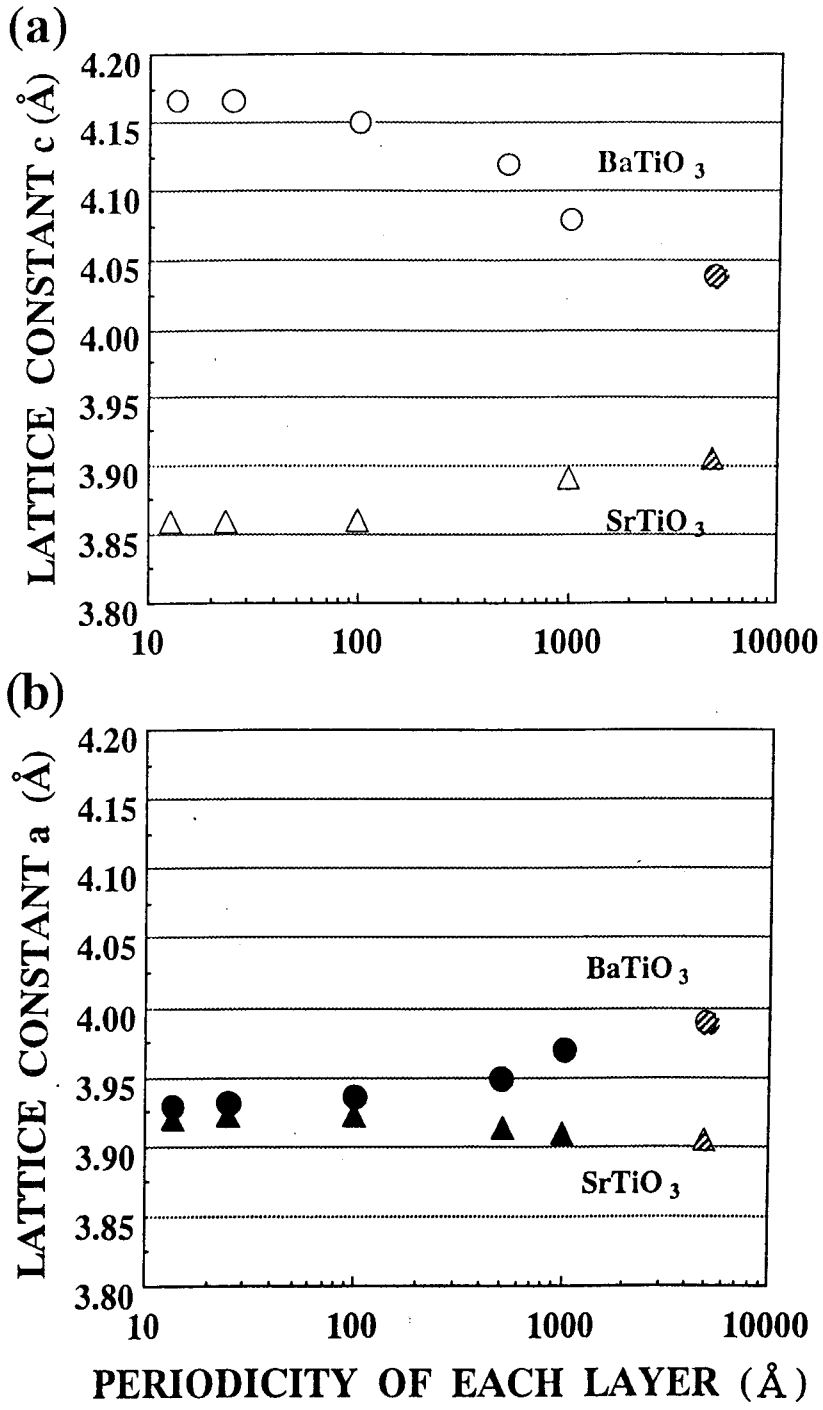

Fig. 5-3-6. Variation of the lattice constant a and c of BTO(○, ●) and STO(△,▲) layers in the STO/BTO superlattices against the layer thickness of each stacking periodicity. The total thickness of these superlattices is 2000Å. Shaded circle and triangle show the lattice constant a and c of single phase film with thickness of 5000Å.

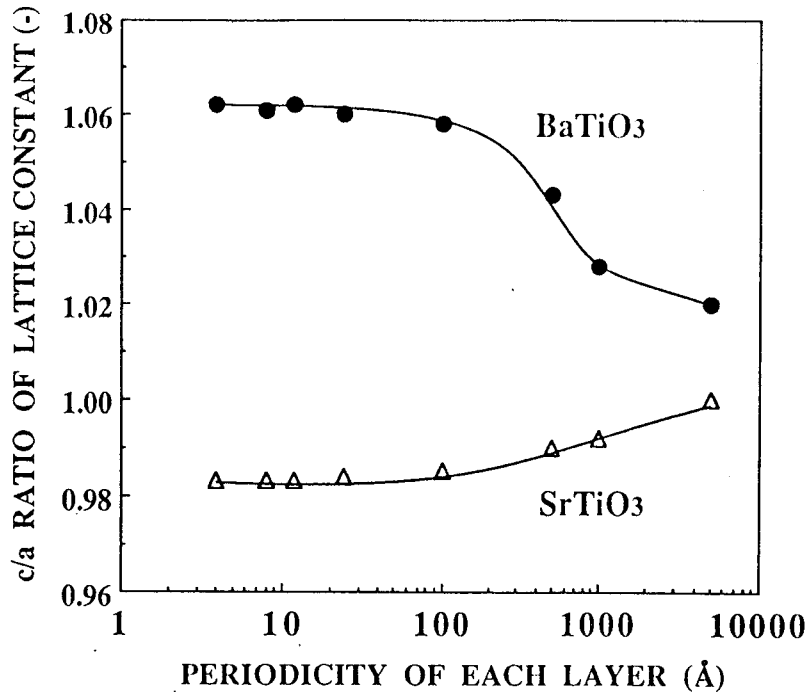

Fig. 5-3-7. The c/a ratio of BTO and STO layer in STO/BTO superlattices. (arranged the data of Fig. 5-3-6)

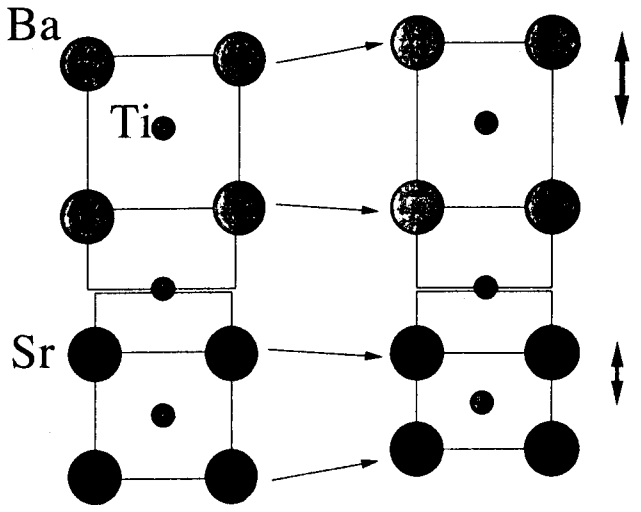

Fig. 5-3-8. Structure of STO/BTO superlattice projected on (010) . The compressing strain is introluced to the BTO layer along the a-b plane and expanded blong c-axis direction. STO layer changes reverse behavir

(a)

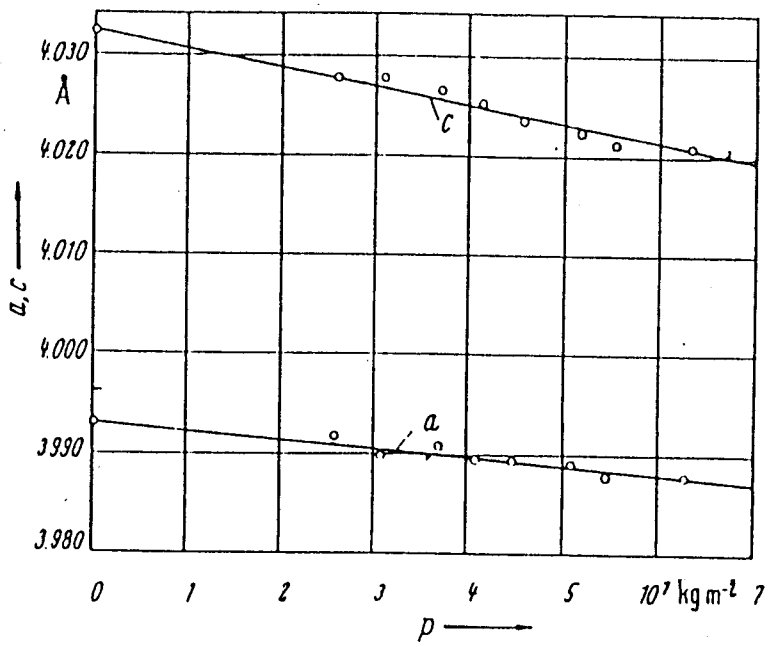

(b)

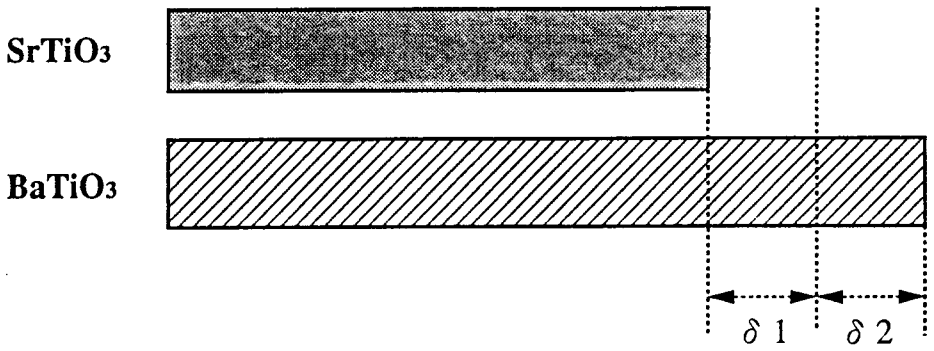

Fig. 5-3-9. (a) lattice constant a and c dependent on pressure in experiment of isostatic pressure. [23)]

(b) Elastic calculation model in the BTO/STO multilayer.

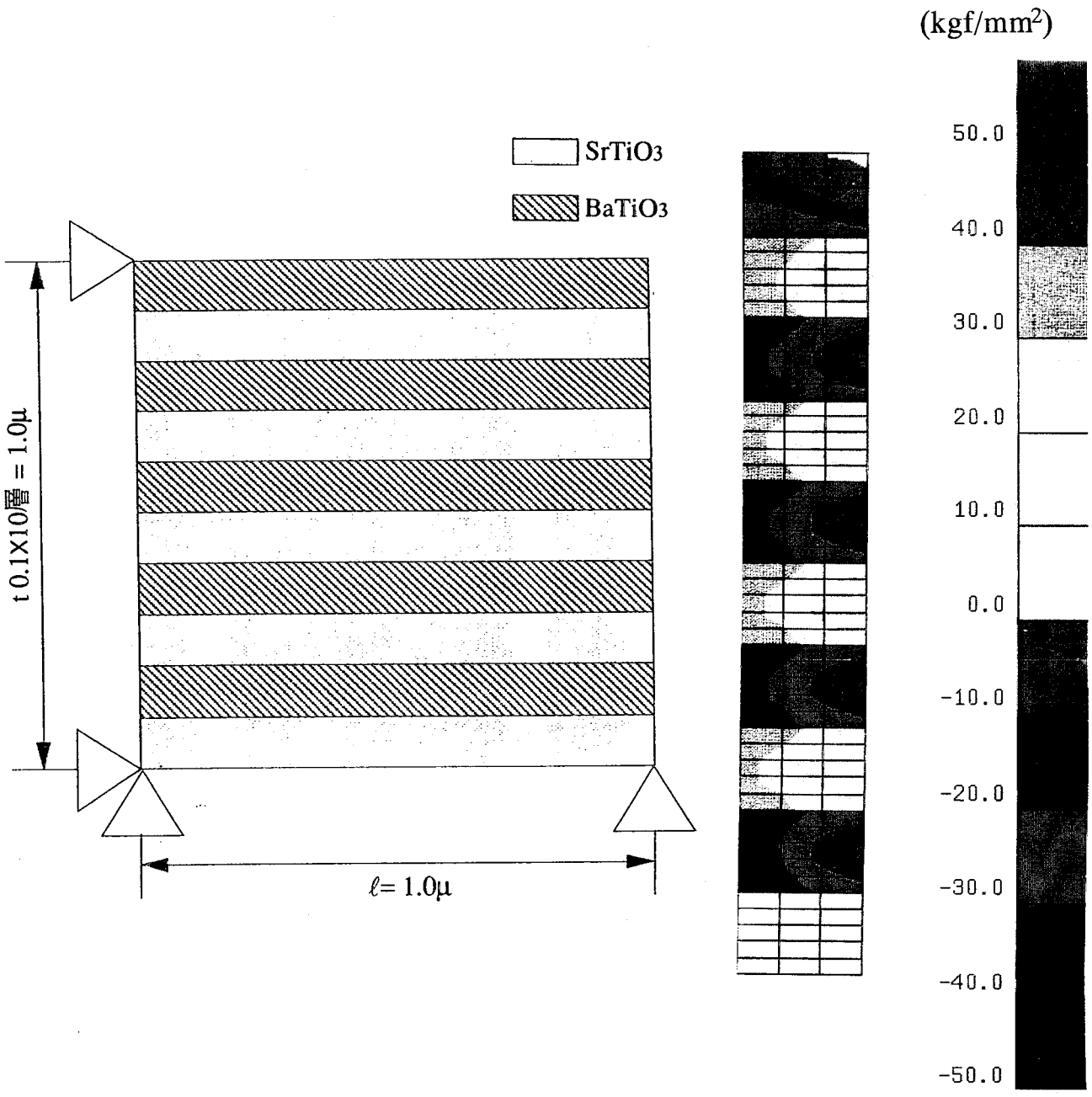

Fig.5-3-6 (c) The stress distribution map of the strained SrTiO3/BaTiO3 superlattice calculated by finite elements method.

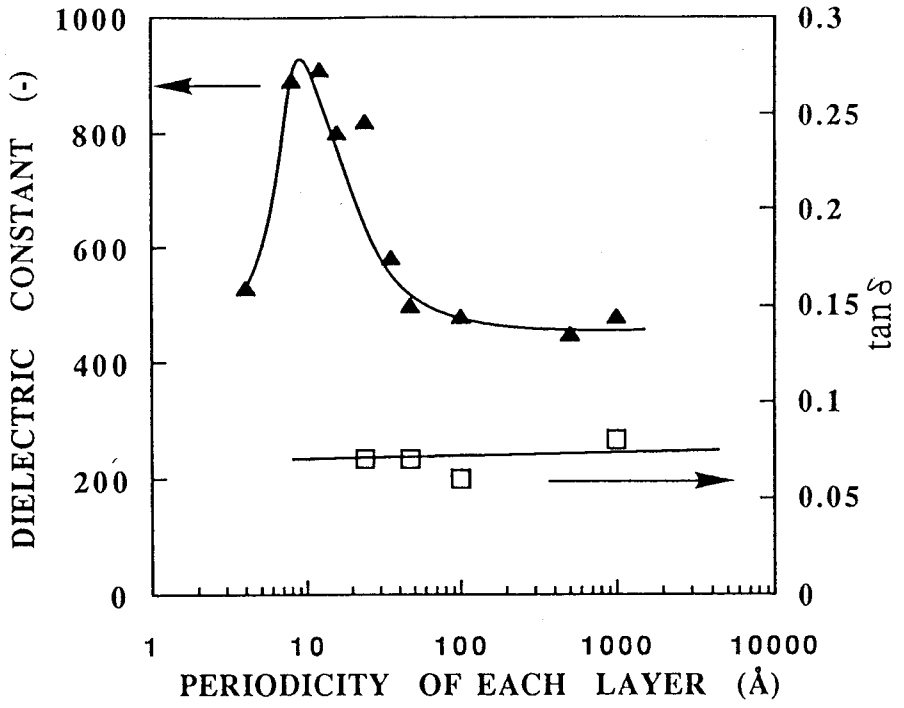

Fig. 5-3-10 Dielectric constants (▲) and tan δ (□) of BTO/STO superlattice vs stacking periodicity of each layer (BTO and STO)

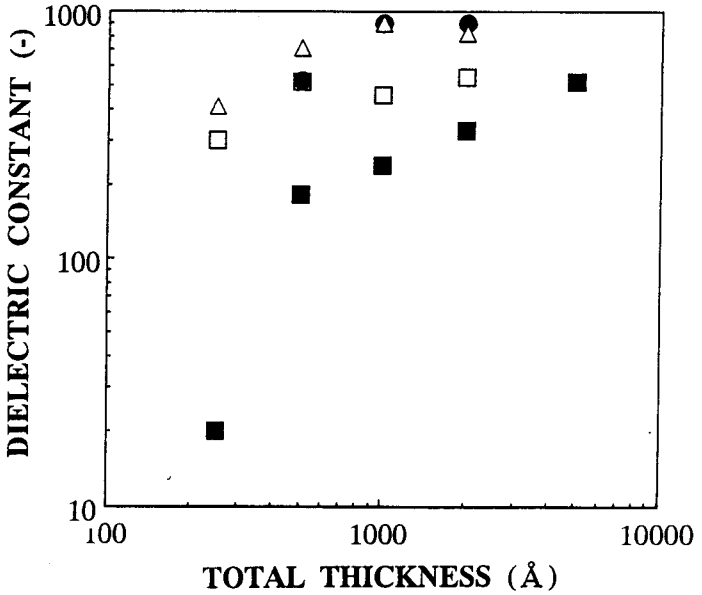

Fig. 5-3-11. The dielectric constant of the STO/BTO superlattices and solid solution SBTO against the total thickness.

□; 1/1 unit stacking, ●; 2/2 unit stacking

△; 4/4 unit stacking ■; SBTO solid solution

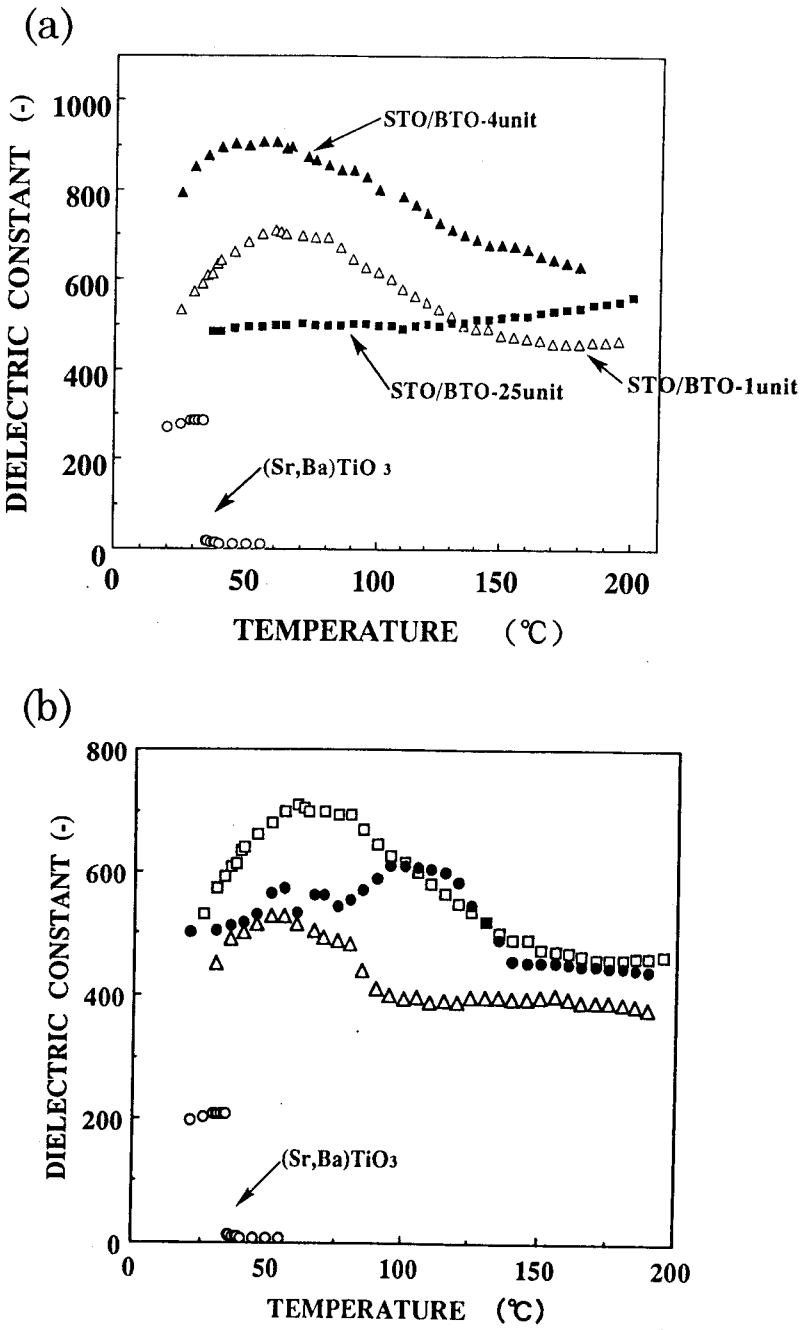

Fig. 5-3-12. (a) Temperature dependence of dielectric constant of various BTO/STO superlattices. (total thickness is 2000Å)
(1) △ : STO/BTO with 1 unit cell stacking, (2)▲ : STO/BTO with 4 unit cell stacking, (3)■ : STO/BTO with 25 unit cell stacking, (4) ○ : (Sr,Ba)TiO_3 solid solution film.

(b)Temperature dependence of dielectric constant of various BTO/STO superlattices against changing thetotal thickness from 2000Å(□), 1000Å(●) and 500Å(△).

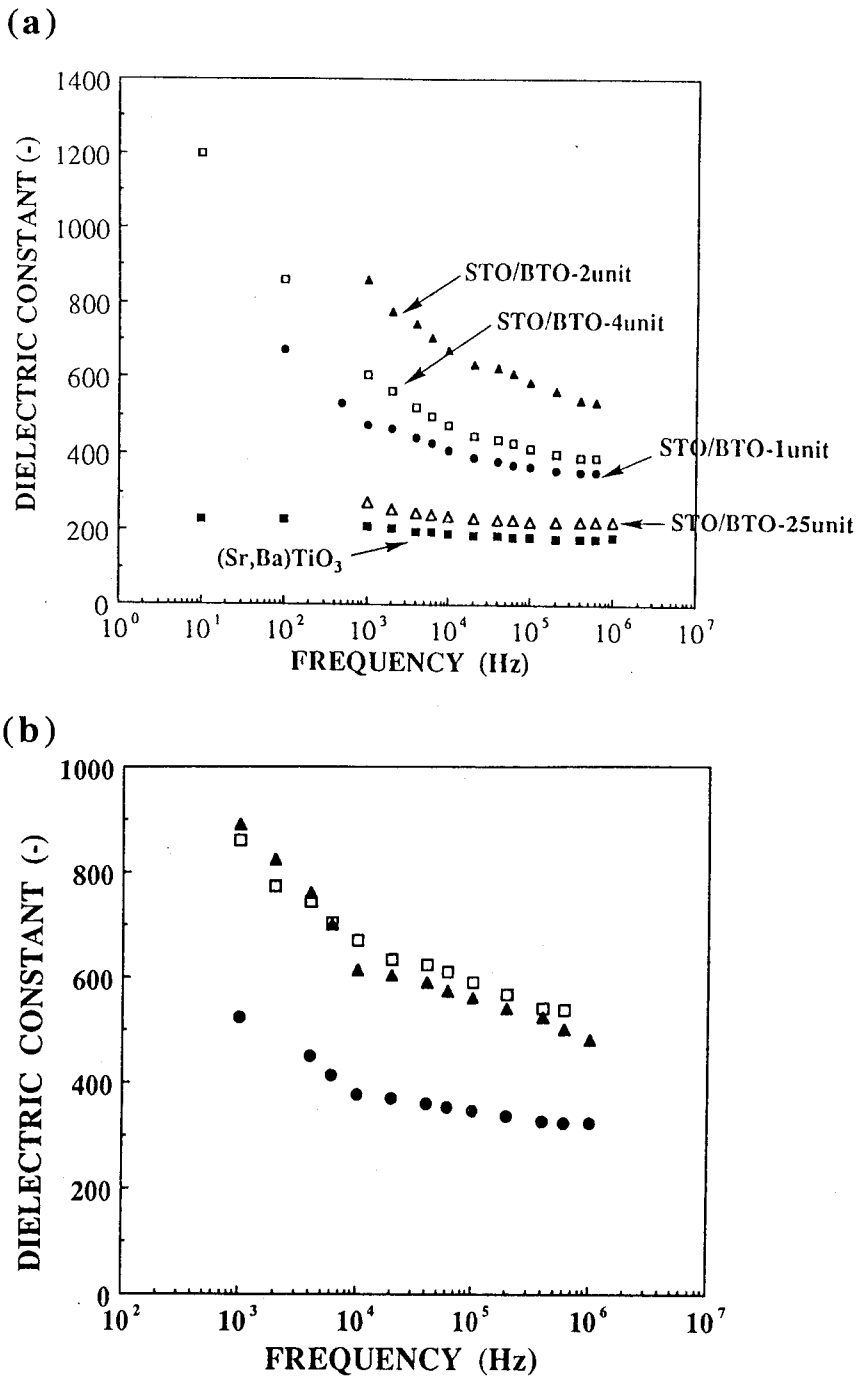

Fig. 5-3-13. (a)Applied frequency dependence of dielectric constant of various BTO/STO superlattices. (total thickness is 2000Å) (●;1 unit stacking, ▲; 2 unit, □; 4 unit, ■;25 unit and △;SBTO solid solution)
(b) Applied frequency dependence of dielectric constant of BTO/STO superlattices (2/2 stacking periodicity) against changing total thickness. (□;2000Å, ▲;1000Å, ●;500Å).

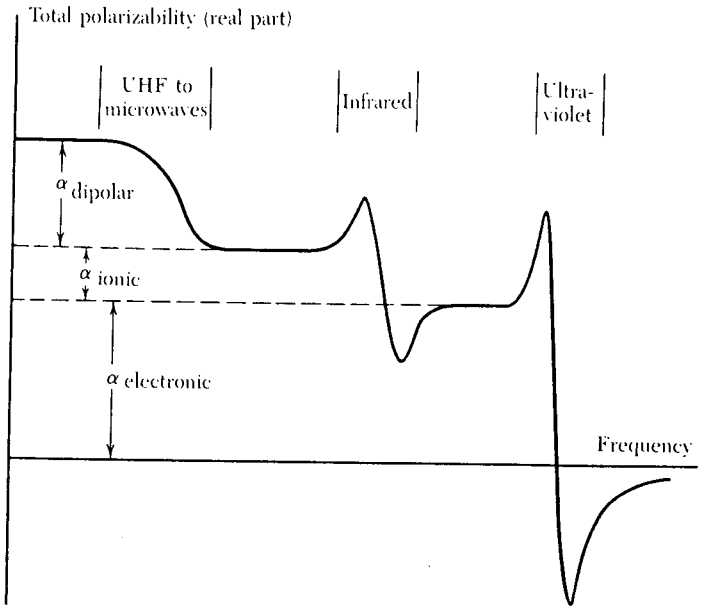

Fig. 5-3-14. Change of the polirizability of ordinal dielectric materials against the frequency

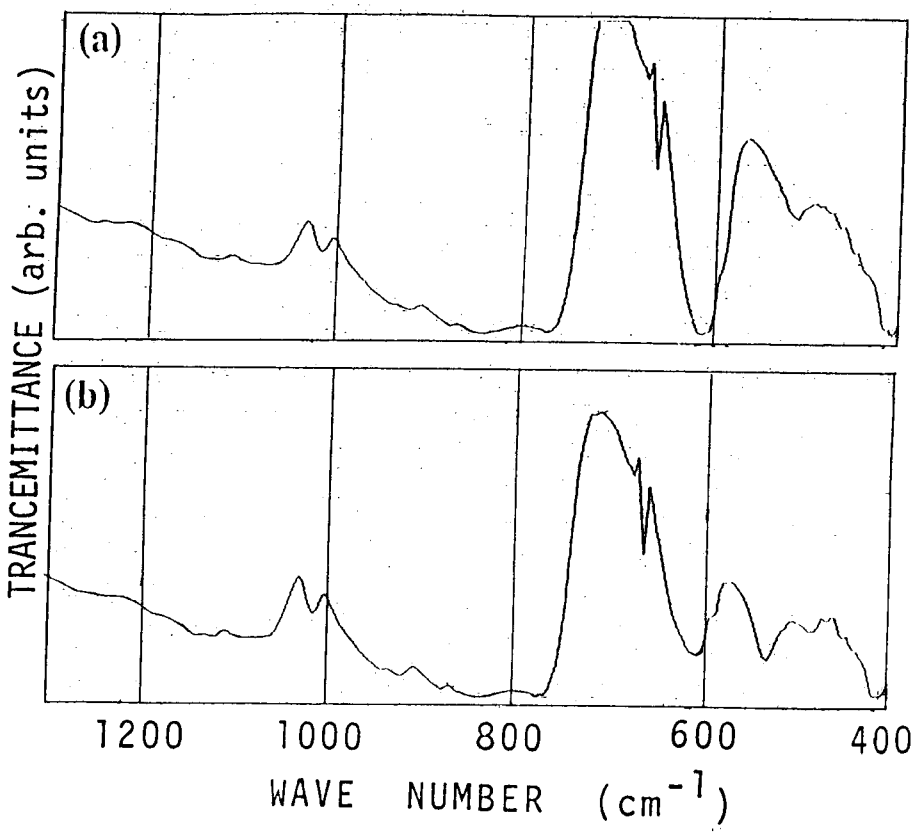

Fig. 5-3-15. FT-IR absorption spectra of (a) BTO/STO film (100/100 unit) and (b) SBTO film fromthe reflection-mode measurements. Total thickness is 2000Å

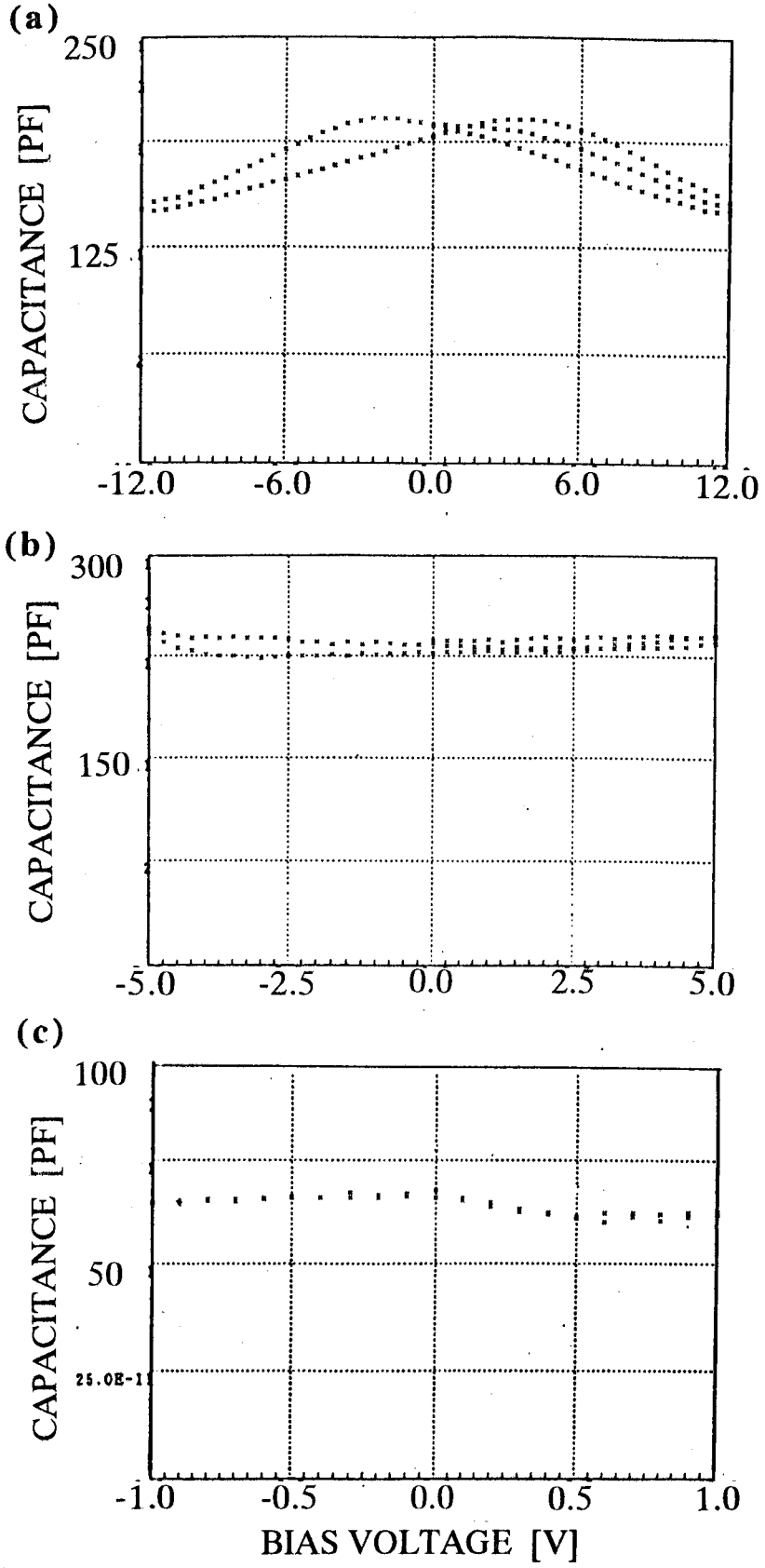

Fig. 5-3-16. Capacitance-voltage curves of (a) $BaTiO_3$ single pahse film, (b) STO/BTO (total 500 Å) and (c) STO/BTO (total 250 Å) with stacking 4/4 unit cell

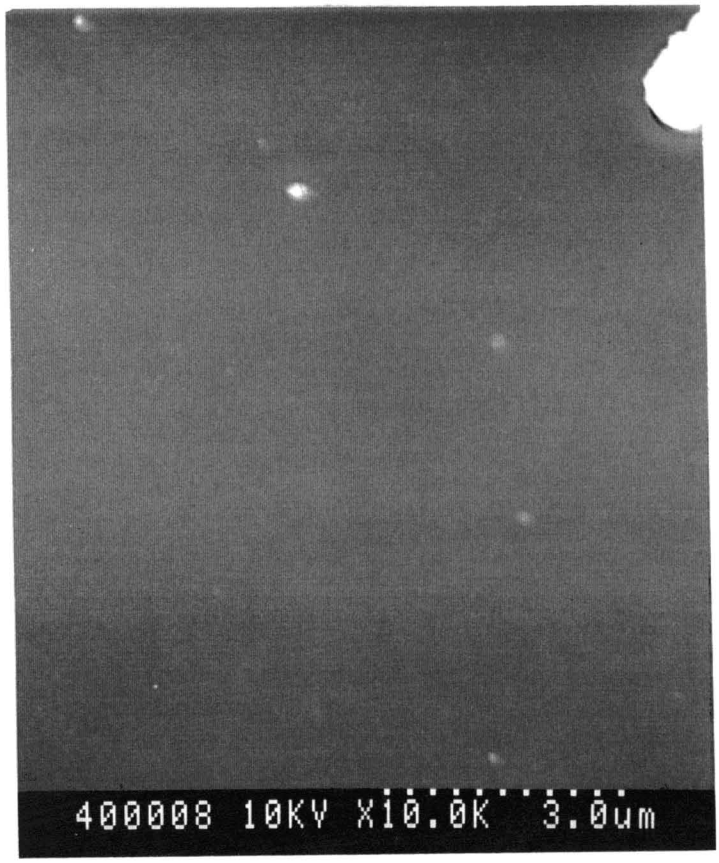

Fig. 5-3-17. SEM image of the $BaTiO_3/SrTiO_3$ superlattice deposited at 500 ℃ under $1x10^{-3}$ Torr $O_2+O_3(8\%)$ with the thickness of about 1000 Å.

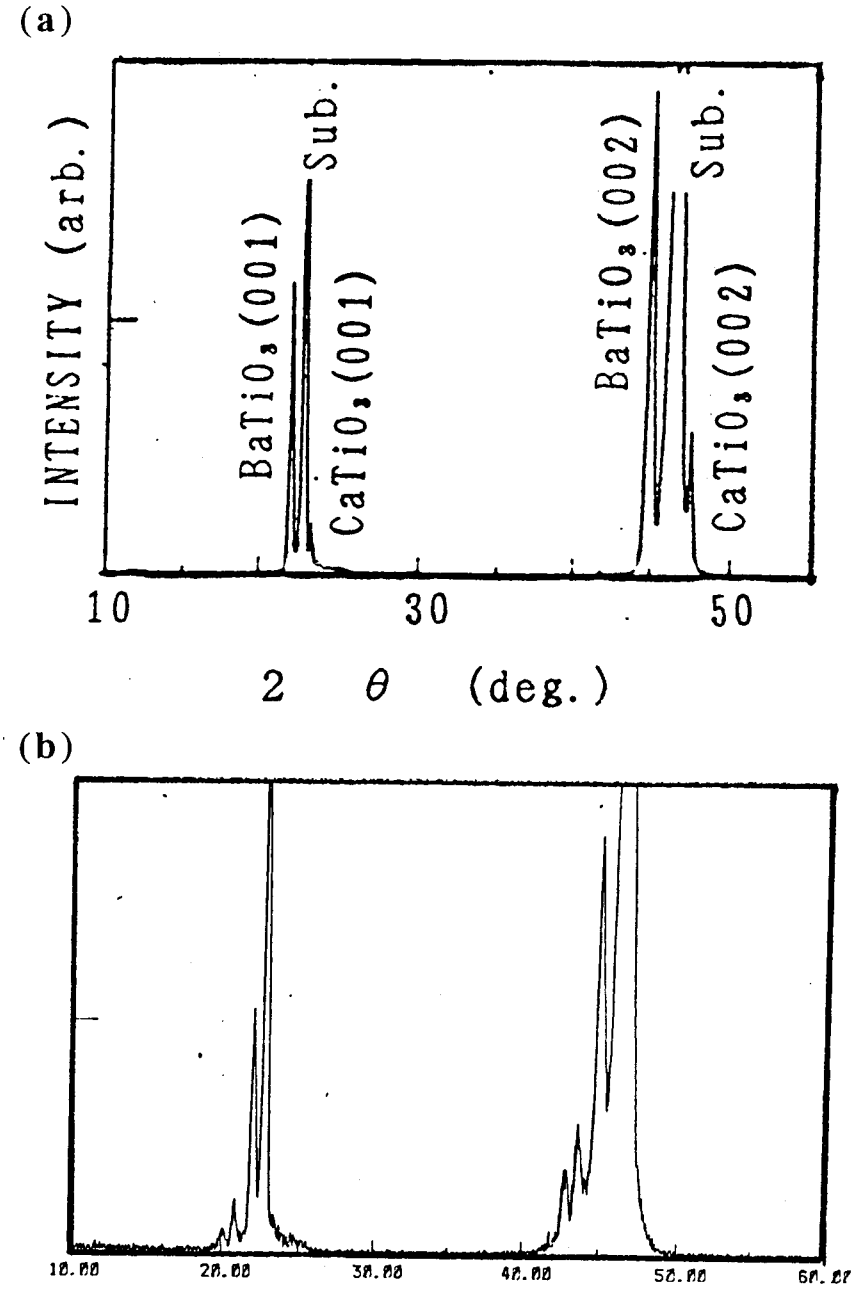

Fig. 5-3-18. (a) X-ray diffraction pattern of $CaTiO_3/BaTiO_3$ superlattice with stacking periodicity of 125 unit cell (500 Å) (b) The X-ray diffraction pattern of observed BTO(20 Å;5 unit cell)/STO(20 Å) superlattice.

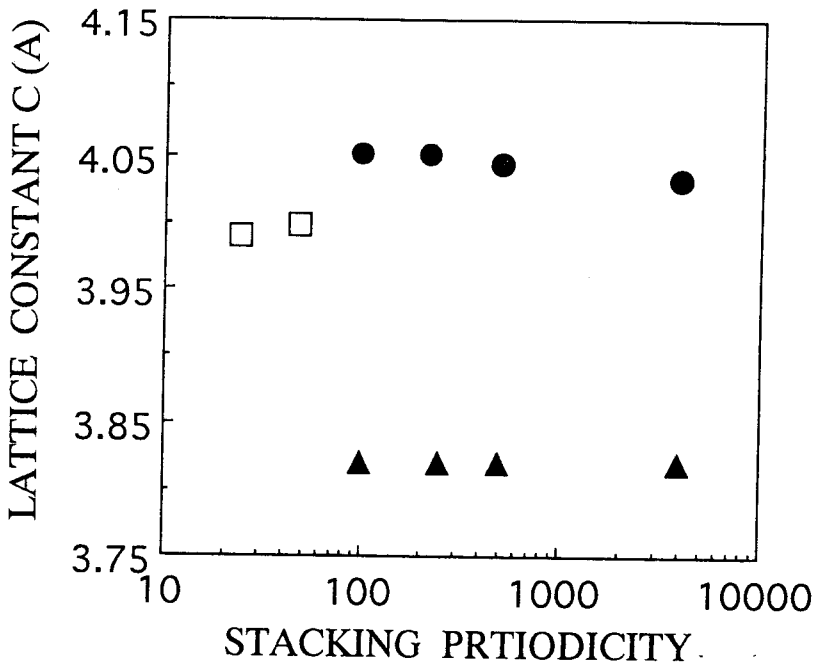

Fig. 5-3-19. Lattice constant c of BTO(●) and CTO(▲) layer in the $BaTiO_3/CaTiO_3$ superlattices against the stacking periodicity

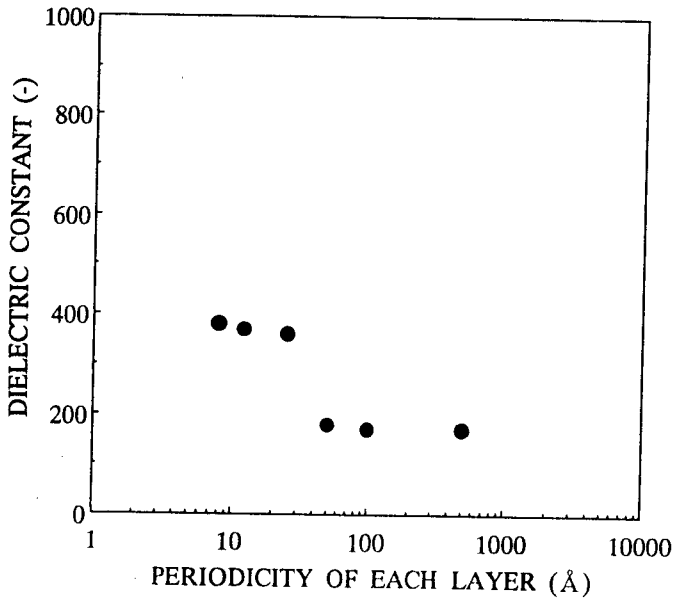

Fig. 5-3-20. Dielectric constant of the CTO/BTO superlattices vs periodicity of stacking each layer of CTO and BTO.

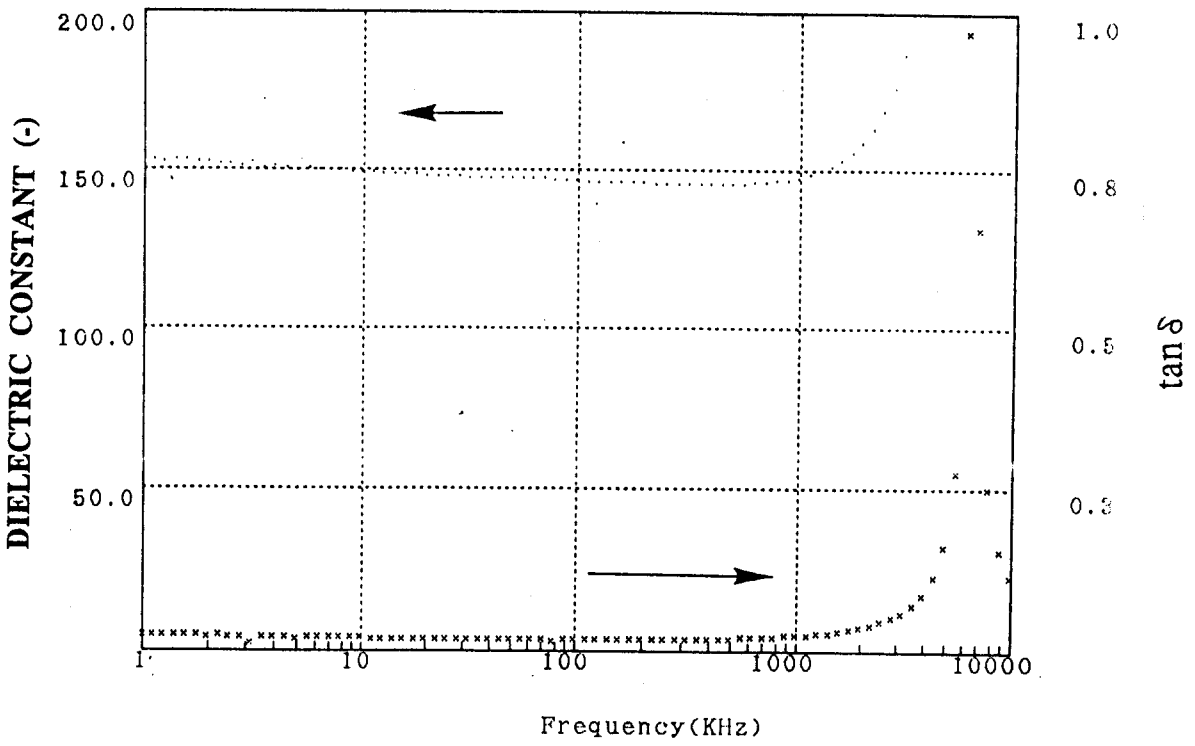

Fig. 5-3-21. Dielectric constant (ε r) and tan δ vs applied frequency at measured at RT.

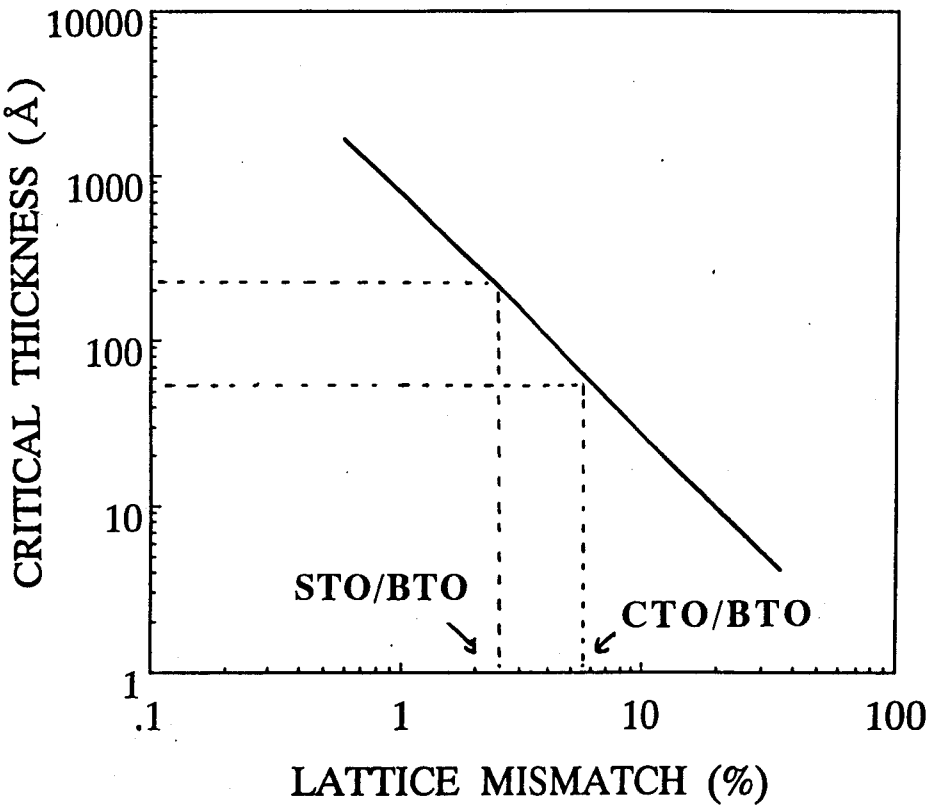

Fig. 5-3-22. Critical thickness for the misfit dislocation against the lattice mismatch (calculated from Matthews's theory)[ref)]

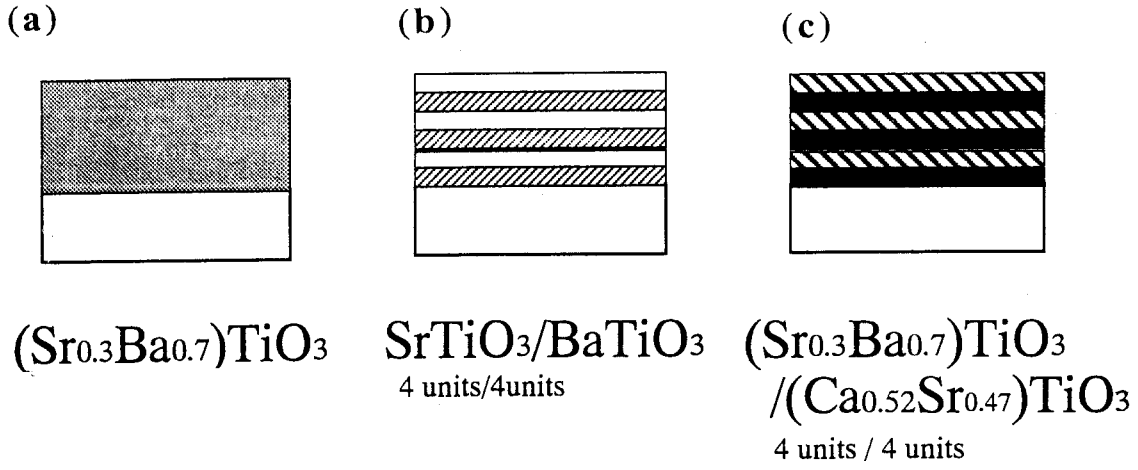

Fig. 5-3-23. Schematic model of

(a) $(Sr_{0.3}Ba_{0.7})TiO_3$ film of solid solution single pahse

(b) SrTiO3/BaTiO3 superlattice with 4/4 unit stacking

(c) $(Sr_{0.3}Ba_{0.7})TiO_3$ /$(Ca_{0.52}Sr_{0.48})TiO_3$ superlattice

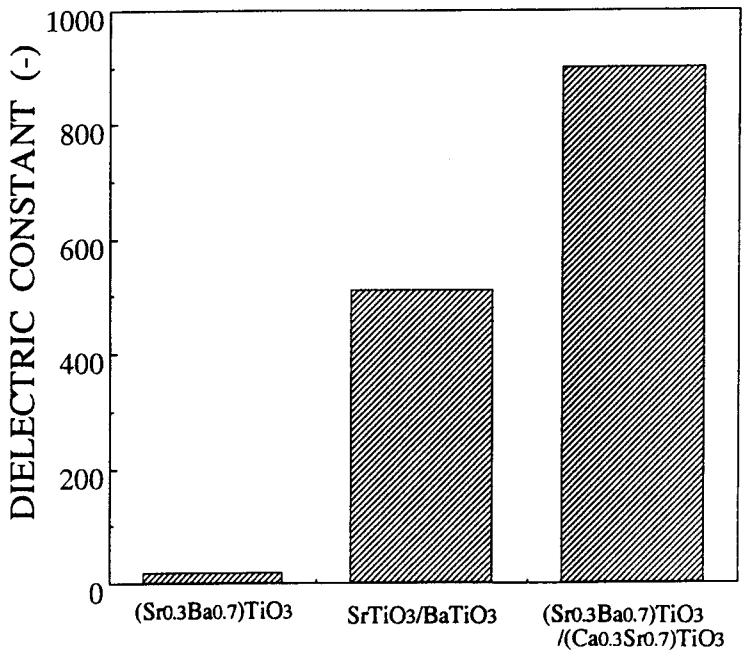

Fig. 5-3-24. Dielectric constant of several kinds of films. total thickness of the film is 500Å.

5-4. Artificial control with atomic layer scale

- Atomic layer growth of $SrTiO_3/BaTiO_3$ and $CaTiO_3/BaTiO_3$ -

Abstract

$SrTiO_3/BaTiO_3$ and $CaTiO_3/BaTiO_3$ superlattices have been formed with atomic layer scale. Monitoring the total diffraction pattern make it possible to control the film growth with atomic order accuracy.

Experiment

For the control of the crystal structure with atomic layer scale, metallic strontium(Sr), barium(Ba), calcium(Ca) and titanium oxide(TiO_2) were used for the targets. The pulsed laser (ArF excimer : wavelength = 193nm) beam was focused onto the targets of Sr, Ba, Ca and TiO_2 targets alternately and energy fluence of 1 - 0.5 J/cm^2, and the STO(Sr/TiO_2), CTO (Ca/TiO_2) and BTO(Ba/TiO_2) layers were stacked up layer-by-layer on the substrate (see Fig. 5-4-1). The thickness of each layer was varied from 4 Å (it means 1 unit cell) to 250Å (about 60 unit cells). The total thickness of these superlattices were varied 500, 1000 and 2000Å. The substrate used was 1%-Nb doped conducting $SrTiO_3$ single crystal(100) with a conductivity of $< 10^{-4}$ ohm cm. The films were formed at the substrate temperature of 650 ℃ in an oxygen (O_2:O_3=92%:8%) ambient a pressure of 1 mTorr. The epitactic formation of the films were monitored by reflection high energy electron diffraction(RHEED) measurement in situ and pole figure measurement using four circle X-ray diffraction method ex situ. The deposition rate was 3-

5 Å/min.

Results and Discussion

1). Growth of $BaTiO_3$ - BaO/TiO_2 with atomic layer scale -

Figure 5-4-2 shows the oscillation of RHEED intensity during formation of BaTiO3 film by depositing Ba / TiO_2 sequence on $SrTiO_3$(100) substrate. One cycle of the oscillation exactly corresponds to the growth of one atomic layer of BaO or TiO_2. Fig. 5-4-3 shows cross section image of RHEED pattern along <100>. From this result, lattice constant a (that is; in-plane lattice parameter) can be estimated. The change of the lattice constant a during the film formation is shown in Fig.5-4-4. It is interesting that the lattice constant a of $BaTiO_3$ film shows similar value to $SrTiO_3$ substrate at first step of film growth. The lattice constant a of BaTiO3 layer keep constant at 3.90 Å up to pile up 10-12 layers of $BaTiO_3$. After the number of $BaTiO_3$ layers above around 15 layers, the lattice constant a increases to suddenly from 3.90 Å → 4.08~4.10 Å.

2). Growth of artificial $BaTiO_3/SrTiO_3$ and $BaTiO_3/CaTiO_3$ superlattices with atomic layer scale

Figure 5-4-5 and 5-4-6 shows a RHEED intensity oscillation of the specular beam observed <100> azimuth during the formation of STO/BTO and CTO/BTO superlattices by layer-by-layer successive deposition, respectively. To determine the growth unit of Sr, Ba, TiO_2 corresponding to an oscillation period, we have independently measured the thickness of STO/BTO and CTO/BTO superlattices. It is sure that one cycle of the oscillation corresponds to one molecular layer growth of SrO,

TiO_2 and BaO by comparing with the number of the stacking cycles and the total thickness of the film. Furthermore, the RHEED patterns showed streaks throughout the film growth process, indicating that these materials can be formed by layer-by-layer growth with flat surfaces. With this technique, STO and BTO layer are deposited followed by each layer alternately. Monitoring the total diffraction pattern make it possible to control the film growth with atomic order accuracy.

Conclusion

In conclusion, the strained dielectric superlattices have been constructed with the stacking combination of STO and BTO layers. The in-situ monitoring of RHEED oscillation is effective technique to control the crystal structures at atomic order accuracy. The STO/BTO superlattices show larger dielectric constants than that of SBTO single phase films. The formation of dielectric and ferroelectric superlattices are the essential approach to create the new high-dielectric materials and to elucidate the mechanism of ferroelectricity.

References

1) M.Y.Chern, A.Gupta, B.W.Hussey and T.M.Shaw, J.Vac. Sci. Technol. 11 (1993) 637.

2) R.A.McKee, F.J.Walker, J.R.Conner, E.D.Specht and D.E.Zelmon, Appl. Phys. Lett. 59 (1991) 782.

3) Y.Shibata, K.Kaya, K.Akashi, M.Kanai, T.Kawai and S.Kawai, Appl. Phys.Lett., 61 (1992) 1000.

4) E.N.Bunting, G.R.Shelton and A.S.Creamer, J.Am.Ceram.Soc. 30 (1947) 114.

5) A.Wailenhorst, C.Doughty, X.X.Xi, S.N.Mao, Q.Li, T.Venkatesan and R.Ramesh, Appl.Phys.Lett. 60, (1992) 1744.

6) Z.Q.Shi, Q.X.Jia and W.A.Anderson, J.Vac.Sci.Technol., 11 (1993) 1441.

7) K.Iijima, T.Terashima, K.Yamamoto, K.Hirata and Y.Bando, Appl.Phys.Lett., 56 (1990) 527.

8)S.Marais, V.Heine, C.Nex and E.Salje, Phys.Rev.Lett. 66 (1991) 2048.

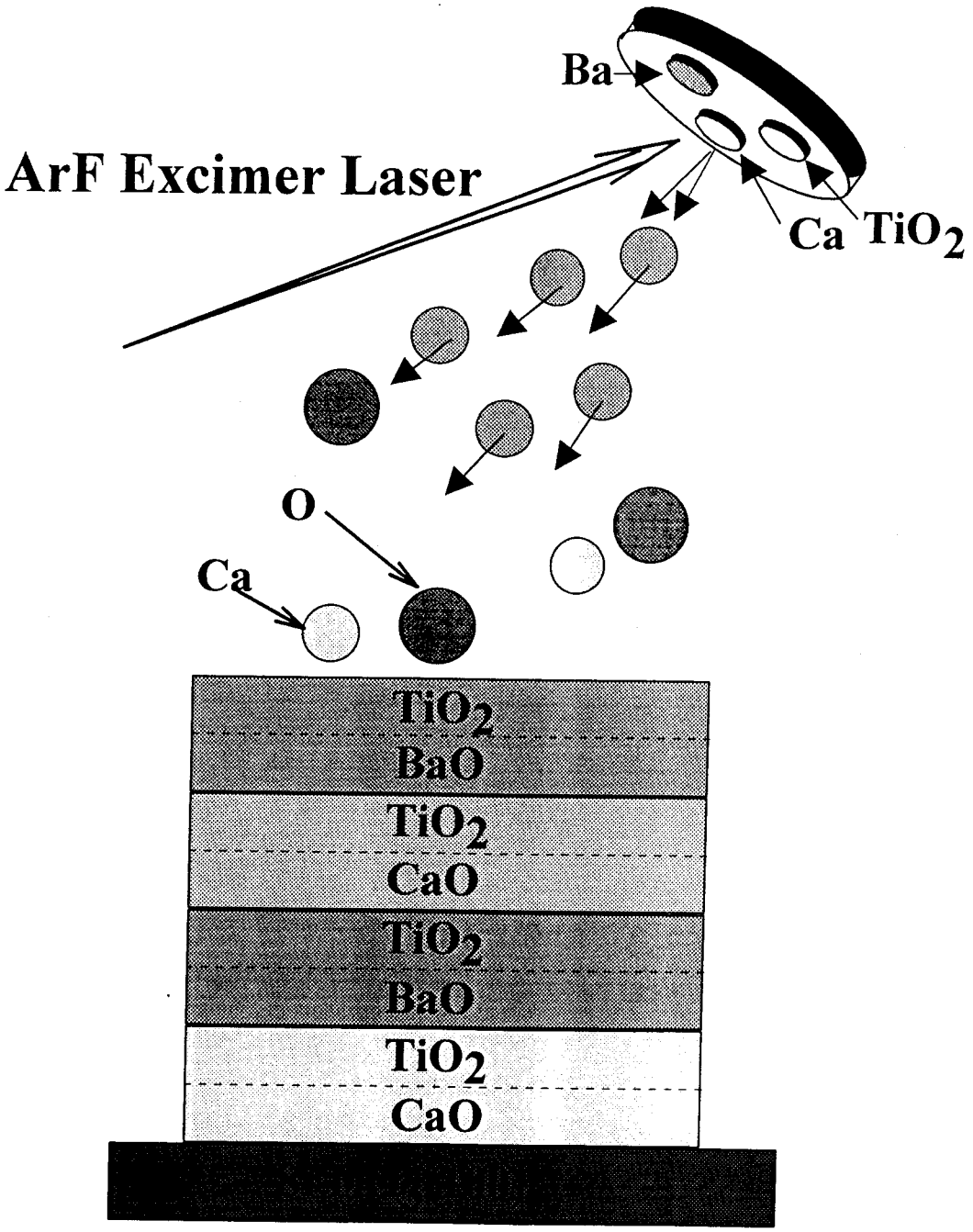

Fig. 5-4-1. Schematic image of forming the $BaTiO_3/SrTiO_3$ superlattice controlled with atomic scale

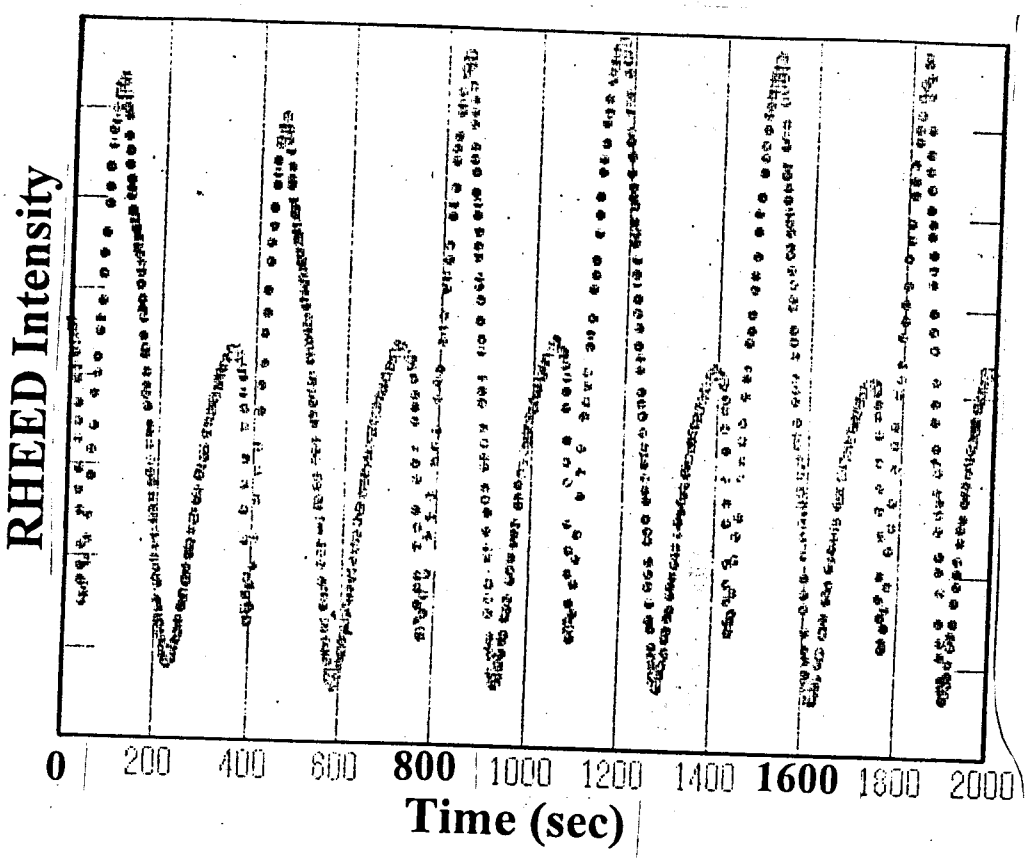

Fig. 5-4-2. Oscillation of RHEED pattern during the formation of $BaTiO_3$ with atomic scale control by depositting with BaO/TiO_2 sequence

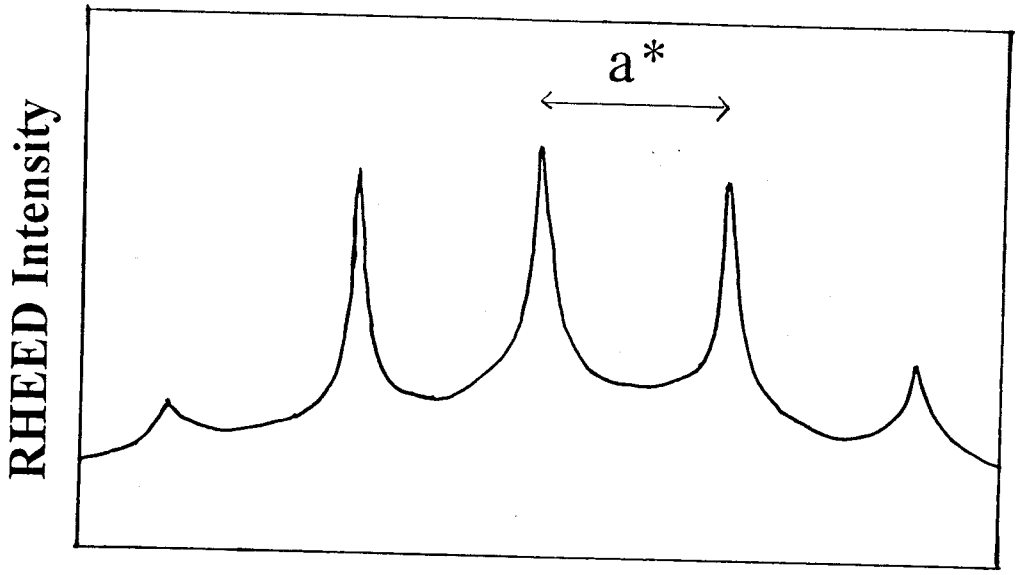

Fig. 5-4-3. Cross veiw of intensities of RHEED pattern

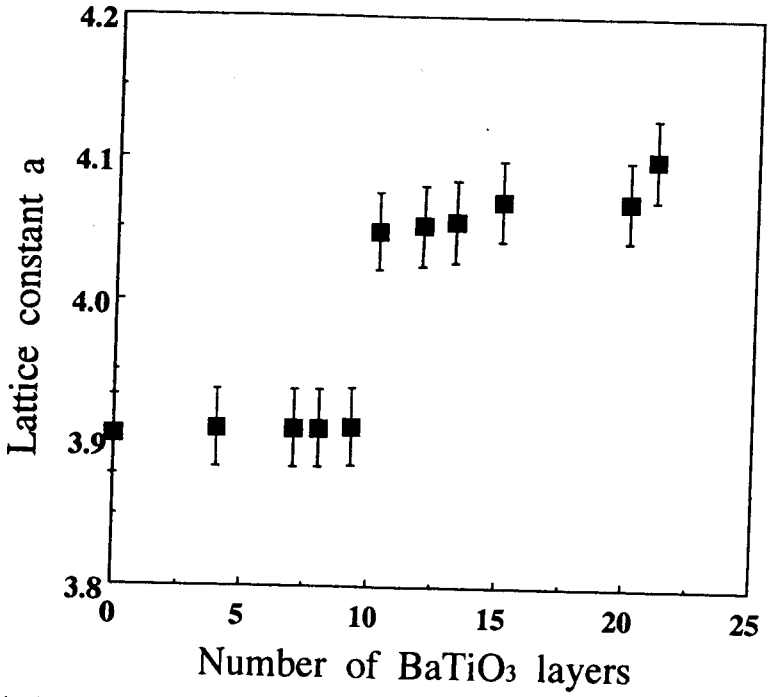

Fig. 5-4-4. Lattice constant a of $BaTiO_3$ formed with layer by layer with atomic layer acculacy vs nubmer of growth layers.

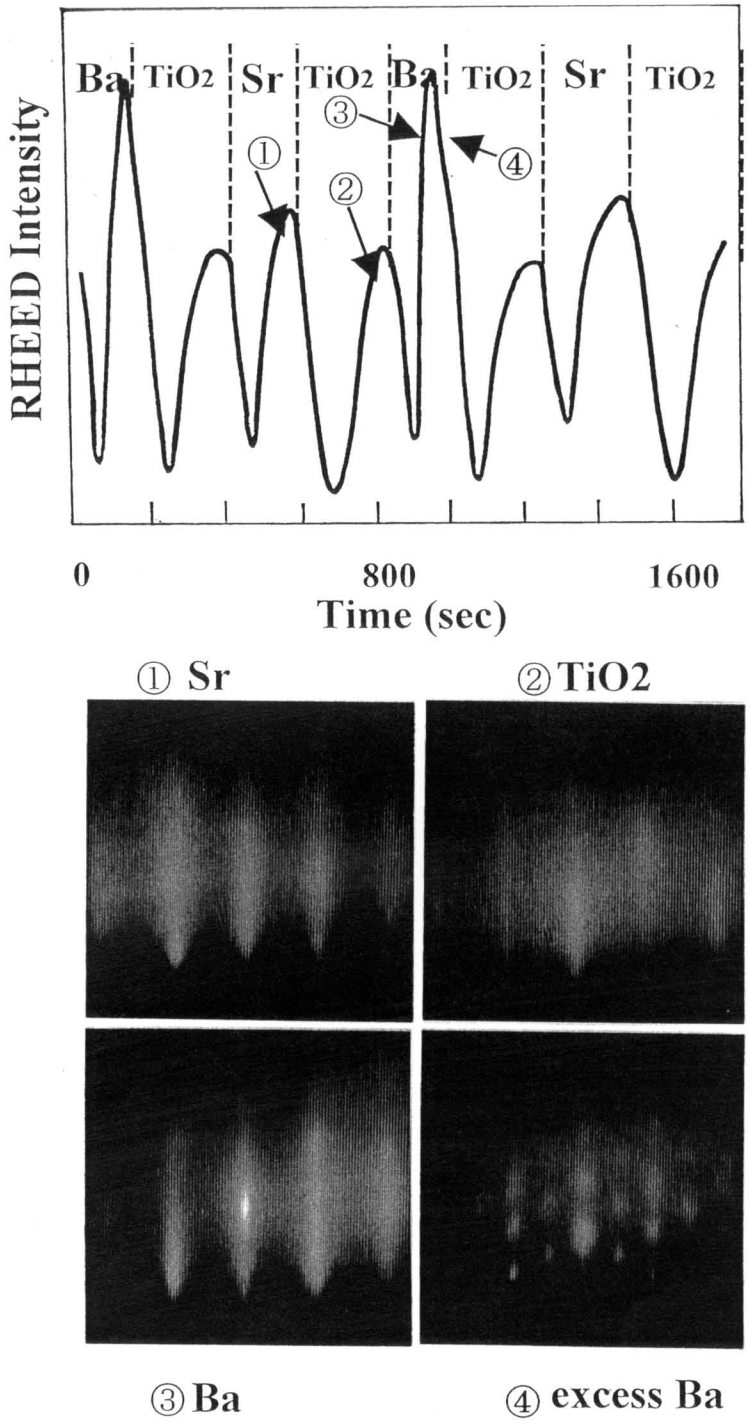

Fig. 5-4-5. Variations of RHEED pattern and intensities of oscillation through formation of $BaTiO_3/SrTiO_3$ superlattice.

①after deposition of SrO layer, ②after deposiiton of TiO2
③after deposition of BaO,
④after deposition of above BaO monolayer

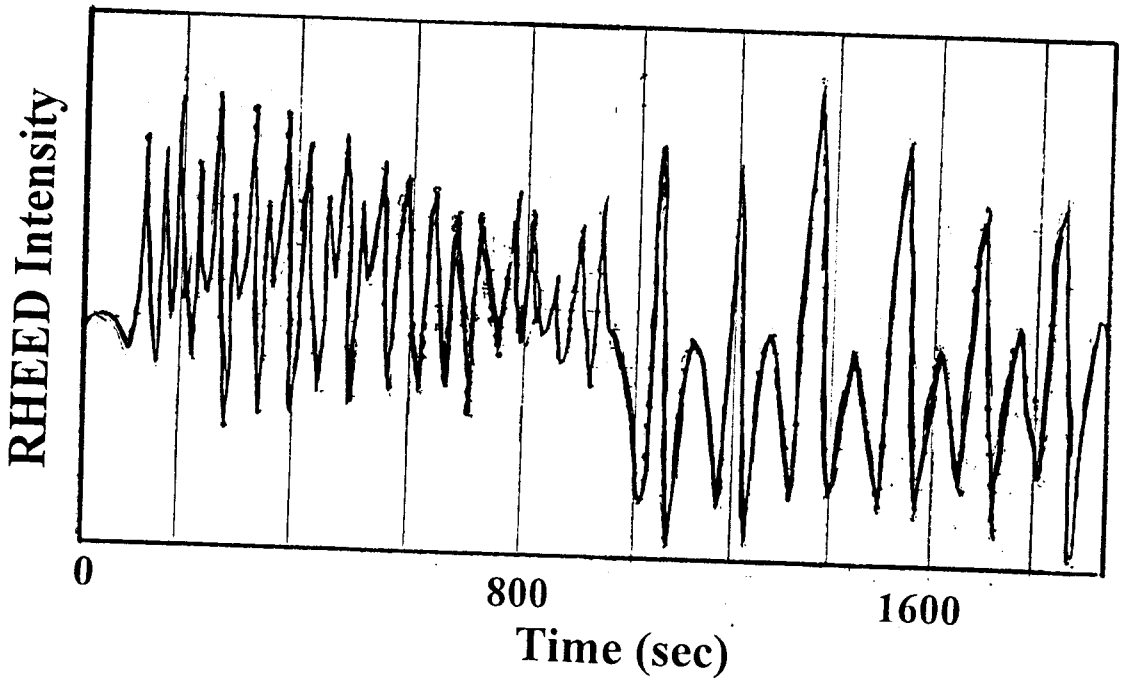

Fig. 5-4-6. Oscillation of RHEED pattern through formation of $BaTiO_3/CaTiO_3$ superlattice.

Chapter 6

6. Summary and future

In this study, comprising a fundamental research of "artificial superlattices" for the metal oxide films, the focus has been put on the construction and characterization of the superconductors and ferroelectric materials as well as related artificial superlattices. The molecular beam epitaxy is employed for the film formation of 3d-transition metal-oxides. For example, copper-oxide superconductors and titanium-oxide ferroelectric and their superlattices.

①Superconducting artificial lattices ; $(La,Sr)_2CuO_4/Sm_2CuO_4$, $(La,Sr)_2CuO_4/La_2CuO_4$(semiconductor), and $(La,Sr)_2CuO_4/(La,Sr)_2CuO_4$(over doped; metal)

②Ferroelectric artificial lattices ; $BaTiO_3/SrTiO_3$ and $BaTiO_3/CaTiO_3$

Site selective substitution is also demonstrated for the first time by the layer-by-layer successive deposition with laser MBE in $Bi_2Sr_2Ca_1Cu_2O_8$ compound.

The control sequence of the artificial lattice formation is as follows,

①unit cell level ; Superconducting artificial lattices and Ferroelectric artificial lattices

②sub-unit cell level ; Superconducting artificial lattices

③atomic level ; Ferroelectric artificial lattices

The factor for determining the thin film growth is lattice matching and the charge neutrality of each separated layer.

In chapter 3, the important factors for constructing 3d metal-oxide films is elucidated in the formation of metal-oxide compounds. Perovskite $PbTiO_3$ phase is constructed at the substrate temperature around 450℃ and in the oxygen pressure of 10-40 mTorr. In this case, the stability of PbO phase plays an important role for the $PbTiO_3$ film formation. Namely, one of the most important factor is metal oxide with low melting point (PbO) rather than that of high melting point (TiO_2). This is the guiding principle to form the metal oxide film which is constructed with the combination of high melting points and

low melting point compositions.

For controlling crystal orientation, the cooling rate as well as lattice matching is the important factor. Perfect c-axis oriented film can be formed with a cooling rate faster than 75℃/min. The laser ablated films exhibit good ferroelectric properties. The dielectric constant and rematent polarization of the 100% c-axis oriented $PbTiO_3$ films are 120-130 and 80 $\mu C/cm^2$, respectively. This large remnant polarization, which is quite similar to that of theoretical predicted, can be achieved for the first time by laser ablation.

The laser excitation process is one of the most typical feature of the laser ablation. The second laser irradiation at the substrate surface is quite effective for crystallization of the films at low temperature. The suitable energy density of the irradiation laser is in the range of 50-80 mJ/cm^2 in both substrate irradiation and vapor irradiation. And the laser irradiation effect is some kinds of photo-chemical effect.

In chapter 4, the new layer-by-layer technique enables us to control the larger number of the CuO_2 layers (n) sandwiched by the thick $Bi_2Sr_2CuO_6$ layers. With this technique, the number of "n" can be changed not only n=1-3 but also n=4-8 in $Bi_2Sr_2Ca_{n-1}Cu_nO_{2n+4}$. This basic concept and the particular synthesis technique will be useful to understand the mechanism of the high T_c superconductivity and also to create new compounds. This method will be applied to the other high T_c superconductors, since all the copper based superconductor have layered structure based on the $(Ca,Sr)CuO_2$ layers.

The superlattices of $(La,Sr)_2CuO_4/Sm_2CuO_4$ were formed onto $SrTiO_3$ substrates at unit cell accuracy by an excimer laser deposition technique. These superlattices can be classified into three regions. The controlled variations of the in plane Cu-O bond length and interlayer proximity coupling have been produced in $La_{1.85}Sr_{0.15}CuO_4$(LSCO) based superlattices. In $LSCO/Sm_2CuO_4$ strained superlattices, the in-plane lattice constant of the LSCO layers is increased and the

transition temperature (T_c) is decreased. The effective pressure is estimated about 8 GPa and the in plane Cu-O bond length is an important factor controlling T_c. For the LSCO /$La_{1.65}Sr_{0.35}CuO_4$(metallic) superlattices, a proximity-induced coherence length of 50Å is calculated for the metallic layer using the de Gennes-Werthamer theory.

In chapter 5, ferroelectric or dielectric materials ($BaTiO_3$, $SrTiO_3$ and $CaTiO_3$) are formed by the laser ablation on the $SrTiO_3$, $LaAlO_3$ and MgO single crystal (100) substrate. All the films can be formed epitaxially on the $SrTiO_3$ substrate with c-axis orientation. The electrical behaviors of these films such as dielectric constant and remanent polarization are quite similar to that of single crystals in bulk samples.

Artificial dielectric superlattices of $SrTiO_3/BaTiO_3$(STO/BTO) and $CaTiO_3/BaTiO_3$(CTO/BTO) have been formed by a pulsed laser ablation technique with an in situ monitoring of RHEED(reflection high energy electron diffraction) oscillation. The crystal structures can be controlled with atomic order accuracy and a large strain of 400-500 MPa is introduced at the interface between the BTO and STO layers. The superlattices show higher dielectric constant than that of $(Sr_{0.5}Ba_{0.5})TiO_3$ films with changing temperature or applied frequency. A large dielectric constant of 900 was observed for the superlattices with a stacking periodicity of 2 unit cells / 2 unit cells. The superlattices show drastically different electrical behavior from that of the solid solution (Sr,Ba)TiO_3 films, both with changing temperature or applied frequency. Broad maxima of the dielectric constants occur around 40-50 ℃ and the values remain large even for temperature above 200 ℃. On the contrary, in the case of CTO/BTO superlattices, lattice constants and dielectric constant do not change so much comparing with STO/BTO cases. Lattice mismatch in the STO/BTO and the CTO/BTO superlattices are 2.5% and 5.5%, respectively. In the case of CTO/BTO, the misfit dislocation such as

stacking faults may occur at the interface between CTO and BTO layers owing to large lattice mismatch.Therefore, lattice strain is introduced effectively below the lattice mismatch of about 3 %.

Finally, the strained dielectric superlattices have been constructed with the stacking combination of atomic scale with SrO/TiO_2 and BaO/TiO_2 layers. The in-situ monitoring of RHEED oscillation is effective technique to control the crystal structures at atomic order accuracy. The $SrTiO_3/BaTiO_3$ superlattices show larger dielectric constants than that of $(Sr,Ba)TiO_3$ single phase films. The formation of dielectric and ferroelectric superlattices are the essential approach to create the new high-dielectric materials and to elucidate the mechanism of ferroelectricity.

Chapter 7

7. Appendix

7-1. Preferential orientation in the thin film growth of $PbTiO_3$

Abstract

Orientation of the ferroelectric $PbTiO_3$ (PTO) thin films can be controlled with controlling the cooling rate after the film formation as described in Chapter 3-2. In these experiments, ferroelectric $PbTiO_3$ epitaxial thin films have been formed on a base electrode of Pt(100)/MgO (100) using ArF excimer laser ablation. The X-ray diffraction patterns of these films show c-axis orientation with a rocking angle of 0.5° when the film is cooled faster than 75℃ /min after the deposition. The films exhibit clear and large ferroelectric hysteresis loops of $80\mu C/cm^2$. C-axis orientated PTO film show a large pyroelectrical behaviors of 1000-1500 V/W without poling treatment.

Introduction

A considerable amount of research has been focused on the growth and device fabrication of ferroelectric then films for a variety of applications including: nonvolatile memories; ultrasonic sensors; and IR detectors. Recently, epitaxial ferroelectric films. such as $PbTiO_3$, PZT, and PLZT, have been successfully grown by a number of deposition techniques. A pulsed laser ablation technique, on the other hand, has been widely used with great success in producing high-quality thin films for high temperature superconductors. These superconductors are multi component oxides and have a perovskite structure just like many ferroelectric materials.

In this chapter I report the formation of preferential c-axis

oriented $PbTiO_3$ epitaxial films using pulsed laser ablation, and describe the pyroelectric behavior of $PbTiO_3$ films deposited on $SrTiO_3$(100) and MgO(100)a base electrode of platinum(100).

Experiment

The deposition system was already described in the earlier reports. Laser pulses from an ArF excimer laser, energy density of 1 J/cm^2, were focused onto a stoichiometric sintered $PbTiO_3$ target. A heated substrate was set parallel to, and at a distance of, 3 cm from the target. The wavelength. the pulse width, and repetition rate were 193 nm. 25 ns. and 10 Hz. respectively. The substrate used was MgO(100), $SrTiO_3$(100) and Pt/MgO(100). The substrate was heated to temperatures in the range of 400-550℃ and the temperature (T_s) was measured with an IR pyrometer and a chromel-alumel thermocouple clamped to the back of the substrate. The deposition experiments were carried out in an ambient oxygen/ozone atmosphere [O_2/O_3 (8%)] of 1-100 mTorr. The deposition rate was about 5nm/min and the thickness of the films was 1 μm.

Pryroelelctric behaviors were measured in the frequency of 10-60 Hz.

Results and discussion

The perovskite $PbTiO_3$ phase is observed in film deposited at an oxygen/ozone (8%) pressure of 10-100 mTorr in the temperature range of 400-500℃. The film composition of the perovskite phase films is stoichiometric $PbTiO_3$, Which is the same as that of the target. However, films deposited below

1 mTorr are Pb deficient, and had a mixed phase of pyrochlore and perovskite.

Figure 7-1-1(a) shows the tendency of the crystal orientation of the $PbTiO_3$ films by controlling the cooling rate. (same figure as Fig.3-2-8) Figure 8-1-1(b) shows the resistance vs cooling rate. The faster the cooling rate is the more the resistivity increase. From the view point of electric properties, The resistivity is required more than 10^8 ohm. Almost all c-axis oriented films are formed at a cooling rate faster than 75℃/min. On the contrary, the slower of the cooling rate is the better for the electric properties.

With the technique described above, the perfect c-axis orientation of the $PbTiO_3$ film can be formed. Pyroelectric voltages are detected on these particular laser ablated epitaxial $PbTiO_3$ films even without poling treatment. This property of the films being polarized in the as deposited state without poling treatment would be very advantageous in the production of one- or two-dimensional array IR detectors of small size because it is difficult to polarize all the elements of a detector uniformly after deposition of the film In addition, the pyroelectric voltage values are in good agreement with the degree of c-axis orientation. Figure 7-1-2 shows the relationship between pyroelectric voltage and frequency of IR irradiation with an intensity of $10^{-7}W/cm^2$. All the data are amplified to 60 dB. The pyroelectric voltage of the 95% c-axis oriented sample (Fig. 7-1-2;■) is twice as large as that of 40% sample (Fig. 7-1-2: ▲). The dielectric constant of the excimer laser ablated films with a thickness of 1 μm was determined to be 120-130 with a dissipation factor (tan d) of 0.03-0.05 at 1 kHz.

Besides this cooling rate effect, the lattice matching at the interface between films and substrates is of great importance for the epitaxial film growth. The $SrTiO_3$ and the MgO substrates have about 0.3% and 7.7% lattice mismatching with $PbTiO_3$, respectively, at 400℃ [Figs 7-1-3(a) and (b)]. Furthermore, the

$SrTiO_3$ substrate has the perovskite structure as $PbTiO_3$. The MgO substrate, on the other hand, has rock salt type structure. Figures 7-1-3(c) and (d) show the x-ray diffraction pattern of the $PbTiO_3$ films deposited on the $SrTiO_3$ and MgO substrate, respectively. Figure 7-1-3(c) shows strong (001) and(002) peaks indicating that the film is preferentially oriented with the c-axis perpendicular to the $SrTiO_3$ substrate.Perovskite $PbTiO_3$ is crystallized at the temperature of 450 and 380℃ on the MgO and $SrTiO_3$ substrates, respectively. This difference derives from the difference of the lattice mismatching. The lattice constant a of $SrTiO_3$ and $PbTiO_3$ are 3.905 Å (at RT), 3.915 Å (at 380℃) and 3.90 Å (RT), 3.89 Å (380℃), respectively. The lattice constant a of the $SrTiO_3$ (100) substrate is identical to that of $PbTiO_3$(100) film . The closely matched lattice constants of the film and substrates (0.2%-2%) result in epitaxial growth of the films at relatively low temperature. The SEM images show the the surface of the film is very smooth. The RHEED patterns show the epitaxial growth of the film.

This result suggests that a good lattice matching between the film ($PbTiO_3$) and the substrate ($SrTiO_3$) has facilitated the formation of the films at low temperature. The epitaxial and c-axis oriented nature of the films account for the high ferroelectrical behavior obtained without poling.

Conclusion

In summary, ferroelectric $PbTiO_3$ thin films have been formed by an ArF excimer laser ablation technique. The crystal orientation of the films can be controlled by the combination with the substrate. The c-axis orientated $PbTiO_3$ films show large pyroelectric properties of1000-1500 V/W at a frequency of 10 Hz without poling treatment.

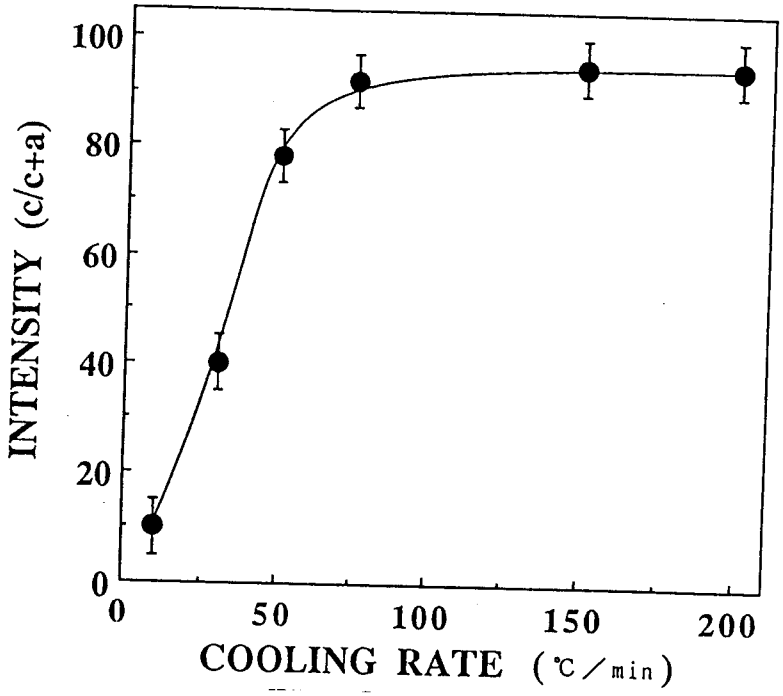

Fig. 8-1-1 (a) c-axis preferred orientation of the PbTiO3 films vs cooling rate after contracting the films.

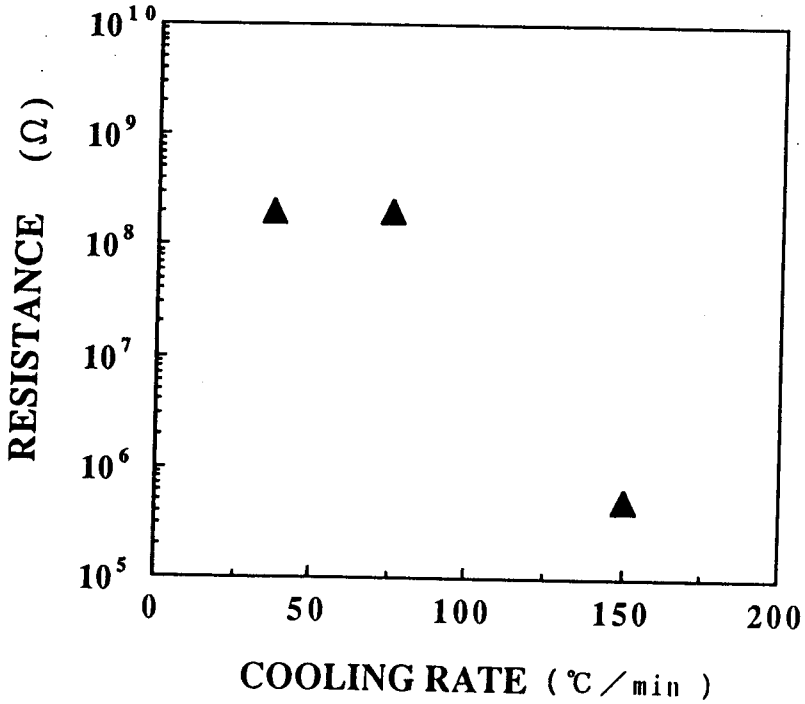

Fig. 8-1-1 (b) Resistance of the $PbTiO_3$ films vs cooling rate.

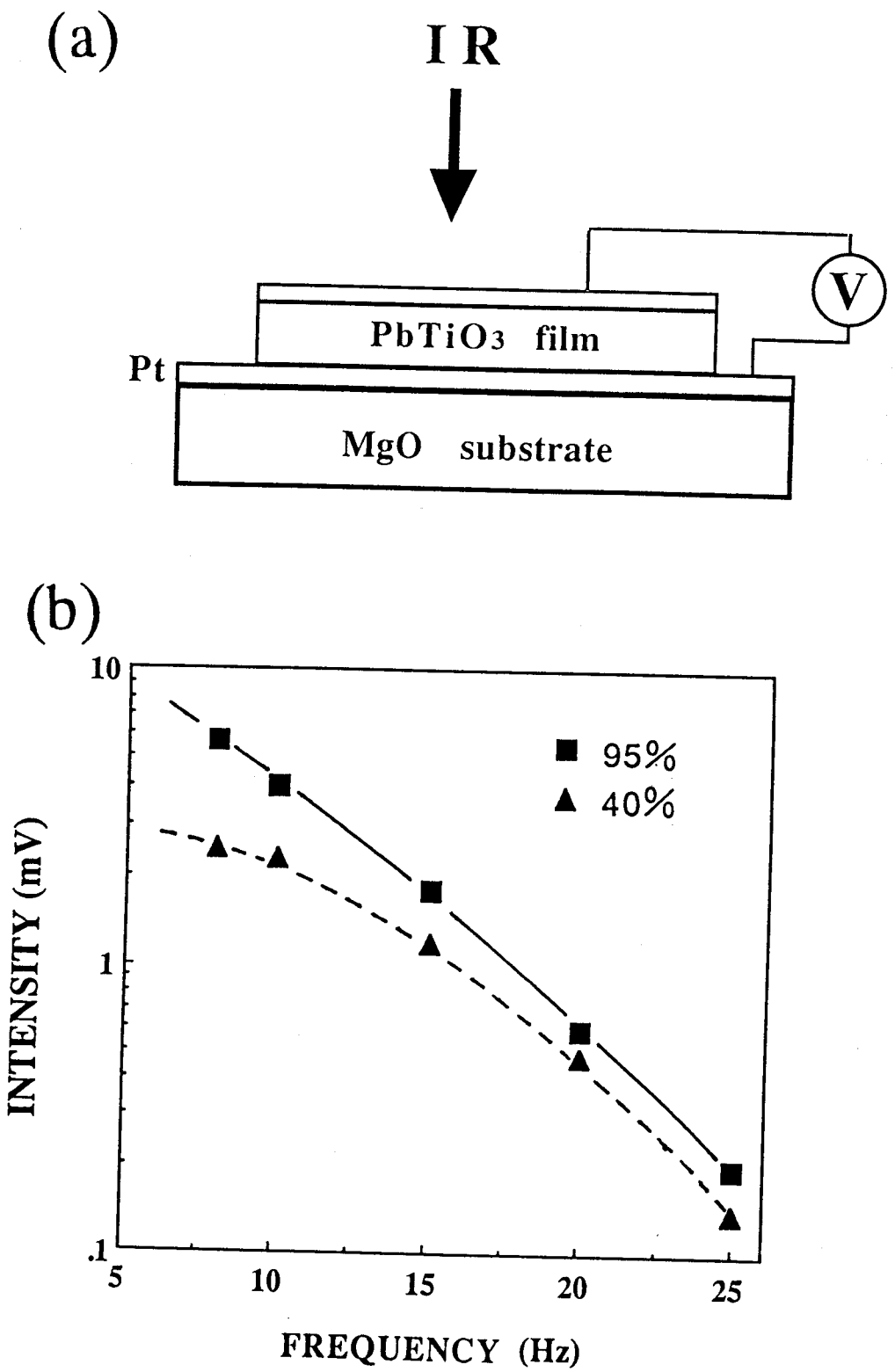

Fig. 8-1-2 (a)Schematic image of pyroelectric measurement. (b) Pyroelectric behaviors against the changes in applied frequency. ■ data of 95% c-axis orientation film, ▲ data of 40% film.

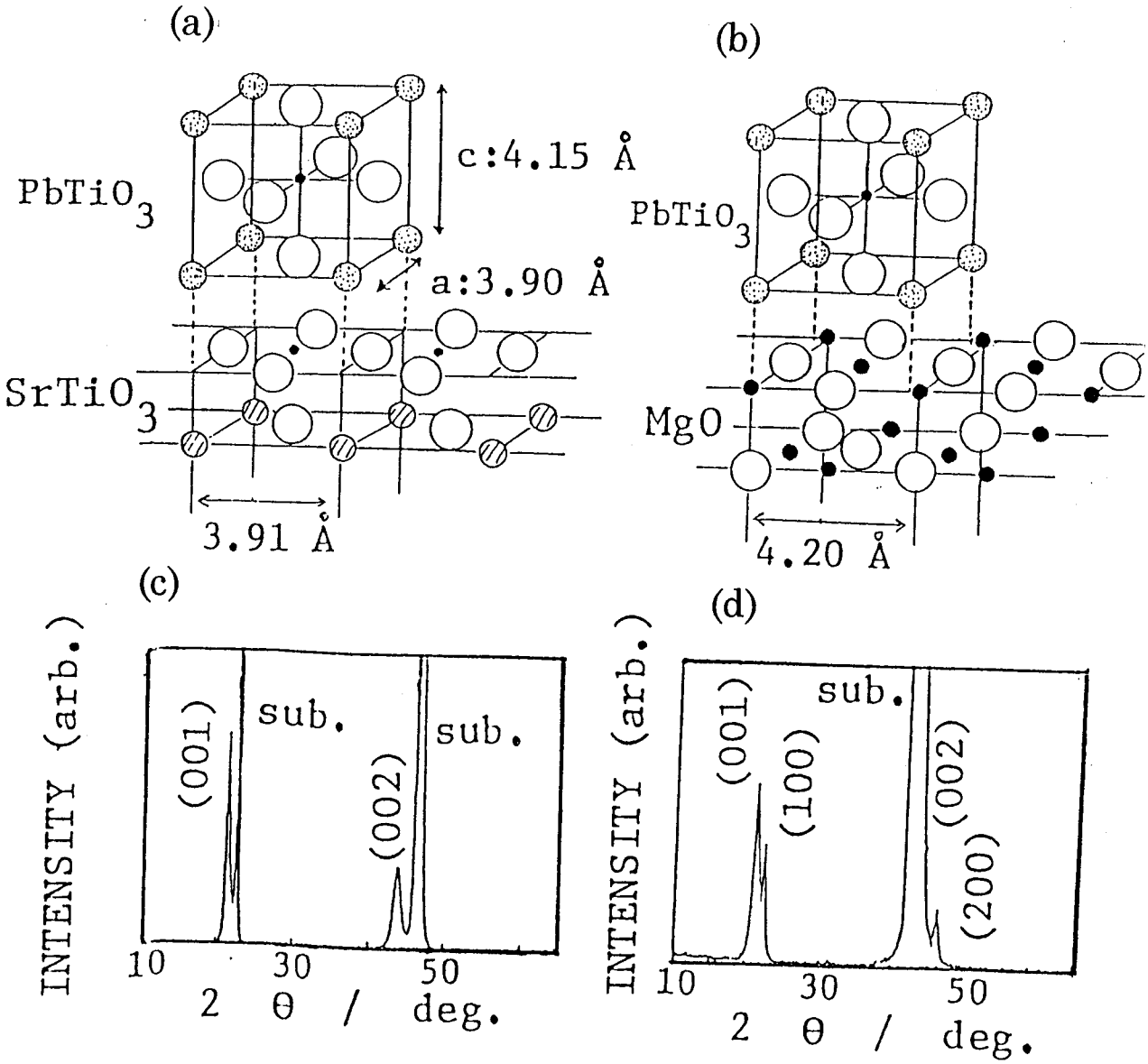

Fig. 8-1-3 Crystal structures of $PbTiO_3$ on (a) $SrTiO_3$ substrate and (b) MgO substrate, X-ray diffraction patterns of $PbTiO_3$ films deposited on (c) $SrTiO_3$ at 380℃ and (d) on MgO at 450℃.

7-2. Heteroepitaxy of ferroelectric films on oxide superconductors

Introduction

When ferroelectric/dielectric materials are used for application and measured their basic properties, a bottom electrode is required. So far, metal electrode, such as Pt, Ti, Au and Al are used. These metal electrodes have good conductivities (< 10^{-5} Ωcm) but the lattice parameter are not suitable for formation of 3d metal oxide materials. The ferroelectric materials and oxide superconductors have quite similar crystal structure of "perovskite". Furthermore, lattice constant is almost same. For example, lattice constant a of $PbTiO_3$ and $YBa_2Cu_3O_7$ are 3.90 Å and 3.84-89 Å, respectively. Therefore, heteroepitaxy between ferroelectric materials and superconductors is very important.

Experiment

For the based electrode, typical three kinds of based electrode is selected, that is Pt(FCC) , Nb-doped(1 mol%) $SrTiO_3$(perovskite) and oxide superconductors $(La_{1.85}Sr_{0.15})CuO_4$ or $YBa_2Cu_3O_7$(perovskite). They were deposited on the $SrTiO_3$(100) or MgO(100) single crystals at 500 ~ 700℃. When the oxide superconductors were deposited on the substrate, oxygen (1-5 x 10^{-3} Torr)was introduced during the film formation. The films were observed with X-ray diffraction pattern and RHEED monitor to determine orientation and crystallinity.

Results and discussion

Figure 7-2-1 shows X-ray diffraction patterns and RHEED pattern of the based electrode films of Pt and $La_{1.85}Sr_{0.15}CuO_4$ (LSCO;oxide superconductor) coated on MgO or $SrTiO_3$ substrate. They show preferred c-axis orientation to the substrate surface. Streak patterns of RHEED image indicate that these film (Pt and LSCO) grow with atomically ordered flat surfaces. The resistivities of (a)Pt film and (b)$YBa_2Cu_3O_7$ are shown in Fig.7-2-2. The resistivities decrease with decreasing temperature below 300K. The $YBa_2Cu_3O_7$ film show metal $\rightarrow$ superconducting transition at around 90K.

Figure 7-2-3 shows the X-ray diffraction patterns of $PbTiO_3$(PTO) films deposited on the bottom electrode of (a) Pt, (b) Nb-$SrTiO_3$ (STO) and $YBa_2Cu_3O_7$(YBCO). In all cases, PTO film have c-axis orientation to the substrate surface. Furthermore, pole figure shows in plane orientation of (a)PTO/LSCO) and PTO/Pt indicating cube-on-cube epitaxial relationship of the multi layers.(Fig.7-2-4) That is ; PTO film can grow epitaxially on the bottom electrode of both Pt and oxide superconductors(YBCO and LSCO). Rocking curves of PTO films at (001) diffraction pattern are shown in Fig.7-2-5. The FWHM(full width at half maximum) are 0.5-0.6° (PTO/YBCO and PTO/LSCO sequence) and 1.0 ° (PTO/Pt). The lattice matching between PTO-Pt, PTO-YBCO and Pt-LSCO are almost same. Therefore, the crystal structure of perovskite and surface energy of oxide/oxide(PTO/oxide superconductor) comparing with metal/oxide(PTO/Pt) play important role for the film formation.

Conclusion

In conclusion, heteroepitaxy of ferroelectric materials on the oxide superconductors have been demonstrated. For the crystal growth and electrical applications, heterostructure of ferroelectric materials / oxide superconductors is essential approach to get the epitaxial thin films.

References

1) J.F.Scott and C.A.Paz deAraujo ; Science 246 (1989) 1400.

2) J.L.Moll and Y.Tarui; IEEE Trans.Electron Devices ED-10 (1963) 338.

3) S.Y.Wu ; IEEE Trans. Electron Devices ED-21 (1974) 499.

4) Y.Yoneda, H.Kasatani, H.Terauchi, Y.Yano, T.Terashima and Y.Bando; J.Phys.Soc.Jpn. 62 (1993) 1840.

5) T.Yamamoto, K.Urabe and H.Banno ; Jpn.J.Appl.Phys. 32 (1993) 4272.

6) W,Kaezing ; Phys.Rev. 98 (1955) 549.

7) M.Okuyama, Y.Matsuji, H.Nakano and Y.Hamakawa ; Ferroelectrics 33 (1981) 235.

8) Y.Miyasaka and S.Matsubara ; Proc.7th Int. Symp.Application Ferroelectric (IEEE, New York, 1991) 3556.

9) K.Iijima, T.Terashima, K.Yamamoto, K.Hirata and Y.Bando ; Appl.Phys.Lett. 56 (1990) 527.

10) R.Ramesh, W.Chan, B.Wilkens, T.Sands, J.Tarascon, J.Keramidas and J.Evans ; Integrat. Ferroelectr. 1 (1992) 1.

11) Y.Watanabe ; Appl.Phys.Lett. 64 (1993) 1295.

12) C.B.Sawyer and C.H.Tower ; Phys.Rev. 35 (1930) 269.

13) C.J.Johnson ; Appl.Phys.Lett. 7 (1965) 221.

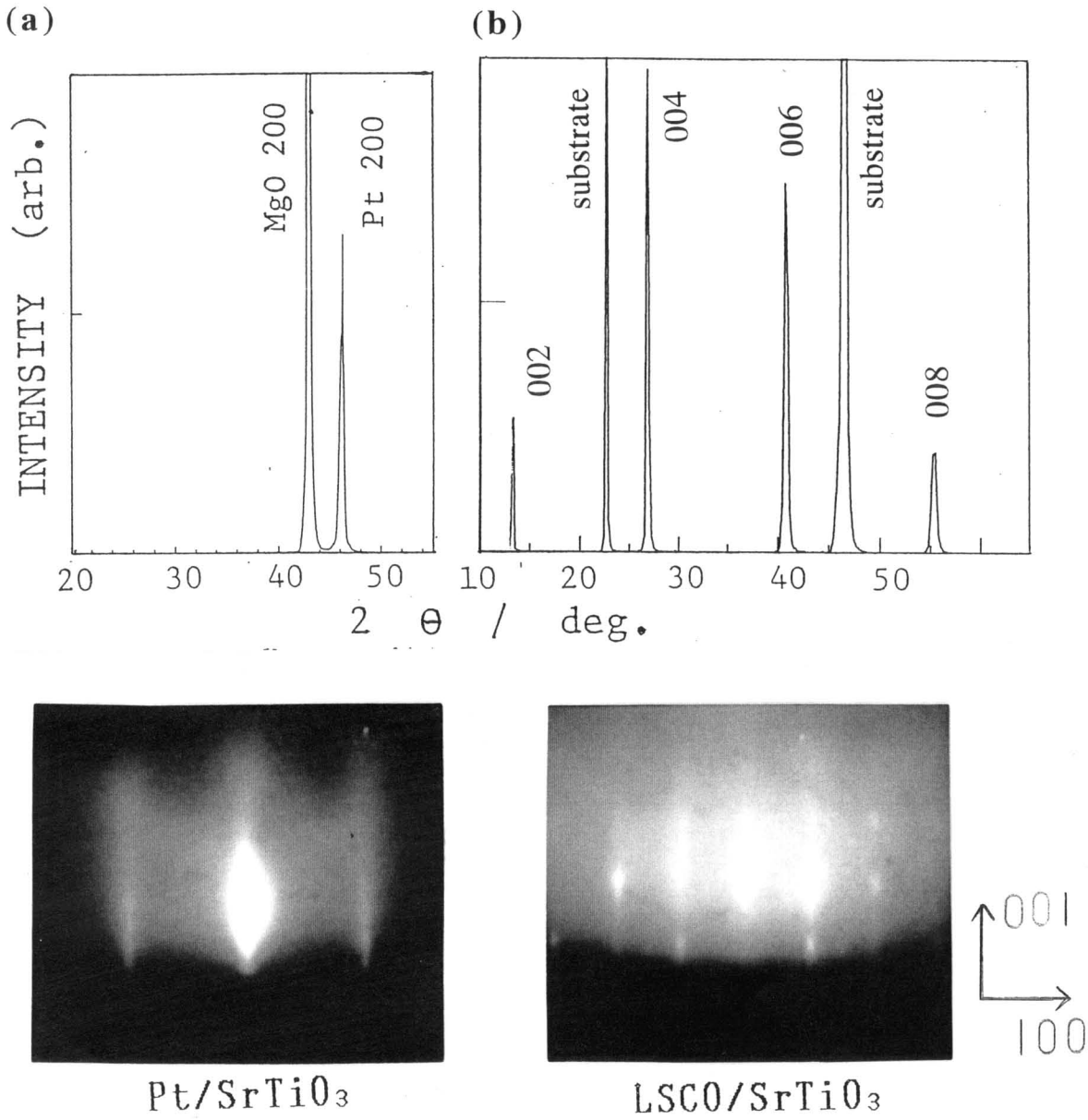

Fig. 7-2-1. X-ray and RHEED patterns of Bottom electrode (a)$Pt/SrTiO_3$ substrate and (b) $La_{1.85}Sr_{0.15}CuO_4$ (LSCO;oxide superconductor)

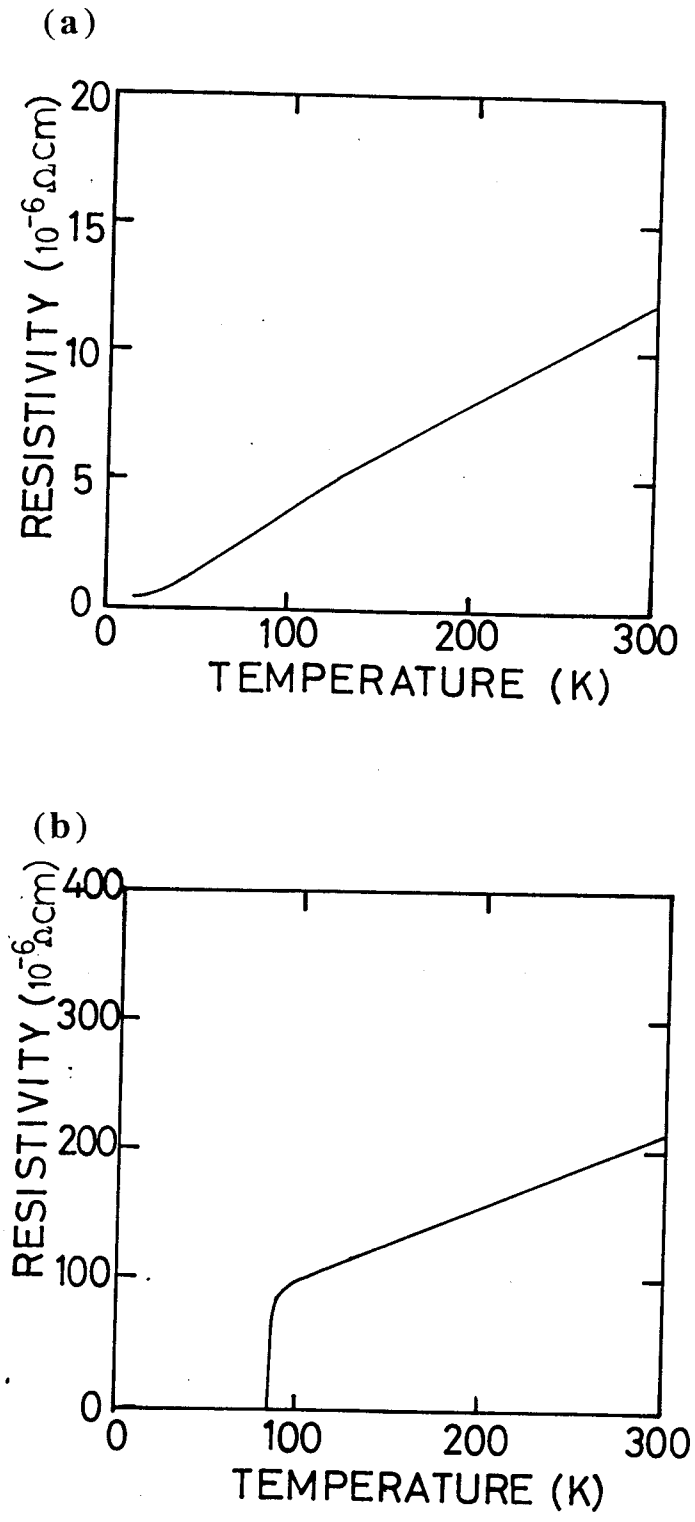

Fig. 8-2-2. Resistivity vs temperture curves of Pt film and $YBa_2Cu_3O_7$ films.

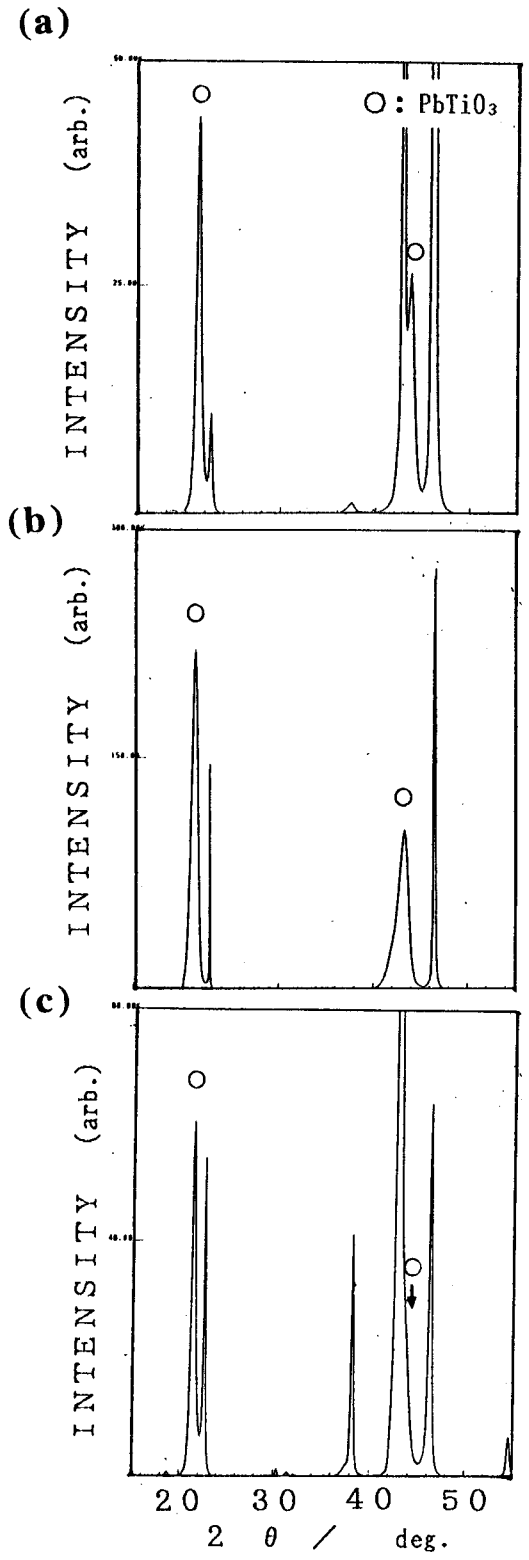

Fig. 8-2-3 X-ray diffraction pattern PbTiO3 films formed on three kinds of bottom electrode. (a)Pt.SrTiO3, (b) Nb-SrTiO3 and (c) $YBa_2Cu_3O_7$.

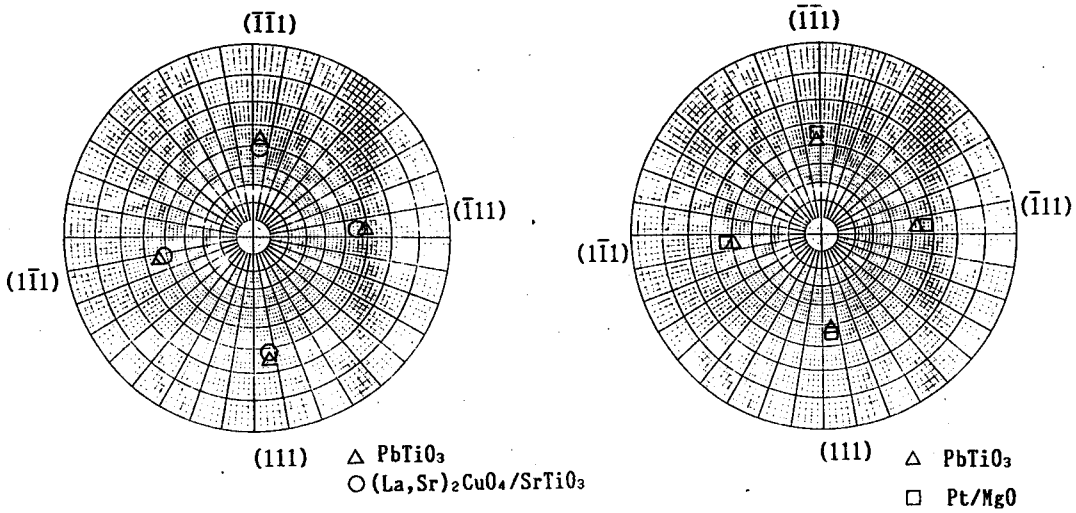

Fig. 8-2-4. pole figrue of the $PbTiO_3/La_{1.85}Sr_{0.15}CuO_4/SrTiO_3$ (right) and the $PbTiO_3$/Pt/MgO(left).

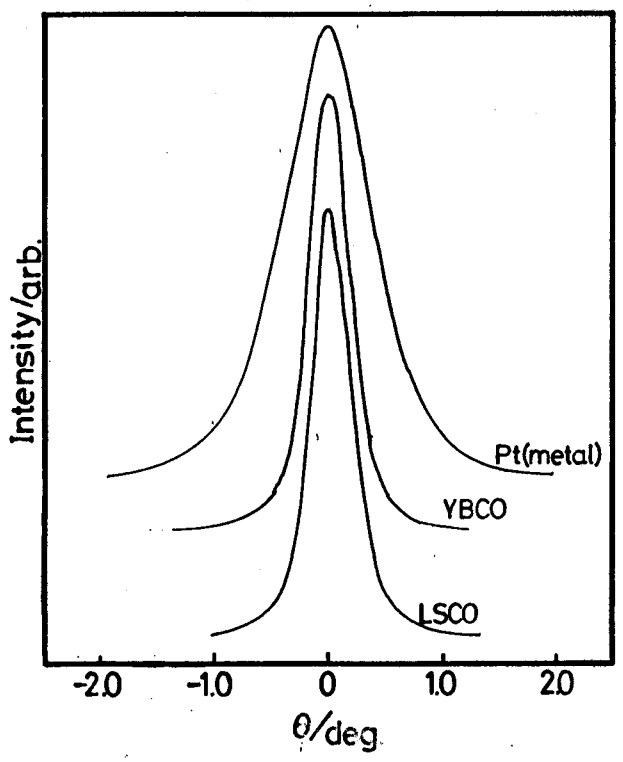

Fig. 8-2-5 Rocking curves of $PbTiO_3$ (001) films formed on

List of publication

[Scientific Journal]

1. H.Tabata, T.Kawai, M.Kanai, O.Murata and S.Kawai: "Formation of the High-Tc the Superconducting Bi-Pb-Sr-Ca-Cu-O Thin Film by Laser Ablation Method", Jpn.J.Appl.Phys. Vol.28, No.3 (1989) L430-433.

2. H.Tabata, T.Kawai, M.Kanai, O.Murata and S.Kawai: "Tailored Thin Films of Superconducting B-Sr-Ca-Cu Oxide by Excimer Laser Ablation Technique", Jpn.J.Appl.Phys. Vol.28, No.5 (1989) L823-826.

3. H.Tabata, O.Murata, T.Kawai and S.Kawai: "Tailored thin films of a superconducting Bi-Sr-Ca-Cu oxide prepared by incorporation of exotic atoms - control of the distance between CuO2 layers- ": Appl.Phys.Lett. Vol.56, No.16 (1990) 1576-1578.

4. T.Kawai, Y.Egami, H.Tabata and S.Kawai: "New Cuprate Superconductors", Nature Vol.349 No.6306 (1991) pp.200.

5. Y.Egami, H.Tabata, M.Kinugasa, T.Kawai and S.Kawai: "Phase Control of Superconducting B-Sr-Ca-Cu-O Thin Films Prepared by Laser Ablation Method", Jpn.J.Appl.Phys. Vol.30, No.313 (1991) L478-481.

6. H.Tabata, T.Kawai and S.Kawai: "Crystal structure and superconductivity of (La,Sr)2CuO4/Sm2CuO4 superlattices prepared by excimer laser deposition", Vol.58, No.13 (1991) 1443-1445.

7. H.Tabata, O.Murata, J.Fujioka, S.Minakata, T.Kawai, S.Kawai and M.Okuyama: "Preparation of PbTiO3 thin films at low temperature by an excimer laser ablation technique": Appl.Phys.Lett. Vol. 59, No.19 (1991) 2354-2356.

8. T.Kawai, T.Matsumoto, M.Kanai, H.Tabata, K.Horiuchi and S.Kawai: "High Tc superconducting artificial lattices as a new material", Physica C, Vol.185-189 (1991) 198-203.

9. K.Horiuchi, H.Tabata, T.Kawai and S.Kawai: "Crystal structures and superconductivities of (La,Sr)2CuO4/Sm2CuO4 and YBa2Cu3O7/(La,Sr)2CuO4 strained superlattices", Physica C, Vol.185-189 (1991) 2049-2050.

10. H.Tabata, O.Murata, T.Kawai, S.Kawai and M.Okuyama: "Preparation of PbTiO3 Thin Films by an Excimer Laser Ablation Technique with Second Laser Irradiation", Jpn.J.Appl.Phys., Vol.31 (1992) 2968-2970.

11. T.Kawai, M.Kanai, T.Matsumoto, H.Tabata, K.Horiuchi and S.Kawai: "Superconducting artificial lattices grown by laser molecular beam epitaxy", Materials Science Engineering, B 14 (1992) 227-230.

12. H.Tabata, T.Kawai and S.Kawai: "Strain and Proximity Effect in (La,Sr)2CuO4 Based Superconducting Superlattices", Phys.Rev.Lett. Vol.70, No.17 (1993) 2633-2636.

[Book]

1. H.Tabata and T.Kawai: "Artificial Construction of High Temperature Superconductors with layer-by-layer Laser Ablation Techniques", Materials Science Forum, Vol. 130-132 (1993) 119-142, Editor J.Puch, Trand.Tech.Publications.

[Related works]

1. M.Kanai, T.Kawai, S.Kawai and H.Tabata: "Low-temperature formation of multilayered Bi(Pb)-Sr-Ca-Cu-O thin films by successive deposition using laser ablation", Appl.Phys.Lett. Vol.54, No.18 (1989) 1802-1804.

2. H.Tanaka, H.Tabata, T.Kawai and S.Kawai; "Dominant factor for formation of perovskite PbTiO3 films using excimer laser ablation.", Jpn.J.Appl.Phys. 15 (1994) L451.

3. T.Tomio, H.Miki, H.Tabata, T.Kawai and S.Kawai; "Control of electrical conductivity in laser deposited SrTiO3 thin films with Nb doping.", J.Appl.Phys. may issure on Nov. 15 1994.

4. H.Tanaka, H.Tabata, K.Matsushita and T.kawai; "Molecular dynamics simulation for the crystal structures of ferroelectric and dielectric materials of BaTiO3-SrTiO3-CaTiO3" submitted to nature (1994).

13. H.Tabata and T.Kawai: "Atomic layer control of the growth of oxide superconductors using laser molecular beam epitaxy", Thin Solid Films, Vol.225, (1993) 275-279.

14. H.Tabata, O.Murata, T.Kawai, S.Kawai and M.Okuyama: "Electric and Pyroelectric behaviors of PbTiO3 Thin Films Formed by an Excimer Laser Ablation Technique", Jpn.J.Appl.Phys. 12A (1993) 5611-5614.

15. H.Tabata, O.Murata, T.Kawai, S.Kawai and M.Okuyama: "C-axis Preferred Orientation of Laser ablated Epitaxial PbTiO3 Films and Their Electrical properties", Appl.Phys.Lett. 64 (1994) 428-430.

16. H.Tabata, H.Tanaka and T.Kawai: "Formation of artificial BaTiO3/SrTiO3 superlattices using pulsed laser ablation and their dielectric properties", may issure in Appl.Phys.Lett. Oct. 3, 1994.

17. H.Tabata, H.Tanaka, T.Kawai and M.Okuyama : "Strained BaTiO3/SrTiO3 superlattices formed by a laser ablation technique and their high dielectric properties.", accepted in Jpn.J.Appl.Phys. 1994.

*18. H.Tabata and T.Kawai: "Effect of laser irradiation during the films formation of PbTiO3. - substrate irradiation and vapur irradiation - " submitted to Appl.Phys.Lett. 1994.

*19. H.Tabata and T.Kawai: "Film Formation of Perovskite Type Oxides by a Pulsed Laser Deposition and Their Ferro/Di-electric Properties." submitted to J. Appl. Phys. 1994.

*20. H.Tabata, H.Tanaka and T.Kawai: "Formation of strained dielectric superlattices of BaTiO3/SrTiO3 and SrTiO3/CaTiO3 and their electrical properties."

[Proceedings]

21. Y.Nishiyama, J.Fujioka, O.Murata, K.Nishio, H.Tabata and T.Yoshihara: "Formation of Y-Ba-Cu-O Films from Chloroform-Formalin Solution of Acetyl Acetone Complexes",
Proc. of the 1st Int. symp. on superconductivity (1988, Nagoya) 331-334. ;
Advances in superconductivity, Springer-Verlag.

22. T.Kawai, M.Kanai, H.Tabata and S.Kawai: "Formation of Bi(Pb)-Sr-Ca-Cu-O Thin Films at 500 ℃ by a successive deposition method using excimer laser",
Proc. of Cof.Sci.Thin film Superconductor (1988, Colorado) 21-26,Editor;
R.D.McConnell, Colorado Springs Plenum.

23. T.Kawai, H.Tabata, M.Kanai, O.Murata and S.Kawai: "Laser Ablation Method for the Formation of Tailored Superconducting Film", 2nd Workshop on High-Temperature Superconducting Electron Devices R&D Association for Future Electro Devices, (1989, Hokkaido) .

24. **H.Tabata** and T.Kawai: "Tailored Thin Films of Superconducting Bi-Sr-Ca-Cu Oxide Prepared by the Incorporation of Exotic Atoms - Superconductivity and the distance between CuO2 layers-", 3rd Annual Conference on Super conductivity and applications, (1989, NewYork Buffalo) 61-69, Editors; H.S.Kwok, D.T.Shaw, Plenum Press.

25. T.Kawai, M.Kanai, **H.Tabata**, K.Horiuch and S.Kawai: "Layered Growth of HTSC Thin Films using Pulsed Laser Deposition", Proc.of Films for High Tc Superconducting Electronics, SPIE Vol.1187 (1989, Santa Clara) 84-93, Editor; T.Venkatesan, SPIE.

26. T.Kawai, M.Kanai, **H.Tabata** and S.Kawai: "Tailored high-Tc Superconducting Thin films Prepared by Layer-by-layer deposition with Excimer Laser", Mat.Res.Soc.Proc. Vol.221 (1989) 533-536.

27. T.Kawai, M.Kanai, **H.Tabata**, Y.Egami, K.Kitahama, K.Ogura, S.Takagi, Y.Hori, T.Horiuch and S.Kawai: "Preparation of Bi-Oxide High-Tc Superconducting Cuprates in the form of ceramics and Thin films", Proc. 6th Japan-Korea Seminor on Ceramics (1989) in osaka

28. **H.Tabata**, O.Murata, T.Kawai and S.Kawai: "Tailored Thin Films of Superconducting Bi-Sr-Ca-Cu Oxide prepared by the Incorporation of Exotic Atoms: Superconductivity and the Distance between CuO2 Layers", Proc. of the 2nd Int. symp.on superconductivity (1989, Tsukuba) 939-942. ; Advances in superconductivity II, Editor T.Ishiguro and K.Kaimura, Springer-Verlag.

29. **H.Tabata**, T.Kawai and S.Kawai: "Superconducting superlattices of (La,Sr)2CuO4/Sm2CuO4 prepared by and excimer laser deposition technique", Proc. of the 3rd Int. symp.on superconductivity (1990, Sendai) 1131-1134, Advances in Superconductivity III(1990), Editors; K.Kajimura and H.Hayakawa, Springer-Verlag.

30. **H.Tabata**, T.Kawai, S.Kawai and O.Murata: "Epitaxial Growth of Thin Films of Ferroelectric Materials at Low Temperature by Excimer Laser Ablation Technique", Mat.Res.Soc.Proc. Vol.221 (1991) pp.41-46.

31. M.Kanai, **H.Tabata**, T.Kawai and S.Kawai: "Synthesis of Tailored Thin Films of Superconductors by excimer laser ablation", High Performance Ceramic Film and Coating (1991) 107-113, Editor; P.Vincenzini, Elsevier Science Publisher.

32. **H.Tabata**, H.Tanaka and T.Kawai: "Film Formation of the Perovskite Type Materials ($MTiO_3$; M=Ca, Sr, Ba, Pb) by a Laser Deposition." Mat.Res.Soc.Proc. (1994) Fall meeting in Boston.

33. **H.Tabata**, H.Tanaka and T.Kawai: "Construction of Strained superllatices and Their Dielectric Properties." Mat.Res.Soc.Proc. (1994) Fall meeting in Boston.

Acknowledgements

The author would like to express his sincere thanks to Professor T. Kawai of Osaka University for the encouragement and stimulating discussions.

Thanks are due to Dr. S.Kawai, Dr.K.Kitahama, Dr.T.Matsumoto, Dr. M.Kanai and Miss N.Fujibayashi for their helpful discussions and encouragement during the course of this study. In Chapter 5, I thank Prof. M.Okuyama for his useful suggestions and discussion. The author expresses his special thanks to Mr. H.Tanaka and Miss M.Kasaya for their considerable assistance. The author would like to thank students in Kawai Lab. in ISIR of Osaka University.

In Chapeter 4, I thank Prof. S.Hirotsu and Dr. Shimizu for TEM and SIMS measurements, respectively.

The author is extremely grateful to Mr. O.Murata, Dr. J.Fujioka and S.Okazaki, manager and general manager of Materials Section, Dr.S.Tsunenari, vice director of Akashi Technical Institute, Dr.K.Mori, general manager and Dr.T.Makimura, manager of Kawasaki Heavy Industris Ltd. for encouragement in the course of this study.

In final, the author would like to express his appreciation to his wife for her patience and understanding.